HYDRODYNAMICS AND MASS TRANSFER STUDIES IN A SCHEIBEL EXTRACTOR

by

JULIO CESAR BONNET RODRIGUEZ

A thesis submitted to the University of Aston in Birmingham for the degree of Doctor of Philosophy

Department of Chemical Engineering
The University of Aston in Birmingham.

February, 1982.

TO ADELINA

AND JUAD

Acknowledgements

The author wishes to thank the following:

Professor G. V. Jeffreys,

for his supervision and for providing the facilities for research.

Dra. Adelina R. de Bonnet,

for her tolerance, patience, encouragement and moral support.

The Concejo de Desarollo Cientifico y Humanistico, Universidad Central de Venezuela, Foninves and UNESCO VEN-31 for their financial support.

The technical staff of the department of Chemical Engineering, for their contribution in this work.

Mrs. N. Armstrong,

for her diligence in typing the thesis.

Hydrodynamics and Mass Transfer Studies in a Scheibel Extractor

Julio C. Bonnet Rodriguez Ph.D. 1982

Summary

A 10 cm diameter four-stage Scheibel column with dispersed phase wetted packing sections has been constructed to study the hydrodynamics and mass transfer using the system toluene-acetone-water.

The literature pertaining to the above extractor has been examined and the important phenomena such as droplet break-up and coalescence, mass transfer and backmixing have been reviewed. A critical analysis of the backmixing or axial mixing models and the corresponding techniques for parameter estimation was applied and an optimization technique based on Marquardt's algorithm was implemented.

A single phase sampling technique was developed to estimate the acetone concentration profile in both phases along the column.

Column flooding characteristics were investigated under various operating conditions and it was found that, when the impellers were located at about $D_I/5$cm from the upper surface of the pads, the limiting flow rates increased with impeller speed. This unusual behaviour was explained in terms of the pumping effect created by the turbine impellers.

Correlations were developed to predict Sauter mean drop diameters.

A five-cell with backflow model was used to estimate the column performance (stage efficiency) and phases non-ideality (backflow parameters). Overall mass transfer coefficients were computed using the above model and compared with those calculated using the correlations based on single drop mechanism.

Key Words:- Scheibel Column
Liquid-Liquid Extraction
Axial Mixing

Contents

List of Tables

List of Figures

CHAPTER I

INTRODUCTION

INTRODUCTION

Liquid-liquid extraction is a unit operation that has become an important separation technique in modern process technology. It is used to separate constituents of homogeneous liquid solutions (the raffinate phase) by adding a second liquid solvent (the extract phase), which is immiscible or only partially miscible with the first, being the components (solutes) of the mixture distributed between the two phases.

The petroleum industry was the first to apply this separation technique on a large scale, starting from the early 1930's when the method was used to separate aromatic hydrocarbons from the kerosene fraction during oil refining. The knowledge gained with this application had repercussions in other industrial organic processes and nowadays, liquid-liquid extraction is an important technique in coal-tar industry, petrochemical industries, essential oil industry and pharmaceutical industry.

In the 1940's, liquid-liquid extraction entered the area of inorganic chemical technology with the process for producing uranium. Since that time, application to other industrial inorganic processes has steadily increased, being some of the latest, metals extraction, production of phosphoric acid and waste disposal treatments.

The rapid expansion in liquid-liquid extraction processes has resulted in the fast development of a great variety of extractor types. Those, like the R.D.C., mixer-settler, perforated plate column, etc., which have withstood the test of adoption and become very popular in the industry, have been the most studied ones in the university laboratories judging by the number of papers which have appeared in the literature during the last two decades. On the other hand, some of the earlier extractors, specifically the Scheibel Column, has received very little attention and not enough data are readily available in the literature as to give the engineer some guidance for the industrial design or at least a pilot plant design.

The Scheibel Column has been identified as a low throughput, high efficiency rotary column. The limited capacity coupled with poor disassembly characteristics has been the major causes of its low industrial application, in spite of presenting the highest mass transfer efficiency of all agitated extraction columns. Early research (1,2) has been concerned mainly with only one characteristic of operating this column, that is the packing material not wetted by the dispersed phase. Some correlations were developed but many fundamental mass transfer and fluid dynamics parameters were not studied, making the design work of a simple pilot plant Scheibel column a matter of trial and error procedure.

Results (3) of a short study of a Scheibel Column had shown that better column capacity is achieved when the column is operated with the packing material preferred wetted by the dispersed phase. Also better mass transfer performance was claimed to be achieved when a total coalescence packing pad was used. Unfortunately, not enough experimental data were collected and consequently no design correlations were reported.

It appeared worthwhile therefore to investigate in more detail the hydrodynamics and mass transfer performance of a Scheibel Column operated under total coalescence in the packing section and eventually to provide guidelines to the design engineer. It was recognised at the outset that difficulties would arise, since:

(a) Guidelines for the selection of the packing material do not exist. Besides the specification of the material from which the pad is made and the percentage voidage, no other information is provided in the literature and certainly this is far from being enough as it is proved in this research.

(b) A detailed analysis and subsequent precise modelling of the mass transfer process require a complete monitoring of the solute concentration in both liquid phases along the columns. This required that uncontaminated samples of both phases must be obtained from a highly turbulent emulsion chamber.

An experimental technique to perform this task has not yet been reported and needs to be developed.

(c) Hold-up determination on a Scheibel Column operating under total coalescence in the packing has not been determined in past research (3,4) mainly because the amount of dispersed phase trapped inside the packing pads could be significant and the well known displacement technique for hold-up measurements may produce misleading results.

In the event an attempt has been made to obtain a useful mathematical model of the Scheibel Column which simulate the performance of the system sufficiently well for practical purposes using a small number of parameters to characterize the mass transfer mechanism and the fluid dynamic behaviour.

CHAPTER II

EXTRACTION EQUIPMENT

EXTRACTION EQUIPMENT

2.1 Classification and Selection

Industrial liquid-liquid extraction contactors may be classified, according to the construction and the operational characteristics, into two broad groups, stagewise contactors and differential contactors. In the former type of contactors there are a number of discrete stages in which the two phases are brought into intimate contact, separated, and passed counter-current to the adjoining stages, whereas in the differential contactors the composition of the phases changes continuously. In the case of stagewise contactors since the phases have to be separated after being mixed in each stage, the settling compartments have to be large and thereby the whole unit may become bulky. Differential contactors are more compact for a given throughput requiring little ground area since they are normally constructed as vertical columns. While such contactors do avoid the problem of large floor space, the presence of axial mixing reduced significantly their performance.

A typical classification of liquid-liquid contactors is presented in Figure 2-1, in which a further subdivision is made according to the means adopted for phase

Figure 2.1 - Liquid-Liquid Contactors

Force producing phase interdispersion	Differential Contactors	Stage wise Contactors
Gravity	- Spray column - Packed column	- Perforated plate column*
Pulsation	- Pulsed packed column - Pulsating plate column	- Pulsed sieve-plate column*
Mechanical agitation	- Rotating disc contactor - Oldshue Rushton column - Kuhni column - Graesser contactor	- Scheibel column* - ARD extractor* - Mixer-settlers
Centrifugal force	- Podbielniak - Quadronic	- Westfalia - Robatel

* Could be considered intermediate between differential and stagewise

inter-dispersion (5).

The selection of a particular extractor to perform a specified separation process is largely dictated by economics and is still based upon experience. Recently a contactor selection chart (6), shown in Figure 2-2, has been published which provides broad guidance and a quick method of preselection between apparatus for a new separation problem which can then be used to implement specific design experiments.

2.2 Design

Once a preselection of possible extractors has been made, the next stage consists in the design of the pilot-scale contactors in which experimentation must be carried out with the products to be processed later in the industrial system. This study provides the criteria and the mass transfer data for the final selection and design of the industrial extractor.

The identification of the parameters which control the design and performance of the extraction equipment under study is highly desirable in order to set up an experimental program and a research strategy. This information can be obtained primarily from equipment manufacturers' literature, unfortunately, not always

Figure 2.2 - Contactor Selection Chart

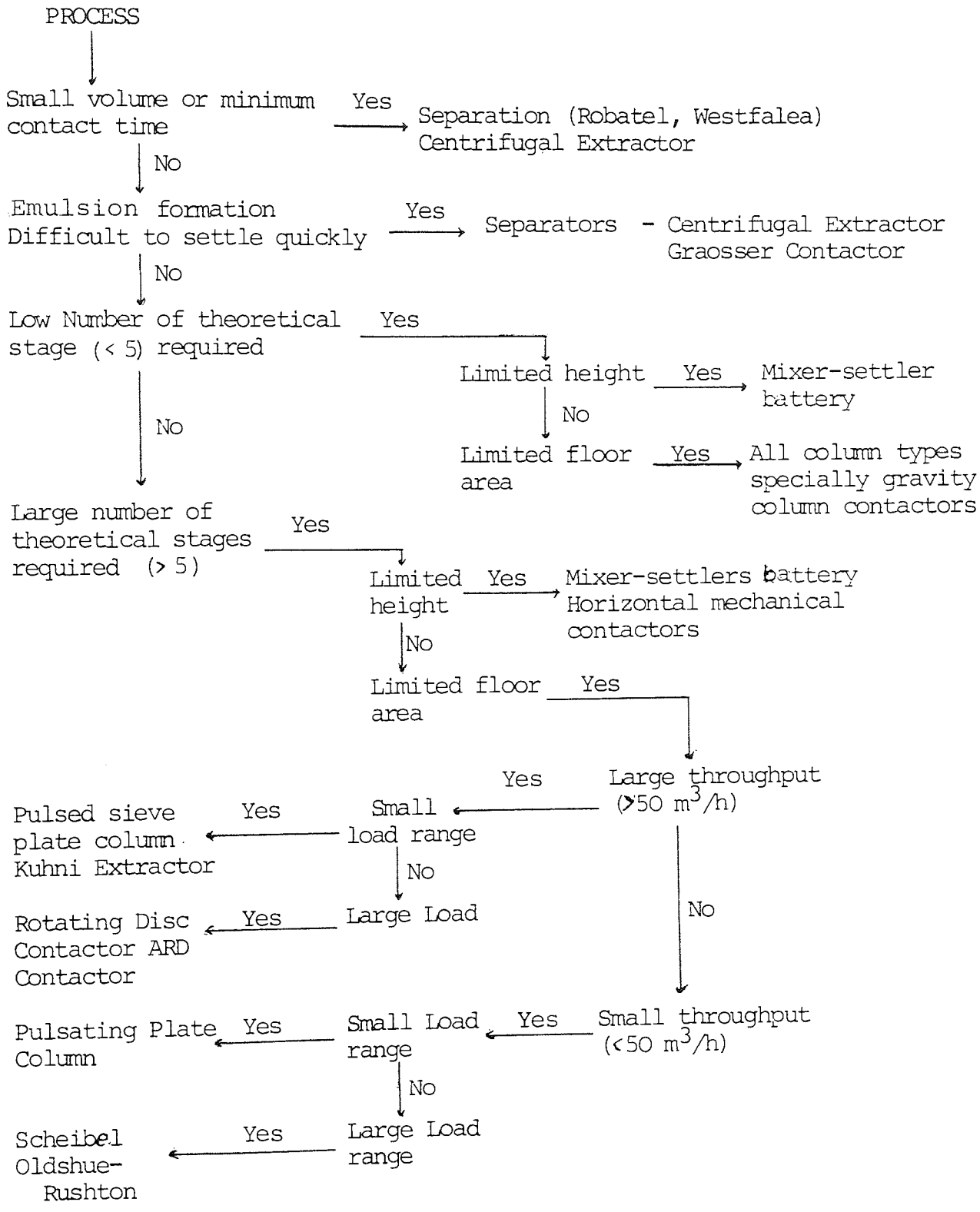

readily available, or as usually occurs, from the general literature in the technical journals.

In order to highlight the most important design parameters in extraction equipments, a presentation is made of the most representative contactor in each of the two broad groups of Figure 1.1, i.e. stagewise and differential.

2.2.1 Discrete Stage Contactor - Mixer-Settler

The mixer-settler could be considered the most representative contactor in the group of stagewise contactors and the one having the most abundant design information. The simplest version of the mixer-settler consists of two tanks in series, one for mixing and the other for settling the mixed phase. Such mixer-settler unit is considered as forming a simple stage. Several such units are arranged in series, horizontally or vertically, to form a continuous multistage countercurrent cascade or battery. Figure 2.3 shows some of the most common mixer-settler battery (MBS) types.

All countercurrent multistage contacting units are schematically represented by the common flowsheet shown in Figure 2.4a. The number of equilibrium stages required to achieve a particular separation in a multistage contactor can be obtained by the simultaneous solutions of the distribution coefficient and mass-balance equations.

Figure 2.3 - Mixer Settler Battery Types

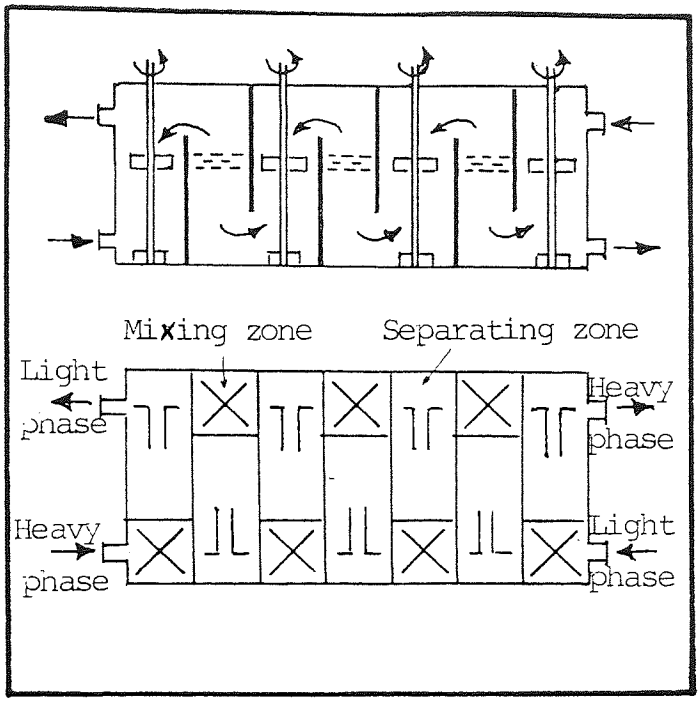

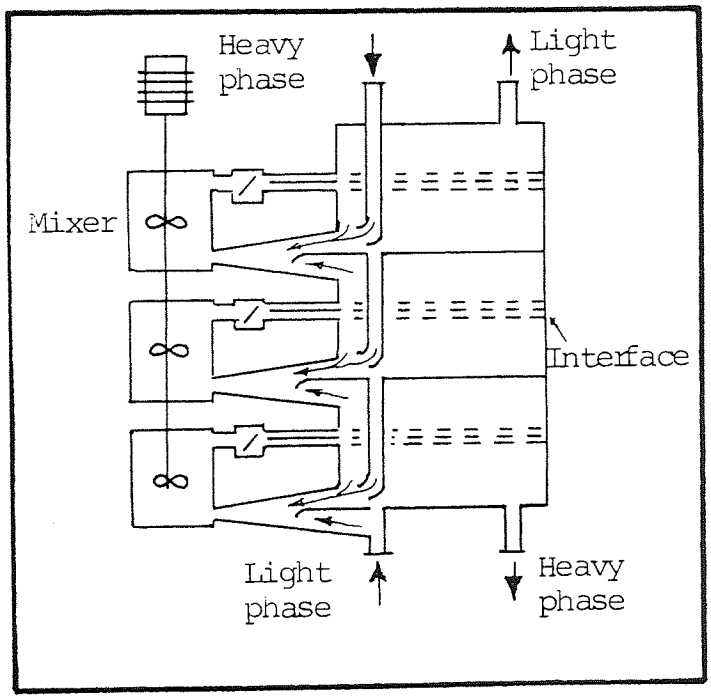

Figure 2.4 - Stagewise Contactor

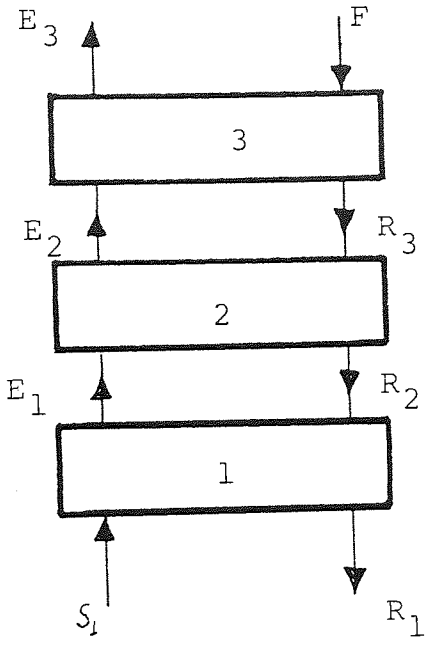

(a) Three stage counter-current liquid-liquid contactor

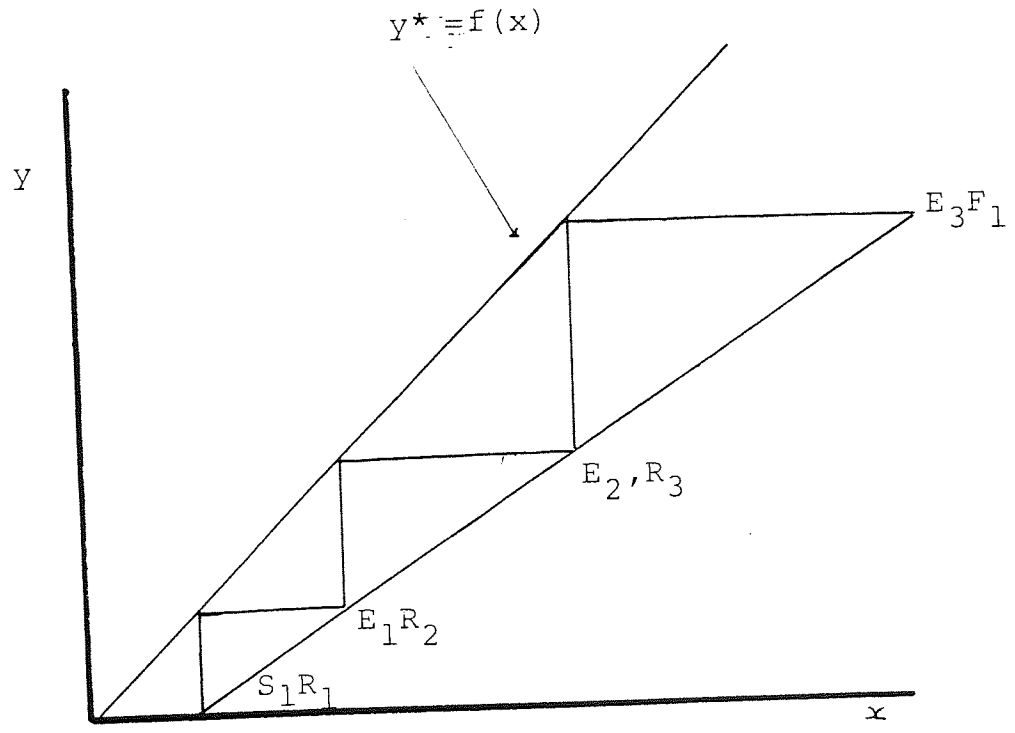

(b) McCabe Thiele construction. 100% Efficiency, plug flow condition

Usually, graphical methods are used such as the McCabe-Thiele construction shown in Figure 2.4b. The number of equilibrium or theoretical stages required is sometimes used as an index of performance and as such was included in Figure 2.2. A more generally used method of expressing performance is by means of calculating the fractional approach to equilibrium attained by the effluents. This quantity is known as the Stage Efficiency. Different stage efficiencies can be defined but the most used is the Murphree Efficiency which measures the approach of one of the effluent streams to equilibrium with the other at its actual final concentration.

In order to estimate the Murphree Efficiency, based on either extract or raffinate phase, from the parameters controlling the kinetics of the process, it is necessary to postulate a model which assumes a specific flow pattern or solute concentration change inside the stage, or specifically in the mixer, since little mass transfer actually takes place in the settler. The selection of an appropriate flow model is based fundamentally on the size and shape of the agitated vessel, method of agitation and internal construction. If a well mixed model or a totally backmixing of the phases is found acceptable then the Murphree Efficiency (E_{MD}) can be estimated by the following equation (7)

$$\frac{K_D \; a \; H}{V_D} = \frac{E_{MD}}{1 - E_{MD}} \qquad (2.1)$$

This equation requires the knowledge of the overall mass transfer coefficient K_D and the specific surface area a. This last variable can be calculated by the expression;

$$a = \frac{6 \Theta_D}{d} \tag{2.2}$$

The average drop diameter, d, can be estimated using the expression based on Kolmogoroff's theory of isotropic homogeneous turbulence,

$$d = \frac{C\, D_I^{5/8}}{(W_e)^{3/8}\, \sigma^{3/8}} \tag{2.3}$$

The fractional dispersed phase hold-up in the mixer Θ_D, is usually assumed equal to the fraction of the dispersed phase in the feed. This is not exactly true for continuous operation unless the level of agitation is sufficiently high.

The estimation of K_D requires in terms the estimation of the continuous phase k_c and dispersed phase k_D mass transfer coefficients, since all three coefficients are assumed to be related by the law of additive resistances given by the following equation;

$$\frac{1}{K_D} = \frac{1}{k_D} + \frac{m}{k_c} \tag{2.4}$$

The calculation of k_D and k_c are based on correlations derived for single drop mechanisms which are extensively discussed in Chapter IV.

Finally, after the calculation of d, Θ_D, a, and K_D the Murphree Stage Efficiency and the number of real stages to accomplish the mass transfer duty can be estimated.

As a final remark, it is necessary to point out that a carefully designed settler is most vital for a good performance. The capacity of a mixer-settler extraction plant is determined by the capacity of the settlers, because the mass transfer work done in the mixers can be dissipated through entrainment from the settlers. Then it is necessary to make the settlers large enough so that sufficient resident time is allowed for coalescence of the phases. Jeffreys and Hawksley (8) had presented a correlation to predict the coalescence time of a single drop at a planar interface. This correlation can be used to obtain an "order of magnitude" of settler size.

2.2.2 Continuous Differential Contactor - R.D.C.

The Rotating Disc Contactor was invented by H. Reman in 1951. It is probably the best known agitated extractor, and the most extensively studied during the last two decades.

Figure 2.5 shows a schematic diagram of the original R.D.C. which consists of horizontal discs, used as agitating elements, mounted on a centrally supported shaft. Offset against the agitator discs, stator rings whose aperture is greater than the agitator disc diameter, are mounted at the column walls simplifying installation.

It is used extensively in the petrochemical industry, for instance for phenol extraction from waste waters. For design and operational reasons, the column can have large diameter, i.e. 6 to 8 meters, but with only low height, i.e. 10 to 12 meters, since the shaft must be continuous without coupling or intermediate bearing. It has been found experimentally, that flooding occurs at the coupling of the shaft.

The extraction efficiency of R.D.C. columns has been expressed either as the number of theoretical stage, or as the "number of overall transfer unit" $(NTU)_o$. The last variable is the most common in use and the knowledge of the "height of a transfer unit" (HTU) is required in order to estimate the height of the effective part of the column according to the following equation

Figure 2.5 - Rotating Disc Contactor

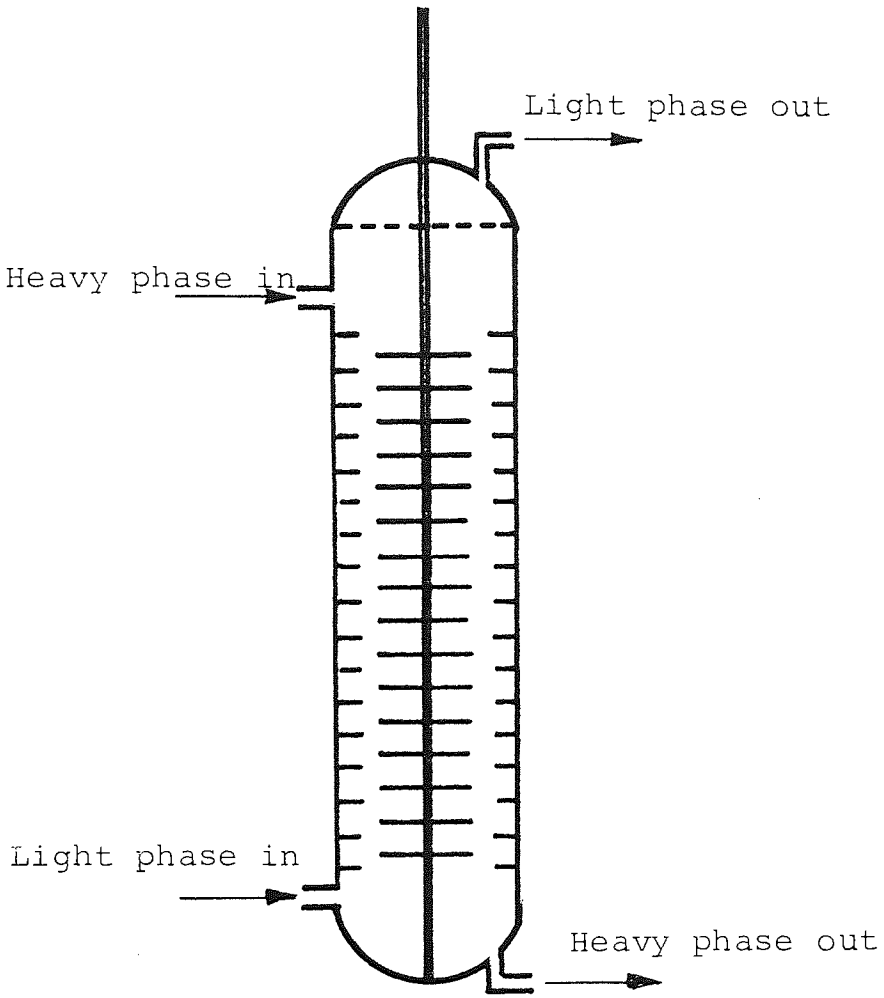

$$(N_{TU})_{OD} = \frac{K_D\ aL}{V_D} = \frac{L}{(HTU)_{OD}} \qquad (2.5)$$

Early methods of design of countercurrent separation processes were usually based on the assumption of plug-flow conditions for both phases. This assumption leads to a simple expression for the number of overall dispersed phase transfer units,

$$(NTU)_{ODP.F.} = \frac{lu\left[\left(\frac{x_i - my_i}{x_o - my_i}\right)(1-F) + F\right]}{1 - F} \qquad (2.6)$$

However, it has been shown in a number of experimental studies that in the majority of types of extraction equipment, i.e. R.D.C., Oldshue-Rushton & Spray Column, this assumption is not fulfilled even approximately. This is due to the presence of longitudinal dispersion or axial mixing of the phases which reduces concentration gradients and adversely affects performance. Methods of taking it into account in the design of extractors have been developed (9,10) but these depend upon having at hand experimental measurements of the axial mixing effect or means of predicting it. Strand, Olney and Ackerman (11) have successfully described the axial mixing in RDC of different diameters by the eddy diffusivity E, concept earlier introduced by Sleicher (10). Their research produced very valuable correlations of the eddy diffusivities in the continuous and dispersed phases as given by the following equations;

$$\frac{(1 - \Theta_D)\ E_c}{V_c\ L} = 0.5 + 0.09\ (1 - \Theta_D)\ (\frac{D_I\ N}{V_c})\ (\frac{D_I}{D_c})^2 \left[(\frac{SS}{D_c})^2 - (\frac{D_I}{D_c})^2\right] \qquad (2.7)$$

$$\frac{\Theta_D\ E_D}{V_D\ L} = 0.5 + 0.09\ \Theta_D\ (\frac{D_I\ N}{V_D})\ (\frac{D_I}{D_c})^2 \left[(\frac{SS}{D_c})^2 - (\frac{D_I}{D_c})^2\right] \qquad (2.8)$$

The solution of the problem for mass transfer between the phases in a continuous column, with eddy diffusion present in both phase has been presented by Sleicher (10), Miyauchi and Vermeulen (11) and Pratt (12). Of all, the most attractive is the Sleicher solution which allows for correction of the plug-flow $(NTU)_o$ to obtain the true $(NTU)_o$. This solution is given as a correlation equation with six empirical constants which are function of the extraction factor F.

$$\frac{(NTU)_{OR}}{(NTU)_{OR,P.F.}} = \frac{(Pe)_R\ (Pe)_E}{(Pe)_R(Pe)_E - (NTU)_{OR,P.F.}\left[a(Pe)_R + b(Pe)_E + c\sqrt{(Pe)_R(Pe)_E} - \rho\sqrt{(Pe)_R + (Pe)_E} + g((Pe)_R - (Pe)_E).e^{-h(NTU)_{OR}}\right]} \qquad (2.9)$$

The parameters $(Pe)_R$ and $(Pe)_E$ are the Peclet Numbers of the raffinate and solvent phases based on the column length L as defined by the following equations;

$$(PE)_R = \frac{V_R\ L}{\Theta_R\ E_R} \qquad (2.10)$$

$$(PE)_E = \frac{V_E \; L}{\Theta_E \; E_E} \qquad (2.11)$$

This definition of the H.T.U. by equation (5) calls for a knowledge of the variables K_R, overall raffinate phase mass transfer coefficient, drop diameter d and dispersed phase hold-up Θ_D, these last two combined by equation (2) to give the specific interfacial area, a.

The estimation of K_R can be done by the procedure outlined in section 2.2.1. Misek (13) has presented different correlations for the determination of drop size, d, in a rotating disc contactor depending on the intensity of mixing. For a fully turbulent mixing region,

$$\frac{d \; N^2 \; D_I^{\,2} \; \rho_c}{\sigma \; e^{0.0887(D_c - D_I)}} = 16.3 \left[\frac{H}{D_c}\right]^{0.46} \qquad (2.12)$$

On diminishing the mixing intensity below a critical value of the impeller Reynolds Number, the drop sizes can be estimated by

$$\frac{d \; N^2 \; D_I^{\,2} \; \rho_c}{\sigma \; e^{0.0887 \; \Delta_D}} = 0.345 \times 10^{-6} \left[\frac{D_I^{\,2} \; N \; \rho_c}{\mu_c}\right]^{1.42} \qquad (2.13)$$

A further decrease in mixing intensity leads to a mechanism of drop formation almost entirely dependent on the equilibrium between buoyancy and surface force, i.e. mechanism analogous to that governing the splitting in packed columns. In this case the drop size d can be estimated by the expression;

$$d = 0.38\sqrt{\frac{\sigma}{\Delta\rho g}} \qquad (2.14)$$

The calculation of the dispersed phase fractional hold-up, ϕ_D, needs to consider the coalescence and break-up of droplets in the R.D.C. Hence Misek (14) proposed that hold-up in an R.D.C. be correlated by the relations

$$\frac{V_D}{\phi_D} + \frac{V_C}{1 - \phi_D} = \bar{v}_o(1 - \phi_D) \exp\left(\frac{z}{\alpha} - 4.1\right)\phi_D \qquad (2.15)$$

Many other variables and considerations enter into the complete R.D.C. design, but those presented in this summary highlighted a phenomonological approach to the design of a rotating disc cont actor. A comparison of the equations presented in this section and section 2.2.1 reveals the existence of variables which are common to any type of agitated liquid-liquid extractors, i.e., the overall mass transfer coefficient K_D, the dispersed phase hold-up ϕ_D and the drop diameter d, as well as variables related to a particular phenomena described by an appropriate mathematical model, i.e., E_R, E_E, axial diffusion coefficients.

The identification of the design variables common to the different equipments within the same unit operation is a very valuable information in the planning stage of a research project of a new or poorly known equipment.

CHAPTER III

THE SCHEIBEL COLUMN

THE SCHEIBEL COLUMN

3.1 Types of Column

The Scheibel extraction column was patented in 1950 (15) for the Hoffmann-La Roche Company. The schematic drawing of the column is shown in figure 3.1. The column consists of an alternate series of mixing sections and packed sections with a centrally located shaft upon which are mounted agitators with vertical blades. The packing or calming section usually consists of a woven wire mesh which acts as an entrainment separator and coalescer for the two liquids. Scheibel (15) suggested to use a packing prepared from a tubular knit wire mesh fabric, which is flattened and may be folded and then rolled up spiralwise to form the packing. It was claimed that with such packing "channelling" is eliminated.

Commonly to all extraction columns, the heavy phase enters near the top of the column and flows downward, through the packing to the mixing chamber where it is brought into intimate contact with the lighter liquid by the agitation in this chamber, leaving through the bottom. The light phase enters near the bottom and is displaced upwards by difference in density. The principal interface is maintained in one end section depending upon which phase is dispersed. The solute may be introduced in either entering solvent or at some intermediate point.

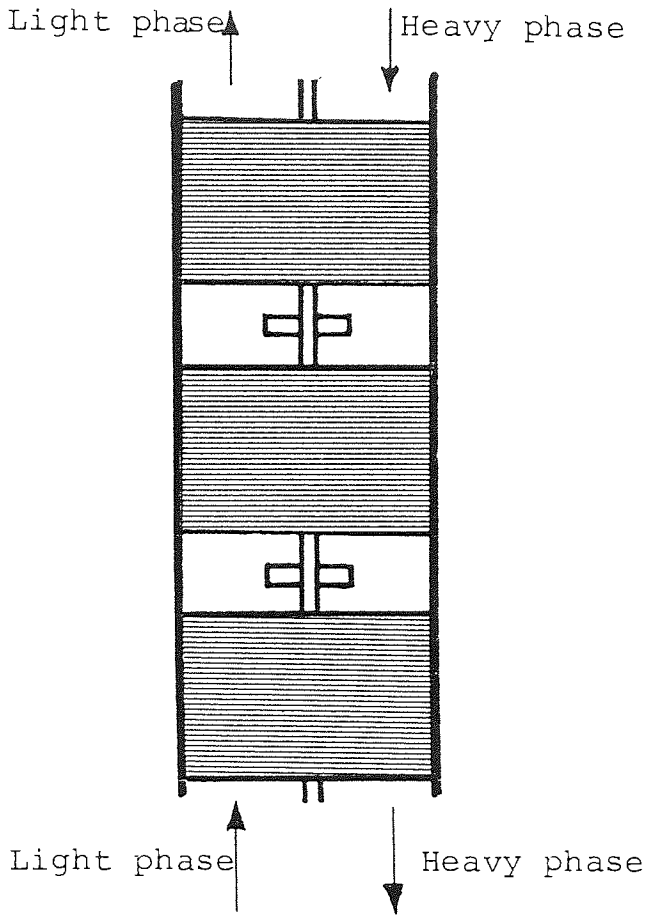

Figure 3.1 - Schematic Diagram of Scheibel Column

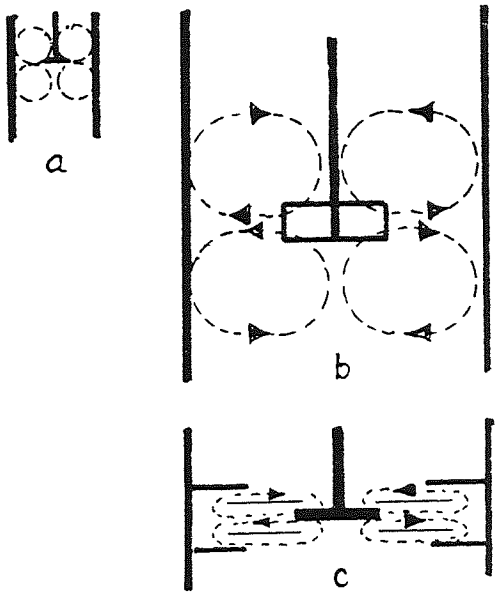

Figure 3.2 - Vertical Flow Components in Agitated Columns

Scheibel (16) expressed the performance of this column in terms of an overall stage efficiency and/or as a "Height Equivalent to a Theoretical Stage" (HETS). The efficiency was based on the assumption that a mixing section and a packing section together comprised a stage.

In general, in internally agitated extractors, the height required for a theoretical stage increases with diameter. Performance data obtained by Scheibel (16,17) in 1 inch and 12 inch diameter columns established that the HETS on this type of column varies as the square root of the diameter. This proportionality represents the tendency of the flow pattern in the mixing section to follow a geometrically similar shape when scale-up is made on the basis of dimensional similitude. This phenomena is represented in figure 3.2(a) and (b). In order to retain the same mixing height at the larger diameter, it will be necessary to direct the flow across the entire diameter by means of the stationary horizontal baffles, as shown in figure 3.2(c). This idea was used by Scheibel (18) in the design of a new column as shown in figure 3.3. It was claimed that the control of the mixing height by means of horizontal baffles will give smaller variations of HETS with diameter. Since only one column diameter was tested this basic idea could not be proved.

Besides the arrangement shown in figure 3.3 Scheibel (18) briefly investigated two more different arrangements. In the second arrangement the packing pads were removed and the mixing chambers were separated

Figure 3.3 - Modified Scheibel Column with Packing Sections

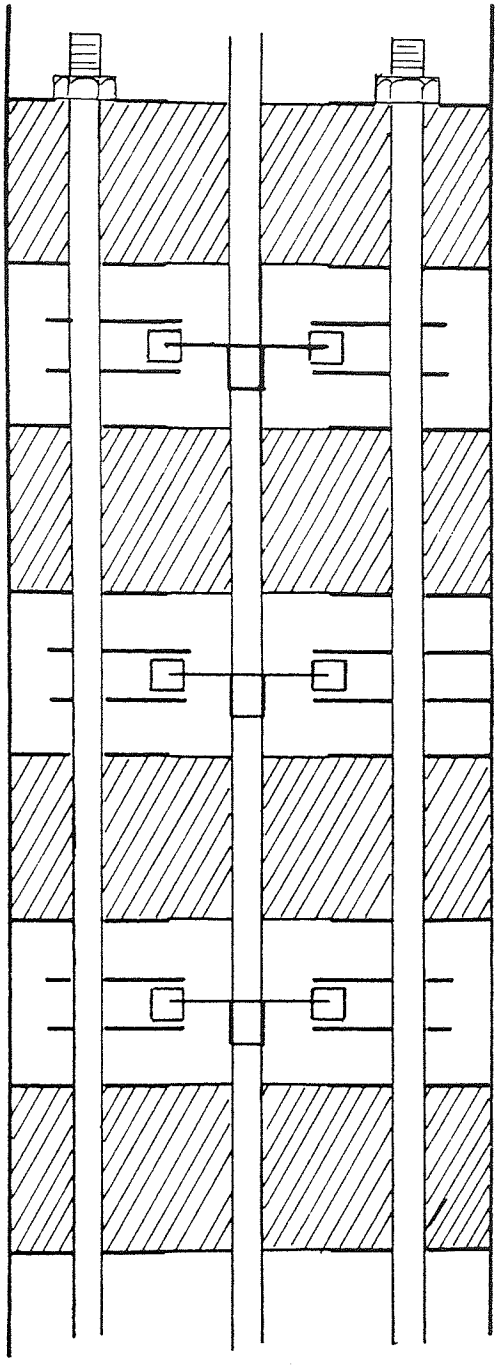

by the void chambers. In the third arrangement baffles and agitators were installed in all the intermediate void sections.

The original version of the Scheibel column shown in figure 3.1 is the most common in industrial use and the one to be considered in this research.

3.2 Hydrodynamics

The Scheibel column presents quite different flow-dynamics according to the wetting behaviour of the packing material. It is then considered appropriate to classify and present past research along this line.

3.2.1 Packing material non-wetted by the dispersed phase

The most extensive study of the flow of dispersions and droplet behaviour in packings wetted by the continuous phase was carried out by Pratt and his co-worker(19) in relation to Raschi g ring packed liquid-liquid extraction columns. In this investigation attention was paid to the droplet size leaving the packing and its dependency on packing size, voidage, flow rates and physical properties of the phases. From results using a 2 inch diameter by 3 ft packed column, Lewis et al (19) suggested the existence of a critical size of packing above which the exit droplet size was independent of the packing size and type. It was further shown in this work that the exit droplet size was independent of the size of the inlet drop. Thus large inlet drops were gradually broken down to some equilibrium

size whilst small inlet droplets grew, by coalescence, to attain the same equilibrium drop size. The expression allowing the estimation of the critical packing size $(dp)_{crit}$ was developed years later by Gayler et al. Based on collision theory, the equation of motion of a spherical droplet was solved to render an expression of the mean distance between collision or path length. By equating this path length to zero, which corresponds to mean void size equals mean droplet size, the following expression was obtained.

$$(dp)_{crit} = 2.42 \left(\frac{\sigma}{\Delta\rho g}\right)^{0.5} \qquad (3.1)$$

Gayler and Pratt (20) correlated the exit drop size (defined using Sauter mean diameter) for a range of organic aqueous systems in a 6 ft packed section in which the packing size was greater than the minimum given by equation 3.1

$$\frac{d_{32}\Delta\rho\sigma}{\mu_c^2} = 1.42 \left(\frac{\Delta\rho\sigma^3}{\mu_c^4 g}\right)^{0.475} \left(\frac{\bar{v}_o \varepsilon\theta_D}{V_D}\right) \qquad (3.2)$$

This equation could be simplified by changing the exponent to 0.5 with slight loss of accuracy to give

$$d_{32} = 0.92 \left(\frac{\sigma}{\Delta\rho g}\right)^{0.5} \left(\frac{\bar{v}_o \varepsilon\theta_D}{V_D}\right)$$

In equation (3.2) $\bar{v}_o$ represents the "characteristic velocity" (20) which is defined as the vertical limiting mean droplet velocity at zero continuous phase and very low dispersed phase flow rates. Under this flow condition $\bar{v}_o$ is proportional to the mean Stokes' law velocity of the isolated droplets (see section 4.1.2.2). The equation defining $\bar{v}_o$ is

$$\frac{V_d}{\Theta_D} + \frac{V_c}{(1 - \Theta_D)} = \varepsilon \bar{v}_o \ (1 - \Theta_D) \qquad (3.3)$$

A similar study was done by Honekamp (21) using knitted wire mesh packings and the low interfacial tension system MIBK-Water in a 4 inch diameter column. His results of exit drop size for different packing heights given in figure 3.4 demonstrate that high voidage knitmesh packing have droplet flow characteristics similar to conventional packings, i.e. Raschig rings and Berlsaddles, greater than the critical packing size. Figure 3.4 also shows that inlet drops smaller than the characteristic size grew only slightly as they passed through the packing. This drop behaviour and the analysis of the data collected from a 4-stage Scheibel Column (21.2) lead to the conclusion that the drop size in a Scheibel extractor is determined by the drop size in the mixing sections.

Honekamp and Burkhart (2) present a table of the Sauter mean drops diameters in the mixing sections of the 4-stage Scheibel Column operated under different dispersed flow and continuous flow rate and stirred speed.

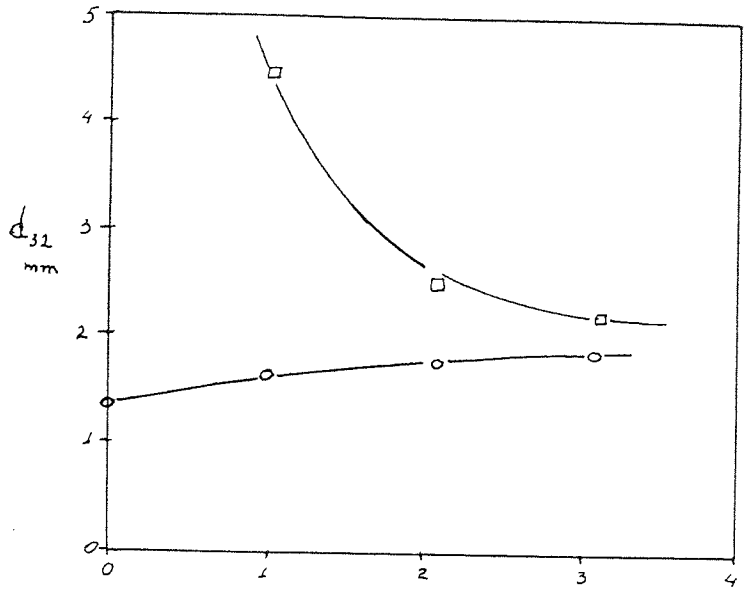

Figure 3.4 - Approach to Equilibrium Drop Size

A statistical analysis of this data was done by the author and the results are given in Table 3.1. Since information regarding the drop diameter distribution curve for each treatment is not available and the experiment was not replicated, the Error Mean Square was estimated from the two and three factor interactions. From this analysis of variance it is concluded that the stirrer speed is the only variable to have a significant effect on drop size.

Dispersed phase hold-up was also measured by Honekamp in the 4 stage Scheibel column using the displacement technique. An analysis of variance done by Honekamp on the hold-up data indicated that the continuous phase flow rate, dispersed phase flow rate and stirrer speed all produced significant effects on the column hold-up. A comparison of hold-up data for packed columns (22), correlated by means of equation 3.3, and Honekamp's data, is presented in figure 3.5. It is clear from the representation that the

Table 3.1 - Analysis of Variance for Honekamp (21) Drop Size Data

S.V.	D.F.	S.S.	M.S.
Total	24	71.6847	
Mean	1	63.537	
Dispersed phase flow rate $\frac{ml}{cm^2 min}$	2	0.0036	0.0018
Continuous phase flow rate $\frac{ml}{cm^2 min}$	1	0.0657	0.0657
Stirrer speed rpm	3	7.516	2.505***
Interaction			
Dispersed phase x continuous phase	2	0.0402	0.02
Dispersed phase x stirrer speed	6	0.169	0.028
Continuous phase x stirrer speed	3	0.0676	0.0225
Dispersed x continuous x stirrer	6	0.2852	0.0475
Error	17		0.118

*** Significant at 1% level

behaviour of the Scheibel extractor at constant stirrer speed, as far as hold-up is concerned, closely paralleled a packed extraction column.

Limiting flow phenomena in a 3.0 inch diameter Scheibel column has been investigated by Piper (3). Three-inch sections of stainless steel knitmesh packing, wetted by the continuous phase; and with 98.75% voidage were used. Attempts were made to correlate Piper's flooding data in a similar manner to that of Crawford and Wilke (23) for the flooding of packed columns. Figure 3.6 shows a plot of $V_C^{0.5}$ vs $V_D^{0.5}$ at the flooding points for different agitator speeds. The data are reasonably well fitted by straight lines indicating that a general flooding rate correlation, similar to that of Crawford and Wilke, is possible.

Jeffreys et al (24) also reported limiting flow data for the same column and chemical system used by Piper. In this work, 5-inch sections of stainless steel knitmesh packing with voidage values in the range 97.5-98.75% were studied.

It was found that a plot of $V_c^{0.5}$ vs $V_d^{0.5}$ (see figure 3.6) generally did not give a straight line unless the drop size was small compared with the interstice size of the packing, conditions corresponding approximately to those found in packed column. They also found that the working range of the packing increased with increasing voidage and that the limiting flow was dependent upon

Figure 3.5 - Hold-up Correlation. Packed and Scheibel Extraction Columns

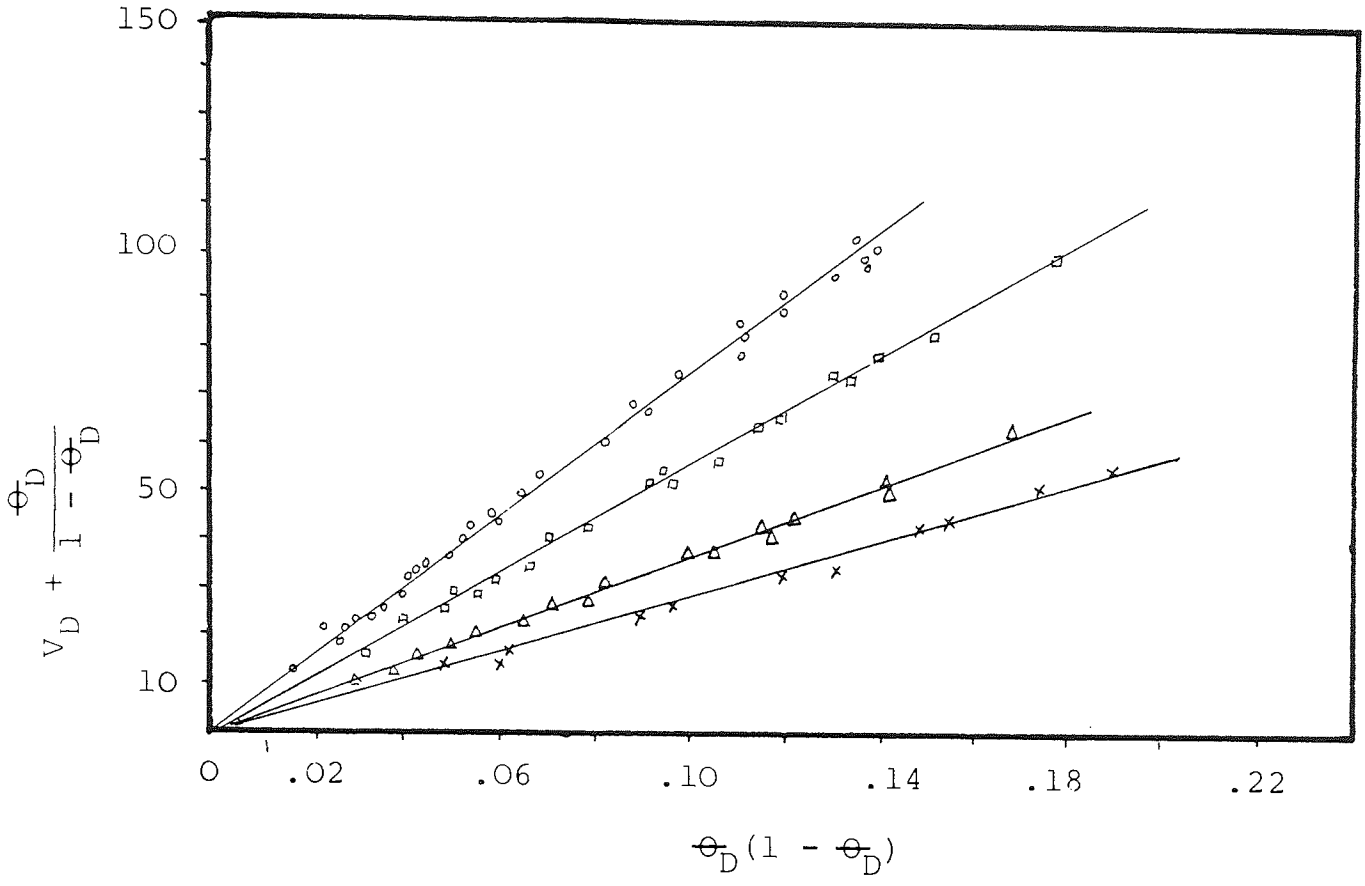

O - i-octane water, 1" Raschig Rings

□ - i-octane-water, ¾" Raschig Rings

Δ - Butyl acetate-water, ¾" Raschig Rings

x - MIBK-water, Honekamp's Data, Scheibel Column

Figure 3.6 - Flooding Rate Data. Scheibel Column

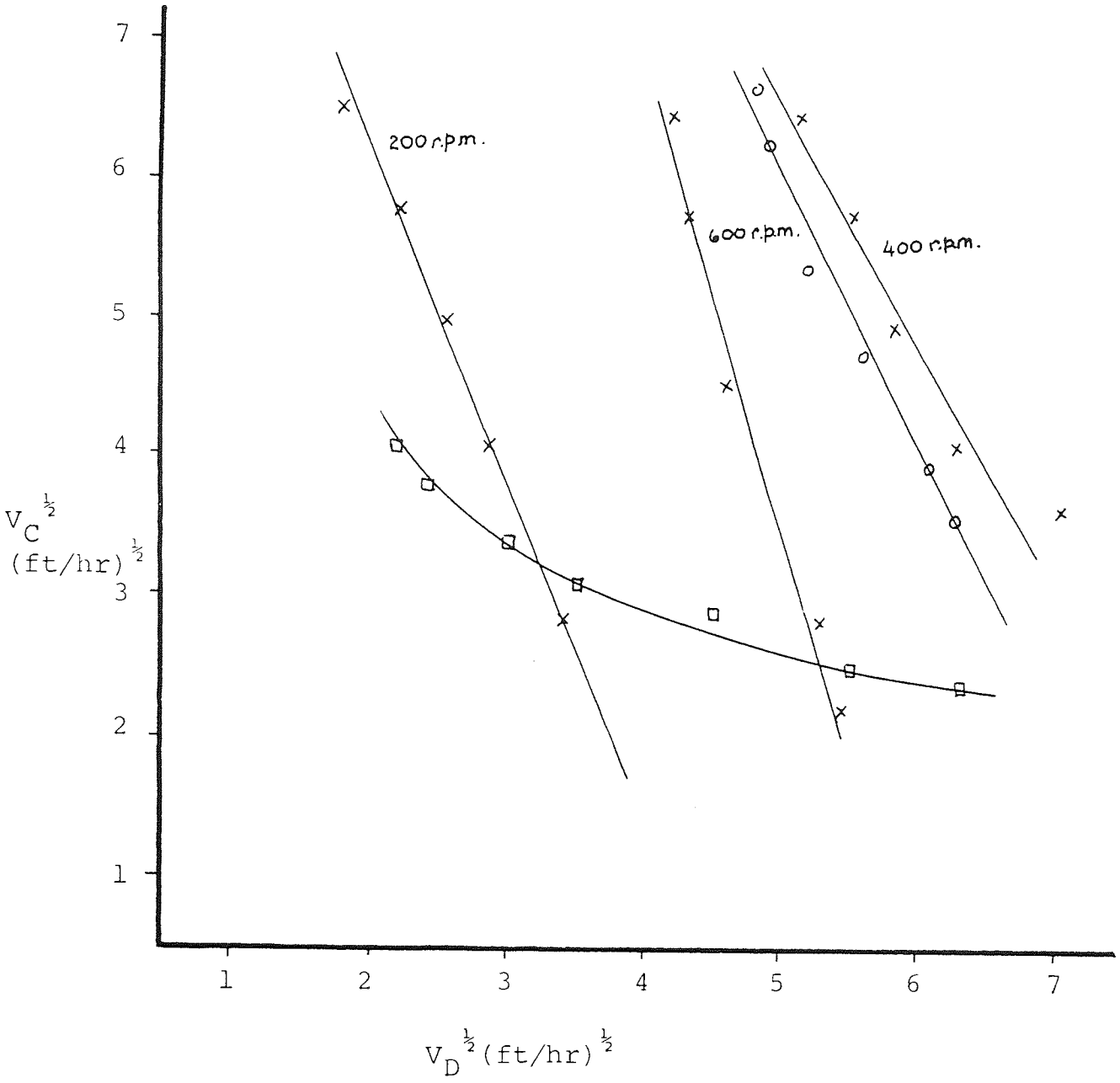

x Piper's. Packing Knitmesh st.st. 4530 - 98.75% voidage

o Jeffreys et al. Packing st.st. 9036 - 98.75% voidage. Large interstice size

□ Jeffreys et al. Packing st.st. - 97.5% voidage. Small interstice size

the inlet droplet size. Their conclusions, with respect to drop behaviour inside the knitted mesh packing indicate a rather more complex mechanism than the one reported by Honekamp and Burkhart and pictured in figure 3.4. Once again the relationship drop size - packing interstice size play a fundamental role on the mechanism by which drops pass through the packing.

Hold-up vs packing type data were not investigated by Piper (3) and by Jeffreys et al (24), but in view of the conclusion arrived at by them with respect to limiting flow rate and drop behaviour it can be said that hydrodynamic parameters on Scheibel columns cannot always be estimated from conventional packed extraction column correlations.

Studies of longitudinal mixing in Scheibel extractors can be considered non-existent. To the author's knowledge the only information available in the literature is the limited work done by Gelperin et al (4) on a 56mm diameter and 500mm length standard Scheibel column. The most extensive part of his work was devoted to the study of the R.D.C. and the modified, without packing, Scheibel column. For the three columns, only the continuous phase longitudinal mixing diffusivity, E_c, was determined by the input-output tracer analysis techniques, using methylene blue as a tracer. The system under study was kerosene-water and the coefficient of longitudinal mixing were calculated from the value of the variance of the C-curve using the equations proposed by Levenspiel and Smith (25).

Figure 3.7 shows the relation between E_c and the agitator speed for the three columns. A common feature in all the curves is the occurrance of a minimum value of E_c, which can be explained from the fact that E_c is made up from the contribution of a back mixing coefficient and an axial diffusion or Taylor diffusion coefficient.

For a low agitator speed, E_c depends basically on the Taylor diffusion. As the rpm increase the continuous phase velocity profile tends to become flat and the Taylor or axial diffusion decrease. However, increasing the rpm produces an increase in the back mixing, which after a specified agitator speed, start to fix the value of E_c. Another important feature shown in figure 3.7 is that the Scheibel column presented the lowest value of E_c for the three columns under study, mainly due to the presence of the packing zones which damp out the turbulence created in the mixing chambers.

Figure 3.8 is a representation of E_c as a function of the linear velocity of the continouous phase, $\bar{V}_c$, under two-phase flow situation and constant agitator speed. The magnitude of E_c increase as $\bar{V}_c$ increase and it can be said that this increase is due to the axial diffusion contribution since practically the back mixing coefficient is independent of the phase linear velocity.

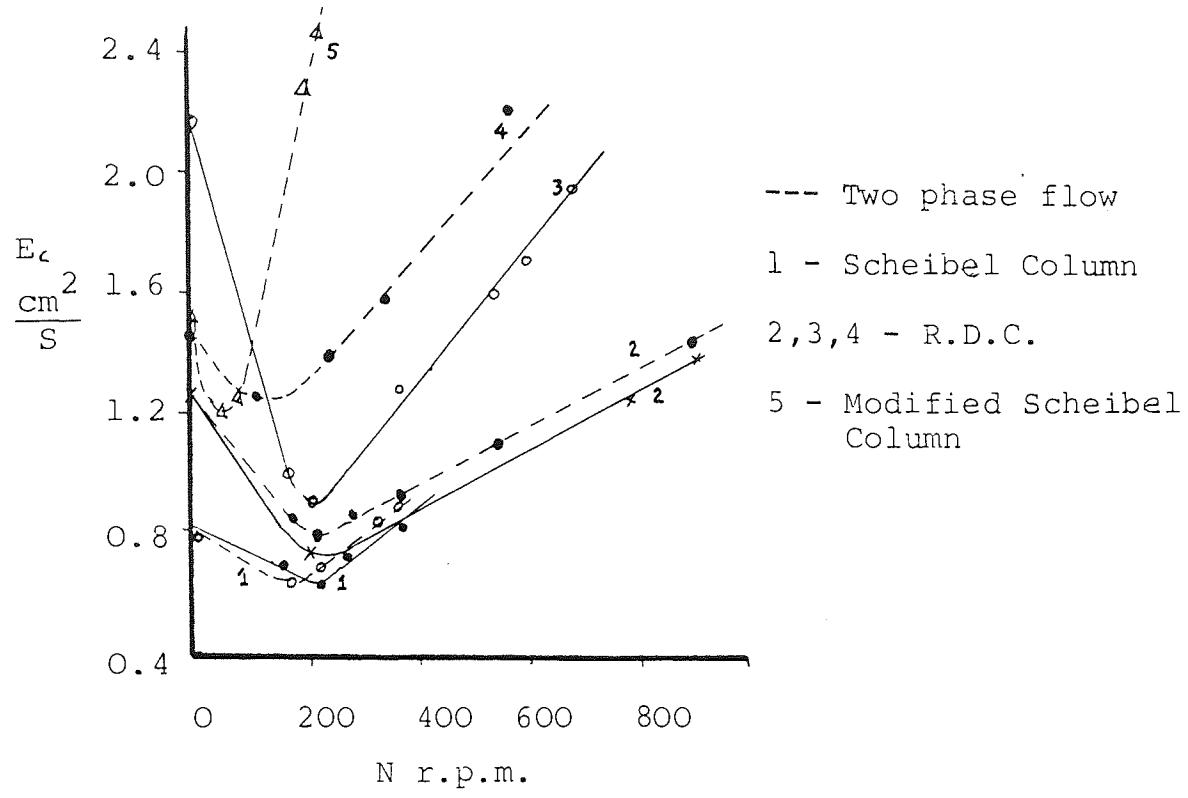

Figure 3.7 - Continuous Phase Axial Diffusion Coefficient E_C vs impeller speed

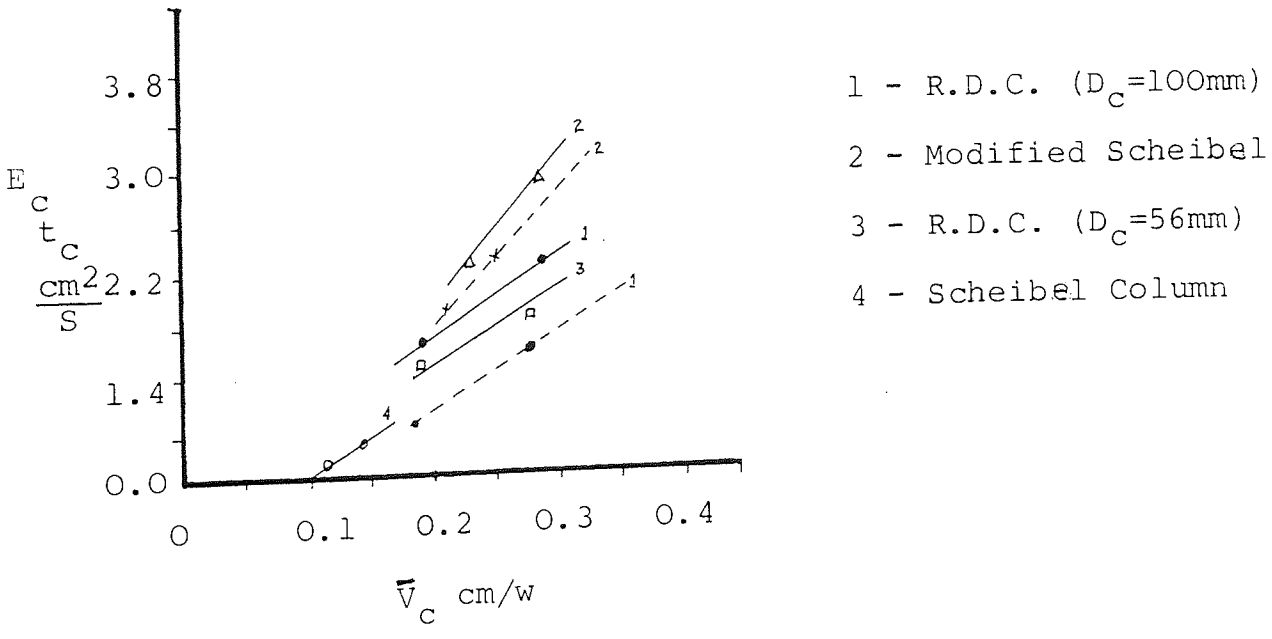

Figure 3.8 - Continuous Phase Axial Diffusion Coefficient E_c vs Continuous Phase Superficial Velocity

A plot of $\frac{E_c}{\bar{V}_c L}$ vs $\frac{D_I N}{\bar{V}_c}$, the same as that done by Guttoff (26), produced the following general correlation, by fitting a straight line through the points.

$$E_c = A\,\bar{V}_c L + BLD_I N \qquad (3.4)$$

The Constant A and B take the values of 0.5 and 0.003 for the Scheibel Column, 0.4 and 0.0038 for the Modified Scheibel and 0.5 and 0.00625 for the RDC. The reliability of this linear correlation is very much questionable firstly because it fails to predict the minimum value of E_c as N increases and secondly, because the large amount of data obtained by Strand et al (11) and Guttoff (26) on RDC could not be correlated, using the same coordinates by a liner equation.

3.2.2 Packing Material Wetted by the Dispersed Phase

A very limited amount of work in Scheibel column with packings made of material preferably wetted by the dispersed phase, has been presented by Piper (3). Knitmesh polypropylene packing, wetted by the kerosene dispersed phase, was used. The flow regime at low stirrer speed for the system kerosene (dispersed)-water-polypropylene packings is shown in figure 3.9. The drops were found to wet the packing fibres and coalesce inside the packing, creating a second continuous phase, leaving the packing surface in the form of a continuous stream for high flow rates or by drip-point mechanism for low flow rates.

Figure 3.9 - Flow Regime. Dispersed Phase Wetted Packing

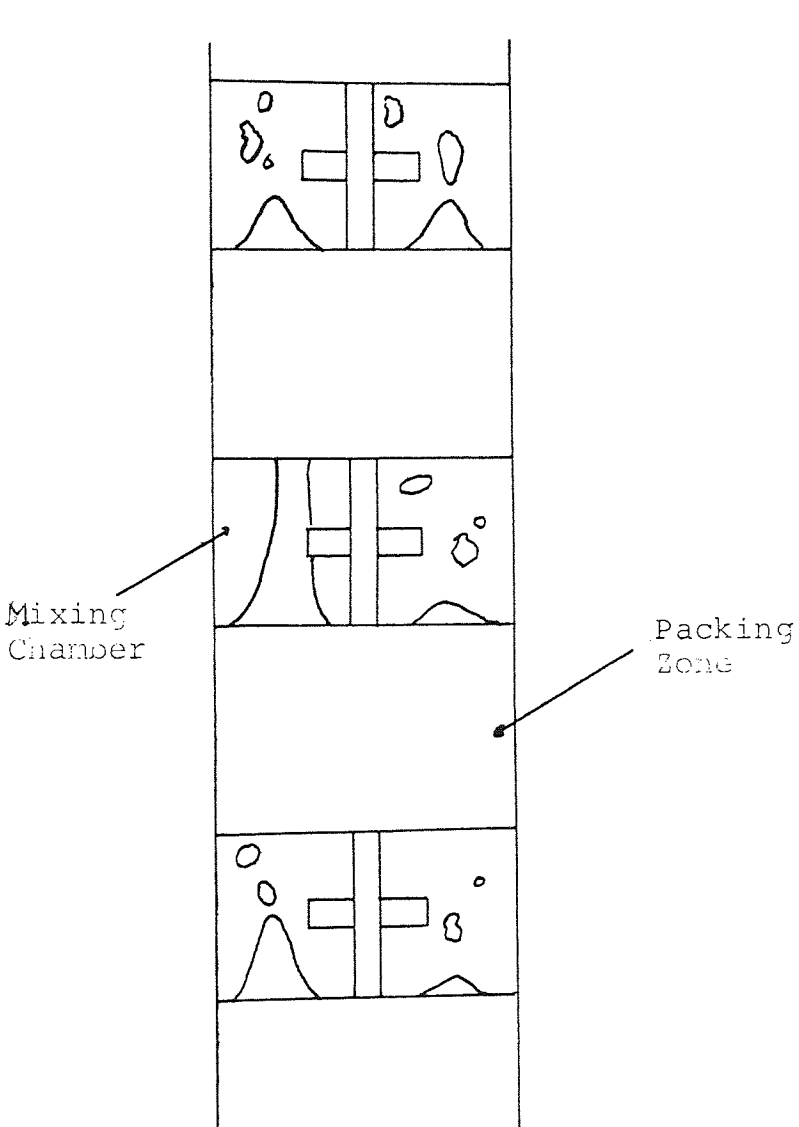

The limiting flow data for the packing wetted by the dispersed phase were found to be higher than the flow regime associated with the packing wetted by the continuous phase.

Piper's flooding point data were plotted using the coordinates $V_c^{\frac{1}{2}}$ and $V_d^{\frac{1}{2}}$ as in figure 3.6. In this case, the data, at different agitator speeds, could not be fitted by straight lines. This result is understandable since the behaviour of the dispersed phase inside the packing is completely different to that observed in conventional and/or non-wetted knitted mesh packing.

3.3 Mass Transfer

The very small amount of information presented in the literature during the last 30 years, regarding the performance of Sheibel columns, has been particularly concerned only with columns containing packing materials non-wetted by the dispersed phase.

Scheibel (16) in the first article describing this extractor, expressed the performance of the column in terms of overall stage efficiency. This efficiency was based on the assumption that a mixing section and a packing section together comprised one actual stage and the theoretical or equilibrium stages were calculated considering plug flow inside the column. Overall stage efficiencies as high as 115% were found in those runs associated with large packing section height and high agitator speed. This high efficiency

is due only to the additional amount of extraction taking place inside the packing due to the countercurrent flow of the phases.

The dependence of efficiency upon packing height and stirrer speed was discussed in this paper. The data indicated that an optimum packing height exists for each liquid system. When the liquids were emulsified readily, the efficiency was more dependent upon the packing height than in the case of a system in which the phase separated easily. In the first case the discrete state of the dispersed phase created in the mixing chambers, is maintained along the packing, while in the last case, significant drop-drop coalescence takes place inside the packing decreasing the mass transfer interfacial area and making any additional length in the packing non profitable. The height of the mixing section was reported to have no effect on the efficiency in the range investigated.

Years later Scheibel and Karr (17) published a further study on a 12 inch diameter column containing three stages and using wire mesh of 97.7% voidage as a packing material. Three liquid systems of very different physical properties were investigated under all methods of operation. Method of operation refers to which phase is dispersed and to the direction of transfer of the solute. The effects of combined flow rate, stirrer speed and packing height on overall stage efficiency were reported.

The overall stage efficiency in all cases, packings wetted and non-wetted by the dispersed phase, increased with agitator speed to a maximum value, then levelled off for a short interval. If flooding was not immediately encountered, a further increase in agitator speed produced a small drop in efficiency. The efficiency also increased with combined flow rate to a maximum then remained substantially constant until flooding.

The effect of packing height was found to be the same as reported for the 1 inch diameter column (16). It was concluded that the overall efficiency consisted of the sum of the efficiency of the mixing section and the additional mass transfer in the packing due to the counter current flow of the phases. These two effects were not determined independently.

The data also indicated that the column capacity is generally higher when the aqueous phase was dispersed, that is packings wetted by the dispersed phase. Also, the dispersion of the water in solvent generally required a higher agitator speed for the same efficiency. This is probably due to the fact that all column internals and walls are wetted by the dispersed water phase requiring then a high agitator speed to achieve a complete dispersion.

In order to separate the effect of the mixing section, Karr and Scheibel (1) continued the investigation with a column designed to eliminate the extraction in the packing as shown in figure 3.10. The area base overall mass transfer coefficients (Ka) in the mixing chamber and the Murphree

Figure 3.10 - Column Used to Determine the Efficiency of a Mixing Section

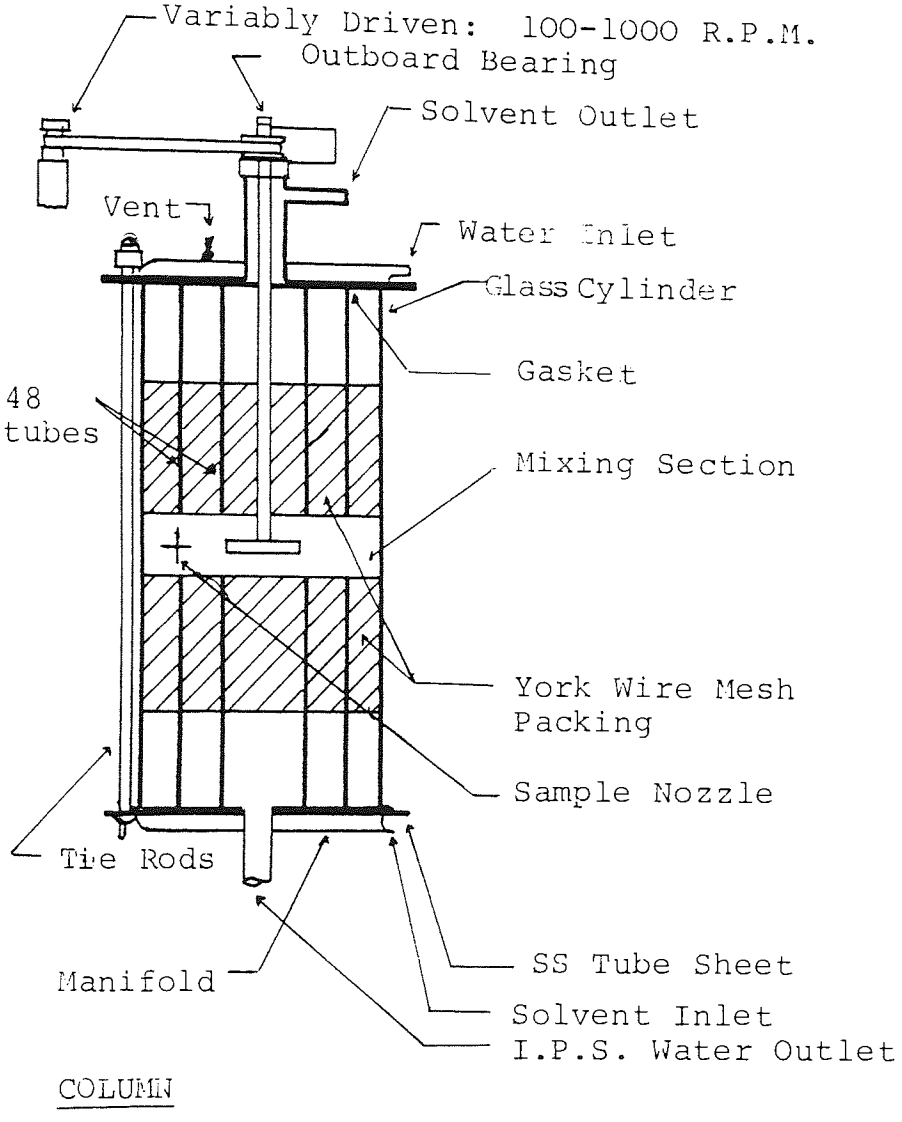

efficiency were calculated assuming perfect mixing in both continuous and dispersed phase. Stirrer speed, the flow rates of each phase and the concentrations of the solute in the feed were the variables studied. Two dimensionally similar columns were employed to test the effect of physical size.

Employing the difference in activity as the driving force for mass transfer, it was possible to develop correlations for the area base mass transfer coefficient for three liquid systems using grapical techniques.

The results indicated that the efficiency of the mixing chamber was independent of the flow rate of the continuous phase. This was attributed to the independence of the hold-up of the dispersed phase on the flow of the continuous phase. However, an increase in the flow rate of the dispersed phase decreased the efficiency of the mixing chamber, as shown in figure 3.11, for some methods of operation. When the system was operated as organic phase dispersed - organic phase extracted the efficiency was substantially constant throughout the entire range of flow rates studied, meaning a linear variation of the area base mass transfer coefficient, Ka, with the dispersed-phase flow rate. This phenomena was explained based on the rate of coalescence of the drop for the different methods of operation.

The effect of the stirrer speed on the Murphree efficiency of the mixing section is shown in figure 3.12 It can be noted that there is an appreciable efficiency at O rpm which is due to mass transfer at drop formation

Figure 3.12 - Murphree Efficiency vs Impeller Speed

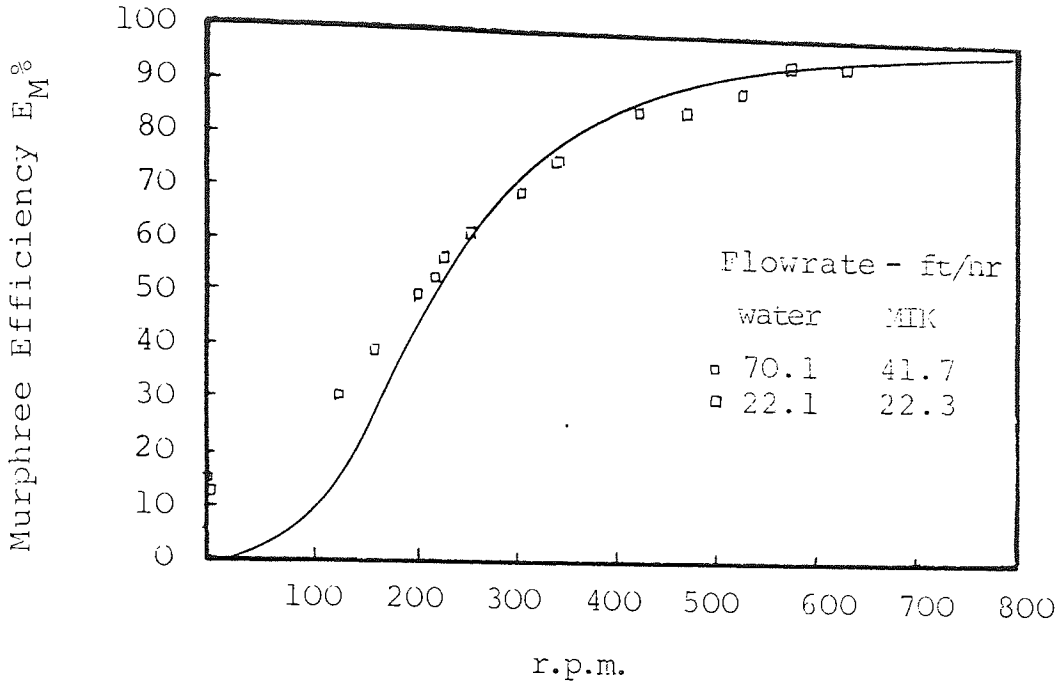

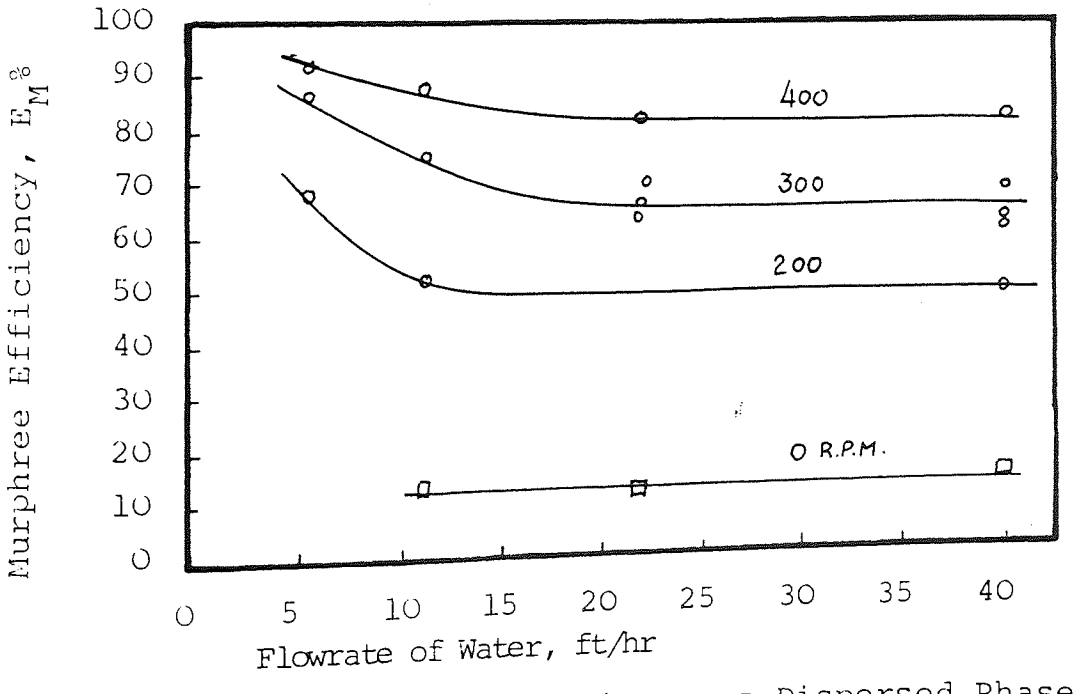

Figure 3.11 - Murphree Efficiency vs Dispersed Phase Flow Rate

at the entrance of the mixing chamber. Karr and Scheibel argue that the data at low agitation speed could not be included in the correlations, mainly because the basic assumption of completely mixed dispersed and continuous phase is invalid. Therefore, the theoretical correlations of Murphree efficiency or area base mass transfer coefficient, developed by these authors, were forced to approach zero and only the data for efficiencies above 50% were used.

Karr and Scheibel also noted that when the light organic phase was both dispersed and extractant, exceptionally high mass transfer coefficient (Ka) and hold-up were obtained compared with the other methods of operation. Visual observation also revealed that for the operation organic dispersed-extractant, the dropsizes were very much smaller, compared with the other cases. All these characteristics were attributed to a high resistance to coalescence of the drops in this type of operation.

The mass transfer direction, under organic phase dispersed operation, was such an important factor that two correlations were necessary depending upon the direction of transfer of the solute. A third correlation was required when the aqueous phase was dispersed. This was the result of a change in drop size and hold-up under this condition. The aqueous phase wet the internal parts of the column causing a much poorer dispersion. All the correlations developed by Karr and Scheibel are presented in Table 3.2.

Table 3.2 - Overall Mass Transfer Coefficient Correlations

Case	Area base mass transfer coefficient	Murphree Efficiencies
Organic phase dispersed-extractant	$\frac{K_a'}{V_D(\frac{\Delta\rho}{\sigma})^{1.5}} = 7.0 \times 10^{-6} N^{4.0}$ (3.5)	$\frac{E_{MD}}{100-E_{MD}} = 1.09 \times 10^{-7} \frac{H}{D_I} \frac{da'}{dC_D} (\frac{\Delta\rho}{\sigma})^{1.5} (ND_I)^{4.0}$ (3.6)
Organic phase dispersed-water extractant	$\frac{K_a'}{(\frac{\Delta\rho}{\sigma})^{1.5}} = 21.5 \times 10^{-6} N^{4.0}$ (3.7)	$\frac{E_{MD}}{100-E_{MD}} = 3.36 \times 10^{-7} \frac{H}{Y_D D_I} \frac{da'}{dC_D} (\frac{\Delta\rho}{\sigma})^{1.5} (ND_I)^{4.0}$ (3.8)
Water dispersed - organic extractant Water dispersed - organic extractant	$\frac{K_a'}{V_D(\frac{\Delta\rho}{\sigma})^{1.5}} = 3.34 \times 10^{-4} N^{3.0}$ (3.9)	$\frac{E_{MD}}{100-E_{MD}} = 7.9 \times 10^{-6} \frac{H}{D_I^{0.3}} \frac{da'}{dC_D} (\frac{\Delta\rho}{\sigma})^{1.5} (ND_I)^{3.0}$ (3.10)

Honekamp (21) measured the amount of extraction taking place in the packings of a 3 inch diameter 4-stage Scheibel column packed with 5 inch stainless steel knit mesh packings and operated with the continuous phase wetting the packings. Concentration profiles of both phases along the column were obtained by measuring the solute concentration of the one-phase samples withdrawn from inside the packings at both ends of each packing pad. From the concentration profile the average concentrations of the mixing sections were obtained and used in the correlations given by Karr and Scheibel, equation (3.6), to calculate the Murphree Efficiency and later the Number of Theoretical Stage (NTS) in each mixing chamber.

The performance of the column was expressed in terms of $(N.T.U._{OE})_M$ for the mixing sections and $(N.T.U._{OE})_P$ for the packing sections. Some of the procedures used to calculate these NTU's, produce performance data of questionable validity. For instance, the total overall Number of Transfer Unit, based on the extract phase $(NTU_{OE})_C$, from which the $(NTU_{OE})_P$ is obtained by substracting the $(NTU_{OE})_M$, is calculated by a graphical integration based on the product concentration. It is known that this procedure gives what it is called the Measured NTU which is lower than the true NTU due to the non-ideal flow conditions or axial mixing.

If one assumes that the calculated $(NTU_{OE})_M$ are the correct and true representation of the performance of the mixing sections, then the reported $(NTU_{OE})_P$ are lower than the true values and the error certainly varies with the column operating variables, especially the agitator speed.

Figure 3.13 shows the performance data plotted as the percent of mass transfer taking place in the packing vs agitator speed for different total flow rates. It is necessary to point out that the % mass transfer were calculated as follows;

$$\% \text{ mass transfer in packing} = \frac{(NTU_{OE})_P}{(NTU_{OE})_C} \times 100 =$$

$$\left(1 - \frac{(NTU_{OE})_M}{(NTU_{OE})_C}\right) \times 100$$

and the error discussed before applies here as well. The decrease in packing performance with increasing agitator speed was attributed to the increase in axial mixing created by the turbulence in the mixing chambers. No attempt was made in this work to estimate the parameters responsible for the axial mixing, nor the kinetic parameter characterizing the rate process.

Figure 3.13 - Effect of Impeller Speed on Mass Transfer in Packing Sections

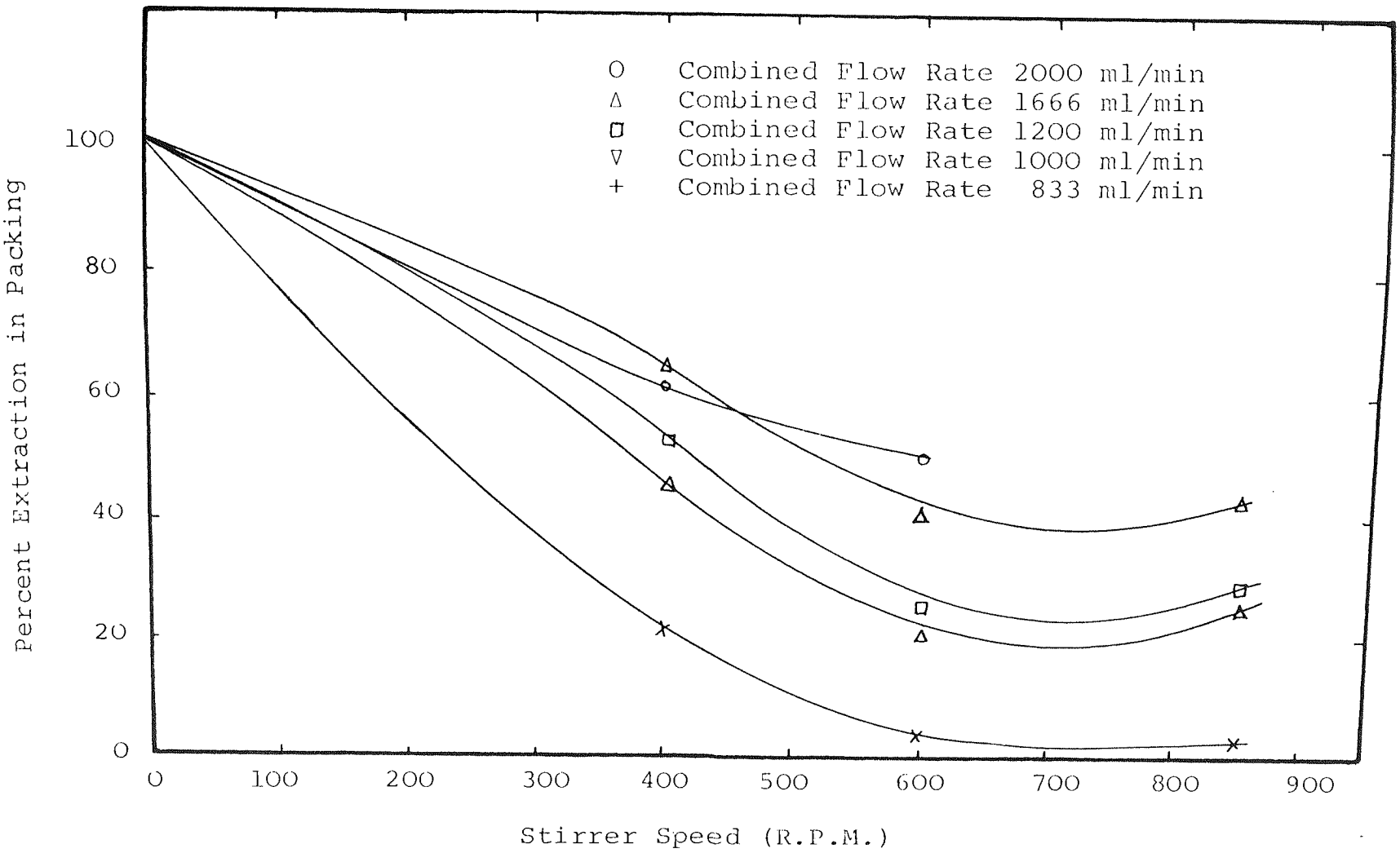

3.4 Conclusions

The very first conclusion with respect to the hydrodynamics and mass transfer characteristics of the Scheibel column is that the amount of research done is not enough so as to attempt a reliable design without a previous investigation of the problems at pilot plant scale.

The conclusions drawn by Honekamp (21) about the hydrodynamic behaviour and associated parameters of a continuous phase wetted packing Scheibel column was seriously questioned by the data reported by Jeffreys et al (24). More work is needed in order to develop equations that allow to estimate hold-up, drop size and non-ideal flow parameters as a function of column and internal dimension variables and operation variables.

A clear and very valuable conclusion of this review is the increased limiting flow obtained when the column is operated with packing material wetted by the dispersed phase as compared with non-wetted pads.

Karr and Scheibel's (1) investigation, whilst being the most important effort toward the correlation of mass transfer data, is limited to the analysis of an isolated mixing chamber. If the effect of packing is considered negligible, then the Karr and Scheibel correlations would be sufficient to allow a reliable column design. Unfortunately, Honekamp's (21) data indicate that 25 to 50% of the mass transfer in a Schiebel column takes place in the 5 inch non-wetted packing pads. Honekamp's prime goal, to complement

Karr and Scheibel's work by studying the behaviour and possible correlation of the mass transfer in the packing sections, did not reach completion since the complicating effect of axial mixing on packing performance could not be quantitatively isolated.

Finally, some authors had claimed that the Scheibel Column can be equally well represented by either continuous or discrete models, depending on the number of stages, as it is the case in the Oldshue-Rushton Column. Nevertheless, not a single work has been reported in the literature to substantiate that claim.

CHAPTER IV

THE DESIGN RATE EQUATION, RATE = K.a.ΔC.

A SURVEY

THE DESIGN RATE EQUATION, RATE = K.a.ΔC.

A SURVEY

In Chapter 2 it was shown that the design of any mechanically agitated extractor requires a knowledge of the parameters controlling the rate process. The rate of mass transfer between two immiscible liquids in an agitated system depends on the concentration difference ΔC, the specific interfacial area a, and the mass transfer coefficient K. These parameters are interrelated by means of the kinetic expression

$$\text{Rate} = K.a.\Delta C \qquad (4.1)$$

The literature review presented in this chapter covers the information available to date on these fundamental parameters, their experimental determination and correlations, which are essential for the optimized design and scale-up of agitated extractors.

4.1 Interfacial Area

The measurement of interfacial area in an operating liquid-liquid extractor is complicated by the fact that this area is composed of a large number of drops of varying size. Although exact measurements can not be made, there are several methods to obtain a good estimate of this area.

The chemical method of measuring interfacial area in liquid-liquid contactors introduced by Nanda and Sharma (27) is an absolute method which is very useful as a standard to check the accuracy of other techniques. It has been applied to packed columns (28) as well as to an RDC and Mixco Column (29) and it is based on the theory of mass transfer accompanied by fast-pseudo first order reactions. The basic equation

$$R_x = a\ A^*\ \sqrt{D_A\ k_2 B^o} \tag{4.2}$$

holds if the following conditions are fulfilled.

$$\frac{\sqrt{D_A\ k_2\ B^o}}{k_L{}^o} << \frac{B^o}{Z_s . A^*} \tag{4.3}$$

$$\frac{D_A\ k_2\ B^o}{(k_L{}^o)} > \sim 10 \text{ (condition of fast reaction)} \tag{4.4}$$

Equation (4.2) indicates that the rate of extraction per unit area of dispersion is a unique function of the physico-chemical properties of the system and independent of hydrodynamic factors. Then a determination of the rate of extraction R_x and a knowledge of the value $A^*\sqrt{D_A\ k_2\ B^o}$ should enable the value of the specific interfacial area a, and later the total interfacial area $\bar{A}$, to be calculated. The limitations of this method are:

1. very few chemical systems fulfil the conditions given by equations 4.3 and 4.4, i.e. the alkaline hydrolisis of formate ester;

2. no information regarding the distribution of drop sizes; only interfacial area and mean drop size can be obtained;

3. too time consuming.

The most popular optical technique employed for the measurement of interfacial area in dispersions is that of estimating the opacity of a dispersion to the transmission of light (30) (31). In principle it is based on Beer's Law

$$\frac{I_o}{I} = \beta A + \ell \qquad (4.5)$$

where I_o/I is the extinction ratio and A is the interfacial area. β is an empirical constant dependant on the ratio of the refractive index of the dispersed phase to that of the continuous phase. It is independent of the drop size distribution provided the particles are spherical or nearly so. This technique presents many limitations.

1. does not give information about drop size distribution,

2. the method usually requires a probe containing a light source and a photocell immersed in the dispersion inside the contactor, which can disturb the flow to a high degree,

3. it is best suited for systems with low hold-up, since at high hold-up and large optical path length, a correction must be made for the multiple reflections of the light as it traverses a dense swarm of drops,

4. the constant β must be determined experimentally, this requires calibration for each combination of dispersed continuous phase system and solute concentration. Normally the calibration procedure is based on photographic methods.

Measurement of interfacial areas by photography involves the determination of a suitable mean size of the dispersed phase drops (d) and of the hold-up ($\bar{\theta}_D$). The specific interfacial area is then calculated from the relations

$$a = 6 \frac{\bar{\theta}_D}{d} \qquad (4.6)$$

Experimentally, the technique is simple and no equipment is needed in the system. Compared to the other two methods above, it has the advantage that it also provides information on the drop-size distribution as well as on particle shapes if a suitable means for photographic analysis is available. However, the technique presents the following draw backs;

1. when photographs are taken through a transparent wall, they provide information on conditions near the wall, and these may or may not be representative of those over the entire cross section of the apparatus i.e., effect of the centrifugal force on high density dispersed phase drops in a mechanically agitated chamber,

2. care needs to be exercised in eliminating the distortions due to curvature of the vessel or column,

3. the analysis of photographs is time consuming.

The physical methods of light transmission and photography are the most appropriate when several chemical systems and a wide range of operation variables are going to be studied. The final selection between those two is based on the type of chemical systems and equipment used as well as on the nature and requirements of the research programme.

Equation 4.6 shows that the interfacial area between the dispersed phase and the continuous phase in a solvent extractor depends on ;

(a) the droplet size,

(b) the dispersed phase hold-up

Each of these will be discussed.

4.1.1 Droplet Phenomena

The sizes and the size distribution of droplets of a dispersed phase in a solvent extractor depends on the method of formation, the amount and nature of the interactions of the droplet with their neighbours as well as with the internals of the vessel, the physical properties of the chemical system, the mode of operation and the geometric arrangements of the vessel.

The dependance of the drop size on the method of formation; on whether the dispersed phase is discharged through some form of orifice or nozzle, or dispersed by mechancial agitation. The former is applicable to spray columns and sieve plate columns and can be further subdivided according to the nozzle velocity in

1. drop formation at subjetting nozzle velocities and

2. drop formation under jetting conditions.

However, in the most common types of extraction equipment the dispersion is normally formed by the high shear stress created by some form of mechanical agitator.

4.1.1.1 Drop Formation in a Turbulent Flow Field

In general, the dispersion of one fluid in another takes place in three stages. When the stirring process has just begun, large lumps of fluid are present at first. These large size lumps are then deformed into long ligaments that break up into drops. In a third stage, these drops may further be broken up by local viscous shearing or by dynamic pressure fluctuation (velocity difference) occurring in the turbulent flow field. This process continues until a dynamical equilibrium is reached between the forces generated in the turbulent continuous phase and the opposite forces of interfacial tension which attempt to retain the drop in its spherical shape. Using dimensional analysis an equilibrium or stable drop size correlation can be derived assuming that the drop

diameter depends upon the interfacial tension and the intensity of the turbulence. For a mechanical agitated vessel the overall turbulent intensity can be described as the rate of energy input per unit mass of fluid. The relation for drop diameter is

$$d = C_1 \sigma^a \left(\frac{P}{V}\right)^b \rho_c^c$$

and by dimensional analysis

$$d = C_1 \sigma^{3/5} \left(\frac{P}{V}\right)^{-2/5} \rho_c^{-1/5} \; ; \quad \text{or} \qquad (4.7)$$

$$d = C_1 \left(\frac{\sigma}{\rho_c}\right)^{0.6} (\epsilon)^{-0.4}$$

A similar result was obtained (32) by a quantitative analysis of the fluid mechanics around a drop in a highly turbulent continuous phase. The theory of local isotropy is qualitively closely related to the analysis leading to the formulation of equations 4.7. This theory, by putting the previous analysis on a more solid fundamental basis, had defined quite precisely the range of its applicability.

For completeness, and because most drop size correlations in agitated extractors are based to different extents, on the Kolmogoroff's theory of local isotropy, a presentation of the basic concepts of local isotropy will be given below.

Turbulent flow consists of unsteady, chaotic movements of parts of the fluid in different directions superimposed on the main flow. Such a movement of any element of fluid is extremely complicated and can only be described in terms of averages. The instantaneous velocity at any particular point in the i-direction is given by

$$U_i = \bar{U}_i \pm u_i \quad (i = 1,2,3) \tag{4.8}$$

where the overscore denotes the time average value and u_i is the instantaneous fluctuation velocity. The root mean square of this fluctuation velocity, denoted u_i', is a measure of the violence or intensity of the turbulence in the i-direction in a particular point in the system.

$$u_i' = \left[\overline{(u_i)^2}\right]^{\frac{1}{2}} \tag{4.9}$$

The turbulence is said to be <u>homogeneous</u> when it has quantitatively the same structure in all parts of the flow field, that is each fluctuation component, u_i', is independent of the position in space. The turbulence is called <u>isotropic</u> if its statistical properties have no preference for any directions, so that perfect disorder exists; that is all fluctuations components are equal. Then in the case of homogeneous isotropic turbulence

$$(u_a')_A = (u_i')_A = (u_b')_B = (u_j')_B = u' \; ; \quad \text{and}$$

$$\overline{(u_i)_A \, (u_j)_B} = 0 \quad \text{for } i \neq j$$

where A and B are any two points in the field of flow, $\underline{a}$ and $\underline{b}$ two given directions at the point A and B respectively and $\overline{(u_i)_A (u_j)_B}$ the double correlations between fluctuation velocity components.

In 1941, A.N. Kolmogoroff (33) stated his theory of homogeneous local isotropy by postulating that at sufficiently high Reynolds number, the turbulent motion in a sufficiently small domain G of any kind of turbulent field, of arbitrary mean-flow characteristics, is homogeneous, isotropic and statistically steady. This first postulate of the theory, is a direct consequence of the Kolmogoroff's conception that a turbulent flow may be thought of as consisting of pulsations or eddies ranging in scale from a dimension characteristic of the mean flow, to a lower limit at which the motion is entirely laminar. At high Reynolds numbers the mean flow due to instability to small disturbances, is superposed by a set of eddies which have characteristic dimensions and velocities one order lower than the corresponding quantities characteristic of the mean flow. This first order flow is in turn unstable and breaks up to form a set of pulsation or eddies with characteristic size and velocities one order lower than the first order flow. This process continues, the $(n+1)^{th}$ order eddies being formed by the break up of the n^{th} order eddies, until an order is reached at which the motion of these smallest eddies is laminar and further formation of eddies is no longer possible. This cascade of instability

may introduce a decoupling effect between the large and small scales motion. If the Reynolds number is sufficiently high (in theory infinite), it is likely that the motion of the smaller eddies (larger order) will be nearly independent of the directional bias and anisotropy of the large scale motion. In this case it is possible to define a domain G with spa tial dimensions such that the relative velocity between any two points of G is determined by motions which present isotropic behaviour.

Hinze (34) has shown that in an isotropic homogeneous turbulent region, the pressure fluctuation and the velocity fluctuations at two neighbouring points with spatial distance r small, are related by the equation

$$\overline{(P_A - P_B)^2} = \rho^2 \left[\overline{(u_A - u_B)^2}\right]^2 \qquad (4.10)$$

We can define a relative velocity at point A with respect to a reference velocity at point B in the i-direction by

$$w_i^A(\xi) = (u_i)_A - (u_i)_B \qquad (i = 1,2,3)$$

where $\xi = \vec{AB}$ is the interval vector of magnitude r with components ξ_i. The formal analogy between local isotropy and ordinary isotropy allows us to calculate the double correlation between the various components of the relative velocity vector by the expression (35)

$$\overline{w_i^A\, w_j^A} = \overline{((u_i)_A - (u_i)_B)((u_j)_A - (u_j)_B)} =$$

$$= \frac{\xi_i\ \xi_j}{r^2}\left[B_{dd}(r) - B_{nn}(r)\right] + \delta_{ij}\, B_{nn}(r)$$

$$= \frac{\xi_i\ \xi_j}{r^2}\left[-\frac{r}{2}\frac{\partial B_{dd}}{\partial r}\right] + \delta_{ij}\left[B_{dd}(r) + \frac{r}{2}\frac{\partial B_{dd}}{\partial r}\right] \qquad (4.11)$$

where δ_{ij} is the Kronecker delta, $B_{dd}(r)$ and $B_{nn}(r)$ are scalar functions of r^2 defined by

$$B_{dd} = \overline{(u_d)_A - (u_d)_B)^2}, \quad \overline{B_{nn} = ((u_n)_A - (u_n)_B)^2} \qquad (4.12)$$

and the suffixed d and n denote components parallel and perpendicular to $\vec{AB}$ respectively.

Equation 4.12 and 4.10 show that if the correlation coefficients B_{nn} and B_{dd} are known, the difference in dynamic pressure at different points is immediately known. In order to derive an expression to calculate the correlation coefficient it is necessary now to complete the physical background to the notion of local isotropy by considering the distribution of the input energy among the different orders of eddies.

In the foregoing we have spoken about turbulent motion, which can be assumed to consist of the superposition of n order pulsations or eddies. Each order can be identified by a characteristic length, velocity, frequency (ratio of the characteristic velocity to length) and it is possible on the average to allocate a certain amount of the

total kinetic energy to a distinct frequency. Such distribution of energy between the orders is usually called an energy spectrum.

The energy supply for the entire motion lies chiefly in the mean flow and the lower order eddies. The nth order eddies absorb some energy from the (n-1)th order eddies and pass it on partly to the (n+1)th order eddies by means of work done to form the next size smaller eddies and partly to the internal energy of the fluid through viscous dissipation. It can be predicted that the ratio of the energy dissipated by viscosity to energy passed on to the next highest order of pulsations or eddies, for any given set of eddies, decreases as the Reynolds number increases. This means that progression to eddies of higher order (smaller characteristic length) and low characteristic Reynolds number, the proportion of energy dissipated by viscosity will increase and for the very smallest eddies the motion is entirely laminar.

In the limiting case of infinite flow Reynolds number, the larger set of eddies contained within the small domain G will pass on to their neighbours (in the direction of decreasing size) an amount of energy in unit time equal to the amount that they receive. This amount of energy must be equal to the energy dissipation, since it is a one-way flow, being the only outlet the viscous dissipation due to the smallest eddies. Then, the motion due to the larger eddies within G is independent of ν and should therefore be determined statistically by the single quantity ϵ which

measures the average total energy dissipation per unit mass of the fluid.

The motion of the smaller sets of eddies within G will not be determined uniquely by ϵ, since these eddies have finite characteristic Reynolds number and therefore dissipate a finite amount of the energy they receive from their larger neighbours. The proportion of energy dissipated will depend on the characteristic Reynolds number of the order of pulsations or eddies concerned, this proportion being unity when the characteristic Reynolds number is low enough for the motion to be entirely laminar.

The whole picture of a turbulent motion is now complete. This physical background was quantitatively summarized by two similarity hypotheses put forward by Kolmogoroff.

(a) Kolmogoroff's first hypothesis: "At sufficiently high Reynolds numbers there is a range of high frequency where the turbulence is statistically in equilibrium and uniquely determined by the parameter ϵ and ν. The state of equilibrium is universal".

Kolmogoroff characterized this equilibrium range with a length scale and a velocity scale both only function of ν and ϵ. From dimensional reasoning

(4.13)

$$\eta = \left(\frac{\nu^3}{\epsilon}\right)^{\frac{1}{4}} \quad \text{length scale}$$

$$v = (\nu\epsilon)^{\frac{1}{4}} \quad \text{velocity scale}$$

Thus the dimensions of the length scale η and velocity scale v' are such that the Reynolds number with reference to this length and velocity is

$$\frac{v'.\eta}{\nu} = 1$$

Evidently, η and v' are a measure of the characteristic length and velocity of the smallest eddies respectively and they mark the region of strong viscous effects, where the inertial forces are of the same magnitude as the viscous shear forces.

Since the first hypothesis requires that all correlation functions, i.e. equation 4.11 must be determined uniquely by ϵ and ν or η and v' and the relevant geometrical parameters, the correlation coefficients B_{dd} defined by equation 4.12 has to have the form (35)

$$B_{dd}(r) = v'^2 . \beta_{dd}\left(\frac{r}{\eta}\right) = (\nu\epsilon)^{\frac{1}{2}} . \beta_{dd}\left(\frac{r}{\eta}\right) \qquad (4.14)$$

where β_{dd} is a universal function.

The mean energy dissipation in locally isotropic turbulence is given by (35)

$$\epsilon = \frac{15}{2}\,\nu\left(\frac{\partial^2 B_{dd}}{\partial r^2}\right)_{r=0} \qquad (4.15)$$

The function $B_{dd}(r)$ is an even function of r taking the value zero at r = 0, then its series expansion must start with the term r^2 and the following expression is valid

$$B_{dd}(r) \simeq \frac{r^2}{2!} \left(\frac{\partial^2 B_{dd}}{\partial r^2}\right)_{r=0} \tag{4.16}$$

By combining equation 4.14 equation 4.15 and equation 4.16 the following expression results

$$B_{dd}(r) \alpha (\nu\epsilon)^{\frac{1}{2}} \left(\frac{r}{\eta}\right)^2 = \frac{\epsilon}{\nu} r^2 \tag{4.17}$$

for $\frac{r}{\eta} << 1$

being $\beta_{dd}(\frac{r}{\eta}) = c(\frac{r}{\eta})^2$

This equation allows to relate the pressure difference between any two points within the domain G for the spatial distance $r < \eta$ with measurable quantities characteristic of the turbulence.

(b) Kolmogoroff's second hypothesis: "If the Reynolds number is infinitely large and if the spatial separation $\underline{r}$ between any two points is large in magnitude compared with η (but still small enough for the points to lie within the domain G), the energy spectrum in this subrange is independent of ν, and is solely determined by one parameter ϵ".

Since in this subrange the inertial transfer of energy is the dominating factor, this is called the inertial subrange.

The second hypothesis thus requires the universal function β_{dd} to have such a form for $r > \eta$ that the corresponding scalar correlation B_{dd} is independent of ν. This condition is satisfying when

$$\beta_{dd}\left(\frac{r}{\eta}\right) = c\left(\frac{r}{\eta}\right)^{2/3} \tag{4.18}$$

where c is an absolute constant. In this case

$$B_{dd}(r) = (\nu\epsilon)^{1/2} . c\left(\frac{r}{\eta}\right)^{2/3}$$

$$B_{dd}(r) \alpha (\epsilon r)^{2/3} * \tag{4.19}$$

for $Le >> r >> \eta$

where Le is the characteristic length of the large and medium size eddies for which isotropic turbulence does not exist. This parameter is called the integral scale of turbulence and it represents approximately the upper limit of the frequencies including the domain G since the

---

* Other authors, like Hinze, had used a shorter approach, but conceptually the same as the one presented here. The link between both approaches lies in the fact that the velocity v_λ of the turbulence eddies of characteristich length λ has an order of mag nitude equal to the change in the average velocity over distances equal in order of magnitude to the scale of the turbulence eddies λ (36)

$$v^2_{\lambda=r} \approx \left[\beta_{dd}(\lambda=r)\right]$$

postulates of local iostropy become invalid when r is of order Le.

It was mentioned at the beginning of this section that it is generally accepted that the fluctuation pressures or pressure difference at two points within a turbulent continuous phase determine the final spectrum of drop sizes. Different dynamic pressures exerted at different points on the surface of the drop will lead, under certain conditions, to deformation and breakup of the drop.

Consider a small volume of fluid in which turbulence is locally isotropic. Within this volume the differences in dynamic pressure are given by combining equations (4.19), (4.17), (4.12) and (4.10)

$$\Delta p \propto \rho_c \left(\frac{\epsilon}{\nu_c}\right) r^2 \qquad r \ll \eta \tag{4.20}$$

$$\Delta p \propto \rho_c (\epsilon r)^{2/3} \qquad Le \gg r \gg \eta \tag{4.21}$$

Assuming that the density and viscosity of the drops inside the volume are of the same order of magnitude as the surrounding fluid, the forces attempting to breakup the drops, given by equations 4.20 and 4.21 will be opposed only by the surface force given by

$$\Delta P_s = \frac{2\sigma}{r_{sd}} . \tag{4.22}$$

where r_{sd} is the radius of the drop. If the density of both phases are very different, in which case the drops of

the dispersed phase do not follow the direction and velocity of the turbulence fluctuations of the continuous phase, the drag exerted by the continuous phase sets the liquid inside the drop into motion. This motion, being rotational or turbulent in nature, creates a dynamic pressure within the drop, directed outward from inside the drop which adds on to the surface force. If in addition, the viscocity of the dispersed phase is high, viscous force within the drop prevents the drop deformations. When these three forces are considered, the complexity is very great and then it is convenient to assume the same order of magnitude for the density and viscosity of both phases.

Inside the small isotropic volume of fluid let us consider a drop of diameter d such as that

$$Le >> d >> \eta$$

If this drop is going to be stable, the surface force must be equal to the external inertial force. Then equating equations 4.21 and 4.22 an expression is obtained which allows to estimate the stable maximum drop diameter within the local isotropic turbulent flow from easily measurable quantities and properties of the system.

$$\rho_c \epsilon^{2/3} d_{sd}^{2/3} = K_1 \frac{4\sigma}{d_{sd}}$$

$$d_{sd} = K_1 \left(\frac{\sigma}{\rho_c}\right)^{3/5} \left(\frac{1}{\epsilon}\right)^{2/5} \qquad (4.23)$$

$$Le >> d_{SD} >> \eta$$

Equation 4.23 was first derived by Kolmogoroff (37) and independently by Hinze (32). It is necessary to indic that in the development of equation 4.23 only the differe in dynamic pressures at points separated from each other by a distance $\underline{d}$, was considered to be responsible for the fragmentation of a drop of diameter $\underline{d}$. This is explained by the fact that velocity differences due to fluctuations with a wavelength equal to $\underline{d}$ will produce a higher dynamic pressure than tho-se due to fluctuations with a shorter wave length. The kinetic energy of a turbulent fluctuatio increases with increasing wave length or eddies character- istic length.

For the change in flow velocity within the zone $<< \eta$ Kolmogoroff derived the expression for the drop diameter in a similar way than for the inertial subrange case It has the form

$$d_{SD} = K_2 \left(\frac{\sigma_{\nu c}}{\rho_c}\right)^{1/3} \left(\frac{1}{\epsilon}\right)^{1/3} \qquad (4.24)$$

$$d_{SD} << \eta$$

Levich (36) has questioned the validity of equation 4. based on the consideration that in the zone of scales below Kolmogoroff's micro scale of turbulence η the motion occurs at Reynolds numbers less than one. At this low Reynolds number, the local flow velocity past a drop becomes regular and no fragmentation of the drop occurs. Furthermore, equation4.24 can be rearranged to the following form

$$d_{SD} = \left(\frac{\sigma \eta}{K_2 \nu_c^2 \rho_c}\right)^{1/3} \eta \qquad d << \eta \qquad (4.25)$$

which requires that

$$\eta < \frac{K_2 \nu_c^2 \rho_c}{\sigma} = \frac{K_2 \mu_c^2}{\sigma \rho_c}$$

If typical values for ρ_c, μ_c and σ ($\sigma \geq 20$ mN - m^{-1}) for oil in water systems are substituted in the inequality, then $\eta < 10^{-6}$ metres which is a quite unrealistic value.

An expression to estimate minimum drop size has been given by Levich. Considering small local Reynolds number of the order of magnitude 5-10 and accepting that the external force to the drop responsible for deformation and fragmentation is chiefly of the viscous nature the following equality can be set

$$\mu_c \left(\frac{v}{d_{min}}\right) = K \frac{4\sigma}{d_{min}}$$

of

$$\mu_c \, Re \, \frac{\nu}{d_{min}^2} = K \frac{4\sigma}{d_{min}}$$

where

$$Re = \frac{v d_{min}}{\nu} \simeq 5 \longleftrightarrow 10$$

$$d_{min} = K_3 \frac{\rho_c \nu_c^2}{\sigma} \qquad (4.26)$$

Other equations (30) have been reported in the literature which cover the region between the inertial subrange and the viscous region.

4.1.1.2 Coalescence of Drops in a Turbulent Flow Field

The preceeding section showed that turbulent fluctuations and some times viscous friction produce forces that tend to break-up the droplets, whereas collision between two drops may result in their coalescence into a larger drop. In practice, the size distribution of droplets in an agitated dispersion is determined by both break-up and coalescence occuring simultaneously and if the dispersion remains in a quasi-stationary flow field for a sufficient duration a dynamical equilibrium between both processes is established.

Interdrop coalescence, as well as drop-liquid or solid interface coalescence, occurs in two basic stages;

1. Drainage of the continuous phase from between the dispersed elements until a critical film thickness is attained.

2. Rupture of this film.

The factors most affecting drainage and film rupture, and which hence control the speed of coalescence are summarised in Table 4.1.

Table 4.1

Number	Variable (increasing)	Effect on coalescence time	Explanation in terms of effect on phase-2 film drainage rate
1	Drop size	Longer	More phase-2 in film
2	Length of fall	Longer	Drop 'bounces' and film is replaced
3	Curvature of interface towards drop (a) Concave (b) Convex	Longer Shorter	More phase-2 in film Less phase-2 in film
4	Interfacial tension	Shorter	Less phase-2 in film (more rigid drop)
5	Phase μ ratio $(\frac{\mu \text{ drop}}{\mu \text{ continuous}})$	Shorter	Either less phase-2 film or increase in drainage rate
6	Phase $\Delta\rho$	Longer	More deformation of drop more phase-2 film
7	Temperature	Shorter	Increases phase μ ratio
8	Temperature gradients	Shorter	Thermal gradients 'weaken' film
9	Vibrational effects	Shorter	Assist drainage rupture
10	Electrostatic effects	Shorter	Increase effective gravitational force
11	Applied electric field	Shorter	Increases effective gravitational force

Continued/...

Table 4.1 (continued)

Number	Variable (increasing)	Effect on coalescence time	Explanation in terms of effect on phase-2 film drainage rate
12	Presence of a third component		
	(a) stabiliser	Longer	(a) Forms 'skin' around drop
	(b) mass transfer in drop	Longer	(b) Sets up interfacial tension gradients which oppose flow of film
	(c) mass transfer out of drop	Shorter	(c) Sets up interfacial tension gradients which assist flow

The study of the influence of a turbulent flow field on the extent of droplet coalescence has had different theoretical approaches. Shinnar (38) attacked the problem in a similar way to the theoretical analysis of drop break-up, that is considering a balance between all the forces affecting the coalescence process, while Howard (39) and Misek (40)) based their theoretical approaches on the theory of coagulation of colloid system in order to derive expressions of the frequency of coalescence.

It is apparent that a high turbulence will increase the frequency with which drops collide and hence increased the probability of coalescence. Shinnar (38) considered that two drops are unlikely to coalesce immediately on collision, but that they may cohere together and be prevented from coalescing by a film of the continuous phase liquid trapped between them. He assumed the cohesion of the drops to be due to attractive forces. The film separating the cohering drops will gradually decrease due to diffusion until it collapses and coalescence follows. However, during the drainage process turbulent velocity fluctuations may communicate sufficient energy to the droplet pair to cause re-separation and should this occur to every cohering pair the dispersion is stabilized against coalescence. The cohesive forces are dependent on drop diameter and there is a minimum size of drops which can be separated at a given intensity of turbulence. The droplet diameter d_{min}, for which the energy due to turbulent velocity fluctuations

is equal to the energy of adhesion can be estimated as follows.

Shinnar showed that the force of adhesion between two drops having diameters d_1 and d_2 is

$$F(h_o) = \frac{\pi\, d_1\, d_2}{d_1 + d_2} \int_{h_o}^{\infty} f(h)dh \qquad (4.27)$$

where h_o is the minimum distance between two drops, i.e. critical film thickness, and f(h) is the force of attraction per unit area between two infinite parallel surfaces separated by a distance h. The energy of adhesion E_a is obtained from the above equation as

$$E_a = \int_{h_o}^{\infty} F(h)dh' = \pi \int_{h_o}^{\infty} \int_{h}^{\infty} \frac{d_1\, d_2}{d_1 + d_2} f(h)dhdh'$$

$$= 2\, \frac{d_1\, d_2}{d_1 + d_2} A(ho) \qquad (4.28)$$

where

$$A(h_o) = \frac{1}{2}\, \pi \int_{h_o}^{\infty} \int_{h}^{\infty} f(h)dhdh' \qquad (4.29)$$

is the energy of adhesion of two drops of unit diameter separated by the minimum distance h_o. Shinnar assumed that the dispersion is a monodisperse system in which case

$$E_a = A(h_o)d \qquad (4.30)$$

Furthermore, he assumed the turbulent flow to have the properties of homogeneity and local isotropy. Under these conditions the kinetic energy of two droplets of diameter d in movement relative to each other is given by

$$\text{Kinetic Energy} = C_1 \rho . (\epsilon d)^{2/3} . d^3 \qquad (4.31)$$

$$Le >> d >> \eta$$

In order to prevent coalescence, the kinetic energy (equation 4.31) must be greater than the energy of adhesion (equation 4.30). The drop diameter for which separation is possible in a given fluid under a specific turbulent field flow is given by

$$\frac{C_1 \rho \epsilon^{2/3} d_{min}^{8/3}}{A(h_o)} = \text{constant} \qquad (4.32)$$

No information is given by Shinnar concerning the estimation of $A(h_o)$ and h_o from the properties of the dispersion. If (h_o/d) is small then $A(h_o)$ and h_o are constant and independent of drop diameter. Also, $A(h_o)$ is constant for different dispersions of a given system.

In figure 4.1 the maximum stable drop diameter (equation 4.23) as determined by the process of break-up; and the minimum stable drop diameter (equation 4.32) as determined by the process of coalescence are plotted against the energy dissipation per unit mass, ϵ. The plot reveals the existence of a critical agitator speed below which coalescence will not occur but above which it may be rapid. The value of ϵ at which these equations intersect

Figure 4.1 - Turbulence Stabilized Dispersion.
Logarithmic Plot

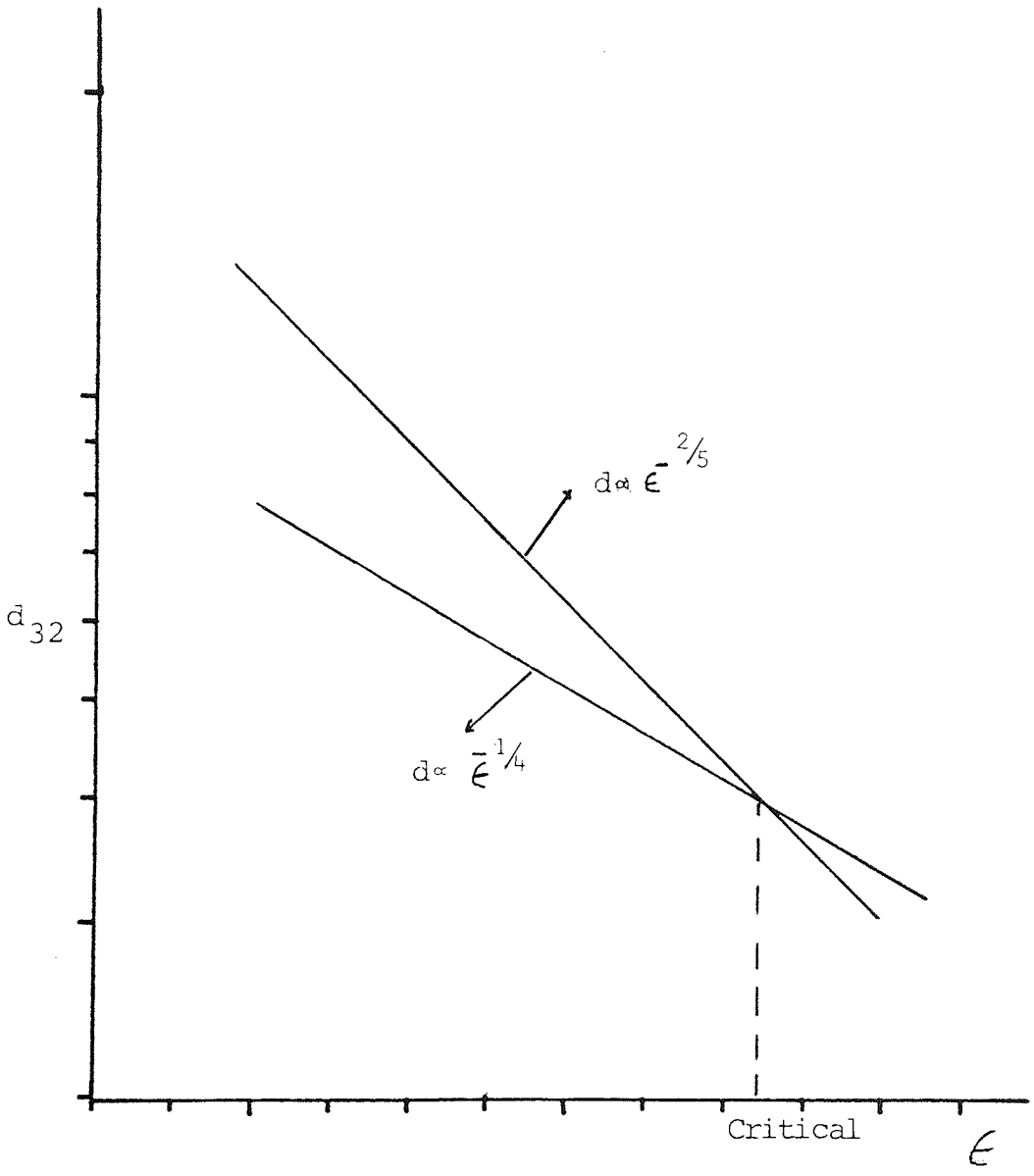

depends on the physical properties of the system. The existence of a critical value of ϵ has been confirmed experimentally. This substantiates the fact that dispersions can be prepared in which no breaking or coalescence occurs by maintaining ϵ constant.

The validity of this theory depends upon the existence of a force of attraction, the nature of which Shinnar did not discuss, strong enough to cause drainage of the film separating two drops in a reasonably short time. The forces referred to by Shinnar are presumibly the forces of molecular attraction, which give rise to the phenomenon of aggregation of colloidal-sized particles and interfacial tension between immiscible fluids. However, such forces are known to be of very short range, and being considerably attenuated over the thickness of the film of continuous-phase liquid separating droplet pairs, would be unlikely to provide a cohesive force of any significance in relation to other forces to which drops in a turbulent suspension are subject. It is therefore unlikely that drainage of the film would proceed to any appreciable extent before cohering drops are separated and the probability of their ultimate coalesence is small. In addition, in the theory proposed by Shinnar, no account is taken of the possibility that a significant fraction of collision may result in immediate coalescence and that the extent of coalescence is a function of drop concentration (hold-up) since the number of drops colliding per unit time increases with dispersed phase hold-up.

The theoretical approach adopted by Howarth (39) and, independently, by Misek (40) avoids the fundamental objections made to the theory of Shinnar. Both authors share the same theoretical base, namely the theory of the coagulation of spherical colloid-sized particles given by Smoluchowski (41). The frequency of collision, arising from thermal agitation of a colloid system, per unit volume, w_c, for uniform spherical particles is given by (42)

$$w_c = 4\pi n_o^2 d_c D_{turb} \qquad (4.33)$$

where D_{turb} is the coefficient of turbulent diffusion of the particles which cohere when their centres approach to a distance d_c (collision diameter) apart. This coefficient characterised the eddy motion of particles and basically the problem of coagulation of colloid particles transported by turbulent eddies is then reduced to a diffusion problem.

It is necessary to express the coefficient of turbulent dispersion D_{turb} in terms of known properties of the flow. Under certain restrictive assumption such as,

(a) Turbulence is homogeneous and isotropic and infinite in extent

(b) The particles are small compared to the smallest wavelength present in the turbulence ($d < \eta$)

(c) The turbulence is not affected by the presence of the particles

(d) Identical particle and fluid densities, which warrant that the particles follow the direction and velocity of the turbulent fluctuations.

Levich (36) gave the following expression

$$D_{turb} \sim \overline{v}_{\lambda} . \lambda$$

and since

$$\overline{v}_{\lambda} \sim \frac{\overline{v}}{\eta} . \lambda \qquad \text{for } \lambda < \eta$$

$$D_{turb} \quad (\frac{\nu \epsilon}{\nu^3/\epsilon})^{\frac{1}{4}} . \lambda^2$$

$$D_{turb} = K . (\frac{\epsilon}{\nu})^{\frac{1}{2}} . \lambda^2 \qquad (4.34)$$

$$\lambda < \eta$$

Furthermore, the energy dissipated per unit mass ϵ can be expressed in terms of the fluid flow velocity $\overline{v}_{Le}$ (characteristic velocity of the largest eddies) and in terms of the scale Le (integral scale of turbulence) of large-scale motions. Using equation (4.19) and the approximation $\overline{v}^2_{\lambda=r} \approx B_{dd}$ $(\lambda=r)$ the following expression is obtained

$$D_{turb} = K(\frac{\overline{v}_{L_e}^3}{L_e \nu})^{\frac{1}{2}} . \lambda^2 \qquad (4.35)$$

Since $d_e \approx \lambda \approx d$ (particle diameter) substitution of equation (4.35) into equation (4.33) gives

$$w_c = K\, n_o^2\, d^3 \frac{\left(\sqrt{L_e}\right)^{3/2}}{\sqrt{\nu L_e}} \qquad (4.36)$$

Strictly speaking, equation 4.36 applies to microdisperse systems, such as emulsions and aerosols, nevertheless, Misek (43) used it to estimate the drop collision frequency by making Le and d equal to column diameter and drop diameter respectively.

Assuming that equation (4.36) can be approximately applied to drop collisions in coarse dispersions, the next step is to determine an expression for the fraction of collisions resulting in coalescence. For the sake of simplicity it can be assumed that every collision leads to a combination of the colliding drops.

In order to determine the effect of coalescence frequencies in the drop size the following procedure was adopted by several authors (44) (45). First, only binary coalescence is accounted for and second the diameter of particles combining at each collision corresponds to the mean diameter after the preceding collision, as shown in figure 4.2.

The following equations are easily derived from the pattern shown in figure 4.2.

$$\left[n_o - (M+1)\right]\bar{d}_{m+1}^3 = d_{m+1}^3 + \left[n_o - (M+1) - 1\right]\bar{d}_m^3 \qquad (4.37)$$

Figure 4.2 - Simplified Coalescence Pattern

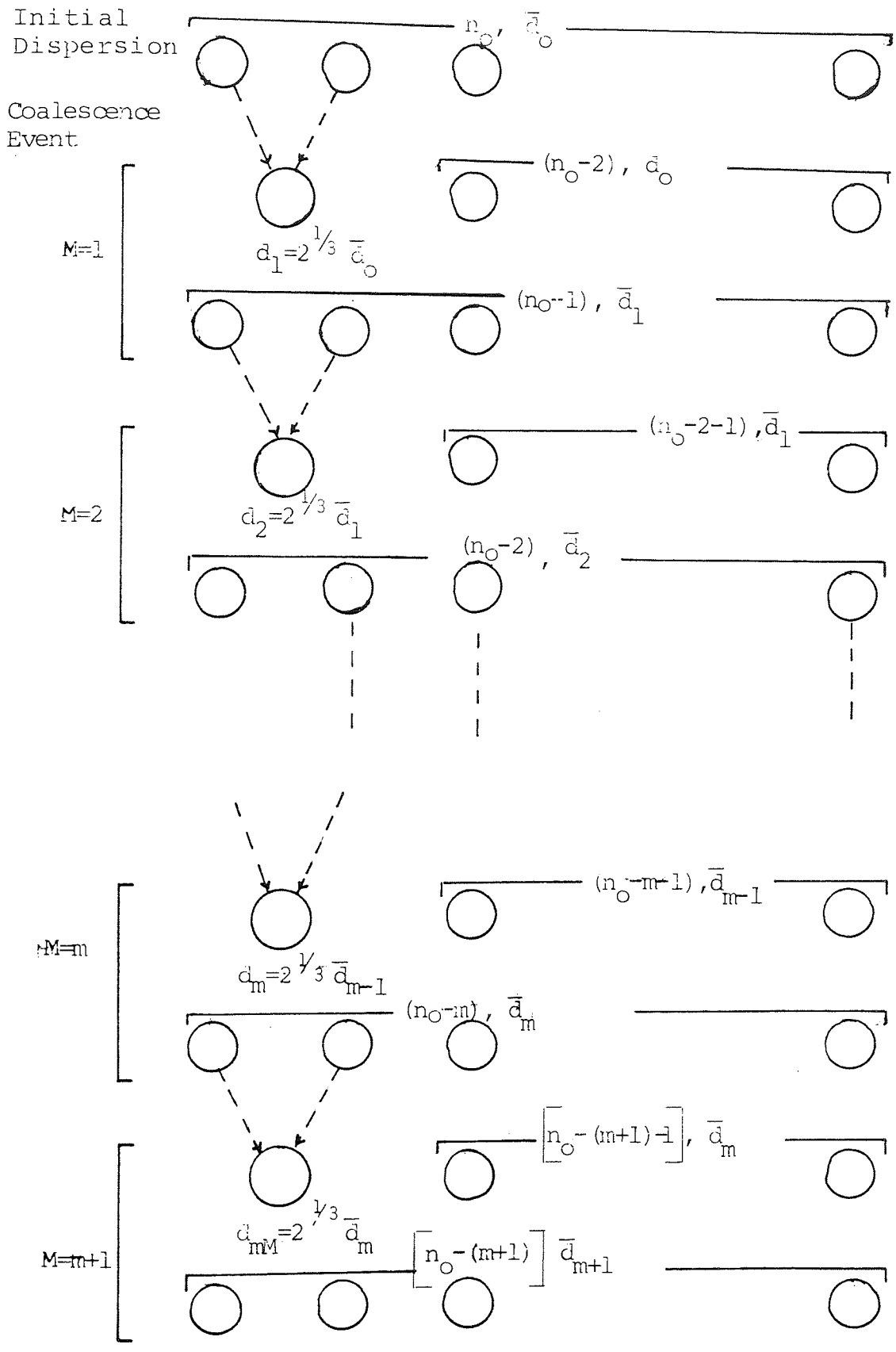

$$d_{m+1}^3 = \frac{2(n_o-(M+1))}{(n_o-(M+1)+1)} \bar{d}_{m+1}^3 \qquad (4.38)$$

Substituting equation (4.38) in equation (4.37), the following difference equation in $\bar{d}$ is obtained

$$\bar{d}_{m+1} - \bar{d}_m = \bar{d}_m \left[\left(1 + \frac{1}{n_o\left(1 - \frac{M+1}{n_o}\right)}\right)^{1/3} - 1 \right] \qquad (4.39)$$

Expanding the expression within the bracket on the right hand side and neglecting powers greater than one;

$$\Delta\bar{d}_m \simeq \bar{d}_m \left[\frac{1}{3n_o\left(1 - \frac{M+1}{n_o}\right)} \right] \qquad (4.40)$$

The frequency of coalescence is introduced now in the following manner

$$\frac{M+1}{n_o} = \frac{w_c t}{n_o} = Q \simeq \frac{M}{n_o} \qquad (4.41)$$

where t is the time during which coalescence of drops occur and Q the relative number of collisions or coalescence events. Substituting equation (4.41) in (4.40)

$$\Delta\bar{d}_m \simeq \bar{d}_m \left(\frac{1}{3\ (1-Q)}\right) \frac{\Delta M}{n_o} = \bar{d}_m \left(\frac{1}{3\ (1-Q)}\right) \Delta Q \qquad (4.42)$$

where $\Delta M = 1$. This difference equation may be reduced to a differential equation by taking the limits and considering that since the number of droplets present in the system is large, the change of their size may be considered as a continuous function of the number of

collisions

$$\frac{d(\bar{d}_m)}{\bar{d}_m} = \frac{dQ}{3\ (1-Q)} \tag{4.43}$$

Integrating this equation with the boundary conditions

$$t = 0 \qquad Q = 0 \qquad \bar{d}_m = d_o$$

$$t = t \qquad Q = Q \qquad \bar{d}_m = d$$

gives

$$\ln \frac{\bar{d}}{\bar{d}_o} = -\frac{1}{3} \ln\ (1 - Q) \tag{4.44}$$

Expanding the right-hand side of the equation (4.44) and neglecting powers greater than 1

$$\ln \frac{\bar{d}}{\bar{d}_o} \simeq k\ Q \tag{4.45}$$

It is important to note that the initial drop concentration n_o, is considered to be very large, in which case the M coalescence events do not affect it significantly and it can be considered constant during the integration step.

Substituting equations (4.36) and (4.41) into equation (4.45) and noting that $n_o d^3$ is proportional to the dispersed phase hold-up, Θ_D, the following relation is obtained

$$\ln \frac{\bar{d}}{\bar{d}_o} \simeq k \frac{(\nu_{Le})^{3/2}}{\sqrt{\nu_{Le}}} t.\Theta_D \tag{4.46}$$

It is necessary to express ν_{Le}, L_e and t in terms of the properties of the system, the geometric characteristic of the equipment and measurable variables that characterise the turbulent flow field. No rules or fundamental reasoning exist as to guide the process which hopefully will produce general expressions. Practical experience on the effect of different operational and geometrical variables on the rate and extent of coalescence is the only guideline available. Misek (43) verified experimentally equation (4.46) in different types of agitated columns adopting the following expressions for ν_{Le}, L_e and t,

$$\nu_{Le} = k_2 \left(\frac{\sigma}{d_o \rho}\right)^{0.5} \tag{4.47}$$

$$t = k_3 \frac{D_c}{\nu_{Le}} \tag{4.48}$$

$$L_e = D_c \tag{4.49}$$

Equation (4.47) is the resulting force balance between the dynamic pressure and the surface force, responsible for the drop break-up process. The validity of the assumption represented by equation (4.49) is doubtful in an agitated vessel. The size of the largest eddy has been normally accepted to be comparable to the disc or impeller diameter. The final expressionswhich quantify the effect of coalescence on the drop size is given by

$$\ln \frac{\bar{d}}{d_o} = k_4 \cdot \left(\frac{D_c}{\nu}\right)^{0.5} \left(\frac{\sigma}{\rho d_o}\right)^{0.25} \Theta_D \tag{4.50}$$

or

$$\ln \frac{\bar{d}}{\bar{d}_o} = Z \, \theta_D \qquad (4.50a)$$

The presentation highlights the great difficulties encountered in the estimation of the extent of interdrop coalescence in an agitated dispersion, mainly because very little data is available. The difficulty lies in the measurement techniques. A non-disturbing technique is required to obtain information within the dispersion away from solid surfaces.

The determination of coalescence frequency is a very active area of research within droplet phenomena. It requires the measurement of the rate of change of physical or chemical parameters and a model describing the mixing process. Here only one of theseveral coalescence models (46) (47) (36) presented in the literature was discussed.

4.1.1.3 Drop Size in Agitated Vessels and Columns

The above two sections presented the mathematical treatments of the phenomena of drop break-up and coalescence considering each one separately. In practice both phenomena occur simultaneously and the extreme complexity of this situation makes it very difficult to obtain a theoretical model from which drop sizes can be predicted All the available drop size correlations in agitated systems are of a semiempirical nature, combining the most important parameters of each of the isolated coalescence and break-up models.

It was mentioned before that in any real dispersion there exists a wide range of drop diameters. In calculating an average drop diameter which characterize the dispersions attention must be given to the ultimate use of this average. Since the final objective is to calculate the total interfacial area, more weight should be given to the small drops. This follows from the fact that the specific surface (i.e. the surface per unit weight) increases as the particle size decreases. The following method has been suggested by Dallavalle (48) to correct for this phenomenon.

Consider the particles to be spheres then,

$$\text{Specific surface} = S_w = \frac{\text{area}}{\text{weight}} = \frac{6}{\rho d}$$

$$\text{Area of a sphere} = \pi d^2$$

$$\text{Weight of a sphere} = \frac{\rho \pi d^3}{6}$$

where ρ is the density of the particle. Let y_i = weight fraction of particles with diameter di, and specific surface S_{wi}. Then,

$$y_i = \frac{n_i d_i^3}{\sum_i n_i d_i^3}$$

The average specific surface $\bar{S}_w$ is given by a weighted arithmetic mean,

$$\bar{S}_w = \frac{\text{Total area}}{\text{Total weight}} = \sum_i y_i S_{wi} = \frac{\sum_i n_i d_i^3 . S_{wi}}{\sum_i n_i d_i^3}$$

Let d_{vs} be the diameter of a fictitious sphere having a specific surface qual to $\bar{S}_w$. Then,

$$d_{vs} = \frac{6}{\rho \bar{S}_w} = \frac{6}{\rho \sum_i Y_i S_{wi}} = \frac{6}{\rho} \left[\frac{1}{\frac{\sum_i n_i d_i^3 S_{wi}}{\sum_i n_i d_i^3}} \right]$$

However,

$$S_{wi} = \frac{6}{\rho_{di}}$$

therefore,

$$d_{vs} = \frac{6}{\rho} \frac{\sum_i n_i d_i^3}{\sum_i n_i d_i^3 . \frac{6}{\rho_{di}}} = \frac{\sum_i n_i d_i^3}{\sum_i n_i d_i^2} \qquad (4.50b)$$

Thus to estimate the total surface area of a particulate material the average volume-surface diameter d_{vs} should be used. This diameter is widely known as the Sauter mean diameter (d_{32} or d_{SM}).

Many studies of drop sizes in stirred tanks, batch and continuous, have been made and numerous correlations have been produced, many supporting Kolmogoroff's theory. This theory, when applied to drop break-up process, was shown to produce the following relationship

$$d_{sd} \text{ or } d_{max} = K_1 \left(\frac{\sigma}{\rho_c}\right)^{0.6} (\epsilon)^{-0.4} \qquad (4.23)$$

Since it is convenient to know the Sauter mean diameter, a relationship between this variable and d_{max} is required. Ratios of d_{32}/d_{max} were reported by Sprow [49],

Van Hauven and Hoevenaar (50) and Brown and Pitt (51), the values being 0.380, 0.5 and 0.675 respectively. No correlation has been developed to estimate the ratio d_{32}/d_{max}, being a common practice to include this factor within the constant K.

Successful application of equation 4.23 requires the existence of local isotropy and within it a limited range of eddy sizes called "the inertial subrange". The only requirement for the existence of this turbulence state is values of Reynolds number sufficiently high as to guarantee that if there is any anisotropy of the turbulence at all, it must be confined to the larger eddies, comparable in size with the integral scale of turbulence Le or larger. Rushton et al (52) assumed that for impeller Reynolds number Re_T > 10.000 the flow field in a stirred vessel may be considered locally isotropic. Other authors (53) gave a criteria very difficult to evaluate, namely the Reynolds number at the level of the micro-scale of dissipation λ_f (not equal to Kolmogoroff's η but of the same order of magnitude) must be greater than 300

$$(Re)_{\lambda_f} = \frac{\sqrt{\lambda_f}\ \lambda_f}{\nu} \qquad (4.51)$$

The criteria put forward by Rushton was experimentally confirmed by Nagata (54). Figures 4.3 to 4.7 present the experimental measurements done by Nagata et al (54) on a baffled vessel equipped with a disc type turbine impeller operated at $Re_T = 6 \times 10^4$. Figures 4.3 and 4.4 show the

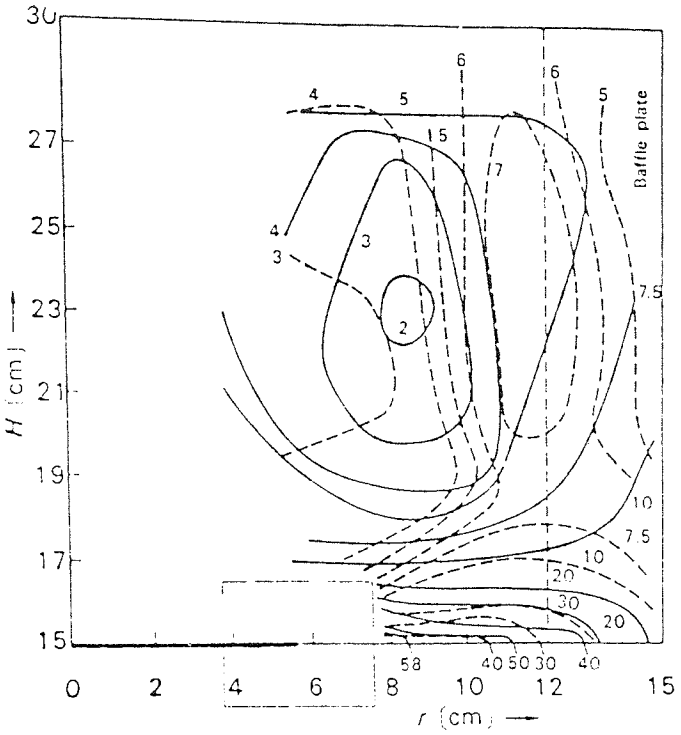

Figure 4.3 - Contour map of longitudinal intensity of turbulence

Figure 4.4 - Contour map of lateral intensity of turbulence

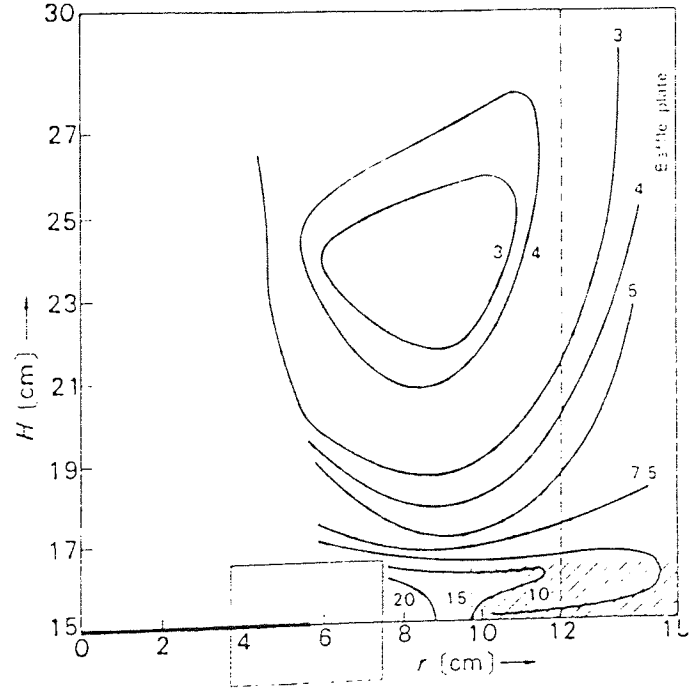

distribution of the intensity of turbulence on the longitudinal and lateral directions (u_r' and u_n' respectively). They show a very large value (u_r') in the vicinity of the impeller, decreasing rapidly as the distance from impeller increases and approaching a uniform distribution. Within the impeller zone u_r' is twice as large as u_n', so the discharge flow is in a state of non-isotropic turbulence. In a remote part of the impeller, u_r' and u_n' have an almost equal value, so the turbulence seems to be almost isotropic. The longitudinal and lateral energy spectra at several heights were also measured by Nagata et al and are presented in figure 4.5. As is evident from the figure 4.5

(a) there is a large difference between E_r and E_n at the impeller height, i.e. $u_r' > u_n$.

This anisotropy, as it was observed also in figures 4.3 and 4.4, is confined to the lower frequency eddies or large eddies, while at frequencies above 1000 c.p.s. (smallest eddies) both energy spectra can be considered approximately equal indicating the existence of a local isotropy. At positions far away from the impeller zone both spectra almost overlap each other indicating that isotropy exist all over the eddy size range.

The turbulence parameter ϵ included in equation 4.23 is a local value of the energy dissipated per unit mass. Figures 4.6 and 4.7, also presented by Nagata, show that there is a distribution of the rate of energy dissipated per unit mass as well as the Kolmogoroff's microscale eddy η. The location where the energy dissipation is most marked

Figure 4.5 - One-dimensional longitudinal and lateral energy spectra at several heights in a baffled stirred tank

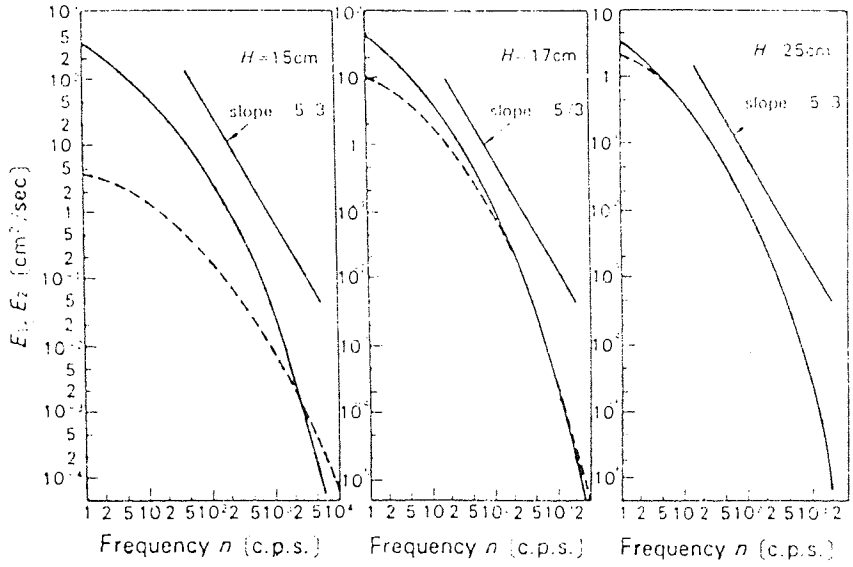

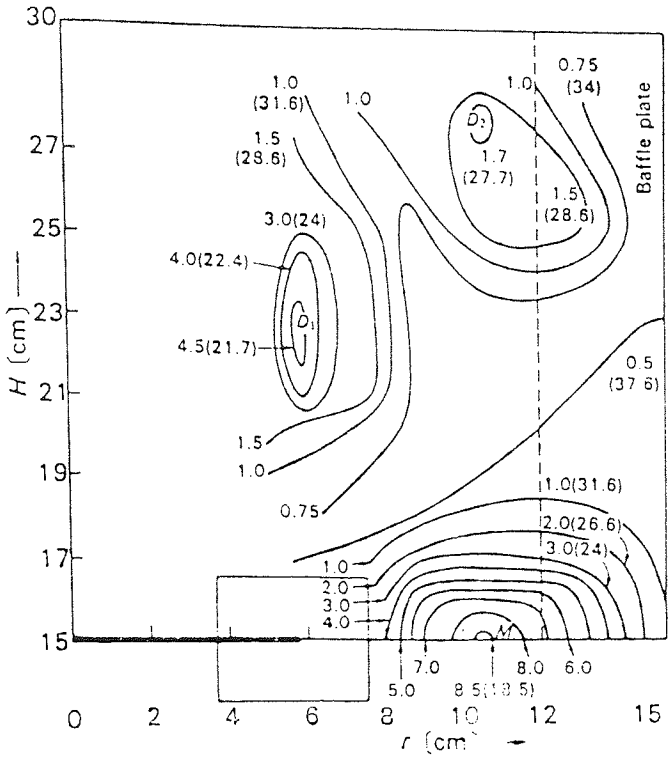

Figure 4.6 - Contour map of dissipation energy and Kolmogoroff's microscale eddy η

Figure 4.7 - Dissipation energy vs impeller speed in baffled stirred vessels

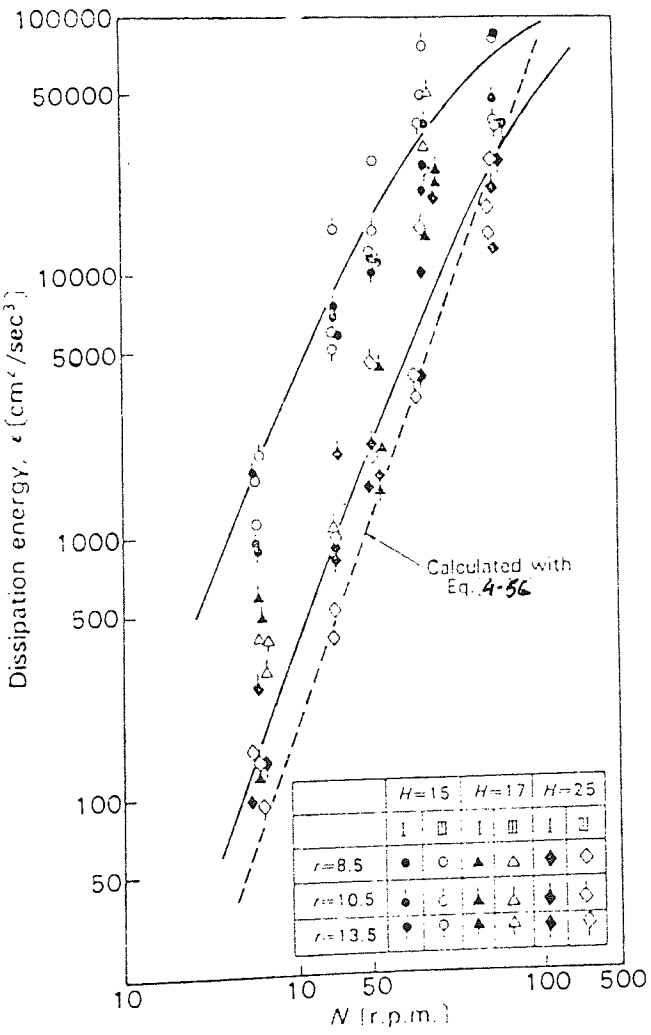

is in front of the baffles at the impeller height (M). There are two other maxima D_1 and D_2, though the dissipation energy was shown to be ½ → ⅓ of that in M. Cutler (55) using the empirical expression

$$\epsilon = \frac{3}{2} A \frac{(u')^3}{Le} \tag{4.52}$$

performed the integration over the impeller stream, and by assuming the turbulence outside to be homogeneous he found that of the total power consumption calculated as

$$P = \int_0^V \frac{3}{2} \frac{(u')^3}{Le} \rho dV \tag{4.53}$$

20% of this input energy was dissipated in the impeller itself, about 50% was dissipated in the impeller stream and that the remainder, about 30%, was dissipated in other parts of the tank.

Several authors have assumed that the average energy dissipation per unit mass $\bar{\epsilon}$, determined as the total power input to the vessel, represented by the following equation valid for fully turbulent flow and geometric similarity

$$P \simeq N_P . \rho N^3 D_I^5 \tag{4.54}$$

divided by the total mass of fluid in the vessel

$$\text{Mass} \propto \rho D_C^3 \tag{4.55}$$

could replace the point value. Then when geometrically similar equipment is used

$$\bar{\epsilon} \propto (N_P) N^3 D_I^2 \tag{4.56}$$

where N_p is the power number, substitution in equation 4.23 gives

$$d_{32} = K_2 \left(\frac{\sigma}{\rho_c}\right)^{0.6} N^{-1.2} D_I^{-0.8} \qquad (4.57)$$

This relationships have successfully been used to represent the Sauter mean drop diameters for a number of liquid-liquid systems for batch operations with low hold-up (56,57,58,49,51).

Recently, McManamey (59) correlated the data presented by Brown and Pitt (60), for a batch system using as $\bar{\epsilon}$ the power input per unit mass based on the volume swept out by the impeller $(\frac{\pi}{4}.D_I^2 W)$.

The effect of hold-up Θ_D (coalescence effect) on Sauter mean diameter has been accounted by expressions of the form

$$d_{32} \alpha f(\Theta_D).d_{32}^{o}$$

$$f(\Theta_D) = (1 + K.\Theta_D) \qquad (4.58)$$

or

$$f(\Theta_D) = 10^{c_1+c_2\Theta_D}$$

where d_{32}^{o} is the Sauter mean diameter for very dilute dispersion (equation 4.57).

Various investigators reported that drop size varies with location, being invariably smallest in the vicinity of the impeller and large at the circulation zones where coalescence effects predominate. Although this

situation can be easily explained with the distribution of ϵ given by Nagata (figure 4.6), the detailed dependence on conditions is not yet known.

Weinstein and Treybal (30) reported that for continuous flow vessels the drop size varies with the phase flow. They demonstrated that as the dispersed phase residence time increases, the drop size distribution approaches that for batch operation and also that fhe ratio $\frac{d_{32\ (flow)}}{d_{32\ (batch)}}$ is larger for larger interfacial tension systems, since the time required for the feed stream to attain steady state drop size increases. Same behaviour was noticed by Coulaloglou (61). No correlation has been developed to explicity account for these effects.

A summary of various correlations available in the literature for Sauter mean diameters in continuous and batch vessels and agitated column is given in Table 4.2. Correlations for drop sizes in Scheibel column do not exist.

All the correlations listed in Table 4.2 were obtained with equilibrated binary systems and they can not, in principle, be applied in a dispersion system under mass transfer conditions. It is well established that the drop size is greatly affected by the presence of mass transfer. A phenomenon which can be attributed to the effect of solute transfer on the rate of coalescence. Many investigators (62) (63) have found that mass transfer aids coalescence when the solute is transferred from the dispersed to the continuous phase but hinders coalescence when it is in the

Table 4.2 - Sauter Mean Drop Diameter Correlations

Investigator	Correlations	Equipment	Reference
Calderbank, Sprow, Chen and Middleman	$\frac{d_{32}}{D_I} = C_1 (We)_T^{-0.6}$	Batch vessels	156,49,58
Sprow	$\frac{d_{32}}{D} = C_3 (\rho_c \mu_c)^{-0.5} \left(\frac{\rho_c}{\sigma D_I}\right)^{-0.25} (W_e)_T^{-0.25}$	Batch vessels	49
Bouyatiotis and Thornton	$d_{32} = 5.38 \left(\frac{\mu_c}{\rho_c g}\right) \frac{\left(\frac{\rho_c}{\rho_c}\right)^3}{\rho_c^2 \mu . g^4}^{-0.16} \frac{\rho_c^3 \sigma}{\mu_c^4 g}^{-0.07}$ + $1.18\Theta_D \frac{\sigma^2}{\rho_c^2 g} \frac{\Delta\rho\gamma^3}{\mu_c^4 g}^{-0.62} \frac{\Delta\rho}{\rho_c}^{0.05}$	Batch and continuous vessels	155
Weinsten and Treybal	$d_{32} = 10^{(-2.316+0.672\Theta_D)} {}^{0.0722}\mu_c^{-0.194} \left(\frac{\sigma g_c}{\rho_c}\right)^{0.196}$	Batch	30

Continued/...

Table 4.2 - (continued)

Investigator	Correlations	Equipment	Reference
Weinsten and Treybal (cont'd)	$d_{32} = 10^{(-2.066+0.732\Theta_D)} \nu_c^{0.047} \left(\frac{\sigma g_c}{\rho_c}\right)^{-0.204}$	Continuous	30
Brown and Pitt	$\frac{d_{32}}{D_I} = 0.051\ (1 + 3.14\ \Theta_D)\ (W_e)_T^{-0.6}$	Batch vessels	51
Mylnek and Reswick	$\frac{d_{32}}{D_I} = 0.058\ (1 + 5.4\ \Theta_D)\ (W_e)_T^{-0.6}$	Batch vessels	69
Coulaloglou and Tavlarides	$\frac{d_{32}}{D_I} = 0.081\ (1 + 4.47\ \Theta_D)\ (W_e)_T^{-0.6}$	Continuous vessel	31
Misek	$\frac{\rho_c N^2 D_I^2 d_{32}}{\exp(0.0887 \Delta D)} = 16.3\ \left(\frac{H}{D_c}\right)^{0.46}$ RDC $Re_T > 6 \times 10^4$ Θ_D - low		13

/Continued..

Table 4.2 (continued)

Investigator	Correlations	Equipment	Reference
Al-Hemeri	$\frac{d_{32}}{D_I} = 4.7 \times 10^{17} \left(\frac{ND_I^2 \rho_c}{\mu_c}\right)^{-3.32} \left(\frac{\mu_d}{\mu_c}\right)^{0.23} \left(\frac{ND_I \mu_c}{\sigma}\right)^{2.0} \Theta_D^{0.225} \text{Exp } 0.40\left(\frac{n}{2}\right)$	RDC	81
Arnold, Mumford and Jeffreys	$\frac{d_{32}}{D_I} = 2.44 \left(\frac{H}{L}\right)^{-0.06} \left(\frac{HD_I^3 N^2 \rho}{\sigma}\right)^{-0.63} \left(\frac{\upsilon_\phi}{ND_I}\right)^{0.18}$	Oldshue Rushton	70

opposite direction. It was suggested that promotion of coalescence when solute was being transferred from the drop is a result of interfacial tension gradients developed in the region of the approaching drops. For most pairs of immiscible liquids, the addition of a solute, soluble in both phases, lowers the interfacial tension. Then when mass transfer takes place from the drop the concentration of solute in the contact zone between the two approaching drops rapidly reaches equilibrium with the drop. This results in a decrease in the interfacial tension locally which causes the interface in the contact zone to dilate drawing with it part of the intervening film which promotes coalescence. When the solute is tranferred into the drop the situation is reversed and material from the bulk continuous phase is drawn towards the contact area, which retards film drainage and hence stabilises the drop.

In a study by Jeffreys and Lawson (64), using a ternary system of benzene-acetone-water, it was shown that the coalescence times change with the direction of mass transfer in accordance with the above theory presented by Groothuis and Zuiderweg (63). Similar results were reported by Sawistowski (65).

4.1.2 Hold-up

4.1.2.1 Determination

For the determination of the fractional volume of dispersed phase (hold-up, Φ_D) several methods are available. The simplest, oldest and most frequently used technique, the diplacement method, consists of closing simultaneously all feed and exit lines, after which the fractional volume of the dispersed phase collected at the column extreme can be measured. This method does not give the true average total Φ_D of the extraction section since the liquid in the top and bottom parts is included in such measurements. Also, when applied to a Scheibel column the results can be highly unreliable because the static hold-up trapped in the packing could be a significant portion of the total column hold-up.

The technique of obtaining Φ_D by determining the average density of the dispersion in the extraction section by measuring pressure differentials has been used in the past in connection with RDC (66) and Kuhni extraction colunns (67,68). Results obtained in this way are free of the end effects affecting the displacement technique but they may not be sufficiently accurate when the extraction section is short. Moreover, the additional pressure effect due to the turbulent motion of the liquid in the column, can not, in general, be totally cancelled out and depending on the position of the static hole; can be a significant fraction of the total pressure difference.

Finally, the sampling technique consists of suddenly draining a part of the contents of the extraction section and determining the fractional dispersed phase content after this sample had settled. It is the only available technique when axial and radial variations of hold-up in agitated vessels and columns are required (69,1,70). Depending of the type of information needed, the sampling device can be a probe inserted inside the dispersion (69,1) sampling at different points, most commonly used in agitated vessels, or side-tubes fitted along the column wall and connected to stopcocks. The size of the sample is very important; small samples reduce the precision of the Φ_D observed and large samples can entrain material from undesirable neighbouring zones. Preferential wetting effects and high shear stress at the entrance and along the drainage tube must bekept to a minimum. This method was adopted during this research and more information is presented in section 7.2.

4.1.2.2 Fundamentals and Correlations

The theoretical interpretation and correlation of hold-up data in extraction colunns start with a series of articles published by Pratt and co-workers (19,20) in relation to their investigations of liquid-liquid extraction in packed columns. Almost all the actually known hold-up correlations applicable to packed, spray and mechanically agitated extraction columns share the same simplified hydrodynamical model put forward by Pratt and collaborators.

Gayler, Roberts and Pratt (22) interpreted the hydrodynamic data obtained in packed ex traction columns using the model defined by the following assumptions:

1. The whole of the void space not occupied by dispersed phase is used for flow of the continuous phase.

2. The effective density difference resulting from a force balance on a drop is given by $(\rho_m-\rho_d)$ rather than by $(\rho_c-\rho_d)$

$$(\rho_m - \rho_d) = (\rho_c - \rho_d)\ (1 - \theta_D) \tag{4.59}$$

3. The droplet diameter is independent of flow rate.

4. The time of passage of the droplets within a void is independent of the continuous phase flow.

5. The mean resistence to the motion of the droplets obeys Stokes' law (creeping flow).

Assumptions 2 and 5 were considered reasonable in view of the results obtained by Steinour (71) on his investigation of the rates of hindered settling of solid suspensions. With regard to assumption 3 it seems at first that a contradiction exists, since Gayler himself in a later publication (72) reported the increase of drop size with increasing flow rates. Also an increase in flow rates produces an increase in the drag force of the continuous phase. Both situations affect the value of the droplet relative velocity, $\bar{v}_r$, defined by equation (4.61) and it is expected that it will also influence the magnitude

of the mean droplet velocity relative to the packing at $V_c = 0$ and low hold-up, $\bar{v}_o$. However, since the plot of hold-up data presented in figure 3.5 shows that the slopes ($\varepsilon \bar{v}_o$) of thelines are constant and independent of the flow rates, it can be concluded that some compensation takes place making $\bar{v}_o$ constant and that assumption 3 is reasonable as far as $\bar{v}_o$ analysis and correlation is concern. Validity of assumption 4 is a consequence of accepting assumption 3 since both are interrelated.

Based on this model a simple relationship between the flow rates of the phases and the hold-up of the dispersed phase was obtained. Thus, the mean velocity of rise, $\bar{v}$, of the droplets relative to the stationary column and packing

$$\bar{v} = \frac{V_D}{\varepsilon \theta_D} \tag{4.60}$$

is given by the value of the velocity of rise, $\bar{v}_r$ of the droplets relative to the moving continuous phase, less theactual velocity of the latter

$$\bar{v}_r = \frac{V_D}{\varepsilon \theta_D} + \frac{V_c}{\varepsilon(1 - \theta_D)} \tag{4.61}$$

Based on assumptions 2 and 5, an expression of the relative velocity $\bar{v}_r$ of a droplet of diameter $d_{32}{}^o$ in terms of a modified form of Stokes' law was presented as follows

$$\bar{v}_r = C_o \cdot \frac{2(d_{32}^o)^2 \cdot g \cdot (\rho_c - \rho_d) \cdot (1-\theta_D)}{36\mu_c} \cdot F(1-\theta_D) \qquad (4.62)$$

where $F(1-\theta_D)$ is a function of hold-up which allows for the effect of hindered settling (cluster of drops) of the drops, C_o is a constant characterizing the resistance of the packing and d_{32}^o the Sauter mean drop diameter at zero continuous phase and substantially zero dispersed phase flow rates and estimated by equation (2.14).

Equation 4.62 can be expressed in terms of the mean Stokes' law terminal velocity, V_s, of the isolated drops as follow

$$\bar{v}_r = C_o \cdot V_s \cdot (1-\theta_D) \cdot F(1-\theta_D) \qquad (4.63)$$

combining equation 4.61 and 4.63

$$\frac{V_D}{\varepsilon\theta_D} + \frac{V_c}{\varepsilon(1-\theta_D)} = C_o \cdot V_s \cdot (1-\theta_D) \cdot F(1-\theta) \qquad (4.64)$$

Analysis of hold-up data showed that $F(1-\theta_D)$ is a constant. Also, an analysis of equation 4.64 shows that for $V_c = 0$ and $V_D \to 0$, $\frac{V_D}{\varepsilon\theta_D} \to C_o \cdot V_s$. Then $C_o \cdot V_s$ can be identified with the mean vertical droplet velocity relative to the packing at $V_c = 0$ and very low hold-up. This velocity was called the "characteristic velocity", $\bar{v}_o$ (see section (3.2.1)). Making the substitution in equation (4.64) the final expression is

$$\frac{V_D}{\theta_D} + \frac{V_c}{(1-\theta_D)} = \varepsilon \bar{v}_o (1-\theta_D) \qquad (4.65)$$

Equations (4.64) and (4.65) resulting from semi-theoretical considerations, have been the basic correlating relations for hold-up in different types of extraction columns. The main difference between the resulting correlations lies in the different expressions of the right hand side of equation (4.65), because each type of column needs specific expressions to calculate the "characteristic velocity" and the hindered settling factor.

For a packed column $\bar{v}_o$ depends on the chemical system and packing under consideration. Based on collision theory and assuming that viscous drag force is the only important force within the void of the packing, a semi-theoretical correlation for $\bar{v}_o$ was developed by Garner et al (22)

$$y = 1 - \frac{y}{x}\left[1 - \bar{e}\,\frac{x}{y}\right] \tag{4.66}$$

where

$$y = \frac{\bar{v}_o}{V_t}\left[1 - \exp.(-7.2D_c)\right] \tag{4.67}$$

and

$$x = \frac{\Delta\rho_g}{\rho_d V_t^2}\left[0.38d_p - 0.92\left(\frac{\sigma}{\Delta\rho_g}\right)^{\frac{1}{2}}\right] \tag{4.68}$$

where $\left[1 - \exp\,(-7.2D_c)\right]$ is the wall effect correlation factor applied to $\bar{v}_o$, $\left[0.38d_p - d_{32}^{\,o}\right]$ represents the mean distance between collision ($\bar{s}$) and d_p is the characteristic packing size. Within this collision model the "characteristic velocity" $\bar{v}_o$ is defined by the following equation;

$$\bar{v}_o = \frac{\bar{s}_c}{t} \tag{4.69}$$

where $\bar{s}$ and $\bar{t}$ are the mean distance and time respectively between collisions. In these expressions the Stokes' law terminal velocity, V_s, has been substituted by the true drop terminal velocity V_t in order to correct to some extent for the acceleration of the drops between collisions, which cause the motion to pass outside the Stokes' law range as well as for the neglected wall drag within the voids. Values of V_t are estimated from the plot of Re vs $C_D{}^2Re^4$, which covers the whole of the Stokes' law, intermediate and Newton's law regions. C_D is the frictional or drag coefficient of a solid sphere moving relative to a fluid with a terminal velocity V_t.

Experimental hold-up data for a 12in, 6in and 3 in packed column were plotted according to equation (4.65) in order to obtain the experimental values of $\bar{v}_o$ (see figure 3.5). The final plot of these values using the coordinates given by equation (4.67) and (4.68) showed that the theoretical line calculated from equation (4.66) represents the data reasonably well with a mean error of ±7%.

It is necessary to point out that equations (4.66) to (4.68) are valid only for conditions in which $d_p \geq d_{p_{crit}}$ where dp_{crit}, given by equation 3.1, corresponds to a packing with sizes of voids equal to the droplet size $d_{32}{}^o$. Another important factor is that the correlation equations (4.66) to (4.68) cannot be applied with certainty in a system undergoing mass transfer since they were obtained under solute-free conditions and no information is given concerning the

effect of the transfer of an undistributed solute on the "characteristic velocity" $\bar{v}_o$.

Equation (4.65) was found to be applicable up to the flooding point for a pulsed column (73) rotary annular columns (74) and spray columns (75). This is based on the fact that all these columns, together with the packed column, share the characteristic that they can be operated up to the flooding point with little or no coalescence of the dispersed phase and consequently it is expected that the "characteristic velocity" $\bar{v}_o$ be substantially constant for a given column and system.

A plot of hold-up data for a spray column (75) obtained at different flow rates gave a straight line with the coordinate system $V_D + \frac{\theta_D}{1 - \theta_D} V_C$ vs $\theta_D(1 - \theta_D)$, demonstrating the constancy of the characteristic velocity. As pointed out above, to predict the hold-up by means of equation (4.65) it is necessary to estimate the value of the characteristic velocity $\bar{v}_o$ for the particular system and column. In the case of spray columns it was found possible to predict $\bar{v}_o$ on the basis of the normal correlation of the free falling velocity for spheres, assuming the size of the droplets produced by different nozzles be given by the Hayworth and Treybal's relationship (76).

The first application of equation (4.65) to a mechanically agitated extractor ($\mathcal{E}$ equal unity) was done by Logsdail, Thornton and Pratt (62). Several systems, with and without mass transfer, were studied in a 3 inch diameter

R.D.C. They found that the characteristic velocity, $\bar{v}_o$ was constant over the entire hold-up regime studied for a particular solute-free system, column geometry and agitator speed. Under these conditions, they correlated $\bar{v}_o$ with the physical properties of the solute-free system, the column geometry and the rotor speed using dimensional analysis

$$\left(\frac{\bar{v}_o \mu_c}{\sigma}\right) = 0.012 \left(\frac{\Delta\rho}{\rho_c}\right)^{0.90} \left(\frac{g}{D_I N^2}\right) \left(\frac{d_i}{D_I}\right)^{2.3} \left(\frac{h}{D_I}\right)^{0.90} \left(\frac{D_I}{D_c}\right)^{2.7} \qquad (4.70)$$

A conclusion arising from the constancy of $\bar{v}_o$ was that the mean droplet size was independent of the phase flow rates and the dispersed phase hold-up and only dependent on rotor speed. Droplet interaction in the R.D.C. is not pronounced within the normal range of operating characteristics, although deviations would be expected at higher flow rates and energy input levels, that is under conditions when the extent of drop interaction becomes appreciable. Logsdail also showed that in those systems with a solute initially present in one of the phases, specifically the rafinate dispersed phase, the characteristic velocity $\bar{v}_o$ at rotor speed N increased with hold-up, implying that the mean droplet diameter also increased. When the mass transfer was in the opposite direction there was no noticeable change in the droplet size. No attempt was made to correlate $\bar{v}_o$ under mass transfer conditions.

In section 4.1.1.3 it was shown (Table 4.2) that several investigators reported variation of mean drop size with dispersed phase hold-up for different systems and extractors even in the absence of mass transfer. In this situation, if equation (4.65) is applied, the characteristic velocity no longer remains constant and independent of the flow rates and a factor quantifying the effect of coalescence on the former is required.

Misek (14) investigated the dependence of the hold-up of dispersed phase on the flow rates of both phases, on the effects of hindered settling and coalescence of droplets in an agitated liquid extractor. His theoretical analysis was based on the assumption that an agitated extractor consists of a series of agitated compartments vertically positioned, that the physical properties of both fluids remain constant during the flow through the system and that neither heat nor mass transfer occur. A population balance on a volume element under conditions of no droplet collision led to an expression of the relative velocity of isolated drop identical to the one proposed by Gayler et al

$$U_x = \frac{V_D}{\theta_D} + \frac{V_c}{(1 - \theta_D)} \qquad (4.61)$$

Misek stated that the relative velocity U_x is in the case of agitated extractor, not constant, even for a given system and intensity of agitation, owing to interactions (collision and coalescence) among the droplets at greater hold-up. This phenomenon manifests itself in two different ways: first the relative velocity of the drops is decreased

with increasing concentration of droplets in a similar way as the sedimentation of solid particles is hindered by collisions among them and second it increases on account of drop coalescence due to the increase of the droplets size.

For the quantitative evaluation of the effect of hindered settling, Misek used the equation derived by Steinour (76) (77) for the settling of non-aggregating solid particles

$$U_{o\Theta} = U_o(1 - \Theta_D)\, e^{-4.1\Theta_D} \qquad (4.71)$$

where U_o is the "characteristic velocity" previously named $\bar{v}_o$ and $\bar{v}_N$ and $U_{o\Theta}$ the settling velocity or relative velocity of drop under no coalescence in a suspension of hold-up Θ_D.

The quantification of the effect of coalescence on the relative velocity, required first an expression which allows to estimate the change of the mean size of the droplets with the coalescence frequency. This expression has been already presented in Section 4.1.1.2 and the coalescence model, on which it is based, was discussed in detail. The equation is

$$\frac{\bar{d}_\Theta}{\bar{d}_o} = e^{Z\Theta_D} \qquad (4.50a)$$

where Z the coalescence coefficient, is given by

$$Z = k \left[\left(\frac{D_c}{\nu_c}\right) \cdot \left(\frac{\sigma}{\rho_c \bar{d}_o}\right)^{0.5} \right]^{0.5}$$

In order to transform the drop size ratio to a relative velocity ratio, Misek assumes that the values of U_x and $U_{o\Theta}$ are very close, so that the respective velocities may be expressed by

$$U_x^{\alpha} = b.\bar{d} \quad : \quad U_{o\Theta}^{\alpha} = b.\bar{d}_o \tag{4.72}$$

which it follows for the velocity ratio

$$\frac{U_x}{U_{o\Theta}} = \left(\frac{\bar{d}}{\bar{d}_o}\right)^{1/\alpha} \tag{4.73}$$

Substituting equation (4.73) on (4.50a) the expression quantifying the change of relative velocity due to coalescence is obtained

$$\frac{U_x}{U_{o\Theta}} = e^{Z/\alpha\ \Theta_D} \tag{4.74}$$

The final equation was obtained by Misek after combining equations (4.61), (4.71) and (4.74),

$$\frac{V_D}{\Theta_D} + \frac{V_c}{(1 - \Theta_D)} = U_o(1 - \Theta_D)\ e^{(Z/\alpha - 4.1)\Theta_D} \tag{4.75}$$

The validity of equation (4.75) was claimed by Misek to have been experimentally checked in different agitated extractors (R.D.C., A.R.D.C. and Oldshue-Rushton columns) with different binary systems of immiscible liquids.

For calculations of Φ_D according to equation (4.75) the constants characterizing the extractor and the binary system must be known, i.e. the characteristic velocity U_o, the coalescence coefficient Z and the velocity exponent α. Misek proposed the following procedures

(a) Characteristic Velocity U_o

It is assumed that U_o can be considered within sufficient accuracy for technical calculations equal to the terminal velocity V_t, of falling rigid spheres. The applicability of this assumption was verified approximately by Misek in the range of low drop Reynolds number (10 to 60). Values of V_t or U_o are estimated then from the plot (77)

$$C_D = \frac{4}{3} \frac{d_{21}\, g\, \Delta\rho}{\rho_c\, U_o^2} = f\left(\frac{d_{21}\, U_o\, \rho_c}{\mu_c}\right) \tag{4.76}$$

where d_{21} is the hydraulic mean drop diameter defined by

$$d_{21} = \frac{\Sigma d^2}{\Sigma d} \tag{4.77}$$

(b) Coalescence Coefficient Z

The coefficient Z is calculated from the physical properties of the system, and geometry of the column according to the following equation

$$Z = 1.59 \times 10^{-2} \left[\left(\frac{D_c}{\nu_c}\right) \left(\frac{\sigma}{\rho_c d_o}\right)^{0.5} \right]^{0.5} \tag{4.78}$$

where d_o corresponds to the diameter of a single spherical drop calculated using the expression proposed by Misek and listed in Table 4.2.

(c) Velocity Exponent α

This factor can be estimated from the relation presented in (a) for the Drag Coefficient C_D vs Reynolds number plot for rigid spheres

Stokes' Law Region: $Re_{(drop)} = \frac{d_o U_o \rho_c}{\mu_c} < 0.3$

$$C_D = \frac{24}{Re} \qquad d_o \propto U_o^{\frac{1}{2}} \qquad \alpha = \tfrac{1}{2}$$

Intermediate Region $0.3 < Re_{(drop)} < 10^3$

$$C_D = \frac{18.5}{(Re)^{3/5}} \qquad d_o \propto U_o^{\frac{7}{8}} \qquad \alpha = \tfrac{7}{8}$$

Newton's Law Region: $Re_{(drop)} > 1000$

$$C_D = 0.44 \qquad d_o \propto U_o^{2} \qquad \alpha = 2$$

These values of α represent characteristic values of each region.

In spite of the claims made by Misek of the applicability of equation 4.75 to any agitated extraction columns, the relation is open to criticism, especially in the following points;

1. The theoretical analysis was based on the assumption that no mass transfer is occurring. The same limitations applied to Logsdail's equation (4.70) and Gayler

et al equation (4.65). It is known that under mass transfer direction continuous → dispersed phase, coalescence hindered. The magnitude of the coalescence coefficient is in this case lower than the value predicted by equation 4.78 and under some conditions may even approach zero.

2. The coalescence model (section 4.1.1.2) from which equation (4.78) is derived, is oversimplified by the assumption that every collision leads to a combination of the colliding drops.

3. The rate of drop interaction depends on the dispersed phase hold-up as well as on the distribution of energy in the agitated compartment. At low hold-up coalescence effects were shown (78) to be significant even in the discharge region of an impeller type agitator. Then it is expected that the coalescence correcting coefficient Z includes a factor quantifying the level of agitation in the system.

4. Only very small drops behave like rigid spheres. The terminal velocity can be greater by a factor of 1.5 than that given by the drag coefficient curve for solids in the 10 to 500 Reynolds number range because of internal circulation within the drop. Correlations of the type given by Hu and Kintner (79) or Klee and Treybal (80) look at the first sight, to be more appropriate to estimate U_o for a wide range of physical properties. Also it is expected some influence of the level of agitation (N) on the value of U_o as it was shown by Logsdail et al.

The hold-up correlations presented above when compared with others reported in the literature can be considered as general for a certain type of extractor. They have the merit of being based on theoretical considerations and proved to be applicable under certain conditions.

Several other correlations based on dimensional analysis (81) or on the relationships presented above (82) had been reported to be applicable to R.D.C. and Oldshue-Rushton columns. No correlation has yet been reported to be suitable to apply in Schiebel column.

4.1.2.3 Flooding

The values of the limiting flow velocity of the dispersed and continuous phase, widely known as "flooding point", are extremely important in extractor design since it is the only information required to estimate the extractor diameter. This condition of "flooding" is a typical hydrodynamic phenomena particulary associated with differential contactors. The increase in flow rates has as a consequence the approach to a limiting value of hold-up and velocity and to limiting conditions under which the velocity can no more be increased under preservation of the original countercurrent flow. Any increase in flow velocity above themaximum leads to one of the following situations:

(a) The entrainment of the dispersed phase into the continuous one (true flooding). Limiting conditions of this sort are characteristic in packed and spray columns.

(b) The occurrance of phase inversion, i.e. the dispersed phase changes into the continuous phase and vice versa. The equilibrium between coalescence and redispersion under steady state conditions is disturbed and shifted towards the former. This phenomena has been reported to occur in R.D.C. and Oldshue-Rushton Columns.

(c) The formation of a second interphase boundary beneath any of the packing sections of a Scheibel Column packed with a material preferably wetted by the dispersed phase.

Brackenfeld and Wilke (83) were among the first investigators to present a correlation for predicting flooding rates in packed columns. They observed that the sum of the square roots of the continuous and dispersed phase velocities were essentially constant for a given packing and liquid system. They developed the following correlation,

$$(V_{c.f}^{\frac{1}{2}} + V_{D.f}^{\frac{1}{2}})^2 = 32.5 \frac{\Delta\rho^{0.98} \varepsilon^{1.98}}{a_s^{0.82} \mu_c^{0.32} \sigma^{0.26}} \qquad (4.79)$$

which was later modified by Crawford and Wilke (84) to cover larger Raschig rings. The theoretical basis for the square root plots of equation (4.79) was provided by Dell and Pratt (85) using a simple hydrodynamical model to

represent the flow behaviour of the phases inside the packing section. Recently, Watson et al (86) presented the correlation

$$V_{c.f}^{\frac{1}{2}} + (0.844\ \Delta\rho^{0.145} dp^{0.298} \mu_c^{-0.084} \varepsilon^{-0.078}) V_{d.f.}^{\frac{1}{2}}$$

$$= 23.8 \Delta\rho^{0.269} dp^{0.494} \mu_c^{-0.084} \varepsilon^{0.5} \qquad (4.80)$$

which it was claimed to be more reliable in predicting flooding rates for new systems since it was based upon more extensive data and a wider range of physical properites.

When the hold-up correlating equation for a particular extractor is of a form similar to equation (4.61), the limiting values of hold-up and velocities may be calculated using a procedure similar to that developed by Thornton (75). At the flooding point the flow rates V_D and V_c reach a maximum value. This condition can be introduced into the hold-up equation by differentiating which respect to θ_D treating V_c and V_D as dependent variables and setting $(\frac{dV_D}{d\theta_D})$ and $(\frac{dV_c}{d\theta_D})$ equal to zero.

Logsdail and co-workers (62) using the above procedure obtained the following equations;

$$V_{D.f} = 2\bar{V}_N\, \theta_{D.f}^{2}\, (1 - \theta_f) \qquad (4.81)$$

$$V_{c.f} = \bar{V}_N\, (1 - \theta_{D.f})^{2}\, (1 - 2\theta_f) \qquad (4.82)$$

$$\theta_{D.f} = \frac{(L_x^{2} + 8L_x)^{0.5} - 3L_x}{4\,(1 - L_x)} \qquad (4.83)$$

where $L_x = \frac{V_{D.f}}{V_{c.f}}$

They showed that these equations are valid for R.D.C. columns under conditions of low or no droplet interaction.

Misek (13) presented other expressions to predict flooding rates, claimed to be applicable for R.D.C., A.R.D.C. and Oldshue-Rushton columns. He solved equation (4.75) for the maximum and then eliminated the characteristic velocity to obtain

$$\frac{V_{D.f}}{V_{c.f}} = \frac{2\phi_{D.f}^2 \left[1 - \phi_f + (z-4.1)\left(\phi_f - \frac{\phi_f^2}{2} - \frac{1}{2}\right)\right]}{(1 - \phi_{D.f})^2 \left[1 - 2\phi_f + (z-4.1)(\phi_f - \phi_f^2)\right]} \quad (4.84)$$

An equation related hold-up and phase velocities at phase inversion in R.D.C. and Oldshue-Rushton column was proposed by Sarkar (87). The hold-up correlation used by Longsdail et co-workers was corrected for droplets coalescence by empirically assuming that $\bar{v}_o$ is given by

$$\bar{v}_o = K \phi_D^n$$

and taken n = 2. After solving the hold-up correlation for the maximum the following expression is given

$$\frac{V_{c.i}}{V_{D.i}} = \frac{(1 - \phi_i)(3 - 4\phi_i)}{\phi_i (4\phi_i - 2)} \quad (4.85)$$

Sarkar found this expression to be in good agreement with the experimental values for $\frac{V_{ci}}{V_{Di}} < 1.0$.

All these flooding correlating equations suffer from the same short-comings as the respective hold-up correlation from which they were analytically derived. Moreover they are strictly valid only for monodisperse behaviour of the dispersed liquid. The actual dispersion is of a polydisperse nature and flooding sets in gradually, not instantaneously. Before noticeable bulk flooding situation is reached in the column, already small velocities of the continuous phase cause drop entrainment, this factor may become the limiting one for the column operation. The practical significance of the type of polydispersion in the column hydrodynamic is illustrated in Table 4.3 (70).

TABLE 4.3

Property of dispersion	Normal	Log-Normal
Proportion of smaller drops	Lower	Higher
mean mass transfer coeffs	Higher because more drops are circulating	Lower - more stagnant drops
Interfacial area	Lower	Higher
Settling rate	Higher	Lower
Tendency to flood column	Higher	Lower

4.2 The Overall Mass Transfer Coefficient K

The overall mass transfer coefficient in terms of the dispersed phase can be expressed, according to Whitmans two-film theory, as the combination of individual resistance to mass transfer of the continuous (k_c^{-1}) and dispersed (k_d^{-1}) phases as follows;

$$\frac{1}{K_D} = \frac{1}{K_D} + \frac{m}{k_c} \tag{4.86}$$

The validity of this simple additivity concept rest upon the assumption that there is no resistance to transport at the actual interface.

Several different mechanisms have been proposed to describe conditions near the interface between two phases. A brief account of some of the most commonly used models is given below.

The film model was originally proposed by Nernst (88) and is the basis of the Whitman's two film theory (89). It assumes that turbulence dies near the interface and the resistances to mass transfer are confined largely to a region quite close to the phase boundary of thickness y_o, in which transport occurs by molecular diffusion. Using the equations for molecular diffusion, the mass transfer coefficient is given by

$$k = \frac{\mathcal{D}}{y_o} \tag{4.87}$$

This concept is a gross over-simplification of the real hydrodynamic conditions near an interface and specially a liquid-liquid interface. Its major pitfall is that it fails to predict the power dependence of the mass flux on the molecular diffusivity $\mathcal{D}$. The actual dependence is known to be between the zero and unit power while the model predict unity. Nevertheless, this theory has been quite useful in several applications.

The penetration model of Higbie (90), contrary to the stationary nature of the transport proposed by the film model, considers that mass transfer occurs during the repeated brief contacts of the two-phases. It proposed that small fluid elements of uniform solute concentration are continually being brought into contact with a phase boundary, remain there for a short and constant penetration time tc and undergo unsteady-state transfer of solute by molecuar diffusion, before being swept away to be replaced by other fluid elements. Application of the Fick's second law

$$\frac{\partial C_A}{\partial t} = \mathcal{D}_{AB} \frac{\partial^2 C_A}{\partial z^2} \tag{4.88}$$

and a subsequent integration along the contact time tc gives the following average flux over tc.

$$N_A = 2\sqrt{\frac{\mathcal{D}_A}{\pi tc}} (C_A - C_o) \tag{4.89}$$

Since $\underline{k}$ is defined by the mass flux per unit concentration difference, the time-average mass-transfer coefficient is given by

$$k = 2\sqrt{\frac{\mathcal{D}_A}{\pi tc}} \qquad (4.90)$$

A procedure to estimate tc is not provided by the theory. It was originally applied to a gas-liquid solute transfer. Higbie assumed that as a gass bubble rises through a liquid, the liquid surface renewal occurs in a time, tc, approximately equal to that required for the bubble to rise one bubble diameter. Substitution of the expression of tc in the equation (4.90) gives the well known Higbie relation

$$Sh = 1.13(Re)^{0.5}\ (Sc)^{0.5} \qquad (4.91)$$

This theory has been widely used and in each application the estimation of tc was done according to the problem and/or the availability of measured variables which after algebraic combinations, produce a characteristic time scale.

The surface renewal model of Danckwerts (91) is an extension of the penetration theory. Danckwerts assumed that the times of exposure of fresh elements of liquid were not identical as assumed by Higbie, but that the probability of replacement of any given liquid element was independent of the time for which it had already resided at the interface. Then the variables contact time may be anything from zero to infinity. The fractional rate of renewal, S, of the area exposed to penetration, in other words, the rate of replacement of the fluid elements

in the surface, is assumed to be constant. Application of these concept to the transient diffusion equation render the following relations

$$N_A = (C_A - C_o)\sqrt{\mathcal{D}} \int_o^\infty \frac{S e^{-St}}{\sqrt{\pi t}}\, dt = \Delta C \sqrt{\mathcal{D}S} \qquad (4.92)$$

$$k = \sqrt{\mathcal{D}S} \qquad (4.93)$$

The eddy cell model of Lamont and (95) Scott considers the surface renewal be due to turbulent eddies. According to this model the very small scale of turbulence in the equilibrium range are considered to be controlling the mass transfer process. Lamont's calculation based on the eddy cell model gives the following relationship for the mass transfer coefficient at a free interface.

$$k \alpha (Sc)^{-\frac{1}{2}} (\epsilon\nu)^{\frac{1}{4}} \qquad (4.94)$$

More details on these and other models are reviewed by Sherwood et al (92), Skelland (93), Treybal (7) and Scriven (94).

4.2.1 Mass Transfer to and from Single Drops

The complex interactions presented when extraction occurs in agitated vessels has made necessary the study of mass transfer to and from single drops in order to gain insight into the practical situations.

The literature dealing with mass transfer between fluid particles and their fluid surroundings is very extensive. Since the individual mass transfer coefficients (k_c and k_d) are expected to depend differently on the liquid properties, operating conditions and vessel and impeller geometry, most of the studies have tried to isolate the resistances to mass transfer into an internal and external one, relative to the phase interface. The resistance to transfer, whether internal or external to the droplet surface, depends upon the motions of the fluid particle and the surroundings. Widely ranging magnitudes of resistance have been reported for drops which behave as rigid spheres (stagnant drops), those performing like circulating fluid bodies (circulating drops) and those exhibiting a fully oscillating regime (oscillating drops). Oscillating drops show a far greater rate of transfer than any other type.

This section will be divided into two main parts. viz. mass transfer in the continuous phase and that in the dispersed phase. The situation for rigid and non-rigid drops will be considered separately.

4.2.1.1 Mass Transfer in the Continuous Phase

(a) Stagnant drop

A drop can be considered essentially rigid if the ratio of dispersed to continuous phase viscosity is high, if it is quite small or if drop circulation is eliminated by the presence of a surfactant. Under this condition, correlations derived for solid spheres

have been used. For drop Reynolds number < 4, where creeping flow around the drop can be assumed, Levich (30) gives the following relation

$$(Sh)_c = \frac{k_c\, d}{\mathcal{D}} = 1.0(Pe)^{1/3} = 1.0(Re.Sc)^{1/3} \qquad (4.95)$$

valid for $Pe > 10^3$.

An equation widely quoted and used for solid spheres at low Re is the one proposed by Ranz and Marshall (96) which is a modification of the Frossling (97) equation

$$(Sh)_c = 2 + 0.6\ (Re)_c^{0.8} (S_c)_c^{0.33} \qquad (4.96)$$

Both previous equations require the drop terminal velocity ( ) which can be estimated from the Hu and Kinter correlation (79).

Above Re > 10 the above equations are not strictly applicable, since wake formation at the rear of the drop needs to be taken into account. Kinard et al (98) proposed the equation

$$(Sh)_c = 2+(Sh)_n + 0.45(Re)_c^{\frac{1}{2}}(S_c)_c^{1/3} + 0.0484(Re)_c(S_c)_c^{1/3} \qquad (4.97)$$

where the figure 2 is for a stagnant continuous phase, $(Sh)_n$ accounts for the natural convection effect, which is important at low fluid velocity and high mass transfer rate. The third term is the contribution at the front of the drop and the last term is the contribution at the rear taking into account the wake effect. Since the concentration at the wake is larger

than in the bulk of the continuous phase at the same level and the k_c is an average value over the entire surface of the drop, the contribution of mass transfer by the wake is therefore not very large. This equation can not be applicable in an agitated system since the wake phenomena has little significance in turbulent flow systems.

An alternate and widely accepted relation for rigid drops with relatively high Reynolds number was presented by Garner et al (99)

$$(Sh)_c = 0.6(Re)_c^{0.5}(S_c)_c^{0.33} \qquad (4.98)$$

It is instructive to mention that all the above equations are of the boundary layer type. The assumed rigid interface of the stagnant drop give rise to the formation of a boundary layer which is represented by the 1/3 power in the Schmidt number.

(b) Circulating drops

For drop Reynolds number in the region 50-200 internal drop circulation develops in clean systems with drops of intermediate sizes. This circulation, due to the drag on the surface of the fluid droplet, increases the drop terminal velocity and the continuous phase k_c. The motion of drop surface should hinder any formation of a boundary layer or at least thinned and then the power of S_c should be larger. Under this condition it is expected that either Higbie or Danckwerts' surface renewal theories should be applicable.

Applying the penetration theory, one may assume the contact time be given by the ratio of the drop diameter to drop terminal velocity. Substituting into equation (4.90) the Higbie relation is obtained.

$$(Sh)_c = 1.13(Re)_c^{0.5}(S_c)_c^{0.5} \qquad (4.91)$$

This equation was also obtained by Boussinesq (100) and Ruckenstein (101) using the velocity distribution for potential flow.

Garner and Tayeban (102) correlated experimental data with the proportionality constant lower than 1.13 because of the existence of the wake

$$(Sh)_c = 0.6(Re)_c^{\frac{1}{2}}(S_c)_c^{\frac{1}{2}} \qquad (4.99)$$

(c) Oscillating drops

It was mentioned above that oscillating drops show a far greater rate of transfer than any other type and a lower terminal velocity than the circulating drops.

Garner and Tayeban (102) studied the effect that drop oscillation had on the continuous phase resistance. They proposed the following equation

$$(Sh)_c = 50 + 8.5 \times 10^{-3} (Re)_c(S_c)_c^{0.7} \qquad (4.100)$$

In the development of a mass transfer model based on interfacial stretch and internal droplet mixing Rose and Kintner (103) used the equation (4.99) given by Garner and Tayeban to predict the outside mass transfer coefficient by a drop assumed to oscillate from a nearly spherical shape to an oblate ellipsoidal

one and back to a spherical shape.

Angelo et al (104) generalised the penetration theory, in an analogous manner as done by Rose and Kintner, by considering the stretching or shrinking of the phase boundaries with special application to forming and oscillating drops. They claimed that their mass transfer coefficient equation holds for both phases with the same characteristic time and the appropriate diffusivity. However, Von Berg and Henkel (157) reported negative dispersed phase coefficient being obtained when the Angelo et al equation was used for the continuous phase coefficients.

4.2.1.2 Mass Transfer in the Dispersed Phase

(a) Stagnant drops

Mass transfer inside a completely stagnant drop can be expected to follow the equations derived by Newman (105) for molecular transient diffusion for spheres

$$E_{f.} = 1 - \frac{6}{\pi^2} \sum_{n=1}^{\infty} \frac{1}{n^2} \exp\left(-\frac{4n^2\pi^2 \mathcal{D} t}{d^2}\right) \qquad (4.101)$$

where $E_{f.}$ is the ratio of the accomplished to total possible drop concentration change during time t. A mass balance across the surface of the spherical drop can be integrated along the rising or falling time t assuming the interface concentration constant to give the following relation between the time

average k_D and E_f

$$k_D = \frac{d}{6t} \ln \left(\frac{1}{1-E_f}\right).$$

then

$$k_D = \frac{d}{6t} \ln \left[\frac{6}{\pi^2} \sum_{n=1}^{\infty} \frac{1}{n^2} \exp \left(- \frac{4n^2\pi^2 \mathcal{D}t}{d^2}\right)\right] \qquad (4.102)$$

Vermeulen (106) suggested an empirical approximation to equation (4.102) by taking only the first term of the series and neglecting the coefficient $6/\pi^2$

$$k_D = - \frac{6}{6t} \ln \left[1 - \left(1 - \exp \left(- \frac{4\pi^2 \mathcal{D}t}{d^2}\right)\right)^{\frac{1}{2}}\right] \qquad (4.103)$$

(b) Circulating drops

As a result of circulations and oscillations the mixing inside the drop can be by laminar and by turbulent circulation.

For the regime of laminar circulation, the generally accepted relation is that drived by Kronig and Brink (107), based on the Hadamard-Rybczynki (108,109) internal circulation flow patterns,

$$k_D = - \frac{d}{6t} \ln \left[\frac{3}{8} \sum_{n=1}^{\infty} A_n^2 \exp \left(\frac{64\lambda_n \mathcal{D}t}{d^2}\right)\right] \qquad (4.104)$$

Equation (4.104) is restricted to regimes for which Re $\lesssim$ 1 and can be applied for the case when resistance to mass transfer in the continuous phase is zero.

Calderbank and Korchinski (10) used a correction factor of the molecular diffusivity $\mathcal{D}$ to account for the increase in mass transfer due to the circulation of the drop. The effective diffusivity was considered to be equal to $(2.25\mathcal{D})$ and used in the Vermeulen equation (4.103) to give

$$k_D = \frac{d}{6t} \ln \left[1 - \left(1 - \exp\left(- \frac{4\pi^2 (2.25\mathcal{D}) t}{d^2}\right)^{\frac{1}{2}}\right)\right] \qquad (4.105)$$

For drops with turbulent motion, Handles and Baron (11) proposed a dispersed phase mechanism consisting of circular and concentric stream lines with mixing in between. Their equation derived for no resistance in the continuous phase is

$$k_D = 0.00375 \frac{V_t}{\left(1 + \frac{\mu_D}{\mu_c}\right)} \qquad (4.106)$$

This model was claimed to be applicable also to oscillating drops. However, photographic studies of oscillating drops revealed that no ordered circulation patterns exist due to the strong oscillation which cause complete mixing of the fluid inside the drop. Therefore, this correlation is not reliable due to a rather unconvincing physical basis.

(c) Oscillating drops

Two of the most important models available for the analysis of oscillating drops are the Rose-Kintner (103) model and the surface stretch model of Angelo et al (104).

Rose and Kintner proposed a model of an interfacial stretch with internal mixing applied to an oscillating drop. They assumed that all the resistance to transfer (both in the continuous and dispersed phases) lie in a thin film near the interface which varies in thickness during the oscillation period. In order to estimate the drop internal mass transfer coefficient they assumed also that the interface would be renewed during each drop oscillation. Hence, two interface concepts are assumed to be applicable, the stagnant film model and the penetration or surface renewal model. The last one was used to obtain an expression of the dispersed phase mass transfer coefficient using as the penetration time the time of one oscillation. Hence,

$$k_d = 0.45 \sqrt{\mathcal{D}_D w} \qquad (4.107)$$

where w is the frequency of oscillation given by

$$w^2 = \frac{\sigma\, b}{(\frac{d}{2})^3} \frac{n(n+1)(n-1)(n+2)}{\{(n+1)\rho_D + n\rho_c\}} \qquad (4.108)$$

in which the empirical amplitude coefficient b is estimated by

$$b = \frac{d^{0.225}}{1.242} \qquad (4.109)$$

the radius of the drop $(\frac{d}{2})$, as a function of the amplitude a_p, is given by

$$(\frac{d}{2}) = (\frac{d}{2})_D + a_p \sin \frac{w}{2}t \qquad (4.110)$$

and n, the mode of oscillation is

n = 2 $\quad$ 200 < Re < 250

n = 3 $\quad$ Re >250

The continuous phase mass transfer coefficient k_c, was calculated by Rose and Kintner using the Garner and Tayeban equation (4.99) which is based on penetration theory with a penetration time equal to the time required for the drop to rise or fall one drop diameter.

The calculated fractional extraction based on this model presented an average deviation of approximately 15% with respect to the experimental values. In spite of the many drawbacks observed in this model (104)(112) it has a more appealing physical basis and is more reliable than that of Handles and Baron.

The Angelo et al (104) model is also based on the surface stretch and complete mixing concepts outlined above. However, only penetration theory is considered and the mass transfer coefficient relation, developed by correcting the basic equation (4.90) for the surface stretch effect, is assumed to be applicable to both sides of the interface. When the model is applied in the analysis of large oscillating drops the following expression of a time average

k_D is obtained

$$k_D = \sqrt{\frac{4\,\mathcal{D}\,w\,(1 + \epsilon' + \frac{3}{8}\epsilon'^2)}{\pi}} \qquad (4.111)$$

based on an assumed surface-time relation

$$S = S_o\,(1 + \epsilon'\,\sin^2 wt) \qquad (4.112)$$

where ϵ', the dimensionless amplitude of the surface stretch is calculated from the values of the maximum and minimum surface area per cycle.

Based on the assumption mentioned above that the coefficients at both sides of the interface differ only in the value of the appropriate diffusivity, the overall dispersed phase mass transfer coefficient is given by

$$K_D = k_D \left[\frac{1}{1 + m\sqrt{\frac{\mathcal{D}_D}{\mathcal{D}_C}}}\right] \qquad (4.113)$$

It should be mentioned that the above expressions are correct only for an integral number of complete oscillations and they will predict low values for a fractional number.

Although the Angelo et al model includes a convective term resulting from the surface-stretching or shrinkage motion, it predicts extraction efficiencies which are in close agreement with the ones obtained using the Rose and Kintner model. Then, as far as the application of these models to oscillating drops, both models can be considered of equivalent reliability.

Recently, Al-Hassan (112) studied large oscillating drops under high mass transfer rate. The data for the system toluene-acetone-water were empirically correlated by

$$K_D = 4.3\ \epsilon'^{2.692}\ E_o^{1.672}\ \sqrt{\mathcal{D}_D w} \qquad (4.114)$$

where E_o is the Eötvos number

$$E_o = \frac{g\ \Delta_\rho\ d^2}{\sigma} \qquad (4.115)$$

Both Rose and Kinter and Angelo et al equations have the real disadvantage that they require a knowledge of the physical motionof the drop. Experience in this area indicates that the oscillations can not always be readily observed and measured, especially in agitated vessels with a high drop population.

4.2.2 Mass Transfer and Interfacial Phenomena

The widely used equation (4.86) employs the assumption that the phases are in equilibrium at the interface, i.e. that there is no diffusional resistance at the phase boundary. However, significant interfacial resistance is encountered when a surface-active agent is present in the system due to its tendency to concentrate at the interface. Furthermore, the transfer of solute, especially at high concentration, sometimes causes interfacial turbulence which substantially increases the rate of mass transfer between the phases. This last is equivalent to a negative

interfacial resistance.

The interfacial phenomena resulting from local changes in interfacial tension may manifest itself in a variety of ways, i.e. rippling of the interface, eruptions and cellular convection. Sawistowski (65) classified all the different types of disturbances in two main categories

(a) interfacial convection of ordered type
(Marangoni instabilities)

(b) disordered interfacial convection
(transient disturbance)

Mathematical analysis of mass transfer induced surface tension driven instabilities (Marangoni instabilities) was first done by Sternling and Scriven (113). The phenomena was studied as a problem of hydrodynamic stability with diffusion and interfacial movement playing a major part. Linearized stability theory was applied to determine the conditions for the onset of instability and the nature of the dominant disturbance. The analysis explained the experimental well known situation that some systems may be stable with solute transfer in one direction yet unstable with transfer in the opposite direction. A complete review of the phenomena is given by Sawistowski (65) and Sherwood et al (92).

4.2.3 Mass Transfer in a Turbulent Dispersion

Derivations of the equations which predict single drop mass transfer coefficients normally make the following restrictive assumptions.

(a) local mass transfer coefficient averaged over the total time of contact of the drop with the continuous phase

(b) no circulatory motion (interfacial turbulence) in the interfacial region

(c) constant physical properties

(d) uniform continuous phase composition

(e) no mass transfer resistance in the continuous phase when k_D is studied

(f) long contact times, as in Newton and Kronig and Brink analysis of k_D or short contact time when penetration theory is applied.

In agitated vessels and extraction columns, the dispersion, or drop swarm, passes through a continuous phase which changes in composition and does offer a resistance to mass transfer.

A drop size distribution exists which gives rise to two complicating factors

(a) a distribution of drop contact time

(b) different drop behaviour (stagnant, circulating,

oscillating) within the same dispersion.

In agitated dispersions the flow pattern of the continuous phase affects the contact time of the drop according to their sizes. Small drops have larger contact time than the calculated from the expression of terminal velocity in a quiescent environment (hindered settling), since they tried to follow the turbulent motion. Drop interaction effects the repeated coalescence and redispersion of the dispersed phase, can be important depending on the extractor geometry and chemical system. Coalescence of drops in swarms causes an increase in oscillations and a decrease in surface area. These factors counteract each other with respect to mass transfer.

Most of the available empirical correlations of mass transfer coefficient in extractors or agitated vessels deals with the resistance in the continuous phase, k_c. Treybal (7) has recommended use of the relation of Barker (114) for baffled vessels using flat blade turbines.

$$\frac{k_c D}{\mathcal{D}_c} = 0.052 \, (Re_I)_c^{0.833} (Sc)_c^{0.5} \qquad (4.116)$$

where Re_I is the impeller Reynolds number. The validity of this relation is highly questionable since it was obtained from the study of solution of crystalline solids in various liquids batchwise. The application of equation (4.116) to liquid-liquid dispersions will certainly under estimate the continuous phase mass transfer coefficient since the surface of a liquid drop is mobile. Nevertheless, equation (4.116) was used by Treybal in the analysis of

the data presented by Karr and Scheibel in relation with their study of an isolated Scheibel column mixing section.

Schindler and Treybal (115) reported that k_c for the continuous flow contact of ethylacetate and water in an agitated vessel, ethylacetate dispersed, were substantially larger than might be expected from consideration of the data obtained from solid particles in agitated liquids. They measured the continuous phase resistance by using the Colburn and Welsh technique. The enhancement of the mass transfer coefficients was attributed to coalescence and redispersion of the drops of ethylacetate as they were thrown radially from the impeller and circulated to the top and bottom of the vessel, eventually around again to the impeller. For baffled vessels they correlated the data by the equation

$$k_c = k_s + 3.94 \left(\frac{\mathcal{D}_A}{\theta_c}\right)^{0.5} \qquad (4.117)$$

where k_s was estimated from the data for suspended solid particles of the same size as the drops (116) and θ_c represents the time between coalescence and redispersion. The latter was empirically estimated from observation of the change in mean drop size from the level in the vessel just opposite the impeller to that at the top and bottom

$$\frac{1}{\theta_c} = 2\left[\frac{(d_{32,T}^{\ 3} + d_{32,B}^{\ 3})/2 - d_{32,M}^{\ 3}}{d_{32,M}^{\ 3}}\right]\frac{1}{t_{ci}} \qquad (4.118)$$

The circulation time t_{ci} was estimated for the baffled vessels from the work of Holmes (117).

Years later, Mok and Treybal (118), using the same equipment as Schindler et al, intended to verify the validity of equation (4.117) which was based on the data of only one liquid-liquid system. They used the same Colburn and Welsh technique applied to paraldehyde saturated with water as the dispersed phase with water continuous. The results of their investigation are summarized:

(a) the coalescence frequency were substantially lower than those observed with ethylacetate-water of Schlinder (115)

(b) the coalescence frequency remains essentially constant with variation of Θ_D (0.1% $\longleftrightarrow$ 10%)

(c) terminal velocity measured in a long glass cylinder indicated that surface active contaminants were probably not present

(d) average drop diameter increase with hold-up

(e) all the k_c's were larger (13% to 61%) than the comparable suspended solids

(f) k_c increase with increasing agitator speed and decrease with increasing hold-up.

The low coalescing rate (point b) of the paraldehyde-water system was explained in base of the small density difference between the phases. The drops are more likely

to follow closely the fluid motion and retain their relative distances, thus offering less opportunity for collision, than with the larger density difference of ethylacetate-water. Hopefully one may use the argument above to explain also the results given in point (b).

An explanation to the increase in k_c, over that expected for solids, in terms of circulation within the drops was found to be unsound. The analysis was made using the correlation of Hughmark(119) for single drops, which estimates the ratio of k_c for circulating and rigid spheres if the particle slip or relative velocity can be estimated. It was concluded that circulation was small for the small drops (0.1 $\leftrightarrow$ 2.5mm diameter) encounted in the experiments. Finally, the situation was left without a convincing explanation.

The decrease of k_c with increased hold-up and drop diameter, at constant coalescence frequency parallels the observation made by Harriot that the mass transfer coefficient decreases with increased suspended solid particle diameter.

An overall conclusion from the work of Mok and Treybal is that much more data have to be analysed before the mechanism of coalescence-redispersion expressed by equation (4.117) and (4.118) can be accepted. One can speculate that the overall behaviour of $k_c > k_s$ and k_c decreasing with increasing Θ_D and d_{32}, may be explained by a combination of surface-drop mobility and a decreasing turbulence intensity with increasing drop population and drop diameter instead of putting all the weight on interdrop coalescence

and redispersion.

A combination of the theory of local isotropic turbulence and conventional mass-transfer correlations has been used by Calderbank and Moo-Young (120). The Kolmogoroff theory was used to give information on the turbulence intensity in the small volume around the drop. The turbulence statistical parameter describing the variation in fluctuating velocity over a distance comparable to the drop diameter $\underline{d}$, $B_{dd}(d)$ or $B_{nn}(d)$ was previously defined by equation (4.12). A square root of B_{dd} or B_{nn} is a scaler function of $\underline{d}$ with the dimensions of a velocity and it may be used in place of the velocity of the particle in correlations of mass transfer rates. According to equation (4.19), valid for the inertial subrange of the local isotropy domain, the relation

$$\sqrt{B_{dd}} = \sqrt{\overline{w^2}_{(d)}} = C(\epsilon d)^{1/3} = C\left(\frac{P}{V}\frac{1}{\rho_c} d\right)^{1/3} \qquad (4.119)$$

give the following Reynolds number for local isotropy,

$$Re = \left(\frac{\sqrt{\overline{w^2}_{(d)}}\ d\ \rho_c}{\mu_c}\right) = \frac{d^{4/3}\ \rho_c^{2/3}\ (P/V)^{1/3}}{\mu_c} \qquad (4.120)$$

If the usual functional relationship between the Sherwood, Schmidt and Reynolds numbers for mass transfer is assumed, the following relation is obtained;

$$\frac{k_c d}{\mathcal{D}_c} \propto \left(\frac{\mu_c}{\rho_c \mathcal{D}}\right)^x \left(\frac{\rho_c^{1/3}\ (P/V)^{1/6}\ d^{2/3}}{\mu_c^{1/2}}\right)^y \qquad (4.121)$$

Mass transfer data for mixing vessels were correlated according to equation (4.121) to give

$$k_c = 0.13 \left(\frac{(P/V)\ \mu_c}{\rho_c^2}\right)^{1/4} / \left(\frac{\mu_c}{\rho_c \mathcal{D}_c}\right)^{1/4} \qquad (4.122)$$

Equation (4.122) originally obtained by Calderbank and Moo-Young for gas-liquid system, has been recommended by Misek (13) for R.D.C. Equation (4.122) can be put in the form of impeller Reynolds Number to yield

$$\frac{k_c D_I}{\mathcal{D}} = 0.13 \ (N_p)^{1/4} (Re_I)_c^{3/4} (Sc)_c^{1/3} \left(\frac{d_I^3}{\text{Tank Volume}}\right)^{1/4} \qquad (4.123)$$

where N_p is the Power Number

Keey and Glen (121) studied the continuous-phase mass transfer coefficient for the system iso-octane-o-nitrophenol (solute)/water in continuously operated baffled vessel agitated with various sizes of six-blade paddles.

An expression was derived on the assumption that the drops are surrounded by a turbulent boundary layer (36)) within it the turbulence is gradually damping in the vicinity of the interface (122), as follows

$$\frac{k_c D_I}{\mathcal{D}} = C_o \ (Re_I)_c^{1.375} \ (Sc)_c^{0.5} \qquad (4.124)$$

Their experimental data, obtained at hold-up values of around 5%, were correlated by the equation

$$\frac{k_c D_I}{\mathcal{D}} = 8.92 \times 10^{-4} (Re_I)^{1.36} D_c^{-0.5} D_I^{-0.36} - 338 \quad (4.125)$$

$$10^4 < Re_I < 10^5$$

Recently, Skelland and Lee (123) presented a mass transfer coefficient correlation based on penetration theory with Kolmogoroff's time scale. The penetration time t_c of the Higbie equation (4.90) was assumed to be equal to the Kolmogoroff's time scale

$$t_k = \left(\frac{\nu}{\epsilon}\right)^{\frac{1}{2}} \quad (4.126)$$

Combining equation (4.90), (4.126) and the expression for energy per unit mass for a fully baffled agitated vessel, the following expression was obtained assuming vessel diameter D_c, equal vessel height H,

$$\frac{k_c}{\sqrt{N\mathcal{D}}} = C_o \left(\frac{D_I}{D_c}\right)^{0.75} \left(\frac{D_I^2 N \rho_c}{\mu_c}\right)^{0.25} \quad (4.127)$$

Influence of the hold-up on k_c was suspected and later confirmed when the data from batch operation of an agitated vessel were correlated by the equation

$$\frac{k_c}{\sqrt{N\mathcal{D}}} = 2.932(10^{-7}) \theta_D^{-0.508} \left(\frac{D_I}{D_c}\right)^{0.548} (Re_I)^{1.371} \quad (4.128)$$

The significant difference between the exponents on any given variable of equation (4.128), (4.127) and (4.125) suggest that these data are not well correlated with expressions derived from penetration theory with Kolmogoroff's time scale and from turbulent boundary layer theory.

Dispersed phase mass transfer coefficient, k_D, in an agitated and turbulent swarms of drops has been much more difficult to analyse and correlate within a theoretical framework. While k_c seems to be possible to analyse with the turbulence theory, and derived hydrodynamic concepts, the interpretation of k_d based on turbulence parameters is extremely difficult. For example, an initially rigid single drop may be transformed into a non-rigid drop during its passage through the turbulent environment owing to a gain of an amount of energy transmitted from the turbulent eddies of the continuous phase. This situation is complicated by the fact that the dispersed phase consists of a distribution of drops spanning different hydrodynamic regimes and each drop will be affected differently by the continuous phase turbulent motion. The situation becomes even worse when the phenomena of interdrop coalesence-redispersion and interfacial turbulence are added.

Under the circumstances that no reliable correlations for k_c and k_d exist, the different relationships applicable to single drops in a quiescent environment are the only available solution. This approach has the advantage that in the design of an agitated column or vessel one takes the conservative basis since the mass transfer coefficients predicted from single drop correlations are usually lower than values obtained in agitated systems.

4.3 The Driving Force - ΔC

4.3.1 Measurement of the Concentration Profiles

A very important requirement in understanding and modelling the operation of a liquid-liquid extraction column is a knowledge of the composition of each phase throughout the length of the column.

Geankoplis and Hixson (124) were the first to obtain continuous phase concentration profiles in a spray column by withdrawing samples at various positions using a hook shaped sampling probe at the end of a tube which was inserted from the top of the column. Slow sampling rates were necessary in order to avoid disturbances in the extraction process as well as entrainment of the dispersed phase and the large hold-up in the tube must have introduced errors.

The use of hypodermic needles for the sampling of the continuous phase was pioneered by Gier and Hougen (125) in their studies of both packed and spray columns. For the first time they obtained samples of the dispersed phase by use of a series of downward-facing funnel-shaped samplers. A fast rate of dispersed phase withdrawal was considered necessary in order to avoid a significant amount of solute transfer when the drops were being coalesced and collected inside the funnel. This resulted in a significant amount of the continuous phase being entrained. Entrainment was reported to occur occasionally in the continuous phase samples. The measured dispersed phase concentration

had to be corrected due to entrainment in order to obtain the true column concentration.

Cavers and Ewanchyna (126) combined the sampling technique of Gier (125) and Geonkoplis (124) in their study of spray columns. They used a hook-shaped probe to obtain continuous phase samples and a funnel-shaped probe for the dispersed phase samples, each being attached to the end of a tube inserted from the top of the column. While clean continuous phase samples were obtained with the hook-shaped probe, it was not possible to obtain uncontaminated dispersed phase samples with the funnel-shaped probe.

Smoot and Babb (127) were among the first to use samplers made from materials preferentially wetted by the phase to be sampled. They sampled both phases in a pulsed column using hypodermic needles. Stainless steel needles, preferentially wetted by water, were used to sample the aqueous continuous phase above each sieve plate. The organic dispersed phase was sampled below each sieve plate using needles with flared polyethylene sleeve pointing downwards. Essentially, the same technique was used by Souhrada et al (128) on a vibrating plate extractor.

The work done by Chiu (129) and Honekamp (2,21) are very important to this research, since both workers investigated the behaviour of a York -Scheibel column. Chiu studied the steady state and transient behaviour of the column by

comparing a perfect-mixed-cell model with the experimental concentration profiles. Samples of each phase were obtained by use of a copper cup soldered onto the tip of a stainless steel hypodermic needle. Samples were removed from the column by withdrawing the liquid into 2.0cc syringes. The aqueous continuous phase was withdrawn when the cup was concave upward and the MIBK dispersed phase when the cup was concave downward. No failures were reported and the significant amount of scattering in some of the profiles was attributed to errors incurred in the chemical analysis of the samples, and to the fluctuations of the composition in the column resulting from the adjustment of the effluent stream at the bottom to maintain the interface.

Honekamp (2,24) determined the amount of extraction that tok place in the York mesh packing of a 4 stage Scheibel column by using a sampling technique to obtain point concentration of both phases inside the packing at the extremes of the packing sections. The principle of using an organophilic sampler for the organic phase and a hydrophilic sampler for the aqueous phase was again applied. For the aqueous continuous phase, an 18-gauge stainless steel hypodermic needle was used. For the MIBK dispersed phase a 12-gauge stainless steel hypodermic needle packed with -28+48 mesh granulated aluminium coated with polyethylene was used. The external surface of the packed needle was also coated with polyethylene. Samples were collected at very low flow rates (0.5 cc per minute) and in some cases contamination was unavoidable

and two-phase samples were withdrawn from the column. The concentration profiles were stagewise, showing a large concentration change across the packing and a small concentration change across the mixing chamber due to the axial mixing.

A completely different approach to sampling was presented by Treybal (130). He withdrew a two-phase sample from the column, allowed equilibrium to be reached and then measured the volumes of the collected phases and their equilibrium concentrations. The simultaneous solution of the sample solute balance equation and the operating line equation gives the composition of each phase within the column. At the time this article was published (1955), the effects of axial dispersion or back-mixing on the concentration profiles were not fully recognised and the assumption adopted by Treybal of plug flow in the column to obtain the equation of the operating line seem justifiable.

Bibaud and Treybal (82) used the single two-phase sampling technique to determine the concentration profiles in an Oldshue-Rushton column. The determination of the operating line was done by the method proposed by Rod (131) which takes into account the axial mixing of the phases. This method requires the knowledge of the overall mass transfer coefficient, the mass transfer specific interfacial area and the eddy axial diffusivity of each phase and the location of the operating line had to be done by a trial and error procedure when axial mixing

was present in both phases. It is clear that the amount and type of information needed to locate the true operating line makes the single two-phase sampling technique of very little value.

The double two-phase sampling technique was first mentioned by Honekamp (2) and thoroughly investigated by Pollok and Johnson (132). It consisted in simultaneous withdrawal of two two-phase samples from essentially the same locations in the column. The samples are allowed to equilibrate and the final concentrations, as well as phase volumes, were measured. Providing that the ratio of the volumes of the two phases are not equal, the concentration of each phase in the column could be determined by solving a pair of simultaneous material balance equations, one equation written for each two-phase sample. The reported (132) experimental results were poor and inconclusive. This problem was attributed to errors in the volume measurements, especially when samples were small, difficulties in achieving a complete phase separation in the collector and obtaining representative samples.

From this review of sampling techniques it can be concluded that:

1. Two-phase sampling techniques, either single or double, are subject to large experimental error and especially the first require information that in general is the final objective of a research programme;

2. The most suitable technique, single-phase sampling, was in general tested in relatively calm regions of extraction columns (with the possible exception of Souhrada (128) for a high frequency of vibration), and no work has been reported of such techniques being successfully applied to highly agitated mixing compartments.

A novel single phase sampling technique suitable to operate in agitated vessels has been designed by the author (133) and detailed presentation of this technique is given in section 7.3

4.3.2 Axial Mixing and Mathematical Models

4.3.2.1 Axial Mixing Concept

It has been common practice in the past to design extraction columns or to interpret experimental results by assuming perfect countercurrent plug-flow for both phases. Since Newman's work (134) it is nowadays completely accepted that considerable nonidealities or deviations from plug-flow exists in the column flow patterns which cause appreciable reduction in the departure from equilibrium, the driving force (Δc) and hence, of column performance. All phenomena that lead to a deviation from plug-flow conditions, distribution of residence times in the phases, are known collectively as "axial mixing" or "longitudinal mixing". The effect on the driving force and the concentration profiles is illustrated in figure 4.8 where it is observed a sudden concentration change at each

Figure 4.8 - Effect of Axial Mixing on Concentration Profiles in the Column

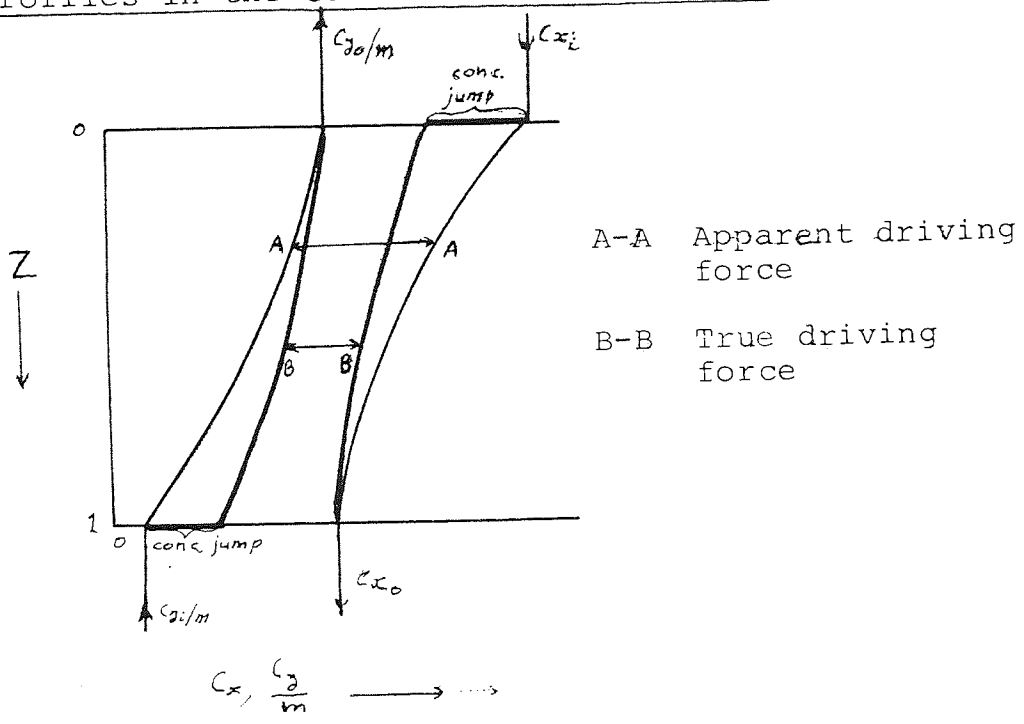

(a) Concentration profile

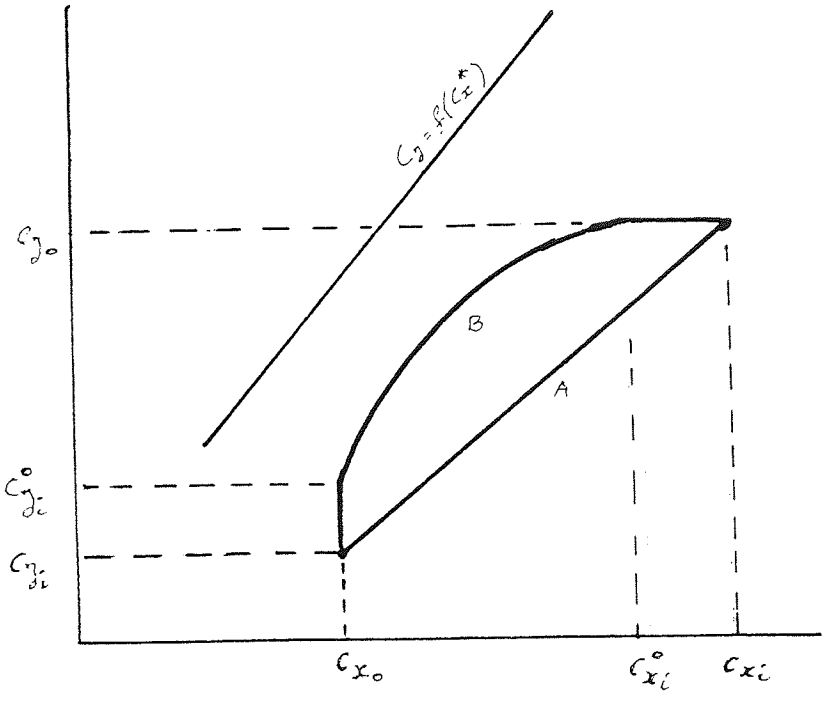

(b) Operating Diagram

inlet and a zero concentration slope at each outlet. The mean potential is much less for curves B than for the piston flow case, illustrated by curves A.

The overall observed effect of longitudinal mixing in liquid-liquid extraction columns are the combined result of several phenomena which will vary according to the type of contactor and the flow conditions within it. Longitudinal mixing in the continuous liquid phase may be considered to be the sum of two effects, the first of which is a true turbulent and molecular diffusion in the axial direction characterized either by an eddy diffusivity or a back mixing coefficient. This may be manifested by vertical circulation currents, or mixing in the eddies from the wakes of the dispersed drops, entrainment of the continuous phase by the drops or forced back mixing action due to turbulence in the column. The second effect is a spreading effect that is specific in the forward direction. This may be caused by non-uniform velocity across the cross section of the column or a channelling phenomenon or a Taylor type of diffusion. This effect predominates over the eddy diffusion in columns operated under non or very small degrees of agitation. Although turbulent effects and drops entrainment may be important for the dispersed phase, an exceedingly dominating contribution to the total axial mixing of this phase is the one caused by the distribution of residence times in the drop swarm, which results from the distribution of the drop sizes and the distribution in rising velocities for the drops. This phenomena is commonly known as "forward mixing".

The determination of the total axial mixing in the column can be done in different ways:

(a) from the concentration profiles

(b) by "stimulus-response" technique

Evaluation of the total axial mixing from solute concentration profiles requires the withdrawal of a sufficient number of samples along the extraction column length during steady state mass transfer. The longitudinal mixing can then be evaluated by comparing the experimental concentration profiles with theoretical values computed from an appropriate non-ideal flow model. Often it is not possible to take internal samples and only the overall performance is available. In this case, the longitudinal mixing is found by the "stimulus-response" technique. This technique uses the injection of tracers into the system during steady state operation and the experiments take two main forms according to whether a steady state or a transient injection of traces is used. In the steady state variation, a steady and continuous stream of tracer is injected into the column and the steady state concentration profile of the tracer is measured in the column upstream of the point of injection. This technique measures only those flow mechanisms that are actually capable of causing physical backflow of material (true physical backmixing). The dynamic method, the truly simultaneous-response technique, imposes a varying tracer concentration at the inlet stream and observes the corresponding response at the exit stream of the system, as in the

standard determinations of residence time distributions in flow systems. Input concentration disturbances may take any form but the most used are the impulse, pulse, step, ramp, parabolic and sinusoidal. This method measures the overall non-ideal flow behaviour, that is the total axial mixing. The break-through curves obtained in the two types of tracer analysis (steady and transient) can be compared with the form of the curves calculated according to the appropriate flow model. From this comparison, it should then be possible to quantify the axial mixing, according to the value of the particular parameter in the flow model which gives the best fit to the experimental and theoretical curves. More details about these techniques are given in the Wen and Fan (135) monograph.

4.3.2.2 Mathematical Models

A description of mass transfer can be made in equipment in which axial mixing of phases occurs by a diffusion model (136, 10,9) differential contact equipment and the so-called cell models with backflow (138,139) for stagewise equipment. Thus:-

4.3.2.2.1 Diffusion Model

In this model, the also called "axial dispersion model" or the "dispersed plug-flow model", the various contributions causing deviations from plug flow are all assumed to follow an eddy diffusion relationship, analogous in form to Ficks law for molecular diffusion, but in which the dispersion

is characterised by a constant value of an eddy diffusion coefficient, appropriate to the given conditions.

The formulation of the model, with a graphical description given by Figure 4.9, is based on the following assumptions;

1. The dispersed phase can be considered as a second continuous phase.

2. Deviation of plug flow may be characterised for the whole equipment by a constant axial eddy diffusivity, E.

3. Mean velocity and concentration of each phase are constant across the column diameter.

4. Solvents are immiscible.

5. Volume rates of solvent and feed raffinate does not change with height.

6. The volumetric overall mass transfer coefficient $K_x a$ or $K_y a$ are constant throughout the column.

7. There is a smooth variation in concentration profiles.

8. The streams coming into the column have uniform concentration and zero axial mixing.

Material balances on each phase over the differential volume of height δ_2 gives

Figure 4.9 - Diffusion Model

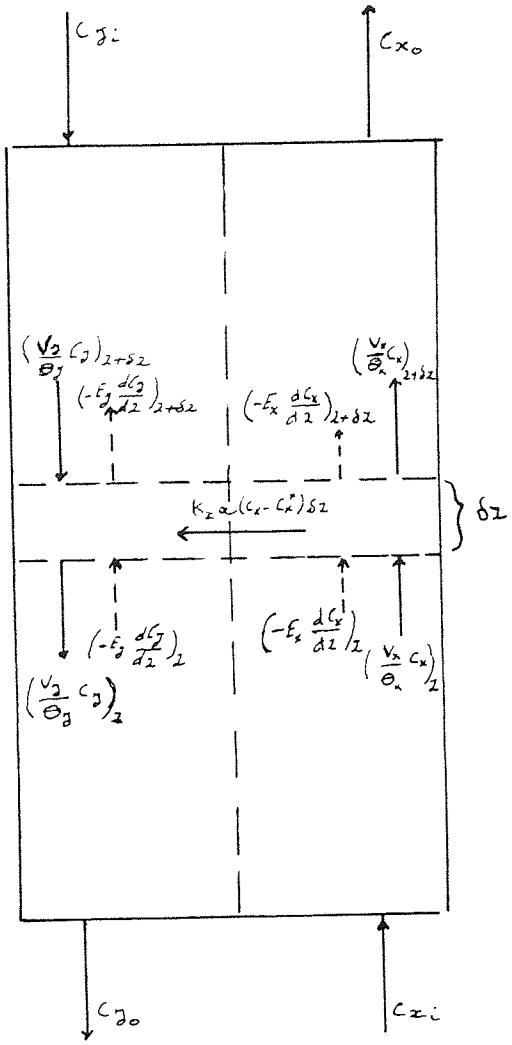

Raffinate phase $$E_x \frac{d^2C_x}{d_z^2} - \frac{V_x}{\theta_x}\frac{dC_x}{d_z} - \frac{K_x a}{\theta_x}(C_x - C_x^*) = 0 \qquad (4.129)$$

Solvent phase $$E_y \frac{d^2C_y}{d_z^2} + \frac{V_y}{\theta_y}\frac{dC_y}{d_z} + \frac{K_x a}{\theta_y}(C_x - C_x^*) = 0 \qquad (4.130)$$

or

$$e_x \frac{d^2C_x}{d_z^2} - V_x \frac{dC_x}{d_z} = K_x a\,(C_x - C_x^*) \qquad (4.131)$$

$$e_y \frac{d^2C_y}{d_z^2} + V_y \frac{dC_y}{d_z} = -K_x a\,(C_x - C_x^*) \qquad (4.132)$$

For a linear equilibrium relationship

$$C_x^* = mC_y + q \qquad (4.133)$$

the following dimensionless variables can be defined

$$X = \frac{C_x - (mC_{yi} + q)}{C_{xi} - (mC_{yi} + q)} \qquad (4.134)$$

$$Y = \frac{m(C_y - C_{yi})}{C_{xi} - (mC_{yi} + q)} \qquad (4.135)$$

$$Z = \frac{z}{L} \qquad (4.136)$$

Substitution of equations (4.134) (4.135) and (4.136) on equations (4.131) and (4.132) gives

$$\frac{d^2X}{dZ^2} - (Pe)_x \frac{dX}{dZ} = (No)_x (Pe)_x (X - Y) \qquad (4.137)$$

$$\frac{d^2Y}{dZ^2} + (Pe)_y \frac{dY}{dZ} = - (No)_x (Pe)_y F(X - Y) \qquad (4.138)$$

where

$$(Pe)_x = \text{Raffinate Peclet Number} = \frac{V_x L}{e_x}$$

$$(Pe)_y = \text{Solvent Peclet Number} = \frac{V_y L}{e_y}$$

$$(No)_x = \text{Raffinate Number of Transfer Unit} = \frac{K_x a L}{V_x}$$

$$F = \text{Extraction factor} = \frac{V_x m}{V_y}$$

The necessary boundary conditions to solve the above system of equations are obtained as follows. Consider a very small boundary region at the x-phase entrance ($z = 0$) such that the amount of mass transfer between the phases can be neglected.

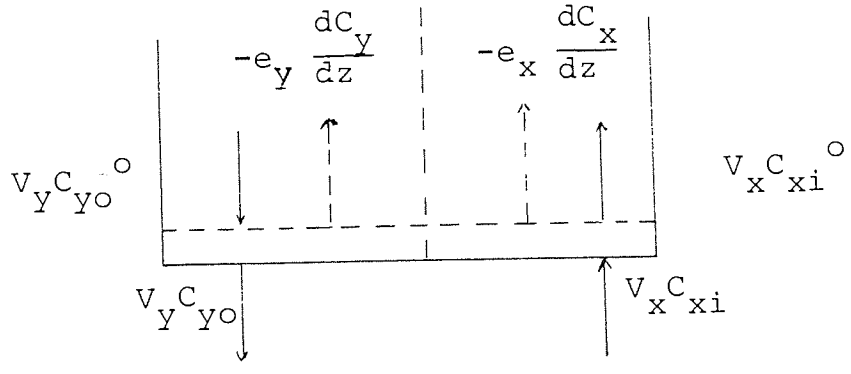

A material balance on the raffinate x-phase gives

$$V_x C_{xi} = V_x C_{xi}^{o} - e_x \left(\frac{dC_x}{dz}\right)_{z=0^+} \tag{4.139}$$

or

$$(C_{xi} - C_{xi}^{o}) = - \frac{e_x}{V_x} \left(\frac{dC_x}{dz}\right)_{z=0^+}$$

where equation (4.139) quantifies the x-phase concentration jump at the column inlet. In terms of the dimensionless variables defined above, equation (4.139) takes the form

$$-\left(\frac{dX}{dZ}\right)_{z=0^+} = (Pe)_x (1 - X_i^{o}) \tag{4.140}$$

A material balance on the y-phase gives

$$V_y C_{yo}^{o} = V_y C_{yo} - e_y \frac{dC_y}{dz} \tag{4.141}$$

or in dimensionless form

$$\frac{1}{(Pe)_y} \left(\frac{dY}{dZ}\right)_{z=0^+} = Y_o - Y_o^{o} \tag{4.142}$$

Since $\frac{1}{(Pe)_y} \geq 0$, $\frac{dY}{dZ} \leq 0$ and $Y_o - Y_o^{o} \geq 0$, the only conditions that satisfy equation (4.142) is

$$\left(\frac{dY}{dZ}\right)_{z=0^+} = 0; \quad Y_o = Y_o^{o} \tag{4.143}$$

A similar analysis at the top of the column gives the rest of the boundary conditions

$$\left(\frac{dX}{dZ}\right)_{z=1^-} = 0; \qquad X_o^{\,o} = X_o \tag{4.144}$$

$$\left(\frac{dY}{dZ}\right)_{z=1^-} = -\,Y_i^{\,o}\,(Pe)_y \tag{4.145}$$

where $Y_i^{\,o}$ is the y-phase inlet concentration jump.

In summary, the mathematical formulation of the model is

$$\frac{d^2X}{dZ^2} - (Pe)_x \frac{dX}{dZ} = (No)_x (Pe)_x\,(X-Y)$$

$$\frac{d^2Y}{dZ^2} + (Pe)_y \frac{dY}{dZ} = -(No)_x (Pe)_y F(X-Y)$$

Boundary conditions:

$$-\left(\frac{dX}{dZ}\right)_{z=0} = (Pe)_x (1-X_i^{\,o})$$

$$\left(\frac{dY}{dZ}\right)_{z=0^+} = 0$$

$$\left(\frac{dX}{dZ}\right)_{z=1^-} = 0$$

$$\left(\frac{dY}{dZ}\right)_{z=1^-} = -\,Y_i^{\,o}\,Pe_y$$

The system of second order differential equations (4.137) and (4.138) is solved by using matrix algebra with the differential operation to give

$$\bar{X} = A_1 + A_2 e^{\lambda_2 Z} + A_3 e^{\lambda_3 Z} + A_4 e^{\lambda_4 Z} \tag{4.146}$$

$$Y = A_1 + A_2 a_2 e^{\lambda_2 Z} + A_3 a_3 e^{\lambda_3 Z} + A_4 a_4 e^{\lambda_4 Z} \tag{4.147}$$

where λ_i, i = 2,3,4 are the roots of the characteristic equation

$$\lambda^3 - ((Pe_x) - (Pe)_y)\lambda^2 - (No_x Pe_x + Pe_x Pe_y + No_x Pe_y F)\lambda - No_x Pe_x Pe_y (1-F) = 0 \tag{4.148}$$

and a_i, i = 2,3,4 are calculated by

$$a_i = 1 + \frac{\lambda_i}{No_x} - \frac{\lambda_i^2}{No_x Pe_x} \tag{4.149}$$

The coefficient A_1, A_2, A_3 and A_4 are determined by substituting equation (4.146) and (4.147) into the four boundary conditions. The resulting four linaar algebraic equations are expressed in maxtrix form by

$$\begin{bmatrix} 1 & (1-\lambda_2/Pe_x) & (1-\lambda_3/Pe_x) & (1-\lambda_4/Pe_x) \\ 0 & a_2\lambda_2 & a_3\lambda_3 & a_4\lambda_4 \\ 1 & (1+\lambda_2/Pe_y)a_2 e^{\lambda 2} & (1+\lambda_3/Pe_y)a_3 e^{\lambda 3} & (1+\lambda_4/Pe_y)a_4 e^{\lambda 4} \\ 0 & \lambda_2 e^{\lambda 2} & \lambda_3 e^{\lambda 3} & \lambda_4 e^{\lambda 4} \end{bmatrix} \cdot \begin{bmatrix} A1 \\ A_2 \\ A_3 \\ A_4 \end{bmatrix} = \begin{bmatrix} 1 \\ 0 \\ 0 \\ 0 \end{bmatrix} \tag{4.150}$$

A computer program to solve equations (4.146), (4.147), (4.148), (4.149) and (4.150) has been written and is given in Appendix 3. The program generates X- and Y- profiles from $Z = 0^+$ to $Z = 1^-$ for different values of the parameters No_x, Pe_x and Pe_y.

Analytical solutions for various special cases, each involving at least one less degree of freedom than in the above general case, were summarised by Miyauchi and Vermeulen (9). Approximate analytical solution (140), (141) suitable for quick manual calculation has also been published. These approximations are useful for design purposes since they can be made explicit in L (length of the extractor).

Until this point we have been concerned only with linear model, that is the rate process is linear with respect to concentration (straight equilibrium line). Only under this condition and with the assumptions listed above, analytical solutions can be found.

For situations of non-linear rate process (curve equilibrium line), solutions must be obtained numerically. Numerical solutions of the diffusional model generally begin with the substitution of standard finite-difference approximations for the differential terms. Rod (131) presented a graphical method to be applied with the distribution diagram which permits solution of the difference equations. The technique is straightforward when axial mixing is present only in one phase, but for the general case of axial mixing in both phases, a trial and error approach based on the method of boundary-value iteration, is required.

Mecklenburgh and Hartland (142) have found that this end to end approach can be very difficult or impossible to converge and they suggested that the set of difference equations be solved simultaneously by Newton-Raphson methods or other high order convergence scheme, or more conveniently to formulate the problem in terms of the cell-backflow model.

4.3.2.2.2 Cell-Backflow Model

This model is closely related to the one used by Sherwood (143) and Colburn (144) to describe mass transfer in absorption towers and distillation columns with entrainment. The basic "perfect mixed cells in series with backflow" model has been introduced by Sleicher (138) in his studies of the entrainment and its effect on the extraction efficiency of Mixer-Settlers. The analytical solutions of the general and special cases of the linear version of this model is well presented by Misek and Rod (145).

Two formulations of the non-linear case exist, that of Prochaska and Landau (146) and that of Miyauchi and Vermeulen (147). Both approaches write the same material balance equations of each stage of a N-cell or stage cascade for rafinate and solvent phase separately obtaining a set of 2N non-linear equations, but different kinetic expressions are used in each model. Prochazka et al. characterized the kinetic of the process using the concept of stage efficiency while Miyauchi et al. adopted the standard overall mass transfer coefficient approach. The former does not require a previous knowledge or

assumption of the flow behaviour inside each cell; on the contrary, the second assumes a perfect mixing situation in both phases in each stage. Axial variation in backflow parameters, distribution coefficient and stage efficiency or mass transfer coefficient can be readily introduced in the model according with the available degree of freedom of the system under study.

A graphical representation of the N-cell backflow model is shown in Figure 4.10 and a detailed derivation of the Prochazka version, adopted in this research, is given below.

Figure 4.10 - n-cells in series with backflow model

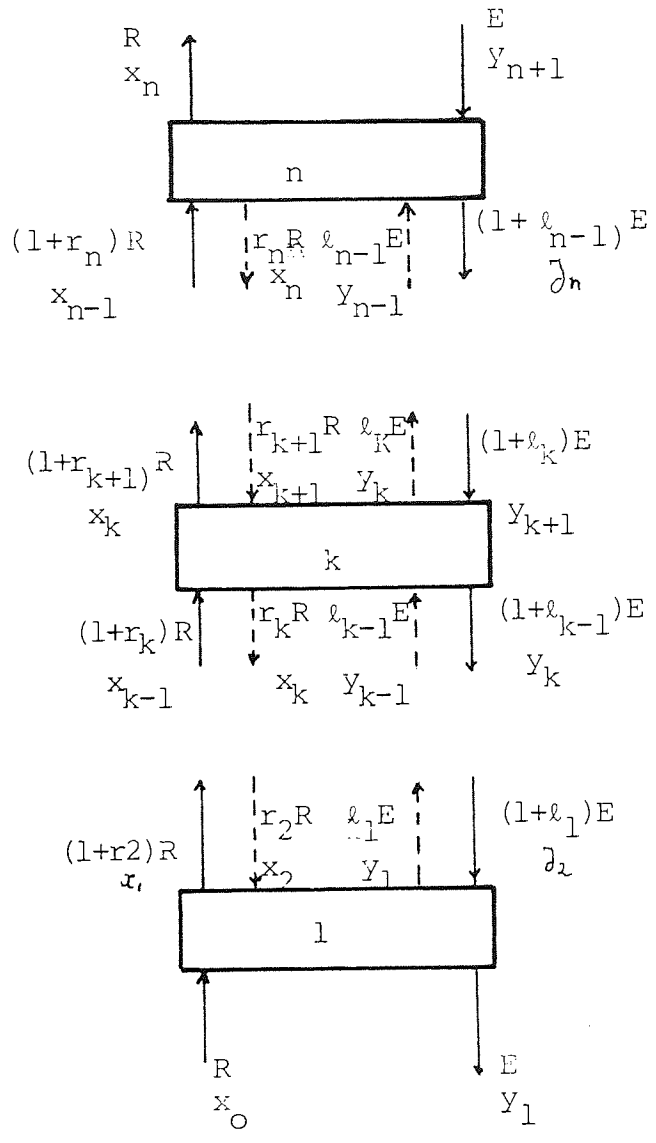

For the case of immiscible solvents, the material balance on the solute for the k^{th} stage can be written as

$$(1+r_k)x_{k-1}^{\alpha} + r_{k+1}x_{k+1}^{\alpha} + (1+\ell_k)y_{k+1} + \ell_{k-1}y_{k-1} =$$

$$(1+r_{k+1})x_k^{\alpha} + r_k x_k^{\alpha} +$$

$$(1+\ell_{k-1})y_k + \ell_k y_k \qquad (4.151)$$

where $\alpha = \frac{R}{E}$

Defining an average stage inlet concentration as,

$$x_{k-1}^{1} = \frac{(1+rk)x_{k-1}^{\alpha} + r_{k+1}x_{k+1}^{\alpha}}{(1+r_k+r_{k+1})^{\alpha}} \qquad (4.152)$$

and

$$y_{k+1}^{1} = \frac{(1+\ell_k)y_{k+1} + \ell_{k-1}y_{k-1}}{(1+\ell_k + \ell_{k-1})} \qquad (4.153)$$

then after substitution of equation (4.151)

$$(1+r_k+r_{k+1})^{\alpha} x_{k-1}^{1} + (1+\ell_k+\ell_{k-1})y_{K+1}^{1} = (1+r_k+r_{k+1})^{\alpha}x_k +$$

$$+ (1+\ell_k+\ell_{k-1})y_k \qquad (4.154)$$

Defining

$$\alpha_k^{1} = \frac{\alpha(1+r_k+r_{k+1})}{(1+\ell_k+\ell_{k-1})} \qquad (4.155)$$

then

$$\frac{y_k - y_{k+1}^{1}}{x_{k-1}^{1} - x_k} = \alpha_k^{1} \qquad (4.156)$$

A stage efficiency corresponding to the kth stage, η_k, is defined as

$$\eta_{k,x} = \frac{x_{k-1}^{l} - x_k}{x_{k-1}^{l} - x_k^*} \quad \text{or} \quad \eta_{k,y} = \frac{y_k - y_{k+1}^{l}}{y_k^* - y_{k+1}^{l}} \tag{4.157}$$

where x_k^* and y_k^* are equilibrium concentrations that satisfy the following material balance

$$(1+r_k + r_{k+1})x_{k-1}^{l}\alpha + (1+\ell_k + \ell_{k-1})y_{k+1}^{l} =$$

$$(1+r_{k+1} + r_k)x_k^*\alpha + (1+ \ell_k + \ell_{k-1})y_k^* \tag{4.158}$$

This last material balance equation can be expressed in the form

$$\frac{y_k^* - y_{k+1}^{l}}{x_{k-1}^{l} - x_k^*} = \alpha_k^{l} \tag{4.159}$$

It can be shown that for the stage efficiency defined above

$$\eta_{k,x} = \eta_{k,y}$$

To complete the formulation of the model a general equilibrium relationship is given by

$$y_k^* = D_k x_k^* + G_k \tag{4.160}$$

and the boundary conditions established by the following equalities

$$r_1 = r_{n+1} = \ell_o = \ell_n = 0 \tag{4.161}$$

Equations (4.156), (4.157), (4.159) and (4.160) plus the boundary conditions equation (4.161) constituted the mathematical formulation of the stagewise model. Algebraic manipulation of these four equations leads to the following set of linear algebraic equations

$$(1+r_k)x_{k-1}^{\alpha} + \ell_{k-1}\, y_{k-1} - (1+r_k + r_{k+1})x_k^{\alpha} -$$

$$(1+\ell_k + \ell_{k-1})y_k + r_{k+1}x_{k+1}^{\alpha} + (1+\ell_k)y_{k+1} = 0 \qquad (4.162)$$

$$(1-\eta_k)(1+r_k)x_{k-1} - \frac{\left[1+(1-\eta_k)\beta_k^1\right]}{(1+\beta_k^1)}(1+r_k+ r_{k+1})x_k +$$

$$\frac{\eta_k(1+r_k + r_{k+1})}{D_k(1+\beta_k^1)}y_k + (1-\eta_k)r_{k+1}x_{k+1} =$$

$$\frac{\eta_k(1+r_k + r_{k+1})}{D_k(1+\beta_k^1)} \cdot G_k \qquad (4.163)$$

where β_k^1 is a modified extraction factor defined as

$$\beta_k^1 = \frac{\alpha(1+r_k + r_{k+1})}{D_k(1+\ell_k+\ell_{k-1})}$$

Equations (4.162) and (4.163) define the state of the system from stage 2 to (n-1) inclusive. The first and last stage have different expressions due to the boundary conditions;

First Stage:

$$\alpha x_o - \alpha(1+r_2)x_1 - (1+\ell_1)y_1 + \alpha r_2 x_2 + (1+\ell_1)y_2 = 0 \quad (4.164)$$

$$(1-\eta_1)x_o - \frac{\left[1+(1-\eta_1)\beta_1^1\right]}{(1+\beta_1^1)}(1+r_2)x_1 + \frac{\eta_1(1+r_2)}{D_1(1+\beta_1^1)}y_1 +$$

$$(1-\eta_1)r_2 x_2 = \frac{\eta_1(1+r_2)}{D_1(1+\beta_1^1)}G_1 \quad (4.165)$$

n-Stage (last):

$$(1+r_n)x_{n-1}\alpha + \ell_{n-1}y_{n-1} - (1+r_n)x_n\alpha - (1+\ell_{n-1})y_n + y_{n+1} = 0 \quad (4.166)$$

$$(1+\eta_n)(1+r_n)x_{n-1} - \frac{\left[1+(1-\eta_n)\beta_n^1\right]}{(1+\beta_n^1)}(1+r_n)x_n +$$

$$\frac{\eta_n(1+r_n)}{D_n(1+\beta_n^1)}y_n = \frac{\eta_n(1+r_n)}{D_n(1+\beta_n^1)}G_n$$

Equation (4.162), (4.164), (4.166) (material balance equations) and equations (4.163), (4.165), (4.167) (kinetic relations) describe the whole system and they can be written in matrix form as;

$$\left[\ A\ \right] \cdot \left[\ x\ \right] = \left[\ C\ \right] \quad (4.168)$$

where

$\left[\ A\ \right]$ = Hexadiagonal coefficient matrix (2n)x(2n+2)

$\left[\ x\ \right]$ = $(x_o, x_1, y_1, x_2, y_2, \ldots, x_n, y_n, y_{n+1})^T$ = concentration vector (2n+2)

$\left[\ C\ \right]$ = vector (2n) of the right hand sides of the kinetic relations

The elements of the coefficient matrix $[A]$ are generated according to the following procedure,

Even rows generated by Equation (4.162):

$$i = 2k; \quad k = 2, \quad \ldots, \quad n-1$$

$$a_{i,i-2} = \alpha(1+r_k)$$

$$a_{i,i-1} = \ell_{k-1}$$

$$a_{i,i} = -\alpha(1+r_k + r_{k+1})$$

$$a_{i,i+1} = -(1+\ell_k + \ell_{k-1})$$

$$a_{i,i+2} = \alpha r_{k+1}$$

$$a_{i,i+3} = (1+\ell_k)$$

Odd rows generated by Equation (4.163):

$$i = 2k-1, \quad k = 2, \quad \ldots, \quad n-1$$

$$a_{i,i-1} = (1-\eta_k)(1+r_k)$$

$$a_{i,i} = 0$$

$$a_{i,i+1} = -\frac{(1+r_k + r_{k+1})\left[1+(1-\eta_k)\beta_k^1\right)}{(1+\beta_k^1)}$$

$$a_{i,i+2} = \eta_k(1+r_k + r_{k+1})/D_k(1+\beta_k^1)$$

$$a_{i,i+3} = (1-\eta_k)\, r_{k+1}$$

Elements generated by the first stage Equations (4.164), (4.165) are,

Even elements:

$$i = 2k; \quad k = 1$$

$$a_{21} = \alpha$$

$$a_{22} = -\alpha(1+r_2)$$

$$a_{23} = -(1+\ell_1)$$

$$a_{24} = \alpha r_2$$

$$a_{25} = (1+\ell_1)$$

Odd elements:

$$i = 2k-1; \quad k = 1$$

$$a_{11} = (1-\eta_1)$$

$$a_{12} = -\frac{\left[1+(1-\eta_1)\beta_1^1\right]}{(1+\beta_1^1)}$$

$$a_{13} = \frac{\eta_1(1+r_2)}{D_1(1+\beta_1^1)}$$

$$a_{14} = (1-\eta_1)r_2$$

Elements generated by the last stage equations (4.166) and (4.167) are,

Even elements:

$$i = 2k; \quad k = n$$

$$a_{i,i-2} = \alpha(1+r_n)$$

$$a_{i,i-1} = \ell_{n-1}$$

$$a_{i,i} = -\alpha(1+r_n)$$

$$a_{i,i+1} = -(1+\ell_{n-1})$$

$$a_{i,i+2} = 1$$

Odd elements:

$$i = 2k-1; \quad k = n$$

$$a_{i,i-1} = (1+\eta_n)(1+r_n)$$

$$a_{i,i} = 0$$

$$a_{i,i+1} = \frac{-(1+r_n)\left[1+(1-\eta_n)\beta_n^1\right]}{(1+\beta_n^1)}$$

$$a_{i,i+2} = \frac{\eta_n(1+r_n)}{D_n(1+\beta_n')}$$

The elements of the $[C]$ vector are generated as;

Even elements = 0

Odd elements:

$$i = 2k-1, \quad k = 1, \quad \ldots n$$

$$c_i = a_{i,i+2} \cdot G_k$$

The matrix equation (4.168) allows the calculation of the stagewise concentration profile if the rafinate and extract back mixing parameters (r_k, ℓ_k) and the efficiencies are known. On the other hand, when experimental concentration profiles are available the model parameters can be estimated from the same equation by a data fitting procedure (148)(149). It is necessary to mention that the degree of freedom of the model limits the number of parameters to be evaluated to 2n according to the following analysis;

total number of unknown parameter:

n	→	η_k
n-1	→	r_k
n-1	→	ℓ_k
3n-2		

total number of equations = 2n

Degree of freedom = n-2

Then (n-2) independent equations or constraints must be introduced in the model in order to make the problem just determined. Several ways are open to specify the (n-2)

equations:

1. Independent measurement of the back mixing parameters ℓ_k or r_k i.e., tracer analysis.

2. Use mean values of r_k and ℓ_k for every two consecutive stage and calculate them by material balance.

3. Based on experience and some known behaviour of the column under studied, assume equal value of the parameters for a specific number of stage. This procedure divides the column in a number of segments.

The possibility of segmentation of the column is an attractive feature of the above version of the cell model. End effects, excluding back mixing of the phases (mass transfer during drop formation, long end sections or settling zones) can be associated with the two end stages and isolated from the main column. This procedure is mathematically valid only when the column contains a number of stages greater than the minimum obtained by an analysis of the degree of freedom similar to the above presented.

CHAPTER V

MODEL PARAMETERS ESTIMATION TECHNIQUES

MODEL PARAMETERS ESTIMATION TECHNIQUES

5.1 Diffusion Model

In this Chapter several techniques for the estimation of the parameters of the models discussed in Chapter 4 are studied. Their validity and reliability are assessed by applying theoretical profiles to the experimental profiles obtained during thepreliminary experimentation.

5.1.1 Sensitivity Analysis

Before presenting the different techniques for parameter estimation to the Diffusion Model, it is convenient to present the results of several test performed to assess the sensitivity of the concentration profiles X (Equation 4.137) or Y (Equations 4.138) to changes in the parameters $(No)_x$, $(Pe)_x$ and $(Pe)_y$.

A computer program was written to calculate the partial derivatives (numerical differentiation using forward difference) of X or Y at different step sizes and levels of the parameters, using as subroutine to generate the concentration profiles, the program listed in Appendix 3.

Table 5.1 presents the results of the analysis Y-profiles for a step size of h = 0.001, being the derivatives evaluated at Z = 0.5 (middle of column).

Table 5.1- Sensitivity Analysis Diffusion Model

F	$(No)_x$	$(Pe)_y$	$(Pe)_x$	$\frac{\partial Y}{\partial (No)_x}$	$\frac{\partial Y}{\partial (Pe)_y}$	$\frac{\partial Y}{\partial (Pe)_x}$
0.794	3.21	5.50	4.40	1.78×10^{-2}	-7.23×10^{-3}	8.67×10^{-4}
0.794	3.21	0.50	25.00	1.27×10^{-2}	-2.27×10^{-2}	1.59×10^{-4}
0.794	3.21	25.00	0.50	2.98×10^{-2}	-2.01×10^{-4}	-2.15×10^{-2}
1.405	4.47	2.70	9.00	1.58×10^{-2}	4.03×10^{-4}	2.15×10^{-3}
1.405	4.47	0.50	25.00	1.20×10^{-2}	9.55×10^{-3}	1.71×10^{-4}
1.405	4.47	25.00	0.50	1.87×10^{-2}	1.99×10^{-4}	-5.53×10^{-3}
0.9552	1.88	7.70	3.70	5.34×10^{-2}	-4.20×10^{-3}	1.86×10^{-3}
0.9552	1.88	0.50	25.00	4.70×10^{-2}	-2.16×10^{-2}	2.21×10^{-4}
0.9552	1.88	25.00	0.50	6.47×10^{-2}	-2.89×10^{-4}	-8.8×10^{-3}

Estimation of the errors due to discretization and rounding off were not done. Instead, different derivative estimates were obtained using step sizes 0.01, 0.001 and 0.0001 and their magnitude were compared, revealing that h = 0.001 gave derivative values of sufficient accuracy for the purpose of a sensitivity analysis.

The following conclusions can be withdrawn from the results listed in Table 5.1.

1. For all cases, the concentration profile is very sensitive to changes in $(No)_x$ and less sensitive, approximately one degree lower, to $(Pe)_x$ and $(Pe)_y$.

2. For values of $(Pe)_x$ and $(Pe)_y$, within the same order of magnitude, the profile is more sensitive to the Peclet Number of the phase in which the concentration profile is under study. This means that Y-profile is more sensitive to $(Pe)_y$ than to $(Pe)_x$ and vice versa for the X-profile.

3. For any phase, if the corresponding axial mixing coefficient decreases (Peclet Number increases) the profile becomes less sensitive and vice versa.

4. For any Peclet Number above 30 the sensitivity is so low that it is better to assume plug flow in the phase (Pe = ∞) and use a 2-parameter model.

From the above conclusion it can be said that in a curve fitting or optimization process using the diffusion model the $(No)_x$ can be estimated more accurately than the two Pedet Numbers.

5.1.2 Parameter Estimation - Mecklenburgh and Hartland Algorithm

Mecklenburgh and Hartland (142) present an algorithm (Algorithm10.21) to evaluate the differential profile of a counter-current solvent extraction with straight equilibrium line.

The method requires an accurate value of the true Number of Transfer Unit $(No)_x$ which is calculated by the following equation

$$(No)_x = \frac{C_{xi} - C_{xo}}{\int_{0^+}^{1-} (C_x - C_x^*)\,dZ} \qquad (5.1)$$

To solve equation (5.1) it is necessary to have concentration data at points very close to the column ends in order to perform an extrapolation and obtain reliable values for the concentration jumps (end effects) which are needed for the solution of the integral. According to the model boundary conditions the limits of the above integral should be $Z = 0^+$ and $Z = 1^{-1}$ (column ends inside the column).

The algorithm does not take into account the whole concentration profile; it only requires a central value (Cx or Cy at Z = 0.5) to start the iteration, the first root, λ_2, of the characteristic equation (4.148) and the Peclet Number of the x-phase are approximately estimated. The values of the other two roots of the characteristic equation and $(Pe)_y$ can now be estimated and from these better values of λ_2 and $(Pe)_x$ obtained. The iteration continues until convergence of $(Pe)_x$ and $(Pe)_y$ is achieved.

In order to assess the validity of the algorithm several theoretical profiles were studied using a computer program designed to process the algorithm. The choice of which profile tostudy, was made based on the results of the sensitivity analysis regarding Peclet numbers. One of the conclusions of the analysis was that the larger the value of (Pe), the lower the sensitivity and less reliable is its estimate. Then, theoretical profiles with Peclet Number ratio in the range 0.1 - 8 were studied and the results are as follows:

	x- Theoretical Profiles			Estimated Values	
F	$(No)_x$	$(Pe)_x$	$(Pe)_y$	$(Pe)_x$	$(Pe)_y$
0.955	2.00	60.00	8.00	43.00	7.00
0.955	2.00	45.00	10.00	34.00	8.65
0.955	4.00	40.00	6.00	30.60	6.67
1.405	2.00	40.00	10.00	40.20	10.10
1.405	6.00	50.00	10.00	68.90	9.80
1.405	10.00	60.00	8.00	57.00	8.00

Overall, it can be said that the estimation is good and the table corroborates the conclusion of the sensitivity analysis regarding the expected accuracy in the estimated values of large Peclet Numbers.

The experimental concentration profiles obtained during the preliminary experimentation were then analysed. The procedure to estimate the true $(No)_x$ is given in Section 5.1.4. For all the profiles the algorithm did not converge and the programme stopped due to numerical overflow or underflow of the Peclet Numbers.

It seems that the algorithm cannot converge when there are large experimental errors in the profiles. Moreover, the estimation of the true $(No)_x$ for each of the experimental concentration profiles could not be done accurately since no data points close to the column ends were available and the algorithm itself did not improve the values of $(No)_x$. Another reason for the failure of the algorithm is simply that the diffusion model may not be the most suitable one to represent the behaviour of the column.

5.1.3 Parameter Estimation - Rod's Graphical Techniques

V. Rod had published two graphical techniques to evaluate concentration profiles based on the diffusion model. Both techniques can be applied to the case of a non-linear equilibrium relationship.

Technique 1 (131)

The diffusion model is approximated by a finite difference model and the difference equations are solved graphically on a distribution diagram. The technique is basically a boundary iteration marching solution method. The three parameters need to be guessed initially and a suitable height increment ΔZ selected. The trial and error procedure in the parameter estimation terminates when the calculated length of the column matches the real length.

The properties of a marching solution method has been extensively discussed by Mecklenburgh and Hartland (142). They show that when backmixing exists in both phases, marching is mathematically unstable in both directions and its application is strongly discouraged. On the other hand, if backmixing is absent in one of the phases, the difference equations are stable if matching is started from the exit of the phases with non-zero backmix.

To assume that the experimental concentration profiles obtained during the preliminary exerimentation have no longitudinal mixing in the dispersed phase, is highly questionable. The fact that the true backflow or entrainment did not exist in the dispersed phase is not sufficient to consider plug flow of the phase. Based on the above, the technique was considered impractical and it was not applied.

Technique 2 (158)

This technique uses a completely different approach. The evaluation of the concentration profiles is performed by graphical integration of the expressions for the Number of Transfer Units and the Peclet Numbers derived from the basic differential backmixing equations as follows:

$$(Pe)_x = \frac{C^o_{xi} - C_{xo}}{\int_0^1 (X^1 - C_x)\,dZ} \tag{5.2}$$

$$(Pe)_y = \frac{C_{yo} - C_{yi}^o}{\int_0^1 (y - Y^1)\,dZ} \tag{5.3}$$

$$(No)_x = \frac{C_{xi} - C_{xo}}{\int_0^1 (C_x - C_x^*)\,dZ} \tag{5.4}$$

where

$$X^1 = C_x - \left(\frac{e_x}{V_x}\right)\left(\frac{dC_x}{dZ}\right) \tag{5.5}$$

$$Y^1 = C_y + \left(\frac{e_y}{V_y}\right)\left(\frac{dC_y}{dZ}\right) \tag{5.6}$$

C^o_{xi} = Concentration jump in the raffinate phase

C^o_{yi} = Concentration jump in the extract phase

The technique suffers from the same drawback of the Mecklenburgh-Hartland's algorithm, the concentration jump at the ends need to be known by means of extrapolation of the C_y and C_x-profiles. Nevertheless, it seems more reliable in estimationg $(Pe)_x$ and $(Pe)_y$ since errors in the concentration profile tend to be smoothed in the graphical integration step and the sensitivity of the solution to inaccurate concentration values will be reduced.

This technique can be used to provide the initial parameter estimates needed in a more complex curve fitting technique.

5.1.4 Parameter Estimation - Miyauchi and Vermeulen Technique

The method proposed by Miyauchi and Vermeulen (9) has been used in this research and the results of its application to experimental concentration profiles are given in Chapter 8.

The technique is iterative and requires an initial estimated value of the "true" Number of Transfer Unit and the concentration jumps in both phases.

A set of variables called jump ratios are defined. Using the dimensionless concentration X and Y defined in Chapter 4, these ratio are as follows:

$$R_x = \frac{1 - X_i^o}{1 - X_o} \qquad (5.7)$$

$$R_y = \frac{Y_o}{Y_i^o} \tag{5.8}$$

The reason for defining these new variables is that they are much less sensitive to variation in the (N.T.U.), than the corresponding concentration jumps X_i^o and Y_i^o and they can be considered constant for the whole iteration.

The procedure consists in constructing a complete grid of theoretical jump ratios using the initial value of the (N.T.U.). Then locate in the grid the experimental (R_x, R_y) point as shown in Figure 5.1. Approximate values of $(Pe)_x$ and $(Pe)_y$ are then read by interpolation. This completes the first cycle of iteration. Using a set of empirical equations based on the estimated $(Pe)_x$ and $(Pe)_y$, a new and better estimate of $(No)_x$ is obtained leading to a second grid jump ratio plot which in turn gives better values of the Peclet Numbers. It was claimed by the authors that convergence is attained with a few cycles.

Three different definitions of the Overall Number of Transfer Unit $(N.T.U.)_o$ has been commonly used in the analyses of longitudinal mixing in continuous columns. They are "true" $(N.T.U.)_o$, $(No)_x$ or $(No)_y$, the "measured" $(N.T.U.)_o$, $(No)_{xM}$ or $(No)_{yM}$ and the "plug flow" or "piston flow" $(N.T.U.)_o$, $(No)_{xP}$ or $(No)_{yP}$

(a) The "true" $(N.T.U.)_o$ as originally defined by Chilton and Colburn (159) is given by the following equation

Figure 5.1 - Jump Ratio Grid Plot

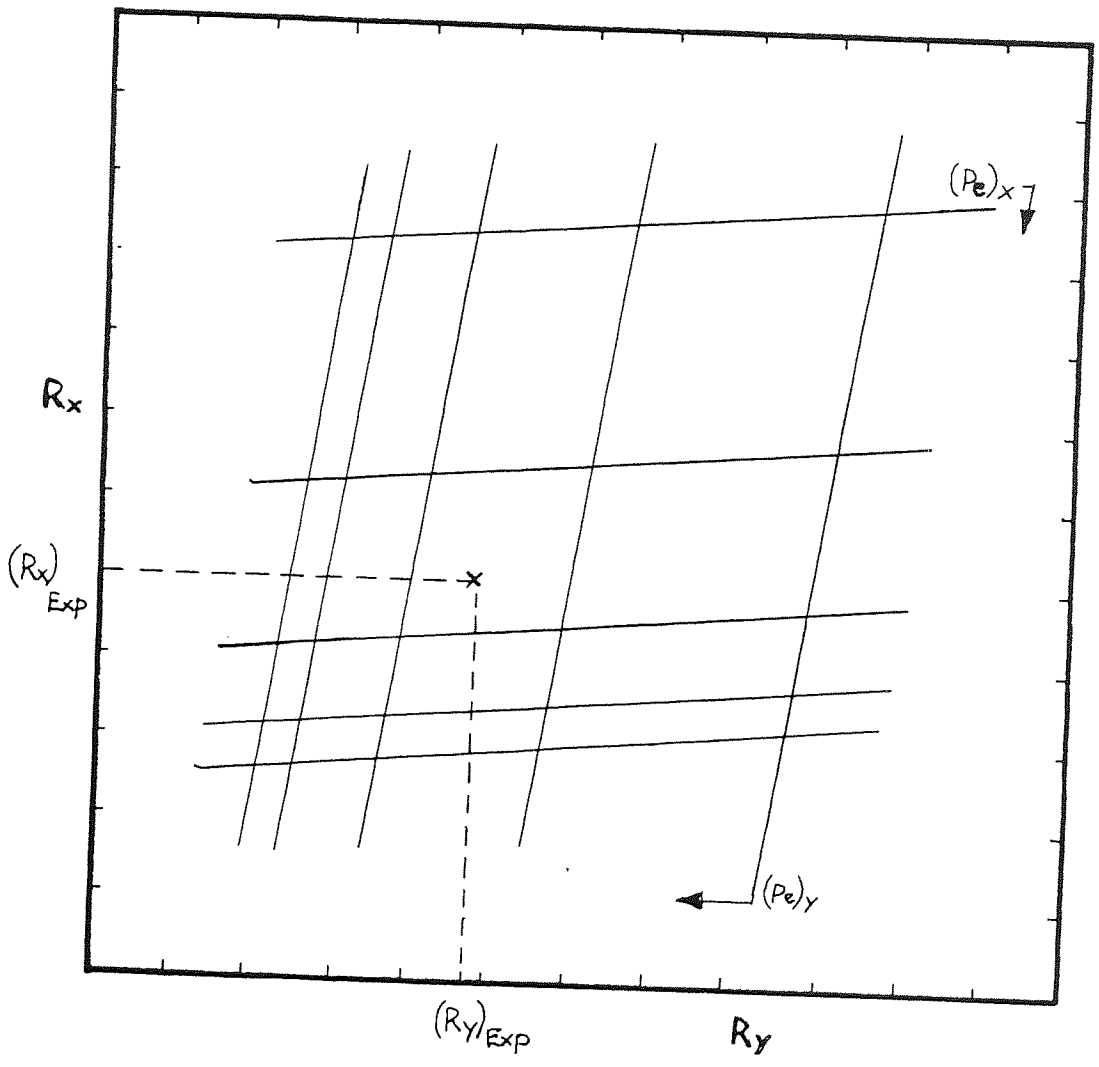

$$(No)_x = \frac{K_x.a.L}{V_x} \qquad (5.9)$$

When the diffusion model is used to interpret the column experimental data, an expression fór the number of "true" overall transfer units $(No)_x$ can be obtained in terms of the x-phase concentrations. The differential mass balance equation (4.31)

$$e_x \frac{d^2C_x}{dZ^2} - V_x \frac{dC_x}{dZ} = K_x a(C_x - C_x^*) \qquad (4.131)$$

can be written in the following form

$$\frac{d}{dZ}\left(\frac{e_x}{V_x}\frac{dC_x}{dZ} - C_x\right) = \frac{K_x a}{V_x}(C_x - C_x^*) \qquad (5.10)$$

or

$$\frac{d\left(\frac{e_x}{V_x}\frac{dC_x}{dZ} - C_x\right)}{(C_x - C_x^*)} = \frac{K_x a}{V_x} dZ \qquad (5.11)$$

Integrating the above expression, assuming V_x constant gives

$$\int_{C_{xi}^o}^{C_{xo}} \frac{d\left(\frac{e_x}{V_x}\frac{dC_x}{dZ} - C_x\right)}{(C_x - C_x^*)} = \frac{K_x aL}{V_x} \qquad (5.12)$$

then

$$(No)_x = \int_{C_{xi}^o}^{C_{xo}} \frac{d\left(\frac{e_x}{V_x}\frac{dC_x}{dZ} - C_x\right)}{(C_x - C_x^*)} \qquad (5.13)$$

A more useful expression is obtained if the hypothetical concentration X^1 defined by Equation (5.5) is used with the dimensionless column height Z. Substituting X^1

$$X^1 = C_x - \frac{e_x}{V_x}\frac{dC_x}{dZ} \qquad (5.5)$$

and

$$\bar{z} = Z.L \qquad (4.136)$$

in Equation (5.10) gives

$$dX^1 = \frac{-K_x aL}{V_x}(C_x - C_x^*)dZ \qquad (5.14)$$

The boundary conditions given by Equation (4.139) and Equation (4.144) lead to

$$Z = 0^+ \quad C_x = C_{xi}^o, \; X^1 = C_{xi}^o - \frac{e_x}{V_x}\left(\frac{dC_x}{dZ}\right)_{0^+} = C_{xi}$$

$$Z = 1^+ \quad C_x = C_{xo}, \; X^1 = C_{xo} - \frac{e_x}{V_x}\left(\frac{dC_x}{dZ}\right)_{1^+} = C_{xo}$$

Integrating Equation (5.14) assuming V_x constant

$$\frac{C_{xi} - C_{xo}}{\int_{Z=0^+}^{Z=1^-}(C_x - Cx^*)dZ} = \frac{K_x aL}{V_x} = (No)_x \qquad (5.15)$$

The solution of the above integral can be obtained by fitting a polynomial to the $(C_x-C_x^*)$ vs Z experimental curve which is then integrated analytically. This approach has been used in the analysis of the experimental data obtained during this research (see Section 8.3.2.2.1).

(b) The "measured" $(N.T.U.)_o$, $(No)_{xM}$ proposed by Geankoplis and Hixson (124) and Gier and Hougen (125) uses the real or correct driving force but omits the transport term $\frac{e_x}{V_x}\frac{dC_x}{dZ}$ of Equation (5.13).

$$(No)_{x,M} = \int_{C_{xo}}^{C_{xi}^o} \frac{dC_x}{(C_x-C_x^*)} \qquad (5.16)$$

(c) The "plug flow" or "piston flow" $(N.T.U.)_o$, $(No)_{xP}$ applies to the ideal situation of $e_x = 0$ in which case

$$(No)_{x,P} = \int_{C_{xo}^P}^{C_{xi}^P} \frac{dC_x^P}{(C_x^P - (C_x^P)^*)} \qquad (5.17)$$

where the superscript P means the hypothetical concentration for the x- and y- phases that would be found in the column if both phases flowed through it in piston type flow. The integration of Equation 5.17 gives the well-known Colburn equation (7) which in terms of the dimensionless concentration defined in Section (4.3.2.2.1) has the form

$$(No)_{x,P} = \frac{\ln\left[\frac{1}{X_o}(1-F) + F\right]}{1 - F} \qquad (5.18)$$

Comparing Equations (5.13) and (5.17) it is seen that $(No)_x$ differs from $(No)_{xP}$ in that it includes the effect of changes in the driving force $(C_x - C_x^*)$ and in the transport term $\frac{e_x}{V_x}\left(\frac{dC_x}{dZ}\right)$.

5.1.5 Optimisation Technique

As it was mentioned in Section 5.1.4, the Miyauchi and Vermeulen technique was used in this research only for the purpose of obtaining the initial values of the parameters needed in a curved fitting or optimization method.

The fitting of the parameters $(No)_x$ $(Pe)_x$ and $(Pe)_y$ to the experimental profile involve, the optimization of a non-linear function in the above parameters. The problem is to compute those estimates of theparameters which will minimize the following objective function.

$$\Phi = \sum_{i=1}^{m} (Y_i - \hat{Y}_i)^2 = \sum_{i=1}^{m} R_i(\beta)^2 \qquad (5.19)$$

subject to the constrains $a \leq [\beta] \leq b$

where

$\hat{Y}_i$ = value of Y_i predicted by $E(Y_i) = f(K,\bar{\beta})$ for the ith observation

Y_i = experimental value of the dependent variable for the ith observation

R_i = residual for the ith observation

m = number of experimental points

n = number of parameters to be estimated

$[\beta]$ = vector of parameters

a,b= lower and upper limit of the parameters

Non-linear techniques are iterative in nature, i.e. starting values are guessed and upgraded by the algorithm until a convergence criterion is satisfied. The method adopted in this research was the Marquardt algorithm (160).

The Marquardt algorithm has been chosen because it combines the best features of the Gauss-Newton and Steepest Descent methods, and avoides their most serious limitations. The algorithm shares with the gradient methods (Steepest Descent) their ability to converge from an initial guess which may be outside the region of convergence of other methods. The algorithm shares with the Taylor series methods (Gauss-Newton) the ability to close in on the converged value rapidly when the vicinity of the converged value has been reached. The algorithm modifies the Gauss-Newton normal equation by adding a scalar factor λ to give the following matrix equation

$$\left[J^T J + \lambda I \right] \delta = - J^T R \qquad (5.20)$$

where

J = Jacobian matrix m x n, $J_{ik} = \frac{\partial R_i}{\partial \beta_k}$ $\begin{matrix} i=1, \ldots m \\ j=1, \ldots n \end{matrix}$

λ = scalar, when equal zero the technique reduces to Gauss-Newton, when approaching $+\infty$ the technique is identical to Steepest Descent

I = identify matrix m x n

δ = correction or direction vector, n x 1, $(\hat{\beta}-\hat{\beta}^*)$

R = residual vector, m x 1, $(Y_i-\hat{Y}_i)$

Thus in the Marquardt procedure, the initial values of λ are large and will decrease towards zero as the optimum is approached.

This algorithm was chosen as the most appropriate based on the fact that convergence can be achieved with a relatively poor starting guess of the model parameters as is the case in this work, especially with the two flow parameters.

The Marquardt algorithm is available in the NAG Routines Library for ICL 1904 computers as Subroutine E04GAF. The initial optimization exercises were done using the above subroutine but it was soon noticed that a better control and monitoring of the computation was required and modifications of the subroutine were needed. As is discussed further in section 5.1.5.1, this situation necessitated discarding the above subroutine in favour of a more easily programmed routine.

The strategy adopted in this study as well as in the stagewise model optimization exercise, was to study first a theoretical profile in order to check the applicability of the regression algorithm to the model under study, its accuracy, different formulation of the problem and the ability to converge to the right answer from different starting points.

Three different formulations of the optimization problem are possible according to the type of function $f(K,\bar{\beta})$ chosen:

Objective Function Formulation 1: Optimization based on the extract phase concentration profile

$$Y = f_1(K_1,\bar{\beta}) = A_1+A_2a_2e^{\lambda_2 Z} + A_3a_3e^{\lambda_3 Z} + A_4a_4e^{\lambda_4 Z}$$

Objective Function Formulation 2: Optimization based on the rafinate phase concentration profile

$$X = f_2(K_2,\bar{\beta}) = A_1+A_2e^{\lambda_2 Z} + A_3e^{\lambda_3 Z} + A_4e^{\lambda_4 Z}$$

Objective Function Formulation 3: Optimzation based on an overall behaviour of the column represented by the difference in concentration profiles of both phases

$$X-Y = f_3(K_3,\bar{\beta}) = A_2e^{\lambda_2 Z}(1-a_2) + A_3e^{\lambda_3 Z}(1-a_3) + A_4e^{\lambda_3 Z}(1-a_4)$$

Any one of the above formulations can be used since all will lead to the same optimum when theoretical profiles are fitted. On the contrary, when experimental profiles are studied, each formulation may give different answers mainly because the model may not be the most appropriate to represent the behaviour of each phase and/or the experimental errors in the profiles are different in each phase.

5.1.5.1 Analysis of Y-theoretical profile

A theoretical concentration profile with the following values of the diffusion model parameters

$F = 0.9552$

$(Pe)_x = 0.050$

$(Pe)_y = 6.045$

$(No)_x = 5.000$

was generated (Appendix 3) and the Y-profile was studied using the Marquardt's algorithm. The above values were chosen in such a way as to impose a severe test on the ability to converge the regression algorithm. The fact that $(Pe)_x$ is so close to one of the constraints, the low sensitivity of Y- profile to $(Pe)_x$ values and the high Peclet Number ratio, creates a difficult problem to optimize, especially when the starting values of the parameters are poor.

The subroutine NAG EO4GAF was used with the following initial values

$$(Pe)_x = 3.00 \qquad (Pe)_y = 3.0 \qquad (No)_x = 3.0$$

and constrains $-10 \leq [\beta] \leq 60$. The iteration progressed satisfactorily with decreasing values of the sum square of the residuals and the program made a normal exit at the point $(Pe)_x = 0.304$, $(Pe)_y = 2.520$ and $(No)_x = 4.430$. This premature stop could be due to an improper criterion for the termination of the computation or more likely to rounding errors in Φ since the subroutine uses a single-precision calculation. In order to make the appropriate modifications, the listing of the NAGEO4GAF subroutine was obtained. The number of auxiliary routines called from the main NAGEO4GAF were so many that a clear understanding of the line of programming and execution of the necessary changes was difficult and too time consuming. It was then decided to use the computer code given by Henley and Rosen (161) (BSOLVE Algorithm), which is more easily programmed and the required modific ations, such as double precision calculation, different criterion of termination of the computation and monitoring the most important Marquardt parameters, i.e. λ angle between steepest descent gradient vector and modified Gauss-Newton gradient vector and the value of Φ at each iteration, can be easily done. A listing of the computer program using the BSOLVE routine is given in Appendix 5.

The results using the BSOLVE Program with the above guess values were

$(Pe)_x = 0.04983$

$(Pe)_y = 6.0476$

$(No)_x = 4.9992$

Number of iterations = 1.0

Sum of square of the residuals = 0.8510×10^{-9}

This clearly indicates that the optimization method works well for the diffusional model and convergence is achieved with a small number of iterations.

No further work was done on the study of the properties of the solution vector, error analysis, etc., since as it is shown in Section 8.3.2.2.1, the adequacy of the diffusion model to the experimental data was found to be unacceptable.

5.2 Cell-Backflow Model

In Figure 4.8 a diagram of an n-cell backflow model is shown. For this case the non-ideal behaviour of the phases is characterized by means of coefficients r_k, $k = 2, \ldots n$ and ℓ_k, $k = 1, \ldots n-1$, which express the "relative" entrainment between individual stages for the respective phase.

As before, approximate methods for the estimation of the model parameters are presented first, followed by the optimization method.

5.2.1 Parameter Estimation - Rod's Method

Rod (158) had published an analytical method to evaluate stagewise concentration profiles assuming that the backflow coefficients r_k and ℓ_k and the overall coefficient of mass transfer are constant, and that the stages are perfect mixers.

A material balance on the rafinate phase of the k-stage of Figure 4.8 leads to the following equation

$$x_k - r(x_{k+1} - x_k) - \left[x_{k-1} - r(x_k - x_{k-1})\right] = - \frac{K_x(aV_k)}{R} (x_k - x_k^*) \quad (5.21)$$

A similar equation for the extract phase enables the following hypothetical variables to be defined

$$X_k'' = x_k - r\ (x_{k+1} - x_k) \quad (5.22)$$

$$Y_{k+1}'' = y_{k+1} + \ell\ (y_{k+1} - y_k) \quad (5.23)$$

which are analogous to the X^1 and Y^1 defined in Section 5.1.3.

Then equation (5.21) can be expressed as

$$X_k'' - X_{k-1}'' = - \frac{K_x(aV_k)}{R} (x_k - x_k^*) \quad (5.24)$$

and the boundary conditions of the model became

$$\begin{aligned} X_o'' &= x_o & Y_1'' &= y_1 \\ X_n'' &= x_n & Y_{n+1}'' &= y_{n+1} \end{aligned} \quad (5.25)$$

Summation from k=1 to k=n on both sides of Equation 5.24 leads to the following expression after proper consideration of the boundary conditions

$$\frac{K_x(a.V_k)}{R} = \frac{x_o - x_n}{\sum_{k=1}^{n} (x_k - x^*)} \qquad (5.26)$$

An analogous procedure is used to derive expressions suitable for the calculation of the backlfow coefficients

$$r = \frac{\sum_{k=1}^{n} (X''_k - x_k)}{x_1 - x_n} \qquad (5.27)$$

$$e = \frac{\sum_{k=1}^{n} (y_k - Y''_k)}{Y_1 - Y_n} \qquad (5.28)$$

The X''_k values to use in Equation (5.27) are calculated by the following expression

$$x_o - X''_k = \frac{K_x(aV_k)}{R} \sum_{i=1}^{k} (x_i - x_i^*) \qquad (5.29)$$

and the corresponding Y''_k by the balance line

$$RX''_k - EY''_{k+1} = Rx_o - Ey_1 \qquad (5.30)$$

The method was applied to the concentration profiles obtained in the preliminary experimentation and the results shown in Section 8.3.2.2.2, Table 8.9 were used as the initial value in the optimization step. Although the summation reduces the random experimental error affecting

the concentrations the errors of fit can be large, as is shown in Figure 8.3 and a least square curve fitting is necessary.

5.2.2 Optimization Technique

The Marquardt's method and its computer code BSOLVE routine, already presented in Section 5.1.5, has also been applied to the stagewise model in a curve fitting using the least square approach.

Two formulations of the sum of squares objective funtion, based on the equation

$$[A][x] = [C] \tag{4.168}$$

are possible;

(i) Objective Function 1

The values of the (2n + 2) concentrations are substituted in equation (4.159) and the optimization consists in minimizing the objective function defined as the sum of the squares of the difference of left-hand and right-hand sides of the above equation

$$\Phi = ||[A] \cdot [x] - [C]||^2 \tag{5.31}$$

(ii) Objective Function 2

The inlet concentrations x_o and y_{n+1} are combined with the vector of the right-hand side $[C]$ making $[A]$ a square coefficient matrix 2n x 2n. Minimization concerns now the sum of squares of the differences of

the measured concentration $[x]$ and the corresponding calculated values $[\hat{x}]$

$$\Phi_2 = ||[x] - [A]^{-1}[c]||^2 \qquad (5.32)$$

Both objective functions are minimized with respect to the vector $[\beta]^T = [\eta, r_k, e_k]$ subject to the constraint

$$a \leq [\beta] \leq b \qquad (5.33)$$

As it is shown in Chapter 9, Section 9.3.4.1, it is convenient not to constrain the parameters r_k and ℓ_k to positive values since the optimum can be approached from the negative side, then $a < 0$.

Both formulations were analysed using a 5-stage theoretical profile. Results indicated that Φ_2 is less affected by round-off error although it consumed more computer time and storage. Another advantage of formulation 2 is that the solution vector $[\hat{\beta}]$ and the fitted concentration profile are obtained simultaneously. Based on this, the Objective Function Φ_2 was used in this research.

5.2.2.1 Model Formulations

In order to solve Φ_1 and/or Φ_2 the number of equations (2n) must at least equal the number of parameters in $[\beta]$. In practice, (2n) usually exceeds the number of parameters to be estimated. Based on this, several models of a 5-stage column with known concentrations and a different number of parameters were formulated.

(i) Model Formulation 1

This is a problem in which ten parameters (n=5) are estimated and three independent equations are stated in order to satisfy the degrees of freedom (Section 4.3.2.2.2).

Vector parameters:

$$[\beta]^T = [\eta_1 \ \eta_2 \ \eta_3 \ \eta_4 \ \eta_5 \ r_2 \ r_3 \ r_4 \ \ell_1 \ \ell_4]$$

Independent Equations:

$$r_4 = r_3$$

$$\alpha x_o - y_1 = (1+r_3)\ \alpha x2 + \ell_2 y_2 - r_3 \alpha x_3 - (1+\ell_2) y_3$$

$$\ell_3 = \ell_2$$

Other independent equations can be chosen but it is considered that the assumption of equal backflow coefficients for the inner stages is close to the real behaviour of a stagewise column.

(ii) Model Formulation 2

In this case eight parameters need to be estimated and five independent equations are specified. This formulation actually divides the column into 3 segments. The first segment consists of stage 1, second segment of stages 2,3 and 4 and the third segment of stage 5 only. The formulation isolates the central part of the column from the two extreme stages affected by end-effects.

Vector of parameters:

$$[\beta]^T = [\eta_1 \ r_2 \ \ell_1 \ \eta_3 \ r_3 \ \eta_5 \ r_5 \ \ell_4]$$

Independent Equations:

$$\eta_2 = \eta_3$$

$$\eta_4 = \eta_3$$

$$r_4 = r_3$$

$$\alpha x_o - y_1 = (1+r_3)\alpha x_2 + \ell_2 y_2 - r_3 \alpha x_3 - (1+\ell_2) y_3$$

$$\ell_3 = \ell_2$$

(iii) Model Formulation 3

This is a five-parameter model requiring eight independent equations to be fixed. No axial variation of the backflow coefficient is assumed.

Vector of parameters:

$$[\beta]^T = [\eta_1 \ \eta_3 \ \eta_5 \ r_2 \ \ell_1]$$

Independent Equations:

$$\eta_4 = \eta_3 = \eta_2$$

$$r_2 = r_3 = r_4 = r_5$$

$$\ell_1 = \ell_2 = \ell_3 = \ell_4$$

In this formulation the end-effects are damped into the efficiencies of the first and last stages.

(iv) Model Formulation 4

This is the simplest of all the model formulations. No axial variation of the parameters is assumed.

Vector of parameters:

$$[\beta]^T = [\eta_1 \ \ell_1 \ r_2]$$

Independent equations:

$$\eta_1 = \eta_2 = \eta_3 = \eta_4 = \eta_5$$

$$\ell_1 = \ell_2 = \ell_3 = \ell_4$$

$$r_2 = r_3 = r_4 = r_5$$

5.2.2.2 Analysis of Theoretical Profile

To generate a theoretical profile $[x]$, requires the solution of the equation (4.168) for a known set of parameters. Initially, the Gauss-Siedel iteration method was used in order to avoid a possible ill-conditioned coefficient matrix $[A]$. It was soon found that for some values of the parameters, the diagonal elements of $[A]$ were of approximately the same order of magnitude than the off-diagonal elements. This caused a very low rate of convergence and in some cases even after 500 iterations the Gauss-Siedel routine did not reach the solution $[x]$. On the other hand, satisfactory results were obtained over the whole range of the parameters when the Crout's Factorisation Method (NAG FOGATF) was used (Appendix 2).

The properties of the models presented in Section 5.2.2.1 were studied from the following points of view,

(i) the influence of data error on the convergence rate and on the accuracy of the results or uniqueness of the solution vector, and

(ii) the influence of the number of parameters of the model on the results. To carry out these studies a 5-stage theoretical profile was generated using the computer program listed in Appendix 2 with the following conditions

$\eta = 0.5, \quad r = 0.8, \quad \ell = 1.0, \quad \alpha = 0.8$

Equilibrium line, $y^* = x$

In order to study the influence of the data error on the solution, the above theoretical profile random errors of magnitude 2%, 3%, and 5% were inserted leading to the three concentration profiles shown in Table 5.2. The selection of the magnitude of the error and its allocation to a particular concentration point was done randomly using a table of random numbers (150). In all the profiles listed in Table 5.2 it was assumed that the feed concentrations x_o and y_6 are controlled.

The computer program listed in Appendix 4 was used to fit the profiles given in Table 5.2 to the models of Section 5.2.2.1.

(i) Case 1

Model Formulation 1 was used to evaluate the exact and the perturbed concentration profiles of Table 5.2. Table 5.3 presents the initial values of the parameters and the fitted solution.

(ii) Case 2

Same as Case 1 but using a different starting point. Only the exact concentration profile was studied.

Initial guess: $\eta_1 = \eta_2 = \eta_3 = \eta_4 = \eta_5 = 0.2$

$r_2 = r_3 = r_5 = 0.3$

$\ell_1 = \ell_4 = 1.50$

Fitted solution - Exact profile:

$\eta_1 = 0.467$, $\eta_2 = 0.537$, $\eta_3 = 0.500$, $\eta_4 = 0.468$

$\eta_5 = 0.515$

$r_2 = 0.970$, $r_3 = 0.794$, $r_5 = 0.974$

$\ell_1 = 0.732$, $\ell_2 = 1.00$, $\ell_4 = 0.905$

Table 5.2 - Theoretical Profiles

	Exact Profile		0% - 2% Error Profile		0% - 3% Error Profile		0% - 5% Error Profile	
k	x_k	y_k	x_k	y_k	x_k	y_k	x_k	y_k
0	0.4000		0.4000		0.4000		0.4000	
1	0.3370	0.3000	0.3431	0.3018	0.3461	0.3027	0.3522	0.3045
2	0.3067	0.2845	0.3074	0.2867	0.3076	0.2879	0.3083	0.2902
3	0.2813	0.2631	0.2825	0.2683	0.2830	0.2709	0.2842	0.2762
4	0.2593	0.2411	0.2618	0.2445	0,2632	0.2462	0.2657	0.2495
5	0.2445	0.2190	0.2484	0.2216	0.2503	0.2229	0.2543	0.2256
6		0.1756		0.1756		0.1756		0.1756

Table 5.3 - Case 1

Parameters	Initial Guess	Profile Solutions			
		1a) Exact	1b) 0%-2% Error Profile	1c) 0%-3% Error Profile	1d) 0%-5% Error Profile
η_1	0.8	0.5088	0.4568	0.4453	0.4410
η_2	0.8	0.4913	0.3736	0.3352	0.2050
η_3	0.8	0.5001	0.5921	0.6434	0.7502
η_4	0.8	0.3074	0.4570	0.4489	0.4680
η_5	0.8	0.5923	0.6053	0.6265	0.6100
r_2	1.1	0.7550	0.6714	0.5770	0.3640
r_3	1.1	0.7947	1.6478	1.852	2.184
r_5	1.1	1.771	2.3560	2.807	3.228
e_1	0.5	1.068	0.8237	0.818	0.964
e_4	0.5	0.4795	0.3669	0.253	0.289

Continued/....

Table 5.3 (continued)

		Profile Solutions			
Parameters	Initial Guess	1a) Exact	1b) 0%-2% Error Profile	1c) 0%-3% Error Profile	1d) 0%-5% Error Profile
e_2	-	1.003	0.5166	0.468	0.449
No. of Iterations	-	6	6	6	7
S.S.R.	-	0.34×10^{-15}	0.23×10^{-18}	0.11×10^{-16}	0.670×10^{-18}

Sum Square of Residual = S.S.R. = 0.17×10^{-19}

Number of Iterations = 9

(iii) Case 3

Model Formulation 2 was used in this case. Table 5.4 lists the initial values of the eight-parameters and the fitted solutions for the profiles of Table 5.2.

(iv) Case 4

The five parameter model of Formulation 3 was studied in this case. Table 5.5 gives the parameters initial guess values and the fitted solutions.

(v) Case 5

No axial variation of the parameters, Model Formulation 4, was studied in this case. Table 5-6 presents the results

The above results presented in Tables 5.3 to 5.6 reveals the following properties of the solution of the model:

1. With the first determined model (Model Formulation 1) and also with the Model Formulation 2 (not shown above) different minima of the objective function are obtained for different starting points with values of S.S.R. (sum square of residuals) indistinguishable within the limits of the used calculation precision (Case 1 and Case 2, exact profile). Since in both Case 1 and Case 2 the theoretical and calculated profiles agree exactly up to the 6th significant

Table 5.4 - Case 3

Parameters	Initial Guess	Profile Solutions			
		3a) Exact	3b) 0%-2% Error Profile	3c) 0%-3% Error Profile	3d) 0%-5% Error Profile
η_1	0.80	0.501	0.354	0.317	0.253
η_3	0.60	0.500	0.5921	0.643	0.750
η_5	0.10	0.499	0.473	0.416	0.289
r_2	0.30	0.795	1.134	1.104	1.00
r_3	1.00	0.795	1.647	1.852	2.184
r_5	0.80	0.793	0.9383	0.456	-0.951
e_1	0.50	1.00	-0.091	-0.346	-0.769
e_4	0.50	1.00	1.060	1.354	2.063
e_2	-	1.00	0.516	0.469	0.449

Continued/....

Table 5.4 (continued)

		Profile Solutions			
Parameters	Initial Guess	3a) Exact	3b) 0%-2% Error Profile	3c) 0%-3% Error Profile	3d) 0%-5% Error Profile
No. of Iterations	-	6	5	5	7
S.S.R.	-	0.34×10^{-19}	0.13×10^{-16}	0.83×10^{-15}	0.48×10^{-19}

Table 5.5 - Case 4

Parameters	Initial Guess	Profile Solutions			
		4a) Exact	4b) 0%-2% Error Profile	4c) 0%-3% Error Profile	4d) 0%-5% Error Profile
η_1	0.80	0.500	0.481	0.462	0.412
η_3	0.10	0.500	0.554	0.583	0.641
η_5	0.30	0.499	0.403	0.357	0.263
r_2	0.30	0.799	0.569	0.506	0.424
e_1	1.00	1.00	1.380	1.53	1.82
No. of Iterations	-	10	10	9	13
S.S.R.	-	0.50×10^{-10}	0.80×10^{-5}	0.19×10^{-4}	0.51×10^{-4}

Table 5.6 - Case 5

Parameters	Initial Guess	Profile Solutions			
		5a) Exact	5b) 0%-2% Error Profile	5c) 0%-3% Error Profile	5d) 0%-5% Error Profile
η_1	0.30	0.500	0.505	0.507	0.510
r_2	0.20	0.799	0.682	0.631	0.543
e_1	0.50	0.999	1.150	1.23	1.38
No. of Iterations	-	12	8	7	9
S.S.R.	-	0.85×10^{-10}	0.27×10^{-4}	0.51×10^{-4}	0.17×10^{-3}

digit it is difficult to find a criterion of choice of the best solution vector. The greatest disagreement between both solution vectors is in the values of the backflow parameter, the efficiencies are less affected and on average, their values are close to 0.50.

2. The backflow parameters ℓ and r are more affected by the number of parameters in the model and data error than the efficiency η. An increase in the number of parameters to be estimated creates a significant bias in the ℓ and r estimates. Concentration profiles with 5% data error lead to high error in the parameters. Analysing the results of Case 5 it is seen that the error in the parameter estimates grows approximately linearly with the data error affecting the profiles and that errors in $\underline{\ell}$ and $\underline{r}$ are almost an order higher than that of η.

3. Only Case 4 and Case 5 gave the same solution vector for different starting points.

4. As the number of parameters increases, the curve fitting improves. For Case 1, even for the profile with 0% - 5% data error, the agreement between calculated and theoretical concentrations was extremely good. This does not mean that Model Formulation 1 is the best model to optimize, on the contrary, the degree of reliability of the estimates, especially the backflow parameters, decreases since the sensitivity of each of the parameters is highly reduced. This

situation can even lead to negative value of the parameters as occurred in Case 3.

The following conclusions set up requirements that have to be met in future practical work and also provide guidelines for future model analysis.

1. The error affecting the concentration profiles, i.e. error due to random variation in the column and error in the analytical determination of solute content, cannot be greater than 5%, prferably 2% at most, if a reliable estimation of the backflow parameters is required. This is a high requirement on the precision of concentration measurements.

2. Assuming that in the real situation, the concentration profiles are affected by error levels of 2%, the comparison between the average values of $\underline{\ell}$ and $\underline{r}$ for all the above Cases (b) reveal that only the solutions obtained in Case 4.b (Table 5.5) and Case 5.b (Table 5.6) are in the neighbourhood of the exact solution, showing the correct relationship between the backflow parameters $\underline{e}$ and $\underline{r}$. Thus, in future analysis of experimental profiles, if isolation of the end-effects is attempted, the Model Formulation 3 is the most appropriate to use.

CHAPTER VI

EQUIPMENT AND OPERATION

EQUIPMENT AND OPERATION

6.1 Description of Equipment

A flow diagram of the equipment is shown in Figure 6.1 and a general arrangement in Figure 6.2.. All lines and vessels were arranged so that the column was accessible from all sides, to facilitate sampling and photography, and all valves were within easy reach. Drain points were incorporated at the lowest points in the system. Two columns with the same number of Scheibel stages but different packing pad thickness were used.

6.1.1 The Columns

The column shown in Figure 6.3, identified as Column 1, consists of a 0.101m diameter 0.70m long Q.V.F. glass section divided into 5 packing sections each 0.06m high, 4 mixing sections each 0.05m high and two non-agitated end sections.

The Scheibel column shown in Figure 6.4 is labelled Column 2 and consists of 0.101m diameter 0.50m long Q.V.F. glass section with the same number of Scheibel stages as Column 1 but with packing pads of 0.03m high. It was intended that the non-agitated end sections of both columns have similar geometrical and dimensional characteristics which hopefully will lead to similar flow dynamics and end effects. This was a very important requirement in the execution of the experimental design since it is desirable to avoid any non-controlled systematic variation which can

Figure 6.1 - Flow Diagram

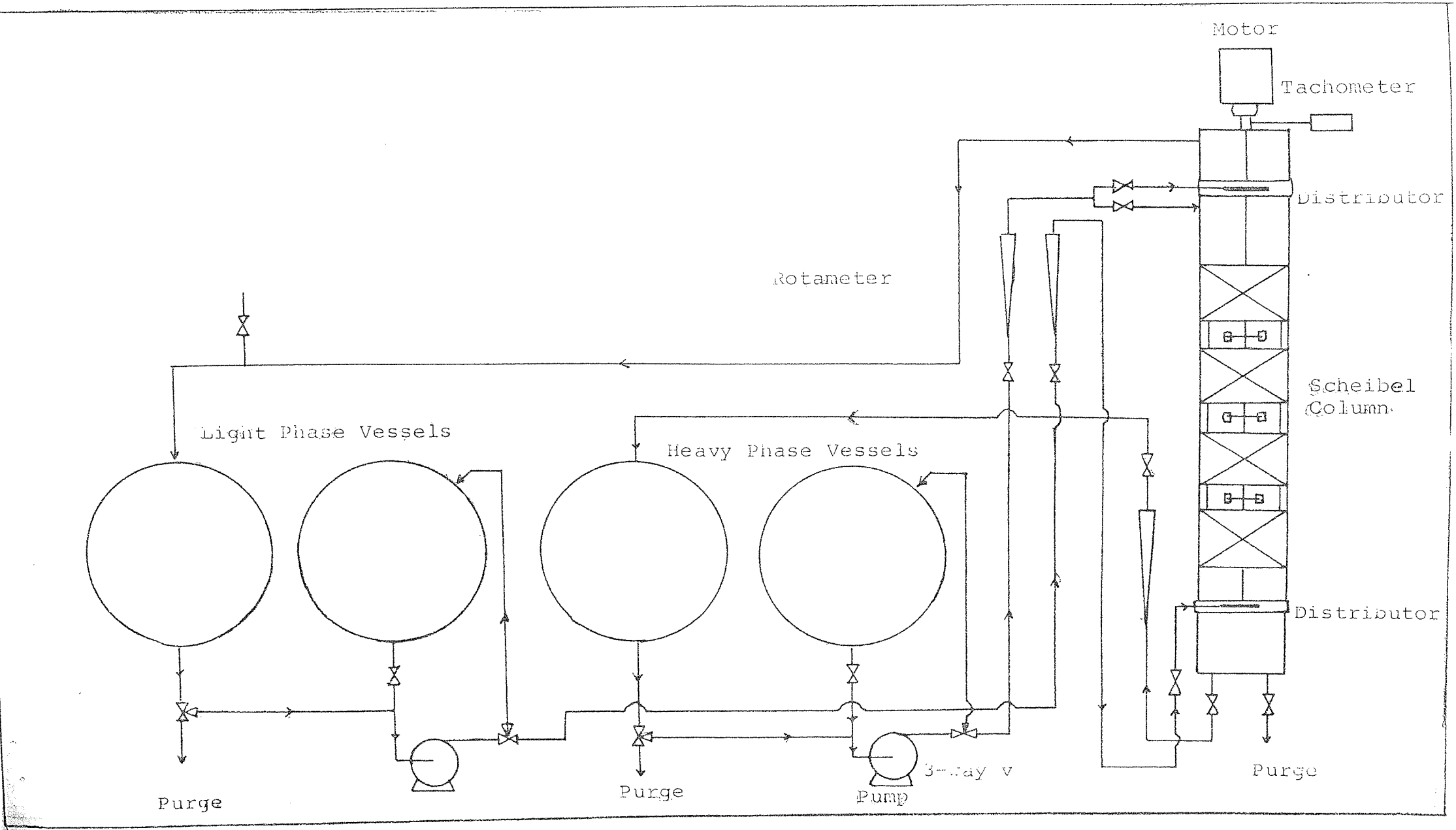

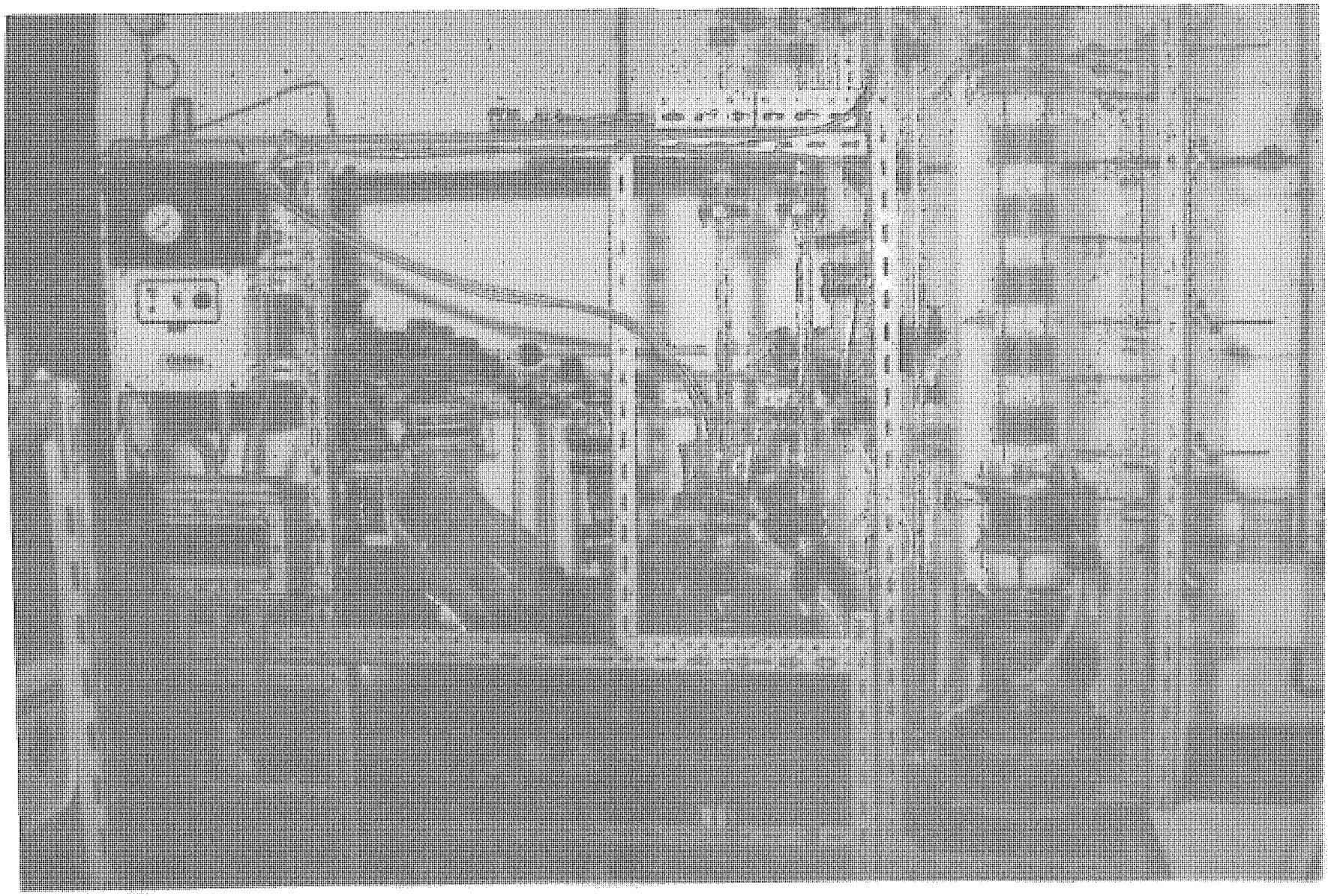

Figure 6-2 General Arrangement

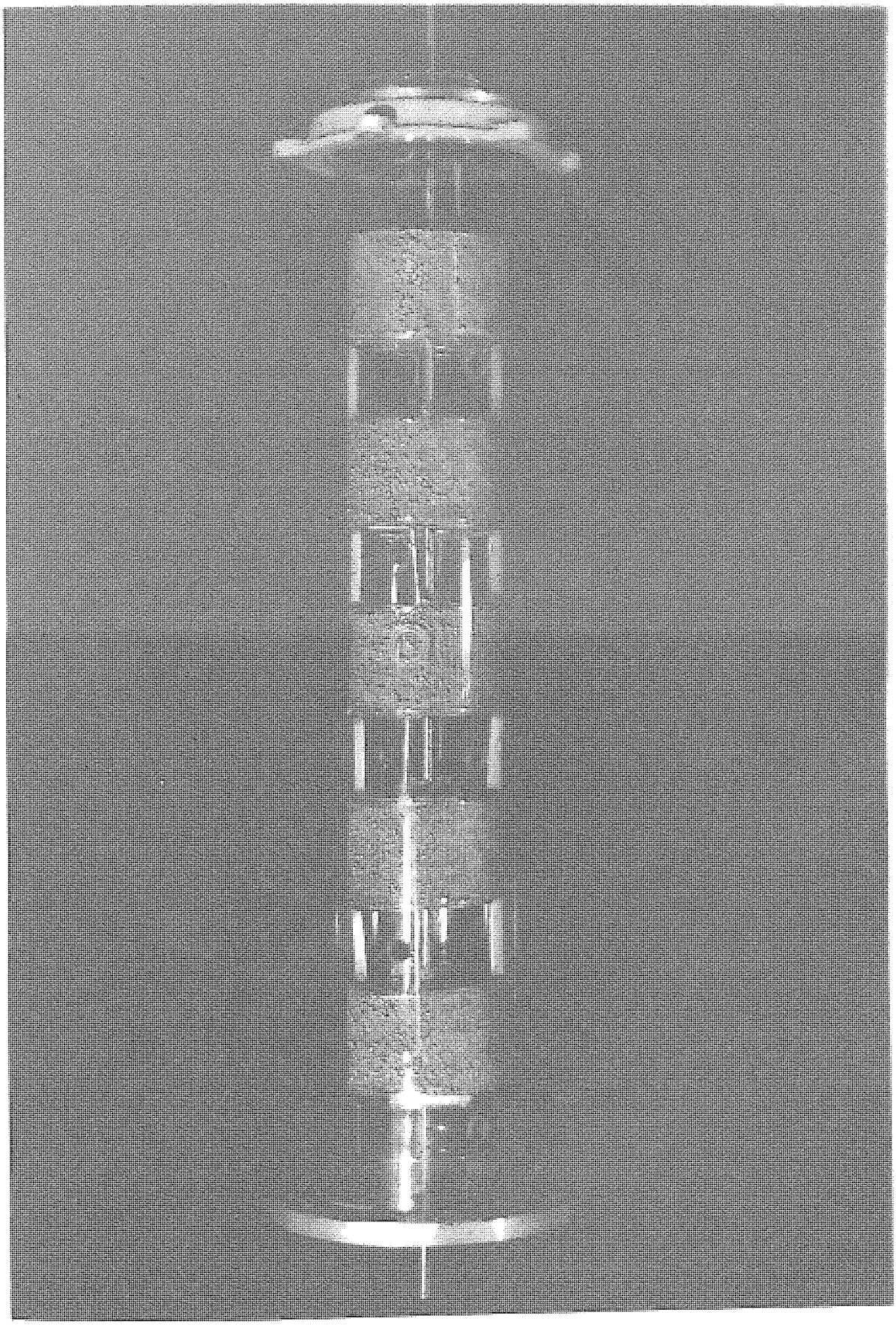

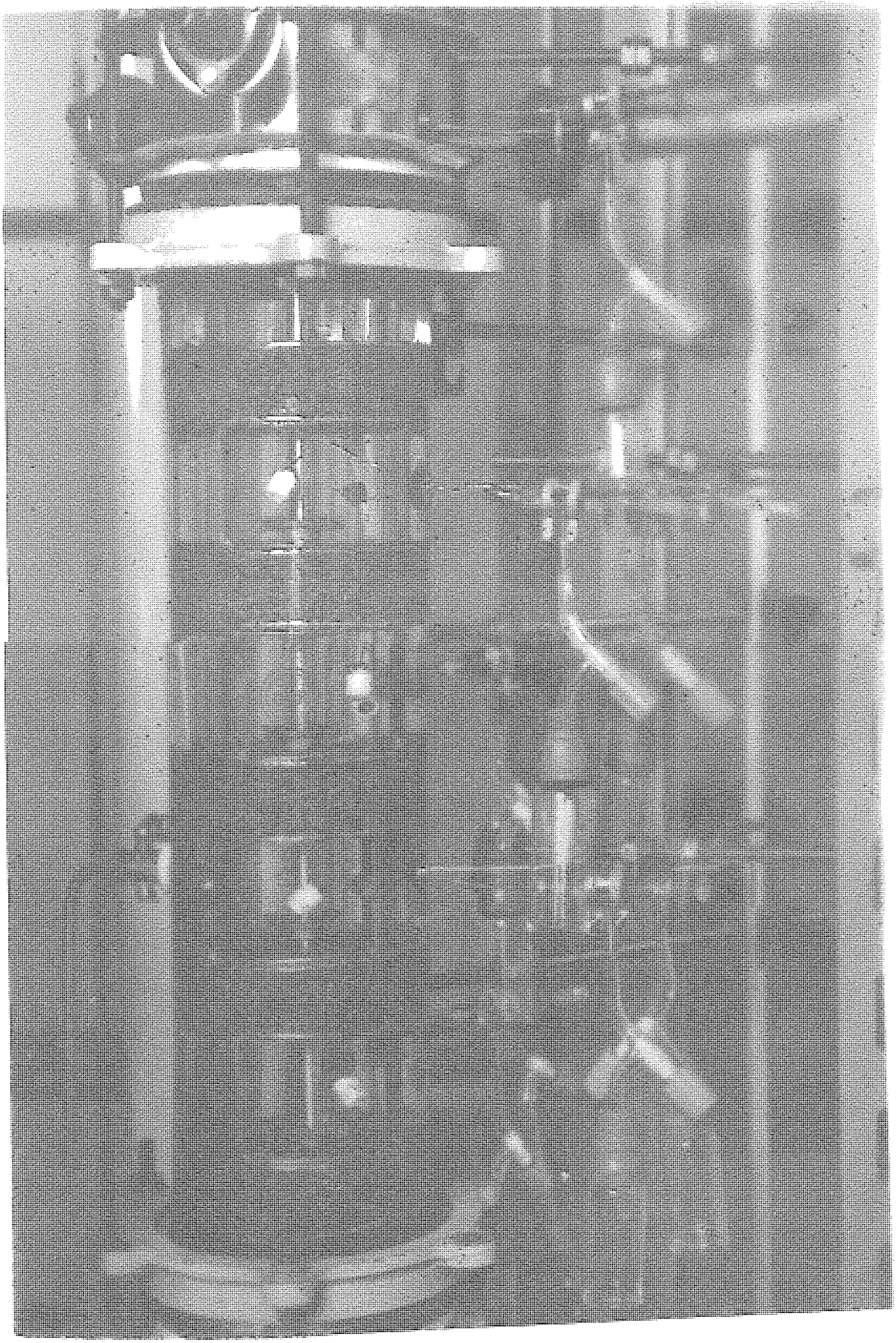

Figure 6.4 Column 2

inflate the error variance and mislead the statistical analysis.

Eight sampling points were provided in Columns 1 and six in Column 2. They were located at the middle of each mixing compartment and at the middle of the top and bottom distributor plates. These last two sampling points were intended to measure the phase concentration jump at the feed inlets. In addition to the above sampling points, a sampling point for each end section was provided in Column 1. Each point comprised a 13mm diameter drilled hole through which the sampling head probes can be set in position.

The column internals were fabricated entirely from 18/8 stainless steel. The rotor shaft, was fabricated from 9.6mm stainless steel rod and was supported by bearings at three points throughout the column length. There was no support bearing within the effective column length. Each 4-bladed standard disc turbines of 33mm diameter was fabricated from 2mm thick stainless steel elements and secured to the shaft by grub screws as shown in Figure 6.5. The packing pad supports shown in Figure 6.5 were made from 2mm diameter stainless steel wire and they were located in each mixing chamber and end sections. Welded to the upper and lower wire ring of the supporter, four vertical baffles each 8mm wide and 2mm thick were located at 90^{o} apart. The baffles were machined to obtain a close fit at the column walls. It is necessary to point out that the original Scheibel column contained

an unbaffled mixing chamber. In this work the baffles were necessary, mainly because, for a low r.p.m. a good dispersion is required for an accurate measurement of hold-up by sampling.

In both columns at the second chamber, numbered from the column bottom, a 1.5cm diameter hole was drilled to accommodate the on-off brass valve for hold-up measurements.

The dispersed light phase was introduced into the column through a stainless steel distributor plate located at the bottom of the column, and left via a lateral pipe above the coalescence interface. The light phase distributor plate assembly as shown in Figure 6.6 was designed such that the feed could, if required, enter directly into the column as a continuous stream. A similar distributor plate assembly was located at the top of the Scheibal column for the introduction of the heavy phase. The two distributor plates were designed according to the methods of Treybal (7). Each consisted of forty-six, 2mm diameter holes arranged on 6mm triangular pitch inside a 0.05m diameter plate. The holes were drilled undersize and then counter-punched to the correct size to provide a small upward projection around the periphery of each hole.

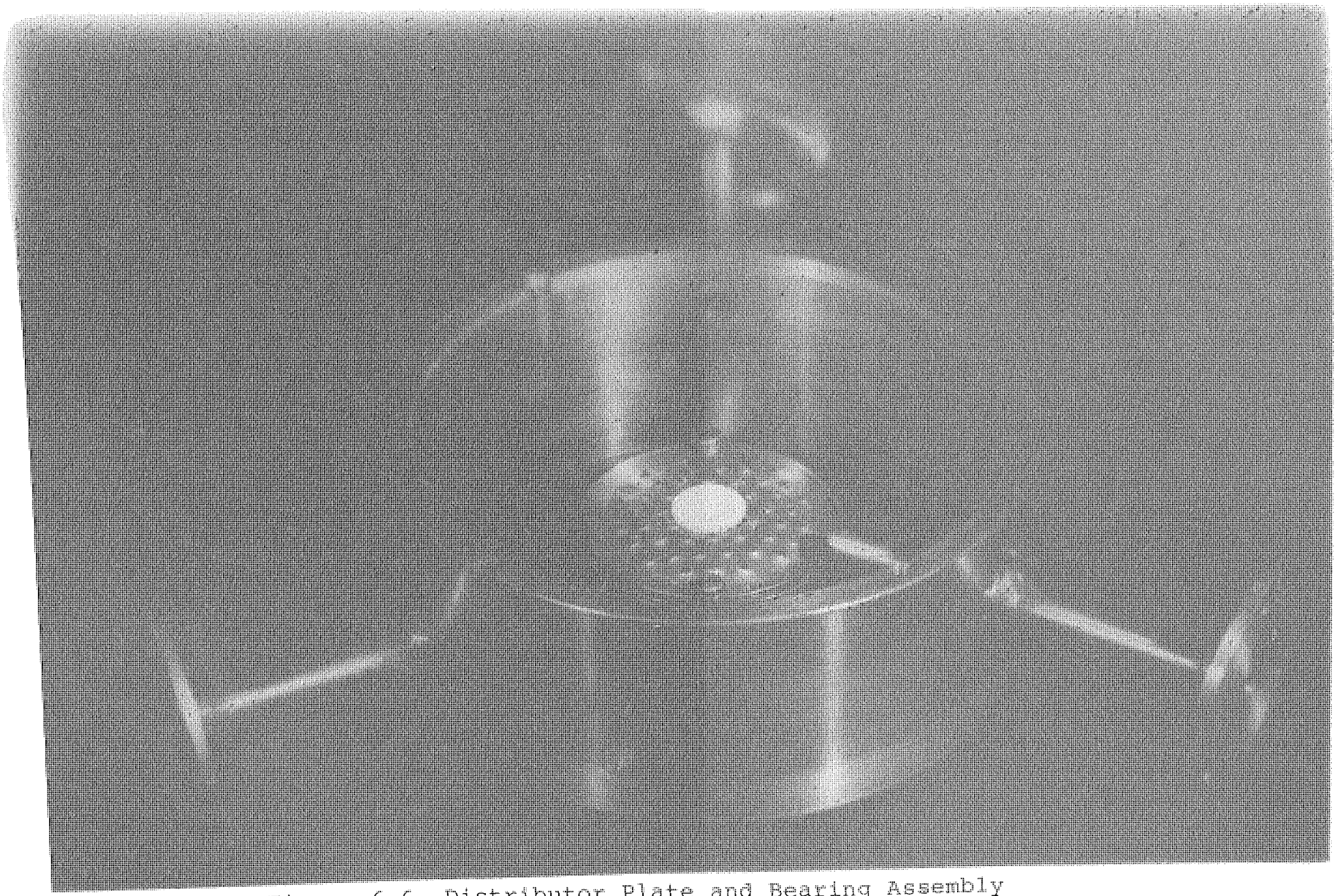

Figure 6.6 Distributor Plate and Bearing Assembly

The column end plates were fabricated from 8mm thick 18/8 stainless steel plate. The bottom plate supports a QFV pipe section located below the low distribution plate and has the necessary lines for draining the column and the heavy phase exit. The top end plate housed a PTFE bearing and a stuffing box filled with 'T-seal' PTFE grannules.

6.1.2 Associated Equipment

The agitator shaft was driven by a ¼ D.C. electric motor, controlled by a single phase 0.25 KW thyristor. The effective speed range was 0-1200 r.p.m. The drive shaft of the motor was coupled to the column shaft via a flexible rubber joint. A 60-tooth wheel was fixed to the top end of the shaft and a magnetic perception head probe positioned at 1cm from the periphery of the wheel send the electrical signal to an electronic tachometer.

Process fluids were stored in any of four 50 litres QVF spherical glass vessels mounted on special supports. Two of these served as reservoir and receiver for the light phase and the other two as reservoir and receiver for the heavy phase. Pipework was mainly of 16mm i.d. borosilicate glass but where flexible lines were unavoidable, 12mm diameter inert PTFE tubing was used.

Flow rates were measured by size 14 rotameters with Korannite ceramic floats type K. Each rotameter was individually calibrated at room temperature using the corresponding liquid phase.

Flow control valves were made of glass with P.T.F.E. stem and seat. Provision was made for the circulation of the liquids within one vessel or between two vessels containing the same liquid by means of by-passes on the pumps.

Fluids were transferred by means of two Stuart-Turner centrifugal pumps, type No. 10 and No. 12 designed to give flow rates of 1.25/0.45 m^3/s at hydrostatic heads of 2.0/ 10.0m. Stainless steel casings and impellers were incorporated in these pumps together with graphite and "Viton A" seals. The speed of each pump could be varied by means of a "Torovolt" variable voltage unit. The pumps were located away from the vessles in order to protect them from any leakage of process fluid. Drip trays were placed underneath the process vessels.

No provision was made for temperature control of the equipment but temperature was always within 18^{o}-$20^{o}C$. The equipment was located in an isolated pilot plant room provided with flameproof switchgear and lighting and an efficient air extraction system.

6.1.3 Packing Selection and Pad Construction

In the Scheibel extractor studies, reported in Chapter 3, knitted stainless steel wire mesh packings were extensively used. Plastic wire mesh wettable by organic dispersed phase was only briefly studied by Piper (3). In all the cases, the only variable used as a criteria for packing selection, for the same material, was the

percentage voidage. A lower limit of 97% was empirically set up and no further information concerning the number of interlocking loops and wire diameter were given. As it will be shown in Chapter 8, pad voidage alone is not a sufficient criterion for the selection of the proper packing mesh.

After testing packing pads made from different materials with various mesh sizes and thickness (see section 8.2, Table 8.1) and considering that the main objective of this research is to study a Scheibel column under the condition of packing wetted by the dispersed phase, a composite knitted mesh called Dual Coalescer (D.C.) .9041 was selected. This packing consists essentially of two dissimilar materials i.e. polypropylene wire of 0.25mm diameter and stainless steel wire of 0.155mm diameter, knitted together to form a mesh structure of asymetrical inter-locking loops of 4 x 5 stitches/inch. This type of packing, patented by Jeffreys and Davies for Knitmesh Ltd., UK (167), uses the concept that at the junction of two dissimilar surfaces, enhanced coalesence takes place, which is termed the "junction effect" (167). Thus, total wettability of the pad by the dispersed phase, with good column capacity performance, is obtained using the above knitted mesh. Immersion tests confirmed that polypropylene wire was unaffected chemically by the process fluids chosen.

The construction of the packing pads required the design and construction of the apparatus shown in Figure 6.7. Plate A, the bottom plate, consists of the

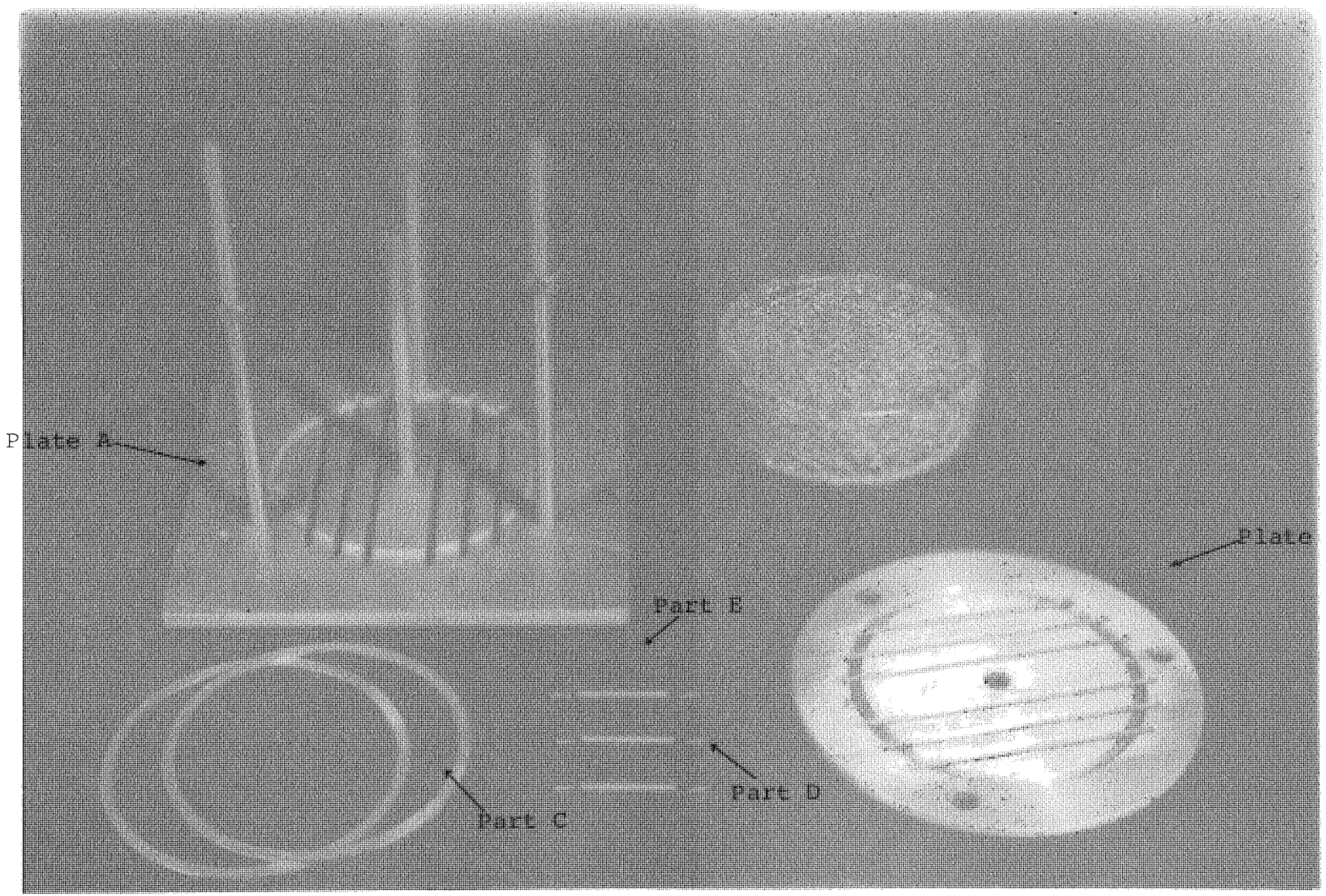

Figure 6.7 Apparatus for the construction of the packing pads

following parts:

1. Three threaded rods to serve as guides for the vertical displacement and position of the plate B. Also they are used to set both plates A and B horizontal.

2. A central rod which simulates the column rotor shaft serves as a guide to the layers of knitted mesh.

3. A circular groove with three small holes slightly greater than the head of the 10BA counter sunk brass screws (part D) drilled all the way through the plate. A stainless steel ring of 0.10m external diameter (part C) also with three holes drilled through it, can be positioned in the groove in such a way that both plates holes and ring holes are aligned. This ring constituted the lower part of the pad. Plate B has also a circular groove with three holes to accommodate another 0.10m external diameter stainless steel ring (part C).

To construct a packing pad the following steps must be observed.

1. Cut the required number of circular (0.10m diameter) knitted mesh layers.

2. Adjust the level of Plate A by using the nuts located below the plate in each of the threaded rods.

3. Located in one of the stainless steel rings in the circular grove of Plate A and the other in the circular groove of Plate B. In both plates, the holes in the ring and in the plates must be aligned.

4. Fix the three spacer rods E to the ring in Plate A using three 10BA¼" countersunk brass screw (part D) which are inserted from below the plate in each of the plate-ring holes and screw into the spacers. Make sure, by locating Plate B in position, that the three plate B-ring holes are aligned with the three spacers.

5. Remove Plate B and start to position the circular mesh layers using as guides the central rod and the three spacer rods. Make sure that the central rod goes through the centre of the layers.

6. After the required number of layers have been positioned, locate the Plate B on top of the pad and fix it in position by the nuts located below and above it on the threaded rods. Check the level of the plate.

7. Fix the spacers to the upper ring in Plate B by locating the remaining three brass screws in each of the Plate B-ring holes and screw them into the spacers. Remove Plate B and the pad.

8. Cut a rectangular piece of knitted mesh of length equal to the perimeter of the pad and width slightly greater than the thickness of the pad. Locate it around the pad side. Pad is now completed.

A total of ten pads of 0.03m and 0.06m thickness were constructed with an average percentage voidage of 96%. The number of circular mesh layers required was calculated using the density of the wire materials, i.e. polypropylene 0.89 gr/cc and 304 stainless steel 8.0 gr/cc and an experimental determined average weight/layer. Twenty layers were required for the 0.03m pad and double for the 0.06m pad.

6.2 Chemical System

High energy levels are created in the Scheibel extractor compartments due to the high degree of turbulence generated by the impellers. It is well established that in a turbulent environment the size of the drops is roughtly proportional to $(\sigma/\rho_c)^{0.6}$. Thus ideally, a high interfacial tension system would be preferred for study since the resulting drop sizes would be larger and thus easier to record and measure.

The system toluene-acetone-distilled water was chosen for the investigation with the distilled water as the continuous phase in all experiments. The advantages of this system are as follows:

(i) The solubility data was available for the system (168) (Figure 6.8)

(ii) Advantages from the point of view of availability, cost, stability and low toxicity have been described (169

(iii) The interfacial tension of the system is affected by the concentration of solute (acetone) in the

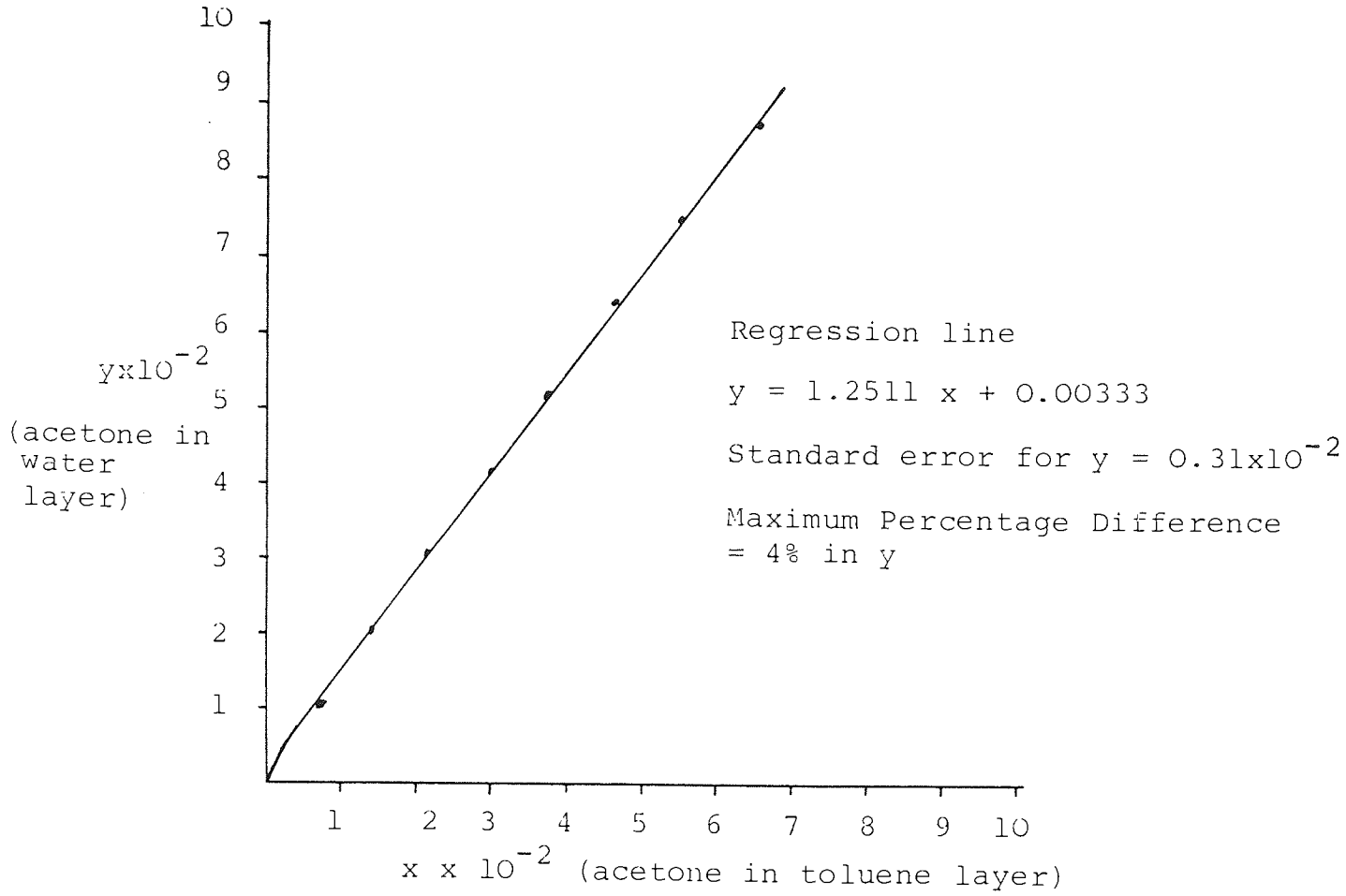

(a) Distribution of Acetone between toluene and water (168) at 20°C in solute free base unit

(b) Interfacial Tension vs Acetone w/w% in organic phase at 20°C

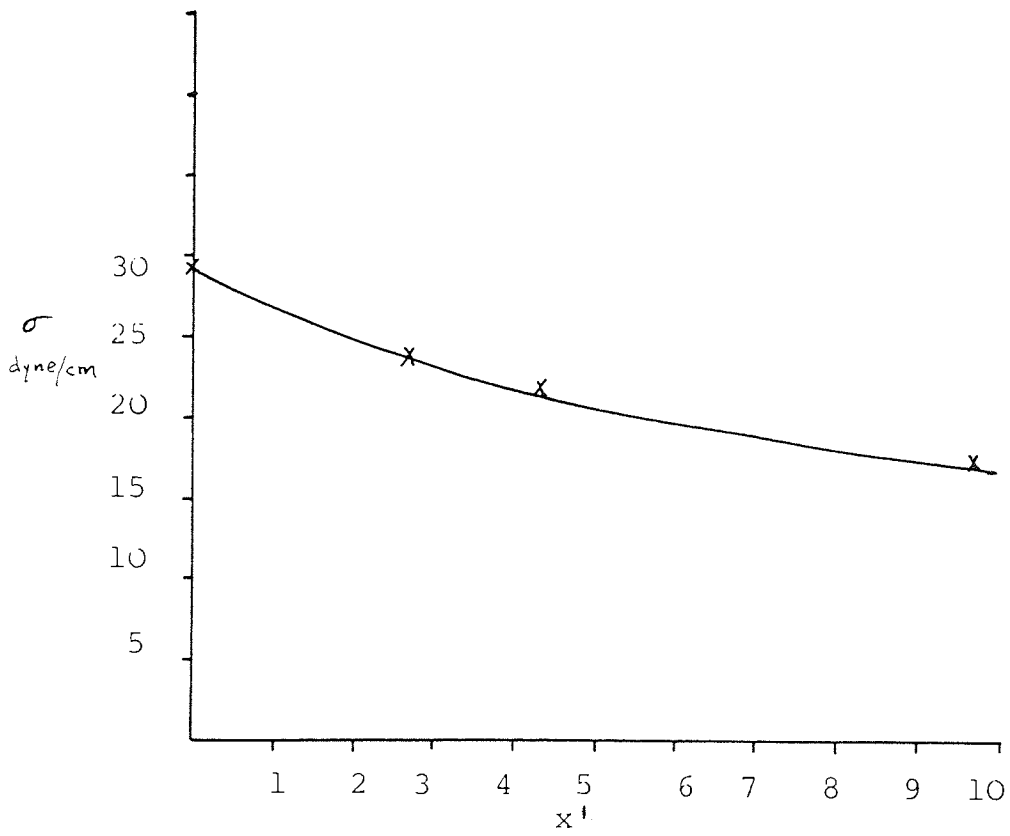

Figure 6.8 - Equilibrium and Interfacial Tension

dispersed phase. Thus, it is expected that the direction of mass transfer to have a large influence on the column hydrodynamics and mass transfer performance. See Figure 6.8.

(iv) The system has been adopted as standard in liquid extraction column research by the European Federation of Chemical Engineering Working Party on Distillation, Absorption and Extraction. This facilitates comparison of results from different sources.

(v) The solvent could be easily recovered and purified.

(vi) Analytical techniques are available for the determination of acetone content in the aqueous and organic phase.

(vii) The equilibrium relationship is approximately linear, in the immiscibility region. This facilitates the theoretical analysis of the experimental data. Also the equilibrium data are not greatly affected by small variations in temperature.

Materials of the highest grade available were used and no further purification was made. The material grades and specifications are listed in Table 6.1 Constant monitoring of the purity of the chemicals by measuring the interfacial tension, was done during the whole experimental work and if there were serious discrepancies, the liquids were discarded.

Table 6.1 - Specification of Material Used

Toluene "Analar"

Wt. per ml at 20°C	0.863 - 0.866g
Refractive Index at 20°C	1.494 - 1.497

Nt less than 92 percent distils within 0.4°C in the range 110.0° - 111.0°C.

Impurities	Maximum Limit Percent
Acidity	0.012
Alkalinity	0.012
Non-Volatile Matter	0.002
Benzene	0.5
Organic Impurities	Passes Acid-Wash Test
Sulphur Compounds	0.0003
Thiophen Homologues	0.0002
Water	0.03

Acetone "Analar"

Wt. per ml at 20°C	0.789 - 0.791g
Boiling Range (95%)	56.0° - 56.5°C
Refractive Index	1.3580 - 1.3600

Impurities	Maximum Limit Period
Water	0.2
Acidity	0.02
Alkanity	0.03 ml N/l
Non-Volatile Matter	0.0005
Aldehyde (HCHO)	0.002
Methanol (CH_3OH)	0.5
Substances Reducing Permanganate	0.0002

The physical properties of the system were measured as follows:

(a) Specific gravity

The standard pyknometer technique was employed for all solutions. Measurements were made at 20°C ± 0.1°C.

(b) Viscosity

The method of timing the passage of the fluid through a capillary immersed in a constant temperature bath (20°C ± 0.1°C) was used. The types of viscosimeter used were Cannon-Fenske B S/IP/CF No. 25 and No. 50.

(c) Interfacial Tension

The standard Du Nuoy ring method was used on a "Cambridge" torsion balance at 20°C ± 0.1°C. The measurement was done with mutually saturated liquid phases.

Table 6.2 presents the measured physical properties.

6.3 Experimental Procedures

6.3.1 Non Mass Transfer Studies

6.3.1.1 Cleaning Procedure

A 2% v/v aqueous solution of Decon-90 decontaminant was used to clean the column vessels and the process lines. The whole system was filled with the cleaning solution for at least eight hours and this was then circulated throughout the system with the agitator on for about an hour. The solution was drained and the system was then flushed through

Table 6.2 - Measured Physical Properties of Fluid System at 20°C

(a) Toluene	
Interfacial tension with water (mutually saturated)	0.0295 N/m
Density	$(0.868 \pm 0.002) \times 10^{3}$ Kg/m
Viscosity	$(0.58 \pm 0.01) \times 10^{-3} \frac{N_s}{m^2}$
(b) Distilled Water	
Density	$(0.99g \pm 0.002) \times 10^{3}$ Kg/m
Viscosity	$(1.02 \pm 0.01) \times 10^{-3} \frac{N_s}{m^2}$

(c) System Toluene-Acetone distilled water

Interfacial Tension - see Figure 6.8(b).

Equilibrium Relationship - see Figure 6.8(a).

with tap water and finally rinsed with distilled water. Care was taken to ensure that all sample points and drainage points were well flushed and free of traces of detergent. Checks were made by measuring the surface tension of the distilled water.

6.3.1.2 Preparation of Fluid System

Toluene was employed as the dispersed phase throughout. It was used without further purification and its purity was carefully monitored. If a significant discrepancy in the value of the surface tension was obtained, it was then purified by distillation in an Oldershaw column with low reflux.

The continuous phase was once-distilled with water throughput produced from an all-glass still. Before use, the phases were mutually saturated by recycling them through the column for at least two hours.

6.3.1.3 Flooding

Flooding rates represent the maximum volumetric capacity of a contactor under a given set of conditions. In the Scheibel columns studied in this research, flooding was characterized by the formation of a second interface underneath any packing pad. If conditions persist the coalesced layer increases occupying the whole stage and eventually spreads to the whole column inverting the physical appearance of the phases.

The operating procedure to determint the onset of flooding was as follows:

The columnwas filled with the aqueous continuous phase up to the plane to be occupied by the interface, generally a distance of 0.15m above the top distribution plate. With the agitator stationary and with no continuous phase flow, dispersed toluene phase was admitted to the column at a low flow rate. When the build-up of coalesced dispersed phase above the interface was sufficiently high it flowed out of the column and back to the reservoir. The agitator was then started and its speed adjusted to the required value. The dispersed phase hold-up steadily increased, and the continuous phase which it displaced was allowed to flow out of the column via the outlet valve. The continuous phase was then admitted to the top of the column at the desired rate.

Careful control of the outlet flowrate of the continuous phase was necessary to maintain the interface at a constant level at the top of the column throughout this start-up period during which the hold-up was increasing. Steady state was achieved when the interface level remained steady and the continuous phase inlet and outlet flowrates were equal.

The dispersed phase flowrate was then increased incrementally until the appearance of a second interface beneath any pad inside the column. Sufficient time (15 minutes) was allowed for steady state conditions to be re-established following each increase. Occassionally

temporary incremental increases in the continuous phase outlet were necessary to maintain a constant interface position during re-establishment.

At the onset of flooding, the dispersed and continuous phase flows and the agitator speed were recorded. As a check, all the flows and agitations were stopped, the dispersed phase allowed to collect above the interface and the whole operation was repeated in order to duplicate the experiment. The flooding data obtained and discussion are given in Section 9.2.1.

6.3.2 Mass Transfer Experiments

6.3.2.1 Preparation of Fluid System

The toluene dispersed phase was prepared in the same manner as described in Section 6.3.1.2, as was the distilled water. Solutions were made up to the required solute concentration by the addition of "Analar" Acetone.

It is customary in mass transfer experimental program to run the experiments alternating the mass transfer direction, i.e. the rafinate phase at one experiment constitutes the extract phase in the next run. This procedure saves time and material. Unfortunately, when the experimental program is based on a statistical factorial design, the above procedure is totally unacceptable since the experiment has to be carried out in a random order. Therefore, it was decided that each experiment will run with fresh solvents and the aqueous phase product will be discarded. The organic phase

product was collected and distilled, except in a few cases, i.e. toluene phase as rafinate phase, in which the organic rafinate was exhausted by multiple acetone extraction with fresh distilled water. In all the runs, the purity of the solvents to be used was checked by measuring the surface tension and the refractive index of each one.

6.3.2.2 Experimental Procedure

The procedure for the mass transfer experiments was as follows:

1. Assemble and clean the sampling head probes as described in Section 7.3.

2. Position the head probes inside the mixing chambers of the Scheibel column using the needle clamp assembly shown in Figure 7.4. Insert also the head probe-needles in the holes provided in the distributor plates in order to measure the feed concentration jumps.

3. Connect the head probe-needles with the sample collector device as shown in Figure 6.9. Each of the 1cc syringes must be filled with the liquid phase to be sampled.

4. Start circulation pumps. The continuous aqueous phase is allowed to fill the column slowly, using the connection between the aqeous feed line and the lower distributor. The reason for filling the column from the bottom at a low rate is to avoid trapping air inside the packing zones.

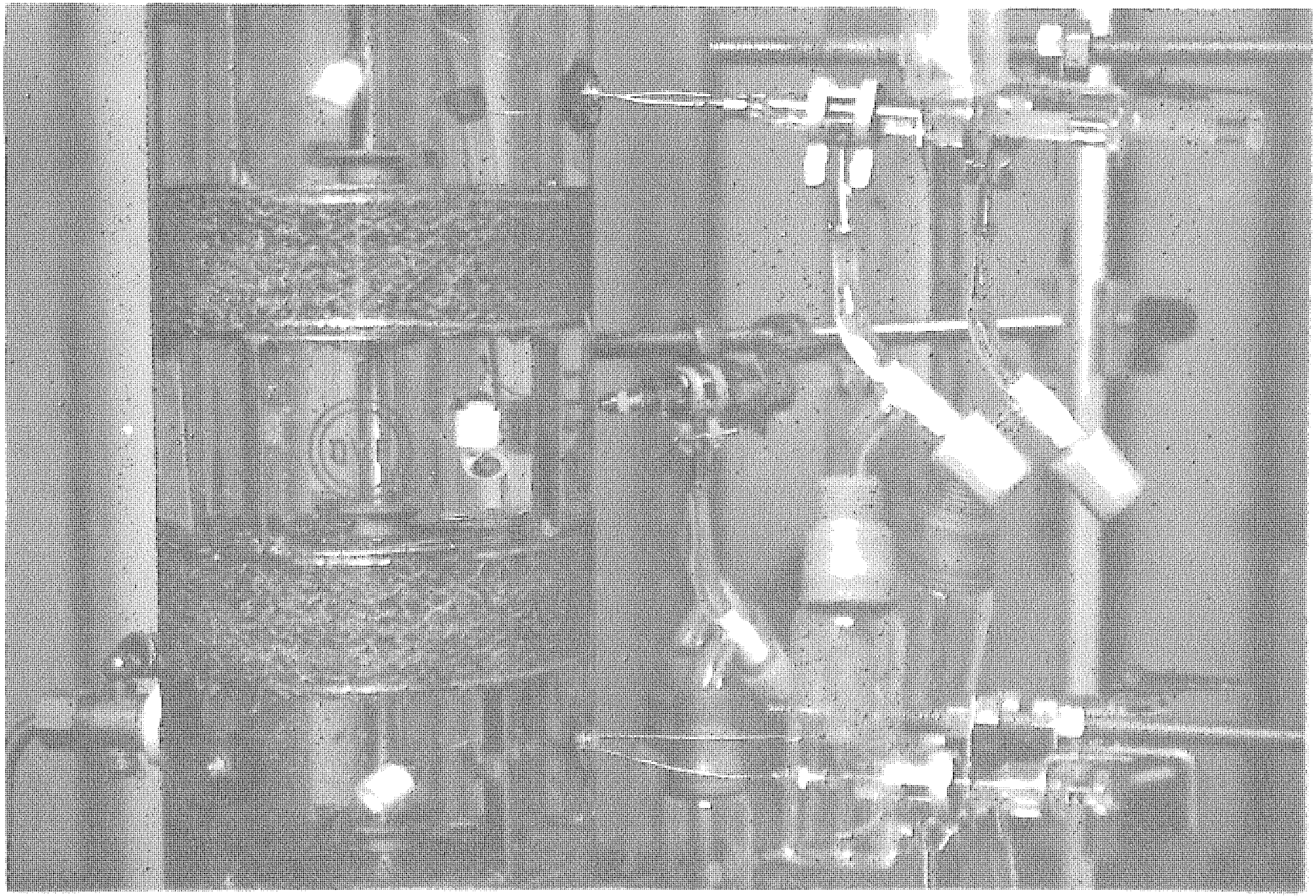

Figure 6.9 Sample collector system positioned at the Column

5. As soon as the head probes in a chamber get immersed, inject half of the content of the syringes into the column and fix the plunger in position using the brass stopper attached at the back of the syringe.

6. Continue filling the column until the level reaches the required height above the top distributor plate. Close the main feed valve located below the heavy phase rotameter. Close the valve connecting the aqueous phase line with the lower distributor and open the valve connecting the aqueous phase line with the top distributor.

7. Start the agitator motor and set the stirrer speed to the desired value. Open the main valve for the organic dispersed phase feed and set the flowrate to the required value.

8. After the coalesced dispersed phase overflowed by gravity from the top of the column, open the valves of the heavy phase feed line and adjust the flowrate at the desired value. Open the valve at the heavy phase exit and maintain the column principal interface at a constant height.

9. Open the small Teflon-Rotaflow valve of each sampling collection system, individual phase start to flow out of the columns. Regulate the sampling rate, preferable very low at the beginning. Check the tip of the syringe for possible entrainment of the undesired phase. If this occurs flush the contents of the syringe

into the column and slowly start moving the plunger back into position.

10. Allow the sampling system to work at low sampling rates for about 5 minutes. In parallel, control the position of the main interface. Occasionally, temporary upset of the heavy phase outlet flow is necessary to keep the level of the interface constant.

11. After 15 minutes of operation, close all Teflon-Rotaflow valves in the collection system and discard all the samples collected in the sample bottles.

12. After 30 minutes of operation, get a 10ml sample of the coalesced dispersed phase at the top of the column and of the heavy phase out let at the bottom.

13. When 45 minutes of operation have elapsed, collect a second sample of the organic phase outlet flow and aqueous phase outlet flow. Start the collection of single-phase samples by opening the Teflon-Rotaflow valves. Adjust the valves to obtain the desired sampling rate. After 5 minutes, start collecting the samples in the 10ml sample bottles.

14. While the sampling is taking place, start taking the pictures of the agitated chambers.

15. When single phase sampling is completed, shut-off all the Teflon-Rotaflow valves and remove the sample bottles.

16. Remove 100ml two-phase sample from Chamber 2 for hold-up measurement. It is necessary to wait 5-10 minutes if a second sample is desired.

17. Stop agitator and shut-off all the inlet and outlet mains valves. Experiment is completed.

CHAPTER VII

EXPERIMENTAL TECHNIQUES

EXPERIMENTAL TECHNIQUES

7.1 Drop Size

The photographic technique was chosen to measure drop size. Photographs of the dispersions were taken on H.P.5 Ilford 35mm film, 400 ASA, using an Asahi Pentax Spotmatic still camera with a Macro Takumar, 100mm lens at a shutter speed of 1×10^{-3}s to "freeze" the movement of the drops.

A fixed focus guide or spacing adaptor was constructed to control the distance between the column wall and the camera and it was used to maintain the plane of focus at the same depth inside the column wall for all the drop size photographs. The focus plane was approximately between 5mm to 15mm inside the column wall, and the depth of field was in the neighbourhood of 3mm. The focus plane could not be moved further into the column because the drops between the wall and the focus plane blurred the picture, especially under operating conditions of aqueous continuous phase rafinate and high r.p.m. Figure 7.1 shows a typical drop size picture.

The light source was a twin Kobold SR2 cine light which produced 1250W at 125V. Light was directed into the mixing compartments at an angle of 90^{o} to the camera. Two photographs were taken for each mixing chamber.

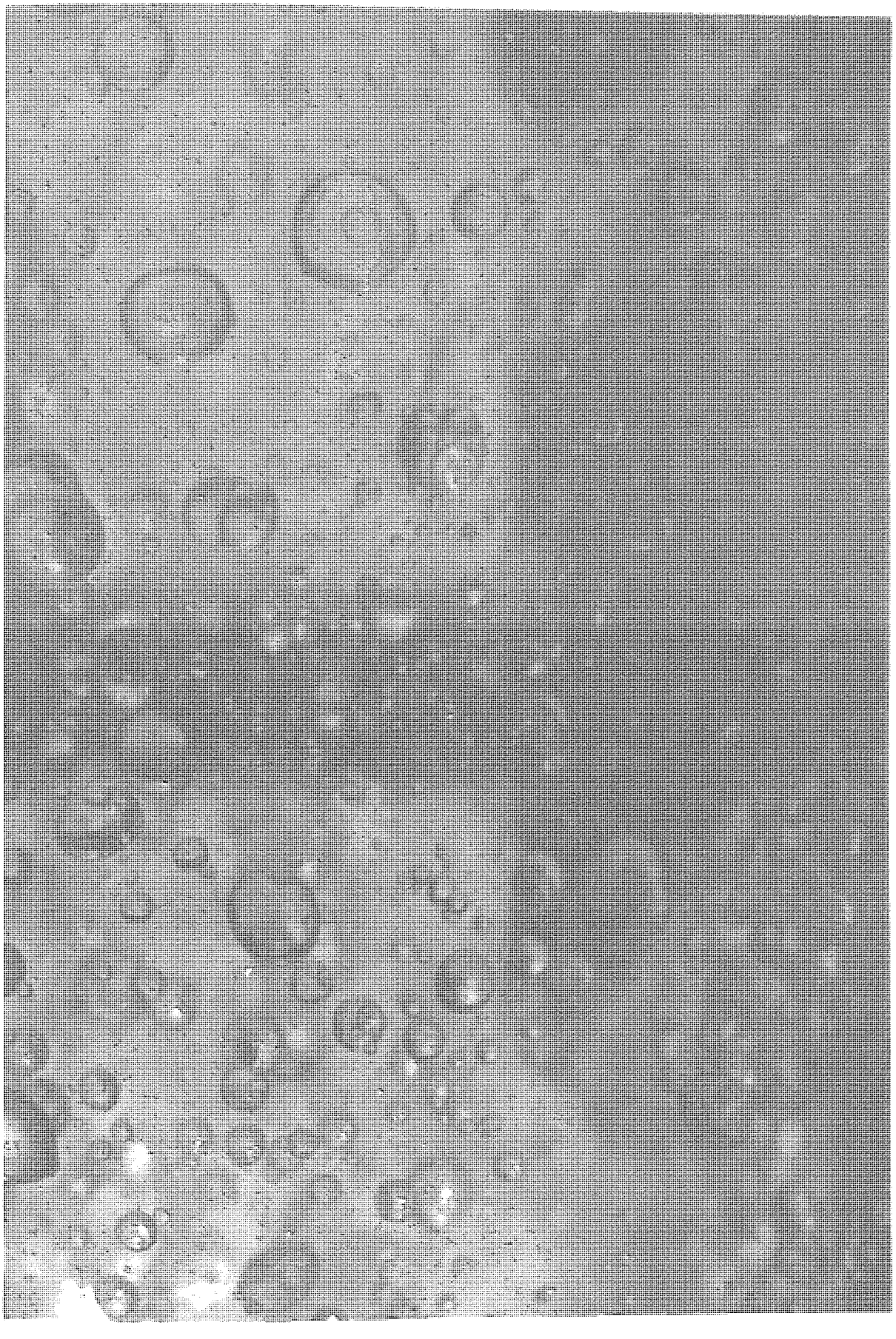

Figure 7.1 Typical Photographs of Dispersion

Distortion in the drop size pictures introduced by the curvature of the column wall was reported (70, 87) to be negligible for columns of similar size to the one studied in this research. Furthermore, the depth of field of the pictures was so shallow that it was reasonable to neglect distortion effects. Nevertheless, the drops at the extreme edges of the picture were not measured because the curvature of the wall may place them too far behind the focus plane and distortion would occur.

Enlargement of the negative to give an overall magnification of 3 to 4 times the true drop size, with printing on Kodak grade 4 "Bromesko" paper, gave sufficient magnification and contrast for counting the drops. Calibration of the measuring procedure was performed by photographing a stainless steel ballotine of 4.0mm diameter immersed in the continuous phase at Chamber No. 2 at a distance of 5 to 15mm inside the column wall. This allowed the focal plane to be fixed for the rest of the experiments pictures and the resulting enlarged photographic print of the ballotini allows the calculation of the magnification factor to be used in the drop size calculations. This operation was done in every experiment before the start up of the plant.

The counting of the drops on the enlarged prints was performed using the Zeiss TG3 Particle Counter. The number of drops to be measured on eachprint is a function of the variance of the drop size distribution and the desired precision of the sample mean. If one assumes

that the drop sizes are normally distributed then for a known variance, the sample size, n, can be obtained by equating the required precision of the sample mean to the 95% confidence interval,

$$\frac{\Delta}{2} = \frac{S}{\sqrt{n}} t_{0.05(n-1)}$$

Δ = precison on the mean diameter (e.g. 0.1mm or confidence interval ±0.05mm)

S = standard deviation of the drop size distribution

n = number of drops measured

$t_{0.05(n-1)}$ = the value of 5% of the Student "t" distribution with (n-1) degree of freedom.

Application of the above equation to various drop size distributions using a precision equal to 0.1mm gave n in the range of 100 to 160 drop. Thus a sample size within the above limits was considered satisfactory. A Honeywell 316 digital minicomputer was used to process the measurements to produce a comprehensive statistical analysis of the distribution. The listing of the computer program in BASIC language is given in Appendix 1.

Additional high speed cine films were taken to record and enable qualitative analysis of the drop formation mechanism at the impeller zone. Kodak 16mm Tri-X Reversal roll film was used in a Milliken R16 with a P3 type, fo.75 lens. Lighting was provided by two 500W photo flood lamps in addition to the Kobold lamp. The films were taken at

500 and 1000f.p.s.

7.2 Hold-up

A substantial amount of time was devoted to find a suitable technique to measure the dispersed phase hold-up. The technique of measuring the difference in static pressure at two points in the column was first examined. The measured pressure drop can be used to calculate hold-up if dynamic pressure variation is negligible, the mean density of the fluid is known and from this value the percentage volume of the dispersed phase can be estimated. Batch tests were performed in an agitated baffled vessel of 0.10m diameter with two 0.015m diameter holes spaced 0.05m axially. These two holes accommodate P.T.F.E. plugs in which 1mm diameter holes (static hole) were drilled in each one and connected to a Differential Pressure Transducer with a working range of 0-5cm water and accuracy better than 5×10^{-2}cm of water. The results obtained for several impeller speeds and locations indicated that the dynamic pressure was of a random nature and constituted a large percentage of the total pressure difference. This led to the conclusion that this technique cannot be applied to the mixing chamber of the Scheibel column under study.

Previous work (70, 87) had reported that the hold-up of the dispersed phase in an extraction column can be satisfactorily measured by sampling in the agitated compartments. A 4mm bore on-off brass valve was located in Chamber No. 2 of the column described in Section 8.2,

Figure 8.1. All the parts of the valve in contact with the dispersion inside the column were made from 18/8 stainless steel and the flexible sealing washers from Viton. Due to the large bore of the valve, 100ml samples could be taken in about two seconds.

The accuracy of the sampling technique was checked by comparison with the results obtained using the displacement technique under the same operating conditions. It is necessary to point out that the displacement technique cannot be normally applied to a Scheibel column due to the high entrainment of the dispersed phase inside the "wetted" pad, but in thecase of the column used in the preliminary experimentation the thickness of the pads was so small, 0.015m, that any entrainment can be considered negligible in comparison with the total column hold-up. The results of applying both techniques are listed in Table 7.1 and they clearly indicate that the sampling method gave reliable data. Replicated experiments using the sampling techniqe gave % hold-up values with an error variance around 0.52 for all operating conditions.

7.3 Concentration Profiles

None of the sampling techniques discussed in Section 4.3.1 can be successfully applied in highly turbulent mixing chambers. In small mixing chambers, as encountered in a standard Scheibel column, the movement of the drops follows quite closely the toroidal flow pattern created by the turbine impeller. Under this condition, it is very

Table 7.1 - Hold-up data. Displacement vs Sampling Technique

$V_D \times 10^3$	$V_C \times 10^3$	RPM	ϕ_D Displacement	θ_D Sampling
1.42	0.98	400	0.0415	0.0432
1.42	1.74	400	0.0454	0.0469
1.42	0.98	500	0.0643	0.0660
2.08	0.98	500	0.0834	0.0946
1.42	0.98	700	0.1438	0.1467
2.08	0.98	700	0.2000	0.2060

difficult to obtain uncontaminated samples of the light dispersed phase using a downward-facing funnel-shaped sampler.

The idea behind the technique developed in this research, as far as the dispersed phase sampling was concerned, is the creation of a spatially fixed droplet coalescence nucleus inside the turbulent chamber from which the coalesced dispersed phase can be withdrawn out of the column by means of a hypodermic needle. The creation of the coalescence nucleus is achieved by the immersion into the dispersion of a small hollow cylinder made from material wetted by the dispersed phase which accommodates inside successive layers of dispersed phase wetted micro-mesh cloth. One end of the cylinder is welded to a 22-gauge hypodermic needle with its open tip protuding into the cylinder chamber.

Sampling of the continuous phase is based on a concept similar to the one applied by Staffin (162). In this situation the sampling probe behaves as a drop filter. A chamber similar to the one described above is made from material wetted by the continuous phase and several layers of micromesh cloth preferentially wetted by the continuous phase are positioned inside it.

The materials used were P.T.F.E. and Nylon micro-mesh (1μ width of opening) for the organic phase sampling head and brass and stainless steel micromesh (27μ width of opening) for the aqueous phase sampler. Figure 7.2

shows schematically the different types of sampling head probes constructed during this investigation and Figure 7.3 is a picture showing all the different components of the head probes.

Based on the principle of operation of the dispersed phase sampler, the rate of withdrawal of the sample depends on the drop population (hold-up) and on the number of drops that hit the head probe with subsequent coalescence. All the factors, operational and physico-chemical, that affect the dispersed phase hold-up and drop-liquid and solid interface coalescence mechanism will influence the performance of the sampler.

Thomas and Mumford (163) have indicated that surface preparation is of paramount importance in the "wetting" behaviour of surfaces. They demonstrated that most surfaces when scrupulously clean and dry, display preferential wetting effects, i.e. that phase which first wets the dry surface will be the "wetting" phase. This behaviour is more pronounced with high free-energy surfaces (stainless steel, glass) than with low free-energy surfaces (polypropylene, P.T.F.E.). The micromesh cloths, both nylon and stainless steel, were therefore cleaned with a concentrated De-con solution, followed by a rinse with acetone and finally left immersed for several hours in the liquid which will constitute the respective "wetting" phase. An analogous treatment was given to the head probes. After the samplers were assembled they were kept immersed in their respective "wetting" phase right up to the moment

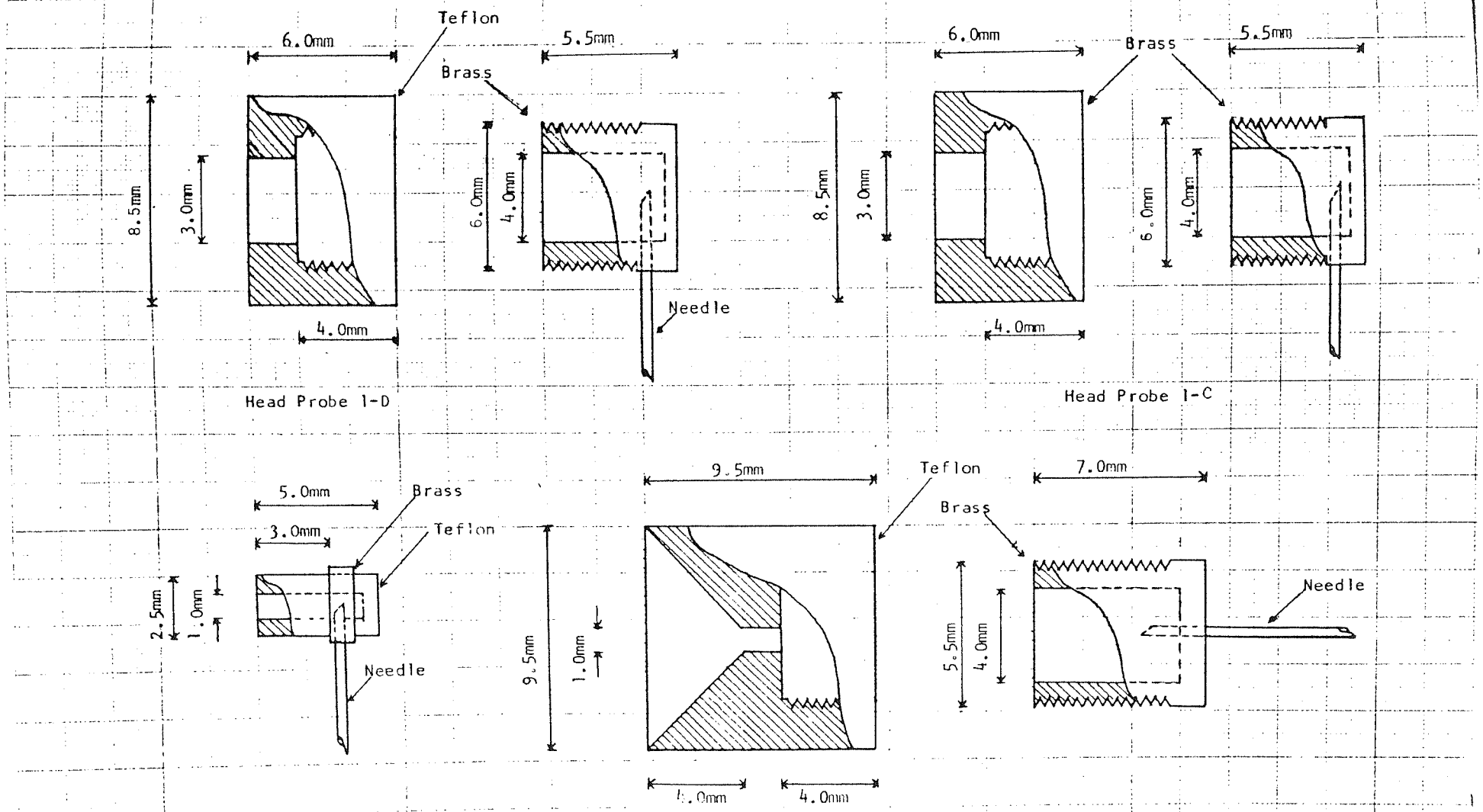

Figure 7.2 - Sampling Head Probes

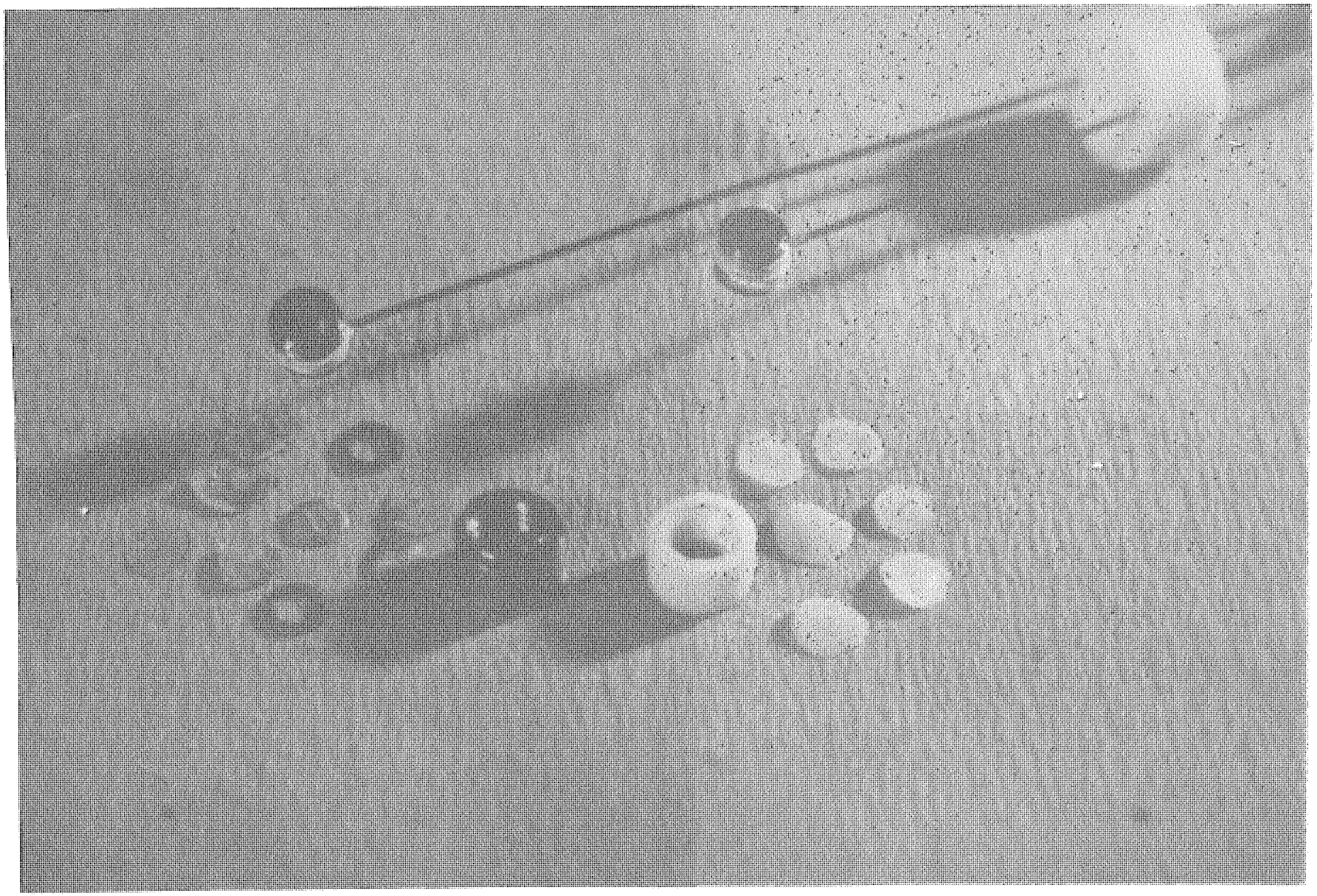

Figure 7.3 Head Probes 1-D and 1-C

to be positioned in the column.

The high standard of cleanliness required for a successful sampling, necessitated removal of the probes from the column to clean them thoroughly at the end of every experiment. This situation calls for a simple, leak-free, plug made from an inert material, which can be easily positioned and removed from the orifices drilled in the columns. Figure 7.4 shows the dimensions and arrangement of the viton plugs. The combination of screw, self-locking washers and nut allows the compression of the viton plug working from outside once it has been positioned in the column hole. The axial compression imposed on the plug induces a radial expansion which gives and excellent seal at the column wall and around the needles.

The head probe-needles were connected outside the column to the sample collector device shown in Table 7.5. The sampling rate was controlled by the small P.T.F.E. Rotaflow valve. Controlled suction for removing the samples was found unnecessary since the hydrostatic pressure inside thecolumn at the different sampling points was sufficiently high. Procedures for starting-up and purging the sampling system were given in Section 6.3.2.2.

7.3.1 Results and Discussion

The column shown in Figure 8.1 of Chapter 8 was constructed to study different designs of the sampling probes as well as to obtain preliminary information about the hydrodynamic behaviour of the Dual Coalescer packing

Figure 7.4 - Needle clamp assembly

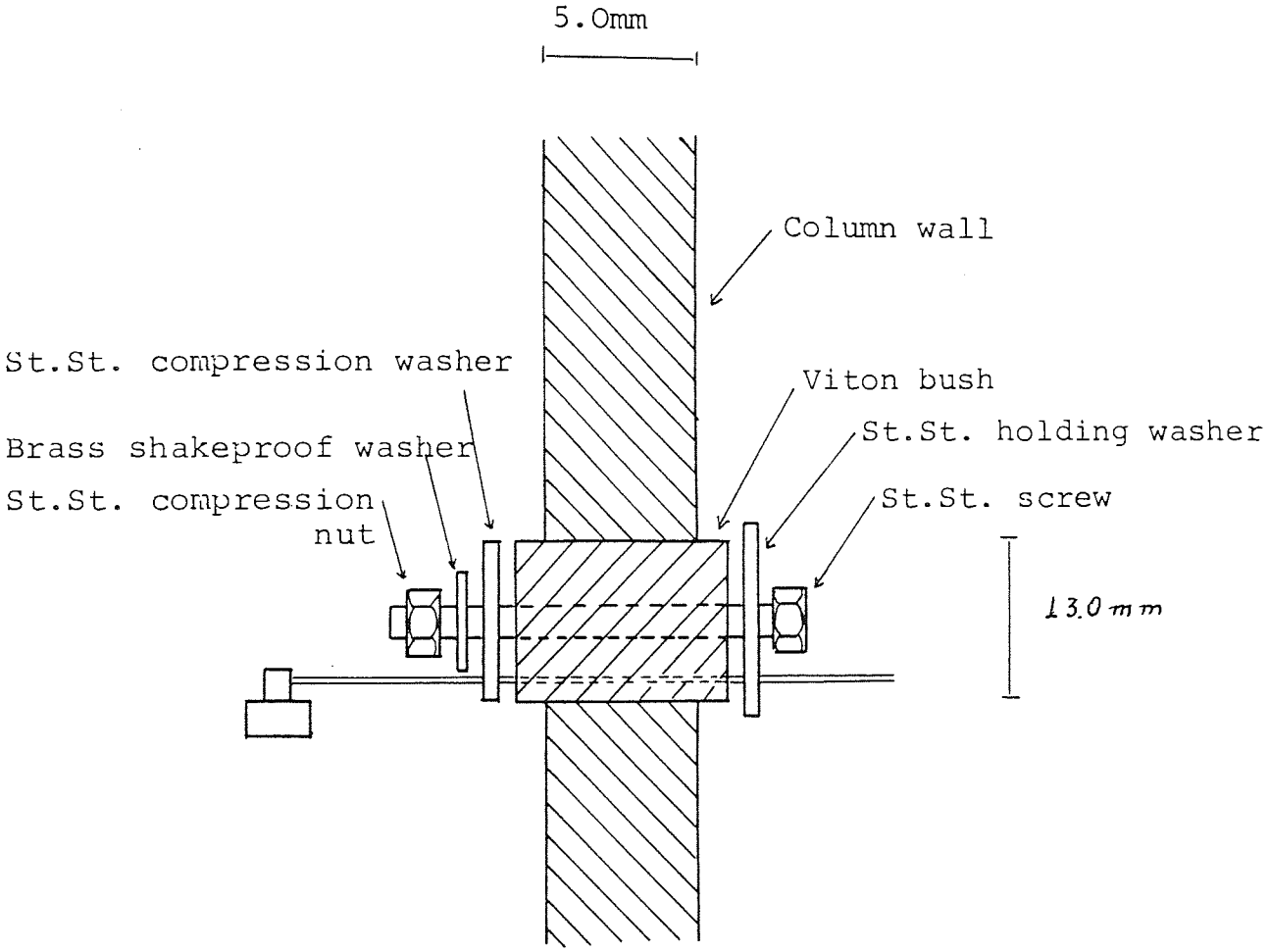

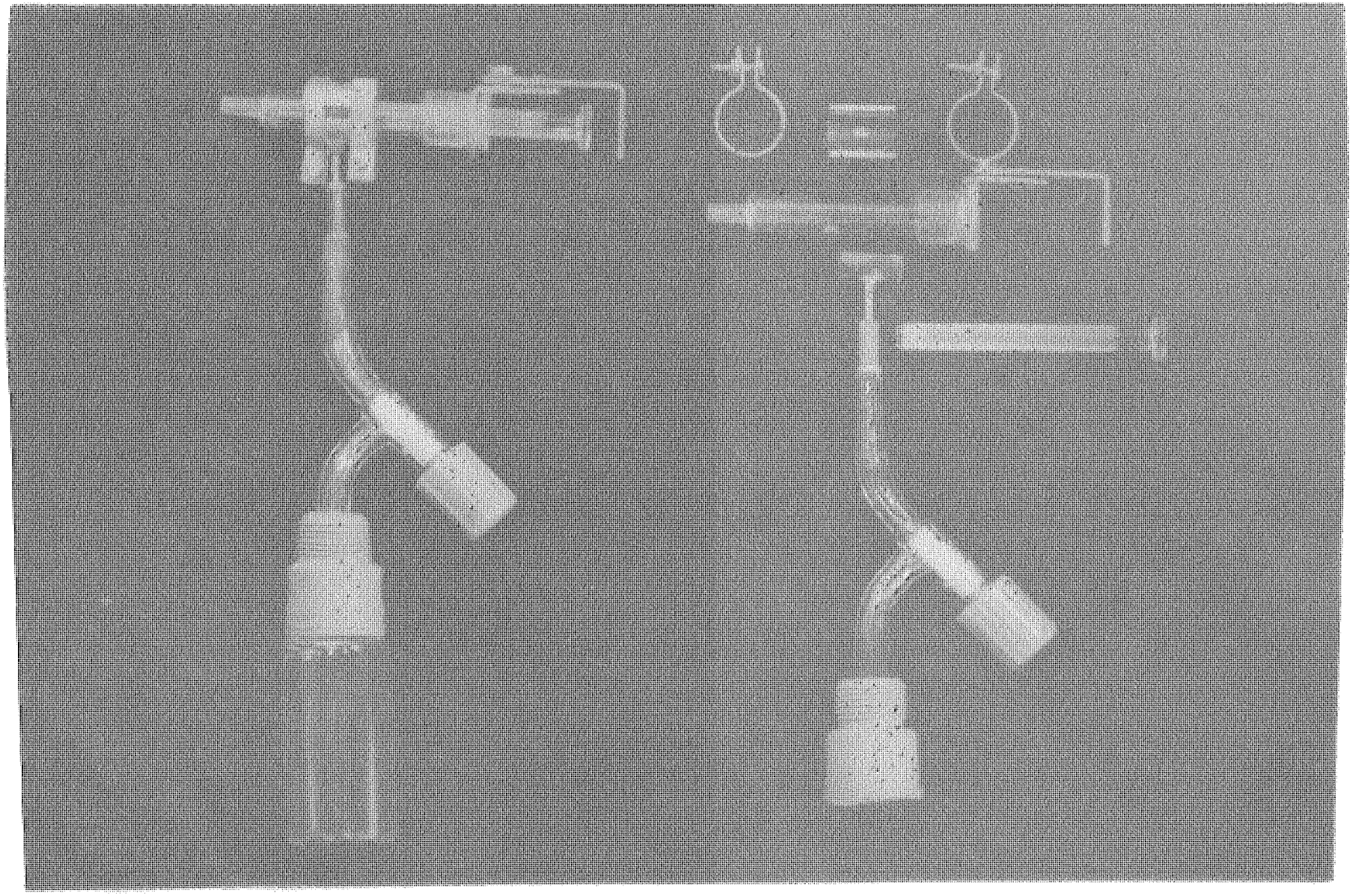

Figure 7.5 Sample Collector System

pads. It was intended to measure the dispersed phase concentration profiles using the P.T.F.E. Probe 1-D shown in Figure 7.2, since batch tests in a one liter beaker demonstrated that the technique was feasible for any sampler positions. Difficulty was encountered when the head of the probe was used in the column. Under all operating conditions the rate of sampling was kept low in order to avoid contamination and in some cases of especially low hold-up with the mass transfer direction dispersed to continuous phase, two phase samples were withdrawn. However, after careful observations of the operation of the column, it was noticed that the mechanism of drop formation in each mixing chamber was mainly jet break-up at the impeller tip which in turn was responsible for the creation of double dispersions. The formation of continuous phase drops within the drops of the dispersed liquid, known as double-multiple emulsions, have been studied by Kessler and York (164). They found that the mechanism of inclusion formation involves the drawing out of a ligament or sheet from the flowing jet, followed by the recoalescence of the free end of this ligament or sheet with the main jet body, entraining in the process a portion of the containing phase. Their observations that large drops contain a higher number of inclusions than the smaller drops was corroborated by photographs taken in this research.

It is then simple to explain the difficulties experienced when sampling the dispersed phase, especially when mass transfer is occurring from the dispersed phase to the continuous phase since this produces the largest drops.

When a large drop of the organic phase coalesces on the P.T.F.E. head of the probe, several small drops of the continuous phase are deposited as inclusions close to or in the suction hole of the head. Repeated coalescence of dispersed phase drops in the head trap an increasing number of inclusions around the head probe and if the coalescence rate of the inclusions with the continuous phase is not fast enough, contamination of the withdrawn sample cannot be avoided. The simple solution of positioning the head with the suction hole in the direction of the continous phase main flow improved the sampling, but still the rate of withdrawal was rather slow (0.5cc per minute). High rates of withdrawal of dispersed phase sample was made possible by using a different head; sample probe 3-D. This probe had an external surface larger than Probe 1-D and the suction hole was positioned at the bottom of a funnel-shaped internal well. The internal funnel as shown in Figure 7.2, enabled a large amount of clean coalesced dispersed phase to be obtained while, at the same time prevented the capture of any inclusions from the suction hole; both conditions were necessary to obtain a fast rate of sampling.

The sampling of the continuous phase by using Probe 1-C was under all conditions satisfactory. However, relatively low sampling rates of about 1cc per minute were necessary when the hold-up was high (20% and above) and the drop size was small (d_{32} = 1.0mm and lower).

7.3.2 Tests on the Reliability of the Sampling Technique

When the problem of obtaining clear single phase samples had been solved, attention was focussed on the reliability of the measured concentrations of the samples.

A possible source of error in the measured dispersed phase concentration might arise from the mass transfer promoted by impingement and coalescence of the drops on the liquid and solid interfaces of the head of the probe before interaction with the continuous phase could be prevented. In addition the amount of solute transfer that can take place during the time the coalesced drops rest on the external surface of the head of the probe can invalidate the sample from being representative of the particular point concentration in the mixing compartment.

Based on the previous publications it appears that the rate of withdrawal of the dispersed phase sample and the dimensions of the head of the probe may have some influence on the reliability of the sample obtained. In order to examine this possibility, the dispersed phase was withdrawn using heads of different sizes, at different rates of sampling and column operating conditions. The concentrations of the collected samples, under steady state conditions, are listed in Table 7.2.

The results of Table 7.2 show that there are no significant effects due to the rate of sampling or the dimensions of the head of the probe on the results obtained for any experimental conditions investigated. Test 3 in

Table 7.2 - Test on reliability of sampling technique for dispersed phase

Test	Superficial Velocity (cm/min) water phase	toluene phase	Agitator Speed (RPM)	Mass Transfer Direction	Sampling rate (ml/min)	Head Probe Type	Conc. of Dispersed phase w/w %	d_{32}*(σ) (mm)
1	6.04	8.65	700	Disp.→ Cont.	1.0	3-D	4.45	2.1(0.7)
					0.3**	2-D	4.20	
2	6.04	8.65	700	Disp.→ Cont.	1.51	3-D	4.33	
					0.4**	2-D	4.21	
3	6.49	7.64	400	Cont.→ Disp.	0.5	3-D	3.80	1.43(0.54)
					1.5**	1-D	3.90	
4	6.49	12.73	400	Cont.→Disp.	2.8	3-D	1.94	2.04(0.98)
					1.2	3-D	2.03	
5	6.49	7.64	600	Cont.→Disp.	3.0	3-D	3.30	0.32(0.26)
					0.33	3-D	3.43	

* $d_{32}(\sigma)$ - Sauter mean drop diameter (standard deviation of drop distribution curve).

** Samples were withdrawn with 1.0 cc syringe.

particular is a very severe check on the reliability of this technique, since the combination of sampling rates and the design of the head of the probe coalescence areas produces extremely different rest times of the coalesced drops. The difference in the resulting acetone concentration is opposite to what would have been expected if the effect of the rate of sampling had been significant. Therefore, it can be concluded that the differences in the concentrations found are due to a wide range drop residence time distribution whose organic feed is proportional to the standard deviation of the drop size distributions tested in Table 7.2. Since in each test, two samples were withdrawn simultaneously from different points inside the mixing chamber, the resulting concentration difference could be interpreted as a deviation from an ideal plug flow situation in the dispersed phase.

The concentration of the continuous phase sample can be considered reliable and free of error. Any concentration difference between the samples taken from the same mixing chamber within any particular run, can only be attributed to incomplete mixing of the continuous phase. Nevertheless, the following test was designed and carried out. After the column reached the steady state level under a particular set of operating conditions, a sample of the continuous phase was withdrawn from the second agitated chamber over a period of five to ten minutes, using the probe head 1-C and the Rotaflow-syringe system. Afterwards, using the large bore on-off valve located at the column wall of the second chamber, a large two phase sample (50 to 80 cc)

was quickly removed into a graduated cylinder and approximately 2cc of the decanted aqueous phase at the bottom of the cylinder were rapidly removed by a pipette already located inside the cylinder. The whole operation did not take more than five seconds since the operating conditions of the column were such as to give dispersed phase hold-up values in the range of 5% to 10%. The results of this test, are presented in Table 7.3, where it can be seen that the validity of the technique and the sample probe is confirmed.

7.4 Solute Concentration Determination

There are a number of methods available to determine the concentration of acetone in the organic dispersed and aqueous continuous phases. The most suitable technique was chosen based on accuracy and practicality.

7.4.1 Refractive Index (R.I.)

Several authors have used the refractive index technique in the system Toluene-Acetone-Water within the acetone concentration range 0-12% in which practical immiscibility of the phases can be assumed.

An Abbé 60 refractometer with temperature control was used in this work to measure the acetone concentration in the samples of the aqueous continuous phase at a temperature of $20^{o}C \pm 0.1^{o}C$. An accurate calibration curve was obtained using as a consolute distilled water saturated with toluene. Figure 7.6 confirms the reported linearity

Table 7.3 - Test on reliability of sampling technique for continuous phase

Test	Superficial Velocity (cm/min) water phase	toluene phase	Agitator Speed (RPM)	Mass Transfer Direction	Continuous phase sample conc. (w/w%) Probe 1-C	Hold-up sampling valve
1	6.04	8.65	700	Disp.→ Cont.	5.06	4.95
2	6.04	8.65	400	Disp.→ Cont.	6.42	6.51

Figure 7.6 - Calibration Curve Refractive Index vs %w/w Acetone in Water

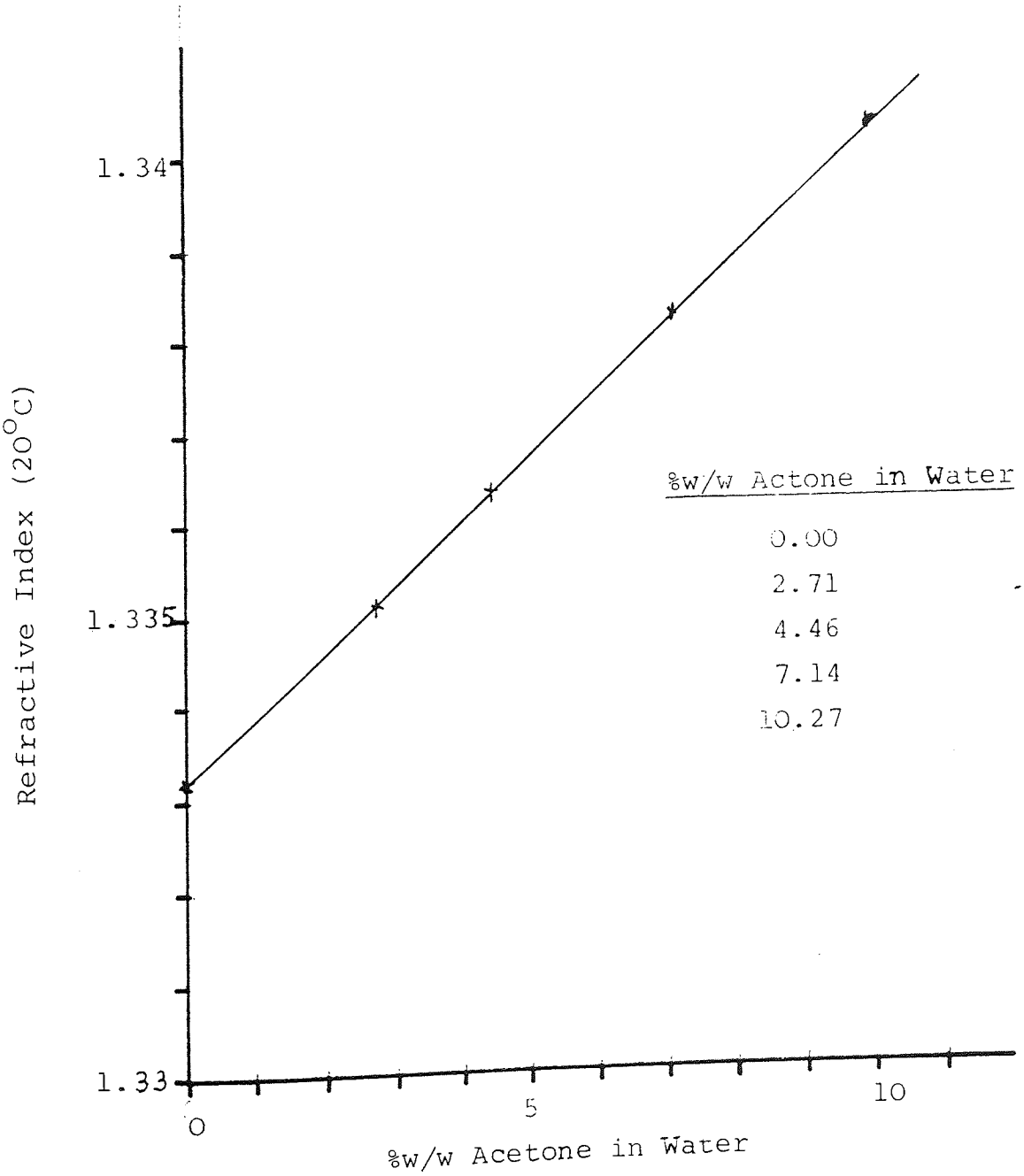

%w/w Actone in Water	R.I.
0.00	1.3320
2.71	1.33516
4.46	1.33638
7.14	1.33841
10.27	1.34050

of R.I. vs % w/w Acetone in Water. Each point in the calibration curve is the arithmetic average of at least six R.I. measurements having a reproducibility of ±0.5 minutes. The following regression line represents the data.

$$w/w\ \%\ \text{Acetone/Water} = 1399.87 \times (R.I.) - 1866.32 \quad (7.1)$$

with a standard deviation on the estimated concentration of 9.02×10^{-2}.

The measurements of the refractive indices of standard solutions acetone/toluene saturated with water did not give reproducible results. While the reproducibility for the pure solvent was satisfactory, it becomes poorer as the acetone content increases. In this case, the demarcation line between the light and dark zones in the refractometer was far from sharp and bright as in the measurement of the aqueous solution samples. This error was totally unacceptable it was decided to use the method of Gas-Liquid Chromatography.

7.4.2 Gas-Liquid Chromatography

The chromatographic unit used in this research consists of a PYE UNICAM Series 204 Gas Chromatograph connected to a Venture MK2 Digital Integrator and a Phillips PM8251 Single Pen Recorder. The chromatograph has two detector/amplifier systems; the Flame-Ionization Detector (F.I.D.) and the Thermal Conductivity (Katharometer) Detector. The F.I.D. was chosen as the most convenient to use in the

analysis of a hydrocarbon mixture since it has higher sensitivity and better linearity when compared with the Katharometer. Its response is proportional to the weight of solute passing in unit time through the burner.

In order to perform a quantitative analysis of a mixture the following steps must be followed:

1. Select a chromatographic column with a suitable stationary phase and length. For an accurate quantitative analysis, partially overlapping peaks cannot be accepted and a complete peak resolution must be obtained. Relative retention data provided by column manufacturers are helpful in solving the above problem.

2. Find the optimum operating conditions of the chromatographic unit. These conditions must produce reasonable small retention times for the sample component, good peak resolution and a convenient amplification of the detector signal which gives a base line with good stability and low noise.

3. Select the method for the quantitative interpretation of the chromatograms.

With different detectors the area under a chromatographic peak (A_i) is related to the amount of substance present (w_i) in the carrier gas by the equation

$$A_i = f_i . w_i \qquad (7.2)$$

where f_i is a factor of proportionality which is not only a functionof the sensitivity of the detector but rather a function of the combination of sample-detector-amplifier-recorder.

Initially, samples of Acetone-Toluene with concentrations (% w/w Acetone) in the range 1% - 10% were analysed using a PEG 400 (polyethylene Glycol M.W. 400, stationary phase) column with 10% stationary phase/support. The resolution of the peaks was good and the retention times obtained were 1.99 minutes for Acetone and 4.23 minutes for toluene. When the "acetone relative peak area"

$$A_{Ac.}\% = \frac{A_{Ac}}{A_{Ac} + A_{tol}} \qquad (7.3)$$

was calculated for each chromatogram it was observed that the repeatability was very poor (10 to 20% variation). This was due to the fact that the chosen concentration range produced toluene peaks with areas 20 to 30 times larger than the corresponding areas for the acetone peak. In this case small changes in the conditions of operation and/or small random perturbations in the apparatus, such as electrical noise, during the analysis seriously affected the repeatability. Also, when a constituent gives a peak so large that its height occupies the whole chromatogram, the peak is badly shaped and its area is not reliable. Thus the Internal Normalisation Method or Total Peak Area Method is inappropriate for the quantitative interpretation of the chromatogram.

The most generally used and convenient method for the quantitative evaluation of a chromatogram, particularly in the analysis of components present in small concentration, is so-called Internal Standard Method (165). This method relates the area of each of the peaks of the mixture being analysed (together with its own factor of proportionality) to the area of the peak obtained by the introduction into the mixture of a known weight (ws) of a standard substance that is well separated from the other constituents. The ratio of the area of a peak to the area of the standard peak is directly proportional to the concentration of the respective component in the sample. Using equation (7.2), the following expression

$$\frac{A_s}{A_i} = \left(\frac{f_s}{f_i}\right)\left(\frac{w_s}{w_i}\right) \tag{7.4}$$

establish a calibration curve from which the ratio of the factors of proportionality is calculated. Having obtained the value of (f_s/f_i) it is possible to take an unknown mixture containing component i, add to it a known weight of the standard component (w_s), inject the sample and obtain A_i and A_s from the chromatogram and finally calculate the amount of component i present in the sample (w_i) using the expression

$$w_i = w_s \left(f_i/f_s\right)_{cal} \frac{A_i}{A_s} \tag{7.5}$$

The choice of the substance to be used for internal standard depends upon the nature of the component to be determined and also upon the concentration range in which they are present. It is generally recommended that the internal standard peak should be located in close proximity to, but not overlapping, the peak to be evaluated (acetone) and that its concentration range be chosen to produce peak heights similar to those of the peak of interest. In this way, the reproducibility of the measurement will be satisfactory.

The following stationary phases and reference substances were tried under different conditons of operation;

Stationary Phase	Internal Standard
PEG 400 (polyethylene Glycol M.W. 400)	- Benzene
DNP (dinonil phtalate)	- Ethyl Acetate
APL 2 (Apiezon-mixture of High Molecular Weight hydrocarbons)	- Butanone
Porapak T (cross-linked porous polystyrene)	- Ethanol
Porapak Q (cross-linked porous polystyrene)	

The best combination was found to be benzene-APL 2 column (1.8m) since it produced short retention time for the three components, toluene (9 minutes) acetone (1.7 minutes) and benzene (4.6 minutes) with good resolution of the peaks. Table 7.4 presents the operating conditions

to run with the combination benzene - APL 2 Column. Figure 7.7 presents the calibration curve which confirms the very good linearity of the detector and Figure 7.8 shows a typical chromatogram.

Table 7.4 - Operating Conditions in G.L.C.

- PYE UNICAN 204 Series with FID 204 Flame Ionization Detector
- Column Apiezon L
- Syringe - Injection volume, 0.3μℓ
  - Needle length, 7 cm

Operating Conditions

- Column Temperature - 180°C
- Detector Injector Temperature - 250°C
- H_2 pressure - 0.7 Kg/cm^2
- Air Pressure - 0.5 Kg/cm^2
- Carrier (N_2) flow rate FID - 0.043 ml/sec.
  Katharometer - 0.645 ml/sec
- Ionization Amplifier
  - Attenuation - 4 x 10^3
- Recorder
  - Range - 5 MV
  - Chart Speed - 300 mm/hr
- Integrator
  - Minimum peak widths - 9
  - Noise filter set - 9
  - Area print - 20
  - Threshold Voltage - 1V, 10 MV

Figure 7.7 - Calibration Internal Standard G.L.C.

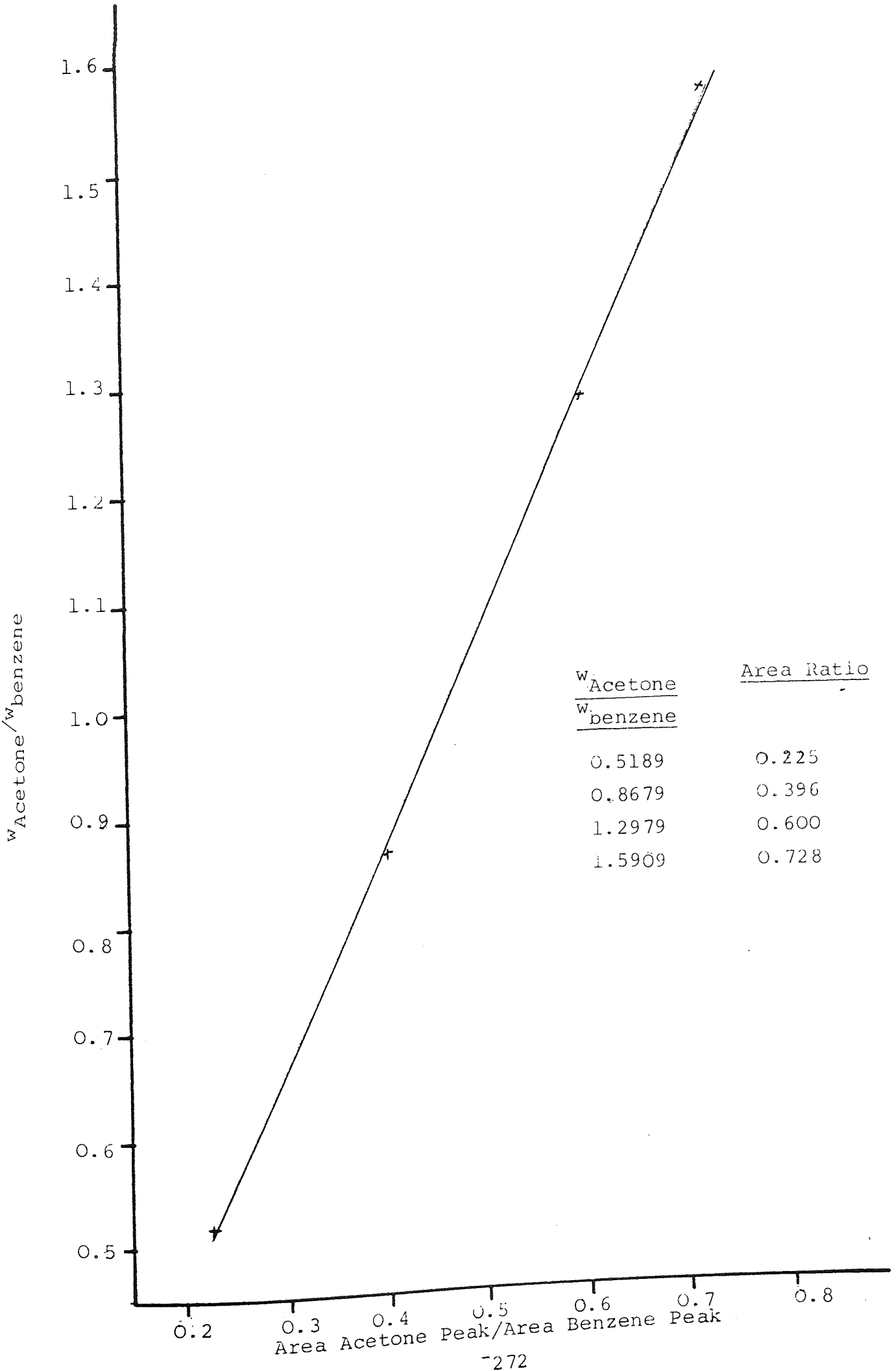

$\frac{w_{Acetone}}{w_{benzene}}$	Area Ratio
0.5189	0.225
0.8679	0.396
1.2979	0.600
1.5909	0.728

Figure 7.8 - G.L.C. Chromatogram Acetone-Benzene-Toluene

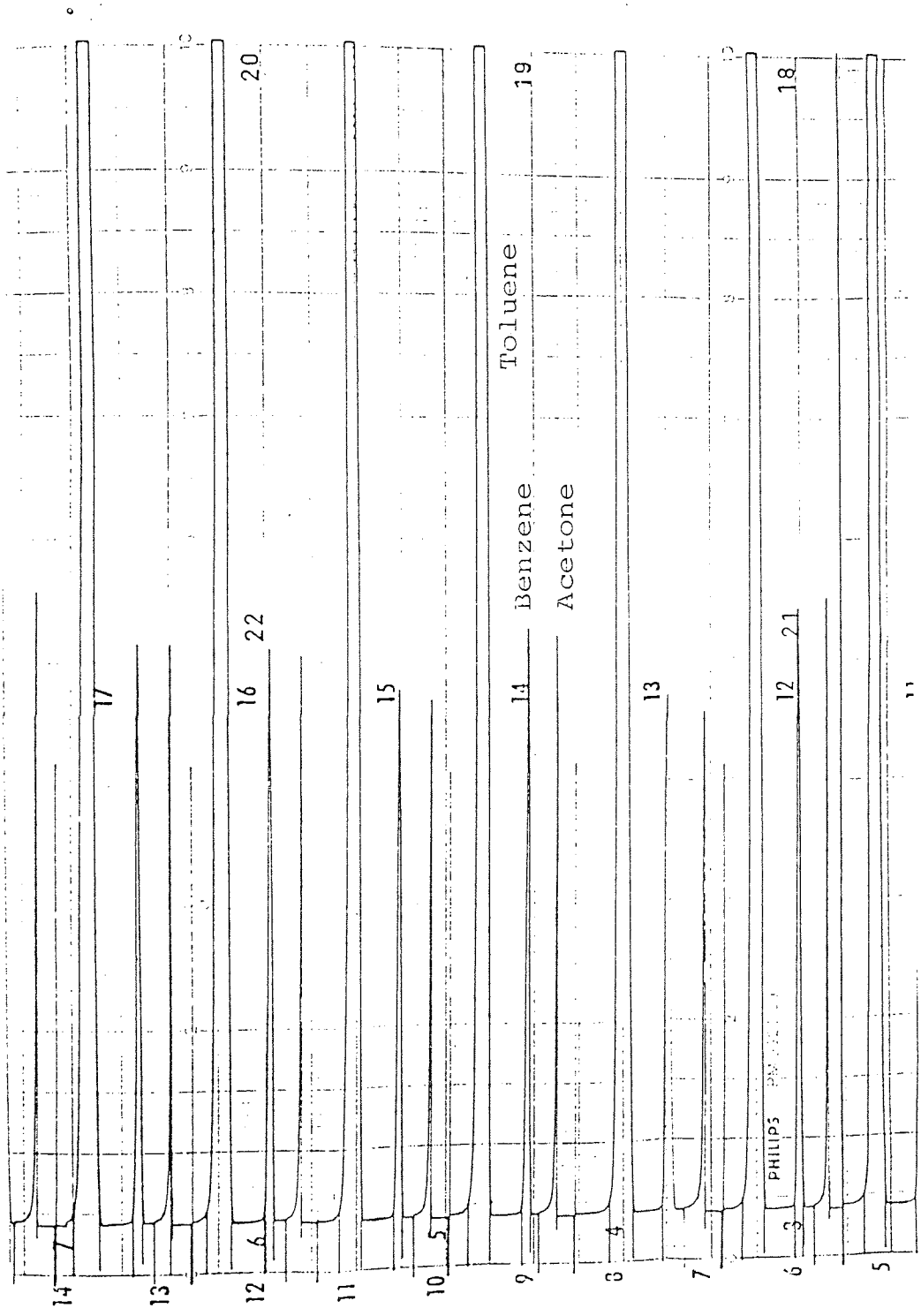

CHAPTER VIII

EXPLORATORY EXPERIMENTATION

EXPLORATORY EXPERIMENTATION

8.1 Objectives

The lack of information about Scheibel column with dispersed phase wetting packings and the need to test new experimental techniques necessitated a substantial amount of time to be devoted to a preliminary experimentation. The objectives of this exploratory work can be summarised as follows:

(i) To test the validity and accuracy of the single phase sampling technique for the determination of the concentration profile.

(ii) To test the accuracy of the dispersed phase hold-up data obtained by two-phase sampling in an agitated compartment

Both techniques, (i) and (ii) and the experimental tests and results have been extensively discussed in Chapter 7.

(iii) Qualitative analysis of the behaviour of different types of packings and fluid dynamic patterns.

(iv) Perform test to establish the existence of back flow between the mixing chambers.

(v) Provide experimental concentration profiles which allow a model searching and a preliminary analysis.

8.2 Experiment and Techniques

The column shown schematically in Figure 8.1 consists of two borosilicate QVF pipe sections of 0.10m diameter and 0.39m and 0.25m of length respectively. The central section of the column was divided in four compartments each of height 0.05m and wire gauze packings of different thickness of mesh size were inserted in each compartment to give a "stage" consisting of a mixing chamber and coalescence chamber. A hole was drilled in the column wall at the middle point of each of the four 0.05m height mixing chambers in order to introduce and position the single phase sampling head probes and needles. In Chamber 2 an extra hole was drilled to accommodate the large bore sampling valve to withdraw two phase samples for hold-up determination. Details of the distributors at the top and bottom of the column and of the impellers and packing support dimensions were presented in Chapter 6.

The following types of wire mesh packing pads of 0.25m, 0.05m and 0.10m thickness were obtained from Knitmesh Ltd. and tested in the above column,

Table 8.1 - Knitmesh Packing Material

Material	Type No	Filament Diameter (mm)	Stitches/inch	% Voidage
Stainless steel	9059SL	2 x 0.12mm	6 x 7	97
Polypropylene	9059SL	2 x 0.13mm	16 x 14	97
D.C. Coalescer (st.st. - Polypropylene	9201SL	1 x 0.12st.st. 1 x 0.13PPL	6 x 7	97

Figure 8.1 - Column for Preliminary Experimentation

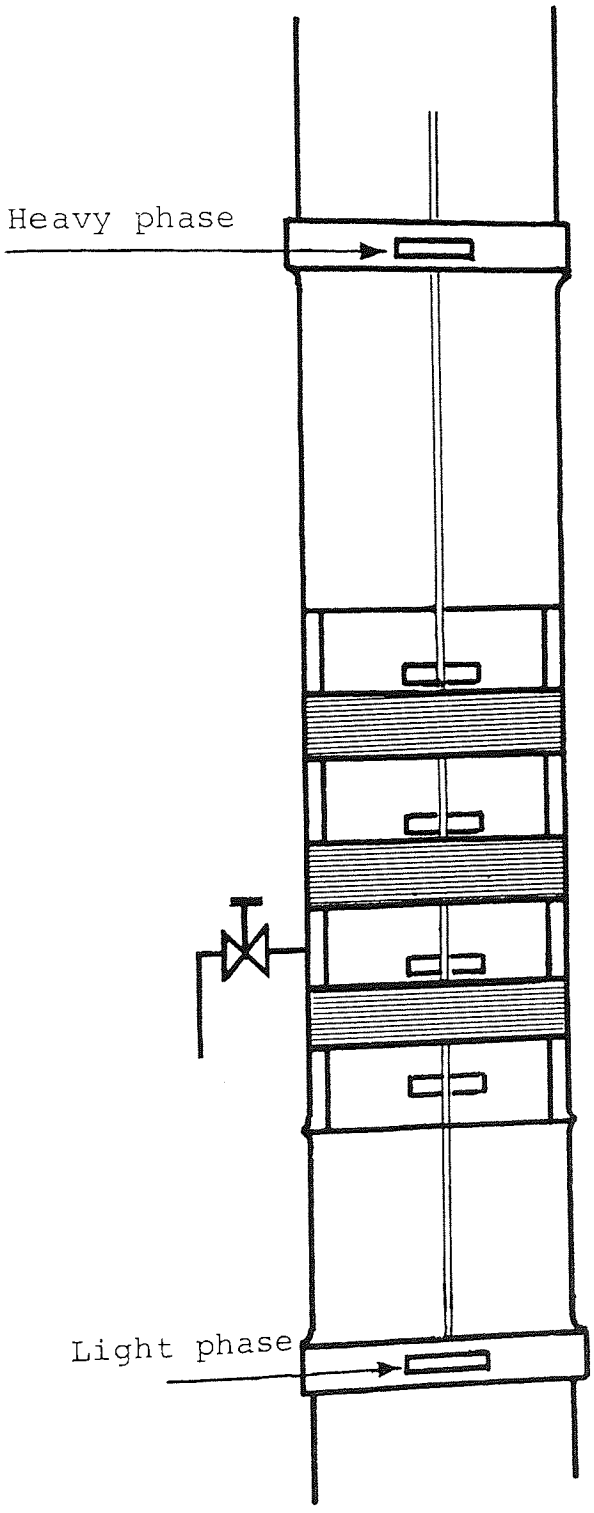

No rules or criteria exist that can help in the selection of an appropriate packing material with the suitable dimensions. The only information available in the literature is the percentage voidage and the type of material from which the pad is made (stainless steel or plastic). The packings listed in Table 8.1 were selected on the basis of manufacturers information and information in the literature. The result was that none of the listed packings worked satisfactorily when the column was operated counter-currently with the binary system toluene-water. For all combinations of packing thickness, packing material, dispersed phase flow rate and agitator speed, premature flooding occurred after the continuous phase was introduced counter-currently. This revealed that, although the packings voidage was correctly chosen, the number of stitches per inch were such that very small interstice sizes resulted, hence large fluid flow resistances developed. The behaviour of the D.C. 9201 was slightly better than the other packings since at low agitator speed and very low throughputs, operation was possible. Then, it was necessary to select a knitted mesh with less stitches per inch in the horizontal and vertical directions. The Dual Coalescer, D.C. 9041, with 4 x 5 stitches/inch, already described in Chapter 6, worked satisfactorily and was used throughout this research. Packing pads of 0.015m thick with 94% voidage were contructed using the apparatus and technique described in Chapter 6 and tested during this exploratory experimentation.

During the mass transfer runs with the system toluene-acetone-water, single phase samples were removed from the top and bottom of each of the 0.05m height mixing chambers after steady state had been reached. This was done using the head probe-needle shown in Figure 8.2 which, by a simple rotation enables samples to be obtained from any position. Eight sample head probes were used to withdraw a total of sixteen samples from the column in each mass transfer experiment. Probes 3-D were used to remove eight dispersed phase samples and Probes 1-C for an equal number of continuous phase samples (see Figure 8.7) At the end of each experiment, samples were obtained from the inlet and outlet streams by using the sampling valves located in the respective pipelines. Still photographs of each mixing chamber were taken in order to measure the drop size distributions and to calculate a representative Sauter mean drop diameter. The dispersed phase hold-up was determined by withdrawing a relatively large amoung of dispersion from Chamber No. 2 using the large bore on-off brass valve. The sample was withdrawn through the valve into a graduated cylinder and the two layers were separated and measured.

8.3 Experimental Results

8.3.1 Non-Mass Transfer Studies

The non-mass transfer investigations were performed to achieve the first three objectives listed in Section 8.1 as well as to find the appropriate values of the operating

Figure 8.2 - Head probe needle for single phase sampling

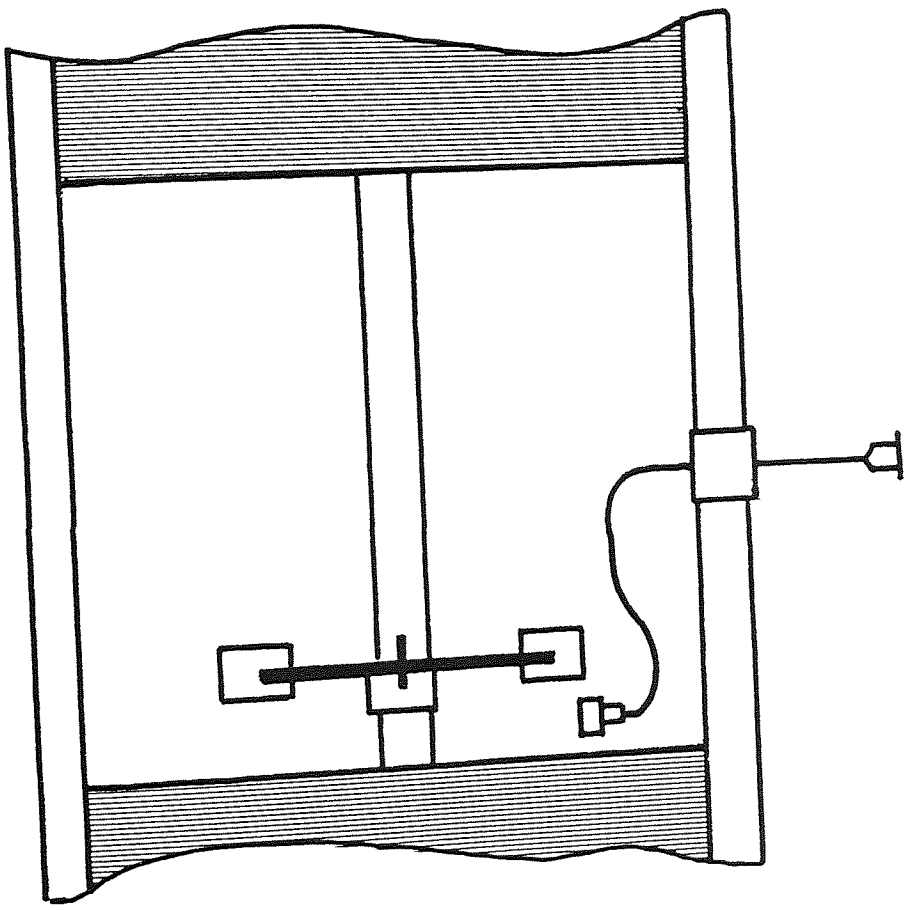

variables to be used later in the mass transfer runs. The column shown in Figure 8.1 was used with the system toluene-water with the organic phase dispersed in all the runs.

8.3.1.1 Flow Regime

The flow regimes obtained for different impeller positions and agitator speeds were observed and they are schematically shown in Figure 8.3. The toluene drops were found to wet the D.C. 9041 packing fibres and coalesce in the packing, leaving the pad surface in streams as shown in Figures 8.3 a-1 and b-1 and Figure 8.4. The position of the impeller at low agitator speed was found to have an important effect on the hydrodynamic of the system as will be seen in Figures 8.3 a-2 and b-2. The resulting differences between the two modes of operation are summarized below;

1. Impellers positioned as in a-2 produced as visually observed in the majority of the low RPM runs, larger drops when compared with the ones obtained under the same operating conditions but with the impellers close to pad as in b-2. This situation arises from the fact tha some of the organic phase exit points at the pad surface are outside the area swept by the impeller. In this case, the organic streams pass through zones of relatively low energy, compared with the high energy zone in the immediate vicinity of the impeller (see Figure 4.6) with the result that breakage

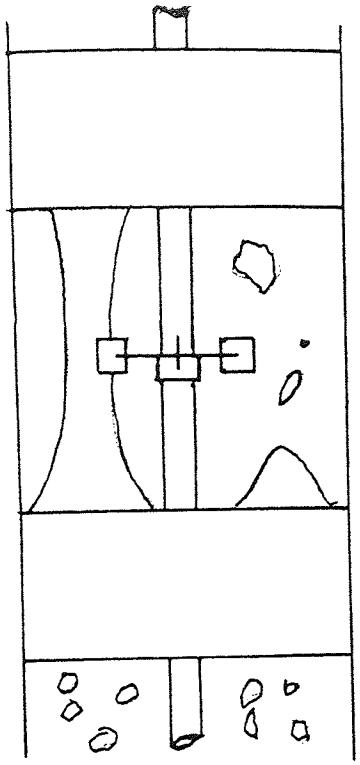

a-1 0 r.p.m.

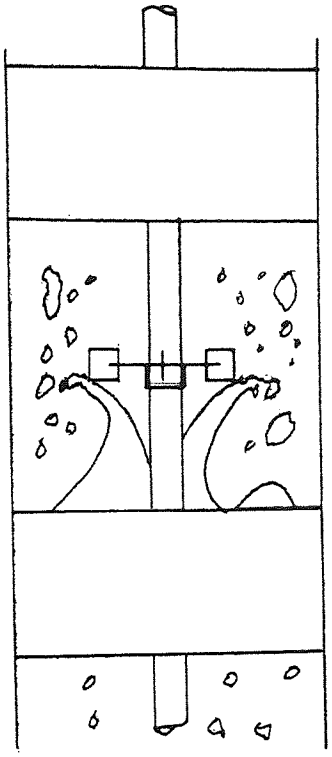

a-2 400 r.p.m.

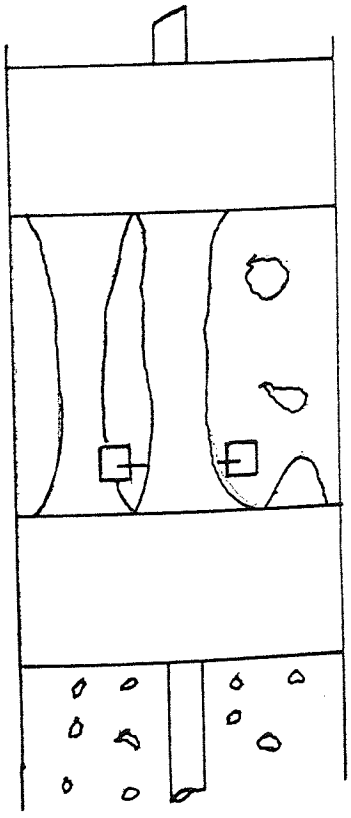

b-1 0 r.p.m.

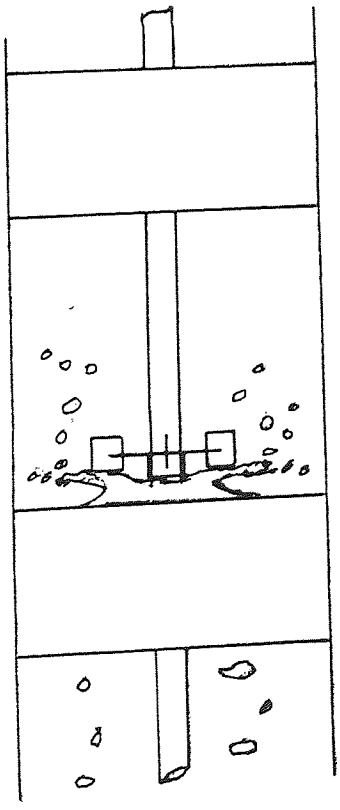

b-2 400 r.p.m.

Figure 8.3 - Flow Regimes. No mass transfer

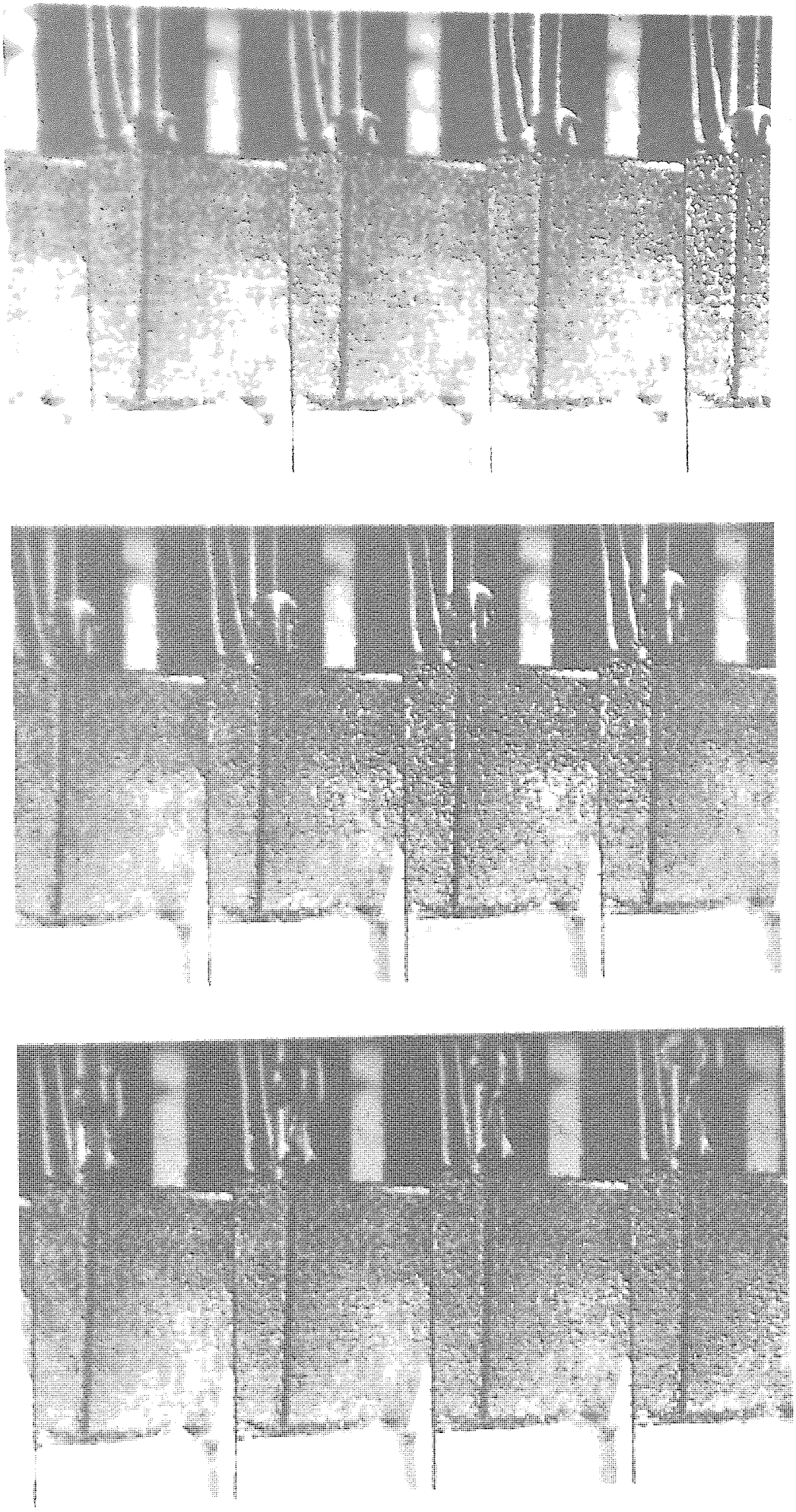

Figure 8.4 Sequence of organic phase exit mechanisms out of pad surface

of the streams are incomplete and large globules are formed. This situation is more pronounced when the exit point is very close to the wall, since, truly by-pass flow can then be produced (see Figure 8.5)

The location of the impellers at a distance about one impeller blade height from the upper surface of the pad as in b-2, eliminates or substantially decreases the randomness in the exit mechanism of the organic phase. The torodial flow pattern generated by the impeller goes deep into the pad forcing the coalesced organic phase to move towards the high voidage centre zone to leave the pad as a single stream surrounding the shaft below the disc of the impeller (see Figure 8.6). This mechanism allows all the fluid elements of the coalesced organic phase emerging from the pad, to be subjected to the same high turbulence intensity, with a much better control over the desired drop size average value and distribution.

2. The formation of large and irregular shaped globules into the mixing chamber presents difficultes in the estimation of interfacial area by optical or photographic techniques and can lead to inaccurate results.

3. The position of the impeller as shown in Figure 8.3 b-2 has as will be discussed in Section 9.3.1, a favourable influence over the column capacity. It was observed that the coalesced organic phase inside the pad was collected, pushed toward the shaft and evenly sucked out by the pumping action of the impeller. This was

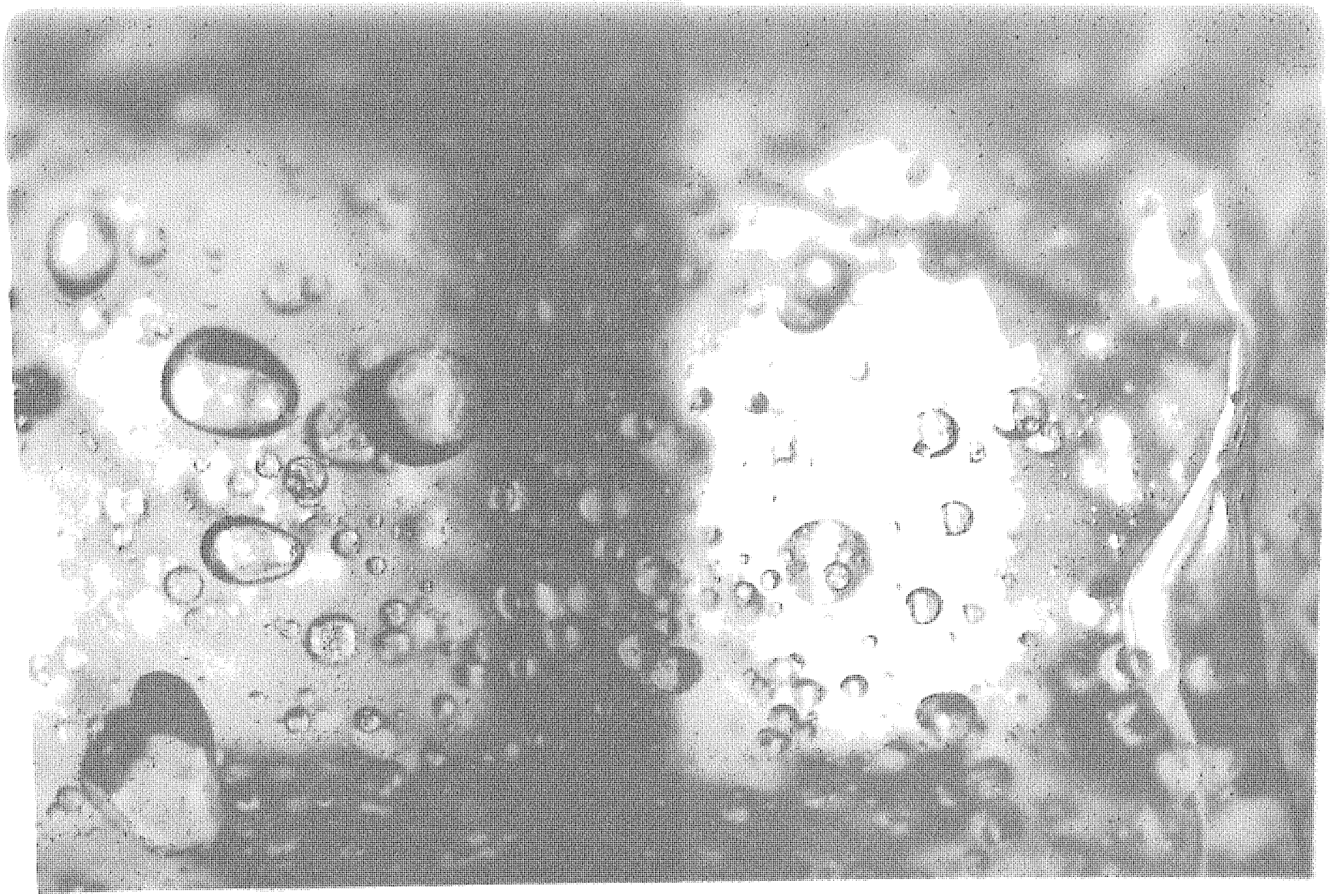

Figure 8.5 Dispersed phase by-passing in mixing chamber

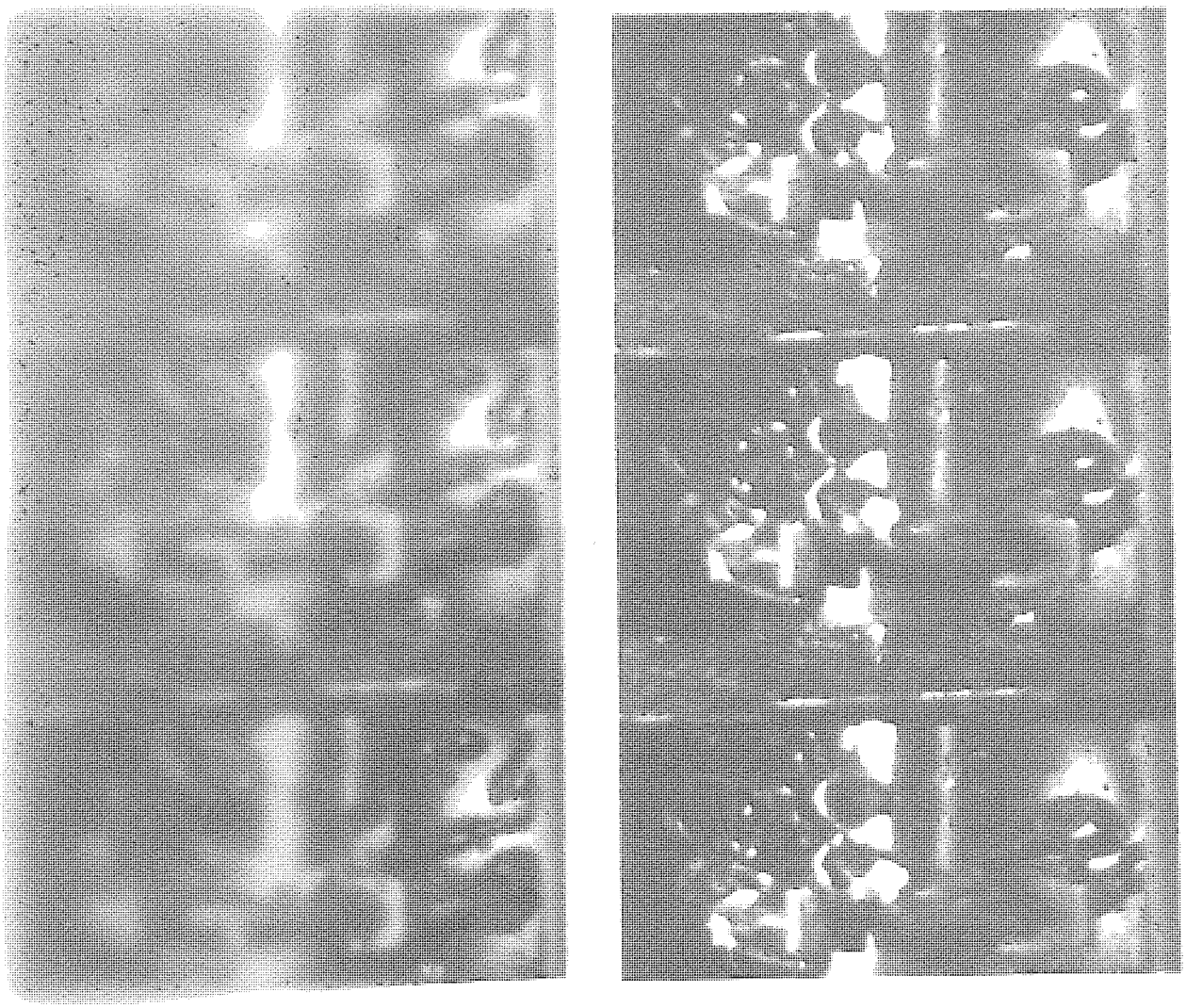

Figure 8.6 Exit mechanism of coalesced phase for impeller close to pad

accepted as a possible explanation for the very unusual observations that the column capacity increased with agitator speed while the column efficiency was not affected. No systematic study of the column capacity was done during these exploratory runs, but this observation was quantitatively confirmed in the final experimental program and these results are presented in Chapter 9 and also clearly indicated in the preliminary runs, numbers 2,3,6 and 8 listed in Table 8.2 . With the impeller positioned for normal operation as shown in Figure 8.3 a-2 it was observed that the relationship of flooding velocities vs RPM followed the usual behaviour; that is, increasing agitator speed decreases column capacity. In this case the pumping effect mentioned above tended to be the less intense, mainly because of the spreading of the organic phase discharge points and the longer distance between impeller and pad upper surface.

8.3.1.2 Drop Size and Hold-up

Table 8.2 shows the values of the hold-ups and Sauter mean drop diameters in different mixing chambers during preliminary non-mass transfer runs. In the experiments at high r.p.m.'s (700rpm) it was not always possible to obtain measurable pictures of all the chambers due to the presence of minute drops sticking at the wall of the chambers and high hold-up of small drops.

Table 8.2 - Preliminary Runs - No mass transfer

Run	$\frac{V_c}{(x10^{-3})}$	$\frac{V_d}{(x10^{-3})}$	N(r.p.m.)	Θ_D	$\frac{d_{32}(*)}{(x10^{-3})}$	Observation
1	1.00	1.43	400	0.041	(2) 2.04 (3) 2.49 (4) 2.43	-
2	1.00	1.78	400	-	-	flooding
3	1.00	1.43	300	-	-	flooding
4	1.78	1.43	400	0.047	-	-
5	1.00	1.43	500	0.064	(2) 1.77 (3) 1.64 (4) 1.60	-
6	1.00	2.12	500	0.090	(2) 1.84 (4) 1.81	-
7	1.00	1.43	700	0.146	(4) 1.06	-
8	1.00	2.12	700	0.206	-	close to flooding

* Sauter mean drop diameter at the specified mixing chamber

Impeller position - D_I/5cm from upper surface of pads (Figure 8.3 b-2)

The drop size data confirmed that drop size was independent of compartment number. This was expected because coalescence and redispersion at each stage. The data were correlated using the regression models presented in Chapter 9 and the ICL Statistical Package XDS3/27 available in the Computer Centre of the University of Aston. The best model was found to be

$$d_{32} = 5.719 \times 10^{-5} \times 10^{(1+1.397\Phi_D)} (\bar{\xi})^{-0.708} \qquad (8.1)$$

with a multiple correlation coefficient of 1.000 and a standard error or residual error of 0.1099×10^{-4}. The hold-up was found to be a significant variable.

More data points need to be obtained and correlated before a reliable conclusion of the exponential variation of drop size with impeller speed be made. From equation (8.1) it is observed that

$$d_{32} \propto N^{-2.1} \qquad (8.2)$$

and the value of the exponent of N for all fitted regression models was in the range of -1.5 to -2.1. This suggests a strong deviation from Kolmogoroff's law.

8.3.2 Mass Transfer Studies

The column shown in Figure 8.1 is not a totally well designed Scheibel column for the execution of a mass transfer experimental programme. The two excessively large end sections and the unrestricted chambers 1 and 4, will certainly create "end effects" larger than those normally

expected in an agitated column. Nevertheless, it was thought convenient to perform a few mass transfer experiments not only to test the validity of the single phase sampling technique but also to study the concentration profiles within the central part of the column. This was confirmed by the preliminary experimentation which helped substantially in saving a large amount of work and time in the final experimental programme.

8.3.2.1 Concentration Profiles

Figure 8.7 presents the concentration profiles corresponding to Runs PM-1 (Table 8.3) and PM-5 (Table 8.7) Large end effects, mainly of the back mixing type, can be readily observed in the profiles. The unrestrictive chambers 1 and 4 produce large back mixing end effects, especially in the continuous phase, where large concentration jumps can be seen to occur at the phase inlet.

The stagewise form of the profiles indicated that, from a practical point of view, the phases within any Scheibel agitated compartment (chambers 2 and 3) can be considered well mixed. Thus in future studies only one sample per phase, per chamber will be necessary in order to characterise the solute content of that phase at the respective stage. The apparent anomaly of a negative mass transfer in chamber 2 and 3 of Run PM-1 is in reality a fluctuating random variation of the solute concentration plus a non-ideal flow behaviour of the phases. In this run, the collected volume of the single phase samples and

Figure 8.7 - Concentration Profiles Run PM-1 and PM-5

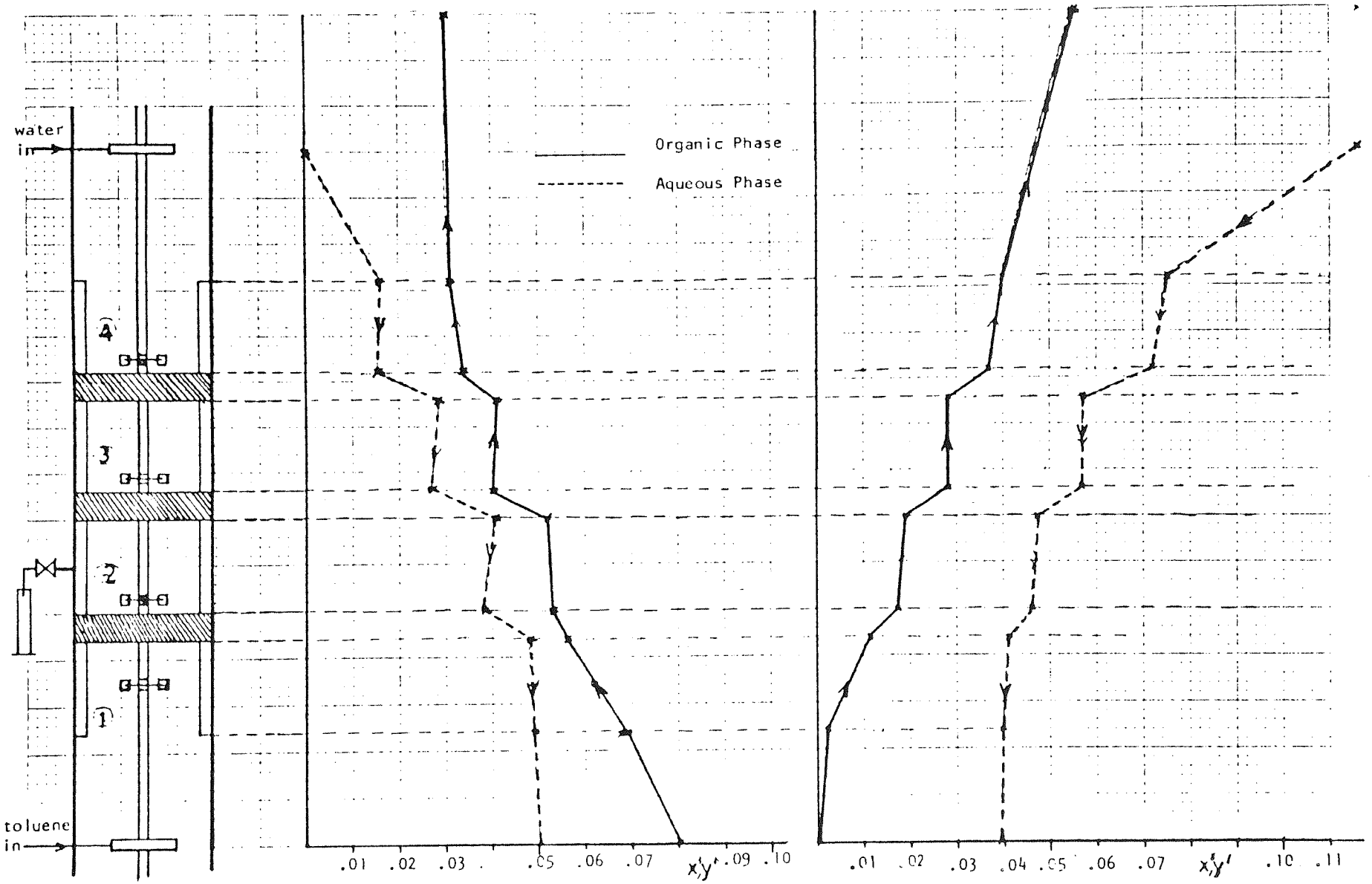

the sampling time was very small (1cc in 10 seconds). In the rest of the preliminary runs several 1.0cc samples of each phase were withdrawn and collected in order to have a better time average concentration. The Continuous Sampling device, as described in Chapter 7, was designed afterwards and used in the final experimental programme presented in Chapter 9.

The large concentration changes across the 0.015mm thickness D.C.pads, observed in Figure 8.7, cannot be attributed to mass transfer within the packing zones. The total coalescence of the dispersed phase on the mixed knitted mesh packing and the short pad height, certainly created a very small mass transfer interfacial area within the pad which cannot account for the large solute transfer across the stage. Therefore, it is reasonable to believe that the major part of the solute transfer within a stage takes place in the neighbourhood of the impeller where the flow pattern induces jet formation and break-up (see Figure 8.6). In order to clarify this point, the following experiment was designed. The column was provided with several single-phase sample points at chamber 3 as shown schematically in Figure 8.8 . Organic dispersed phase samples were withdrawn from the middle of chamber 3 using head-probes 3-D and 2-D and from below the impeller in the same chamber using a standard G18 Stainless Steel needle which was introduced through chamber 2. Another organic phase sample was removed from Chamber 4. Aqueous continuous phase samples were withdrawn from Chamber 3 and 4 using

Figure 8.8 - Mass Transfer at Organic Phase Redispersion Zone

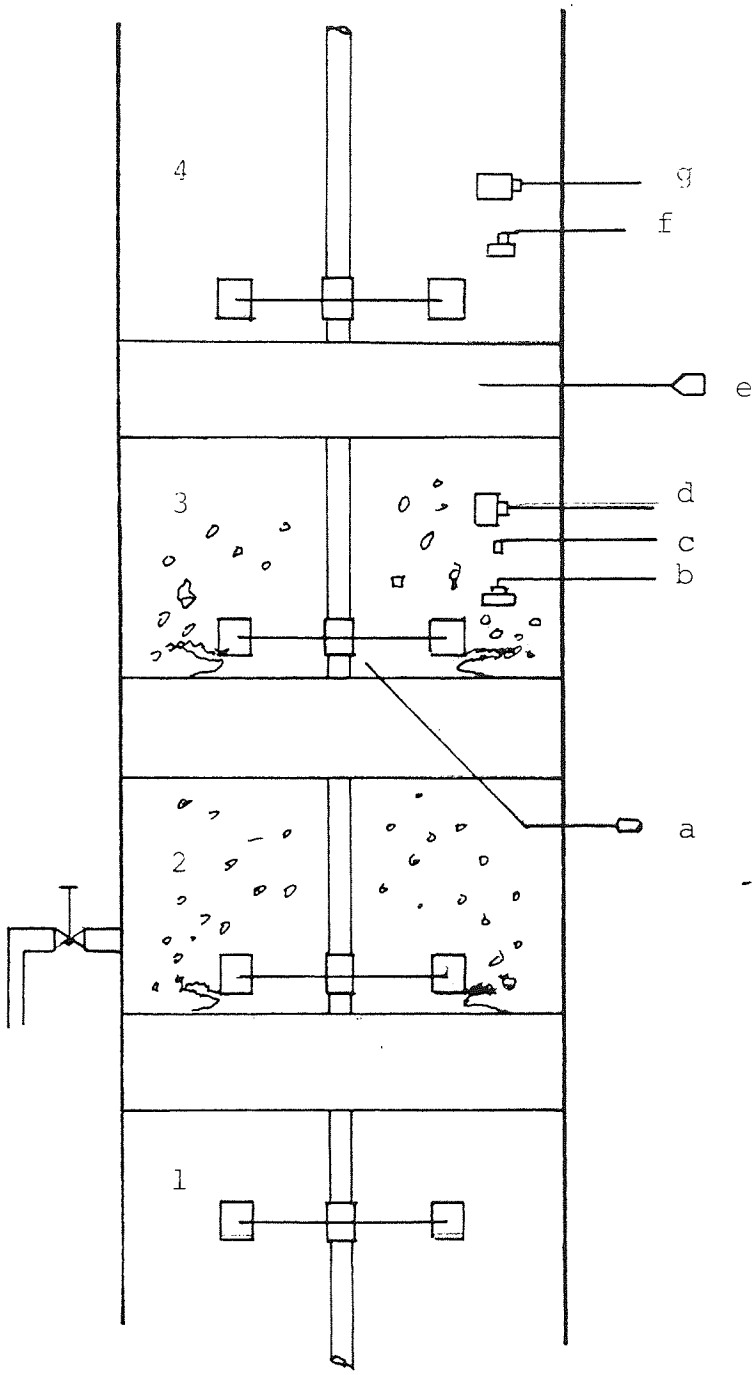

(a) G-18 St.St.needle
Organic phase - 5.00%w/w

(b) 1-C Aqueous pahse, 4.50%w/w

(c) 2-D Organic phase, 4.20%w/w

(d) 3-D organic phase 4.28%w/w

(e) G-18 St.St. needle
Aqueous phase 4.67%w/w

(f) 1-C aqueous phase 5.20%w/w

(g) 3-D organic phase 3.40%w/s

head-probes 1-C and from inside the upper pad using a G18 Stainless Steel needle. Operating conditions and feed solute (acetone) concentration of the rafinate and extract phases were the same as in Run PM-3. The resulting acetone concentrations, in w/w %, at the sample points are given also in Figure 8.8. The following conclusions can be obtained from the above experiment;

1. Comparing the concentration data from this experiment with those obtained in Run PM-3 (Table 8.5) it can be accepted that the acetone concentration (5%) of the sample withdrawn from below the impeller in Chamber 3 is, practically, the same as the concentration of the organic phase in Chamber 2. Therefore it is clear that almost all the mass transfer from Chamber 2 to 3 (5.0% $\longrightarrow$ 4.2%) took place in the impeller region; that is at the zone of organic phase redispersion, and almost none inside the pad.

2. The purpose of sampling from inside the upper pad was to monitor the solute concentration of the organic phase within a whole stage. It was quite a surprise the fact that allthe samples collected from inside the pad (0.02m to 0.04m from column wall) were uncontaminated aqueous phase and not organic phase as it was originally thought, based on the belief that all the voidage inside the pad was occuppied with coalesced organic phase. While a complete description of the flow pattern inside the pad cannot be drawn the experiment revealed that the dispersed phase coalesced

inside the pad and ascended through preferential paths with large areas of the pad being occupied by the continuous phase of the underneath chamber. This situation indicated that for low pad thickness high agitator speed and impeller situated close to upper surface of pad, the pumping action of the impeller can also produce a back flow in the continuous phase. This was confirmed by the following experiment.

The column shown in Figure 8.8 was operated at the same conditions as the above experiment. To test for entrainment in the continuous phase a solution of water and methylene blue was injected in Chamber 1. A strong blue colour appeared in Chamber 2 fading upstream in Chamber 3 and 4, indicating the presence of this back flow. Ananalogous procedure was adopted to test entrainment of the organic dispersed phase. A solution of toluene and iodine was injected at the exit of the upper pad (chamber 3) right below the impeller. A few drops of very small diameter were observed to return backto Chamber 3 at the vicinity of the wall. This was due to the high linear velocity of the continuous phase in the neighbourhood of the wall. The amount and size of the drops entrained in the continuous phase were so small that it is reasonable to conclude that no entrainment of the dispersed phase occurred. This conclusion did not rule out the possibility of the existence of a non-ideal flow behaviour, since only one hydrodynamic factor, out of the many affecting the phases flow pattern was studied.

Tables 8.3 to 8.7 present the concentration profiles of all the mass transfer runs performed in this exploratory experimentation. In Run PM-3 only one sample per phase per chamber was withdrawn. Superficial velocities of the organic and aqueous feed were not corrected for density since solute concentration was low in all the runs.

8.3.2.2 Estimation of the Model Parameters

The axial diffusion model and the compartments with back flow model described in section 4.3.2.2 were applied to evaluate the experimental profiles. Only Run PM-1 to PM-3 were studied because they presented the largest variation of N. These runs proved sufficient to obtain useful information for future modelling exercises.

The process of parameter estimation consisted of two parts, the first was an approximate analytical or graphical method of estimation appropriate to the model under considration, was applied on the experimental concentration profiles. The results of this approximate estimation were then used as the initial guess of the parameters in the final stage of curve fitting by non-linear regression.

The approximate method of parameter estimation and the optimization technique used have been presented in Chapter 5.

Table 8.3 - Run PM-1

Chamber	Z	y'	x'	Y	x	Y	X
	0	5.00	x_i=7.43	0.0526	0.0802	0.507=Y_o	1=X_i
1	0.39	4.65	6.46	0.0487	0.0690	0.471	0.872
	0.468	4.60	5.12	0.0482	0.0539	0.466	0.695
2	0.4836	3.70	5.12	0.0384	0.0539	0.376	0.695
	0.562	4.00	5.02	0.0416	0.0528	0.405	0.681
3	0.577	2.68	3.97	0.0275	0.0413	0.272	0.542
	0.655	2.90	4.00	0.0298	0.0416	0.295	0.547
4	0.671	1.50	3.30	0.0152	0.0341	0.153	0.453
	0.749	1.60	2.97	0.0162	0.0306	0.163	0.408
	1.00	0=Y_i	3.00	0	0.0309	0.0=Y_i	0.408=X_o

V_c = 1.0 x 10^{-3} m/s, V_D = 1.43 x 10^{-3} m/s, N = 400 r.p.m.

d_{32} (chamber 2) = 3.2 x 10^{-3}m, standard deviation = 1.0 x 10^{-3}

Θ_D = 0.04

Mass Transfer Direction = Organic Dispersed to Aqueous Continuous

Table 8.4 - Run PM-2

Chamber	Z	y'	x'	y	x	Y	X
	0	6.25	$8.20=x_i$	0.0666	0.0893	$0.574=Y_o$	$1.0=X_i$
	0.390	6.15	6.46	0.0655	0.0690	0.560	0.792
1	0.468	5.73	5.32	0.0607	0.0561	0.526	0.654
	0.483	5.20	5.32	0.0548	0.0561	0.478	0.654
2	0.562	4.85	5.27	0.0509	0.0556	0.446	0.649
	0.577	3.63	4.33	0.0376	0.0452	0.335	0.535
3	0.655	3.71	4.18	0.0385	0.0436	0.342	0.517
	0.671	2.2	3.20	0.0225	0.0330	0.203	0.398
4	0.749	2.18	2.90	0.0222	0.0298	0.201	0.363
	1.00	$0.0=y_i$	2.70	0.00	0.0277	$0.0=Y_i$	$0.338=X_o$

$V_C = 1.0 \times 10^{-3}$ m/s, $V_D = 1.43 \times 10^{-3}$ m/s, N = 500 r.p.m.

d_{32} (chamber 2) = 2.6×10^{-3}m, standard deviation = 0.85×10^{-3}m

$\Theta_D = 0.058$

Mass Transfer Direction = Organic Dispersed to Aqueous Continuous

Table 8.5 - Run PM-3

Chamber	Z	y'	x'	y	x	Y	X
	0	5.50	$7.80=x_i$	0.0582	0.0845	$0.5431=Y_o$	$1.0=X_i$
1	0.429	5.40	6.00	0.0571	0.0638	0.521	0.773
2	0.522	4.91	5.05	0.0516	0.0531	0.4733	0.647
3	0.616	4.25	4.11	0.0443	0.0428	0.411	0.535
4	0.710	3.01	3.30	0.0310	0.0341	0.291	0.432
	1.0	$0.0=y_i$	3.08	0.00	0.0317	$0.00=Y_i$	$0.404=X_i$

$V_C = 1.0 \times 10^{-3}$ m/s, $V_D = 1.43 \times 10^{-3}$ m/s, N = 700 r.p.m.

d_{32} (chamber 2) = 2.1×10^{-3} m, standard deviation = 0.7×10^{-3} m

$\Theta_D = 0.063$

Mass Transfer Direction = Organic Dispersed to Aqueous Continuous

Table 8.6 - Run PM-4

Chamber	Z	y′	x′	y	x	Y	X
	0	5.10	10.20=x_i	0.0537	0.113	0.681=Y_o	1=X_i
	0.25	3.70	6.60	0.0384	0.0706	0.489	0.647
4	0.328	3.80	6.60	0.0390	0.0706	0.502	0.647
	0.343	3.11	5.40	0.0321	0.0571	0.410	0.529
3	0.422	2.90	5.21	0.0298	0.0549	0.384	0.509
	0.437	2.31	4.45	0.0236	0.0465	0.305	0.433
2	0.515	2.23	4.27	0.0228	0.0446	0.295	0.416
	0.531	1.47	4.05	0.0149	0.0422	0.194	0.395
1	0.609	0.55	2.65	0.0055	0.0372	0.073	0.355
	1.0	0.00=Y_i	3.60	0.00	0.0373	0.00=Y_i	0.349=X_o

V_C = 1.0 x 10^{-3} m/s, V_D = 1.43 x 10^{-3}m, N = 500 r.p.m.

d_{32} = (chamber 2) = 1.3 x 10^{-3}m standard deviation = 0.4 x 10^{-3}m

Θ_D = 0.12

Mass Transfer Direction = Aqueous Continuous to Organic Dispersed

Table 8.7 - Run PM-5

Chamber	Z	y′	x′	y	x	Y	X
	0	5.00	10.40=X_i	0.0520	0.116	0.651=Y_o	1=X_i
	0.25	3.85	7.00	0.0400	0.0752	0.502	0.676
4	0.328	3.55	6.80	0.0368	0.0729	0.463	0.657
	0.343	2.75	5.43	0.0282	0.0574	0.359	0.523
3	0.422	2.80	5.43	0.0288	0.0574	0.365	0.523
	0.437	1.85	4.50	0.0188	0.0471	0.241	0.432
2	0.515	1.70	4.45	0.0173	0.0465	0.222	0.427
	0.531	1.55	3.95	0.0116	0.0411	0.151	0.378
1	0.609	0.2	3.85	0.0020	0.0400	0.026	0.368
	1.0	0.0=y_i	3.83	0.00	0.0398	0.0=Y_i	0.365=X_o

V_C = 1.0 x 10^{-3}m/s, V_D = 1.43 x 10^{-3}m/s, N = 700 r.p.m.

d_{32} (chamber 2) = 1.0 x 10^{-3}m, standard deviation = 0.3 x 10^{-3}m

Θ_D = 0.15

Mass Transfer Direction = Aqueous Continuous to Organic Dispersed

8.3.2.2.1 Diffusion Model

The approximate estimation of $(Pe)_x$, $(Pe)_y$ was done using the Grid Jump Ratio Plot Technique published by Miyauchi and Vermeulan (9) (Chapter 5). This technique requires a knowledge of the inlet concentration jumps, X_i^o and Y_i^o and an initial estimate of the $(No)_x$. The concentration jumps were estimated by extrapolationof the smoothest curve that could be drawn through the pair of concentration points that characterise each mixing chamber, as shown in Figure 8.9 for Run PM-3. These values were used to calculate the Jump Ratios R_X and R_y.

The initial estimated value of the true (N T U), $(No)_x$, was obtained by solving the basic transport equation (5.15) expressed in dimensionless concentration

$$(No)_x = \frac{1 - X_o}{1 - \int_{o+} (X-Y)\,dZ} \qquad (8.3)$$

The solution of this integral was obtained by fitting a polynomial (third degree in Z) to the (X-Y) vx Z experimental points and integrate analytically the fitted polynomial. It is important to point out that for the purpose of estimating the true N.T.U., the value of the concentration jumps at $Z=0^+$ and $Z=1^-$ have to be considered in the polinomial fitting and the integration performed from $Z=0^+$ to $Z=1^-$.

Figure 8.9 - Preliminary Run PM-3. Extrapolation of profile to locate concentration jumps

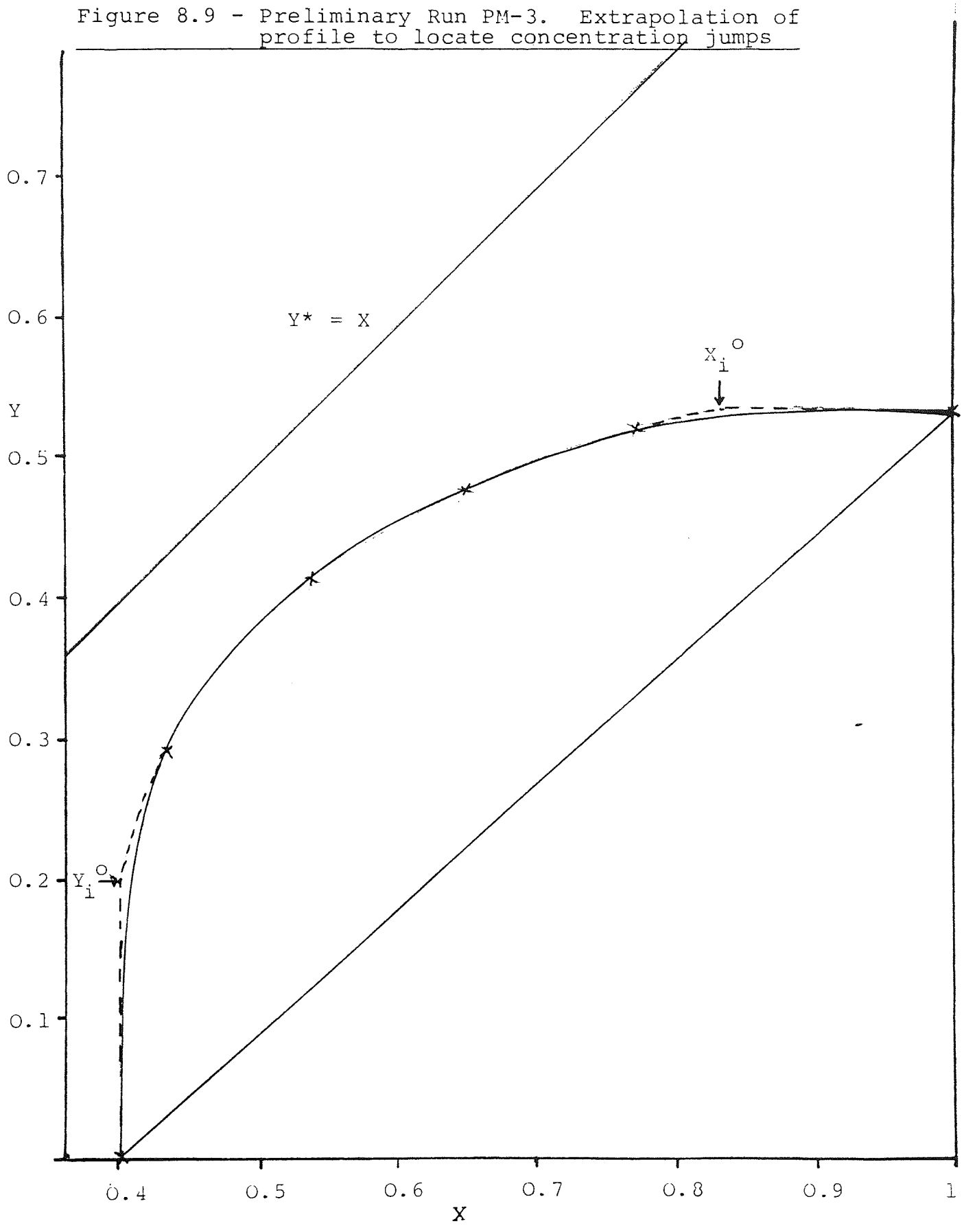

The overall numbers of transfer unit (N.T.U.)o under plug flow condition $(No)_{x.P}$ and the measured $(N.T.U.)_o$, $(No)_{x,M}$ were also calculated in order to make a comparison with the estimated true $(No)_x$.

The $(No)_{x,P}$ was calculated by the equation given in standard text books on mass transfer (7) and the $(No)_{x,M}$ was estimated by the equation

$$(No)_{x,M} = \int_{X_i}^{X_o} \frac{-dX}{(X-Y)_o} \qquad (8.3a)$$

according to the definition given by Gier and Hougen (125).

The initial estimated true $(No)_x$ and the extraction factor F, were used in the computer program given in Appendix 3 to calculate the theoretical concentration jumps at different $(Pe)_x$ and $(Pe)_y$. A complete grid of Jump Ratios for the estimated NTU was constructed and with the experimental R_x and R_y the first estimate of $(Pe)_x$ and $(Pe)_y$ were obtained by interpolation as shown in Figure 8.10 for Run PM-3. Only this first cycle, of the iterative procedure was completed for each run and the results are given in Table 8.8.

The values of E_x in Table 8.8 came out suspiciously high when compared with the axial diffusivities for the dispersed phase obtained by Bibaud and Treybal (82) in an Oldshue-Rushton column with the same chemical system (20.8×10^{-5} m^2/s for N = 150 - 300 RPM). The two unrestrictive mixing chambers especially Chamber 1 and the long end section could be responsible for the apparent high axial diffusivities. Although the absolute values of E_x seem unreliable, its variation with N can be readily understood. The decrease in Ex with increasing speed of agitation is the result of a more uniform drop residence time

Figure 8.10 - Preliminary Run PM-1. Jump Ratio Grid Plot.
$(No)_x = 1.88$, $R_y = 0.21$, $R_x = 0.27$, $(Pe)x = 3.8$, $(Pe)y = 5.0$

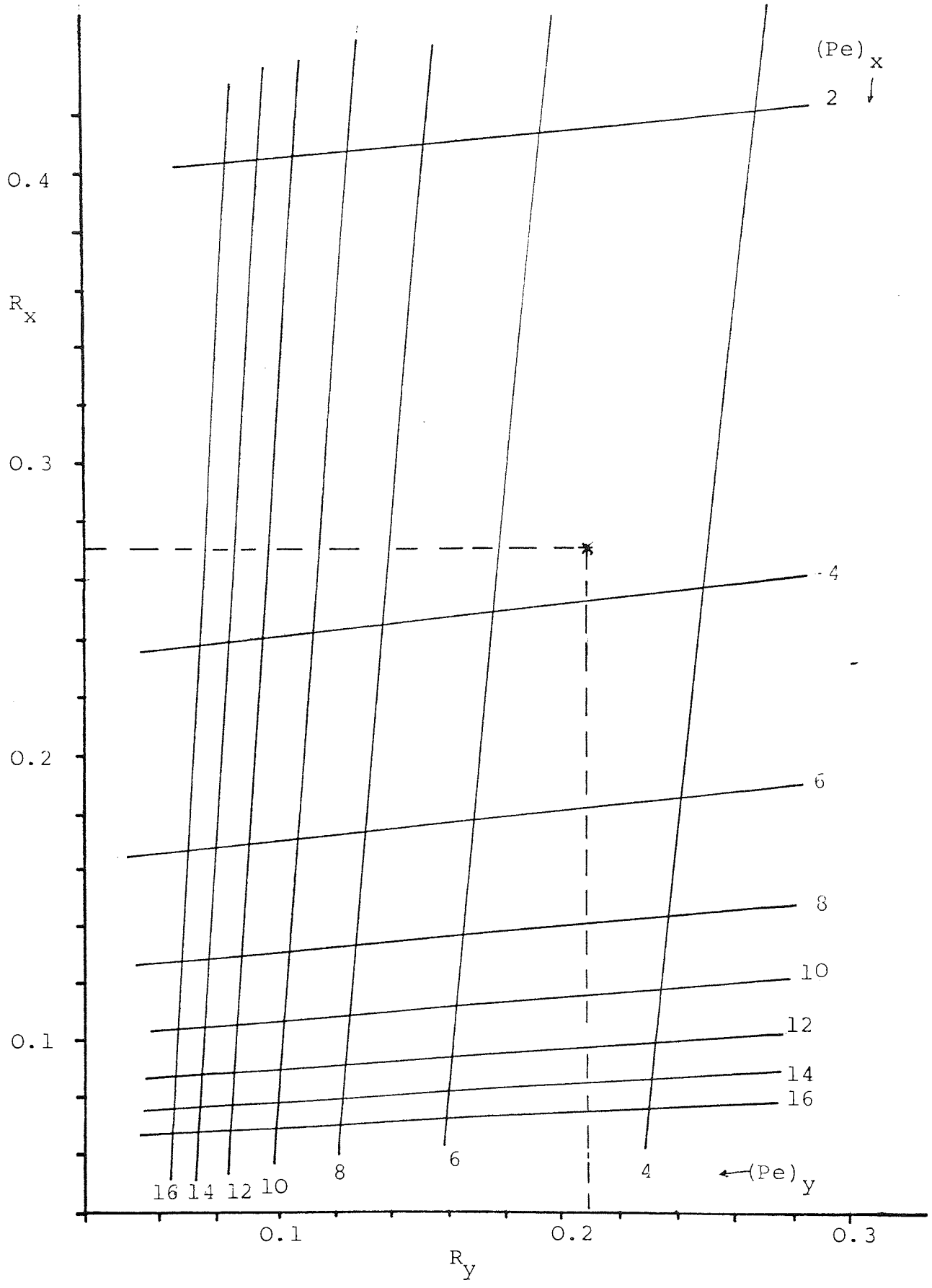

Table 8.8 - Results of Fitting Diffusion Model to Prelimianry Runs

Run	$x10^3$ V_D	$x10^3$ V_C	RPM	F	Θ_D	$x10^3$ $d_{32}(\sigma)$	a	$(Pe)_x$	$(Pe)_y$	$(NTU)_x$	$(P.F.NTU)_x$	$(M.NTU)_x$	$x10^5$ E_x	$x10^5$ E_y
P_{M-1}	1.43	1.00	400	0.955	0.04	3.2(1.0)	75	3.82	5.0	1.88	1.40	1.64	606.6	13.4
P_{M-2}	1.43	1.00	500	0.955	0.053	2.6(0.85)	136	3.80	8.5	3.21	1.87	2.65	411.5	8.05
P_{M-3}	1.43	1.00	700	0.955	0.063	2.1(0.7)	180	3.81	2.5	2.75	1.42	2.24	385	27.5

is the result of a more uniform drop residence time distribution as indicated by the decrease in the standard deviation of the drop size distribution. Increasing the speed of agitation brings more uniform sized drops and rising velocities which in turn reduced the axial spreading effect of the discrete phase. Since it was shown that truly back flow of the dispersed phase did not exist between the components, the above effect is the only one which controls the E_x.

The values of the continuous phase axial diffusivity Ey, presented in Table 8.8 are well within the order of magnitude of the ones reported by Bibaud and Treybal in an Oldshue-Rushton column ($25 - 43.3 \times 10^{-5} \frac{m^2}{s}$). In this case, $E_y = f(N)$ presents a minimum value, which is the result of the competing opposite effects of the radial diffusivity, which increases with N, reducing channeling at the column wall and creating a more uniform continuous phase velocity profile, in addition to the already observed back flow of the continuous phase which increase with agitator speed. As the impeller speed increases from 400 RPM the increase in radial diffusivity results in a decrease in E_y up to a value of N at which the back flow starts to be the predominant factor and as a consequence E_y increases.

The column efficiency represented by the value of the $(No)_x$ presents a variation with agitator speed typical of almost all agitated extraction columns and is analogous with the behaviour reported by Scheibel and Karr (17) in

a 12 inch diameter Scheibel column. An increase in N above 500 RPM did not result in a better performance. Although the mass transfer interfacial area increased, the drop sizes decreased resulting in a lower overall mass transfer coefficient and furthermore, the back flow increased, thereby reducing the concentration driving force. In fact an increase of impeller speed above 500 RPM decreased the $(No)_x$ or column performance as is shown in Table 8.8

The above parameter estimation results were afterwards used in the next step of model fitting by the non-linear regression method. The Marquardt Algorithm was applied to the three different model formulations of the optimisation problem, already discussed in Chapter 5, with the experimental concentration profiles of Run PM-3.

The formulation 1, optimization based on Y-concentration profile was first studied, with the objective function

$$\Phi = \sum_{i=1}^{m} (Y_i - \hat{Y}_i)^2 \qquad (.84)$$

where m, number of experimental points equalled 5 since there are four internal concentration points (Chambers 1 to 4) plus the outlet stream concentration. The feed concentration can not be used since the diffusion model only considers the inlet concentration inside the column (concentration jump) and this value is an output from the optimization process. The starting point of the three parameters optimization was

$$(Pe)_x = 3.80, \quad (Pe)_y = 2.50, \quad (NTU)_{ox} = 2.75$$

These values were fed to a computer program (Appendix 3) being the output of the computation

$$(Pe)_x = 27.8, \quad (Pe)_y = 1.77 \quad (No)_x = 2.38$$

Sum Square of Residuals = 0.1×10^{-1}

The above starting point was also used with the model Formulation 2, optimization abased on X-concentration profile, and the result of the optimization was

$$(Pe)_x = 14.70 \quad (Pe)_y = 34.30 \quad (No)_x = 1.91$$

If comparing the results of Formulation 1 and Formulation 2 it is seen that in Formulation 1 the Y-profile is very insensitive to the parameter $(Pe)_x$ and in Formulation 2 the X-profile is very insensitive to $(Pe)_y$. The substantial difference in the regressed values of the $(No)_x$ indicates that both the profiles are very affected by the experimental error or that the same model can not be applied to each phase separately or both. While experimental error in the concentration profiles can not be ruled out, it is considered a more acceptable explanation in terms of model adequacy.

The model Formulation 3 optimization, based on the overall behaviour of the column, was finally studied using the following least square objective function

$$\Phi = \sum_{i=1}^{m} \left[(X-Y)_i - (X\hat{-}Y)_i \right]^2 \qquad (8.5)$$

where m is equal four; that is only the internal concentration points. The result of the computation was

$$(Pe)_x = 123.60 \quad (Pe)_y = 1.72 \quad (No)_x = 3.44$$

The resulting regressed value of $(Pe)_y$ compares very well with the one obtained with Formulation 1, and can be considered an acceptable estimated value. The situation is quite different when the $(Pe)_x$ value is compared with the one obtained in Formulation 2. The difference between them is so large that an acceptable value can not be assigned to the rafinate phase Peclet Number. A similar situation occurs with the $(No)_x$ value when compared with the first two formulations.

In summary, all the three different formulations of the same differential model produced different answers, which did not adequately fit the experimental profile in Run PM-3 as is shown in Figure 8.11. This analysis reveals that a different modelling approach is needed which must allow for the possible axial variations of the non-ideal flow parameters. The next section presents the analysis of the experimental profiles based on the compartments with back flow model.

Figure 8.11 - Diffusion Model. Parameter Estimation
Run PM-3

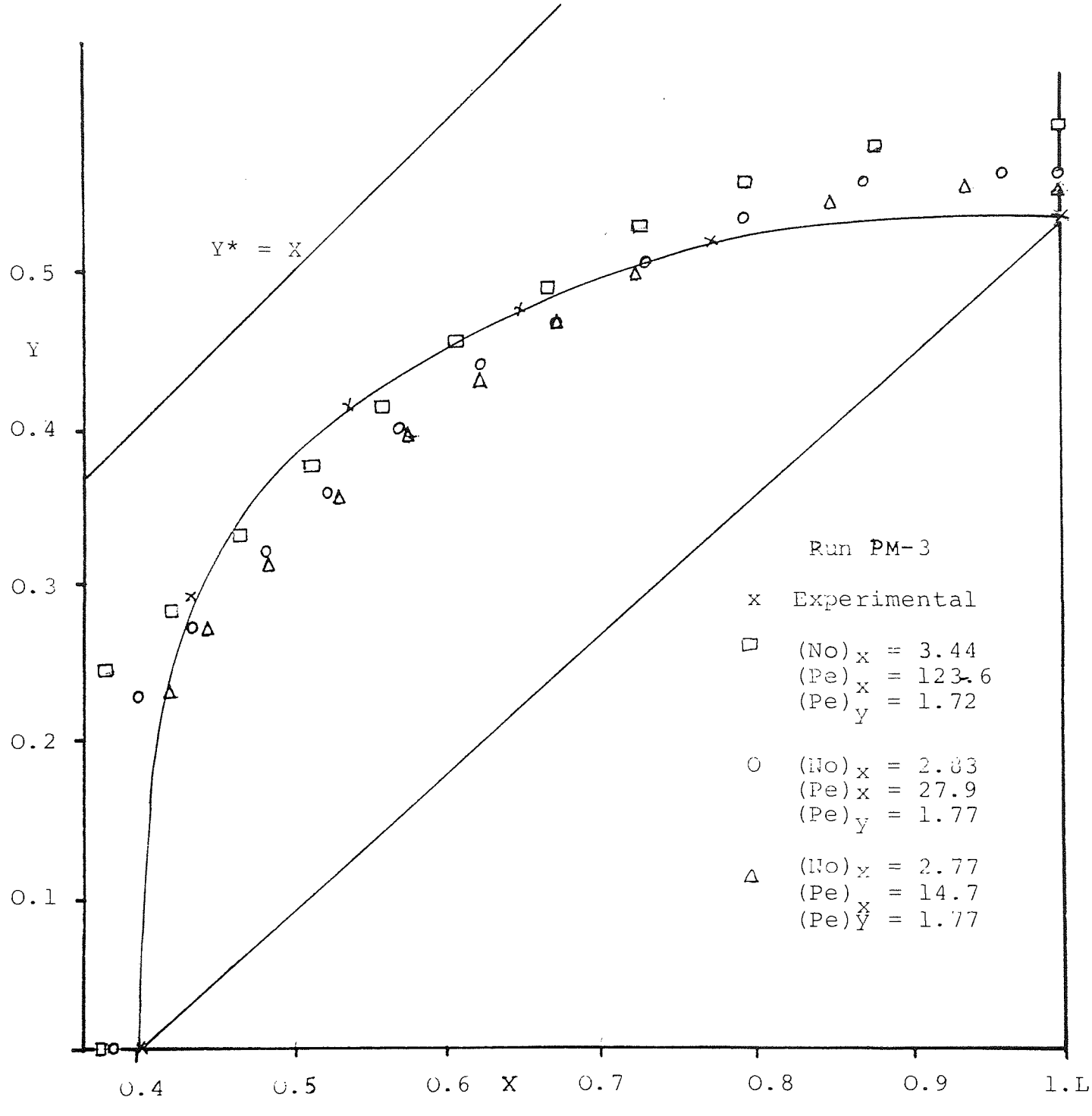

8.3.2.2.2 Compartments with Back Flow Model

The interpretation of the experimental concentration profiles in terms of a stagewise model made it necessary to introduce an important assumption regarding the column construction. This assumption, was made as a result of inspection of the concentration profiles and involved the substitution of ficticious mixing cells for the long end sections. Then the column concentration profiles were interpreted to correspond to a five stage column. This interpretation includes the end effects into the extreme stages, offering the possibility of isolating them from the rest of the column. The Figure 8.12 is the representation of the column and its ficticious end stages.

In this study the solute concentration was expressed in weight fractions on a solute free base (y and x) and the concentration of each phase in the mixing chambers was characterized by a single value resulting from the arithmetic average of the chamber top and bottom concentrations.

The approximate evaluation of the model parameters was done using the Rod technique already presented in Chapter 5. The results are given in Table 8.9 for Run PM-1 to Run PM-3 and illustrated in Figure 8.13

These results were used as the initial values for the next step of model fitting using the Marquardt algorithm. In order to express the kinetics of theprocess in terms of the stage efficiency, η, the values of the group $\frac{K_D(aV_k)}{R}$

Figure 8.12 - Stagewise model. Application to column of Figure 8.1

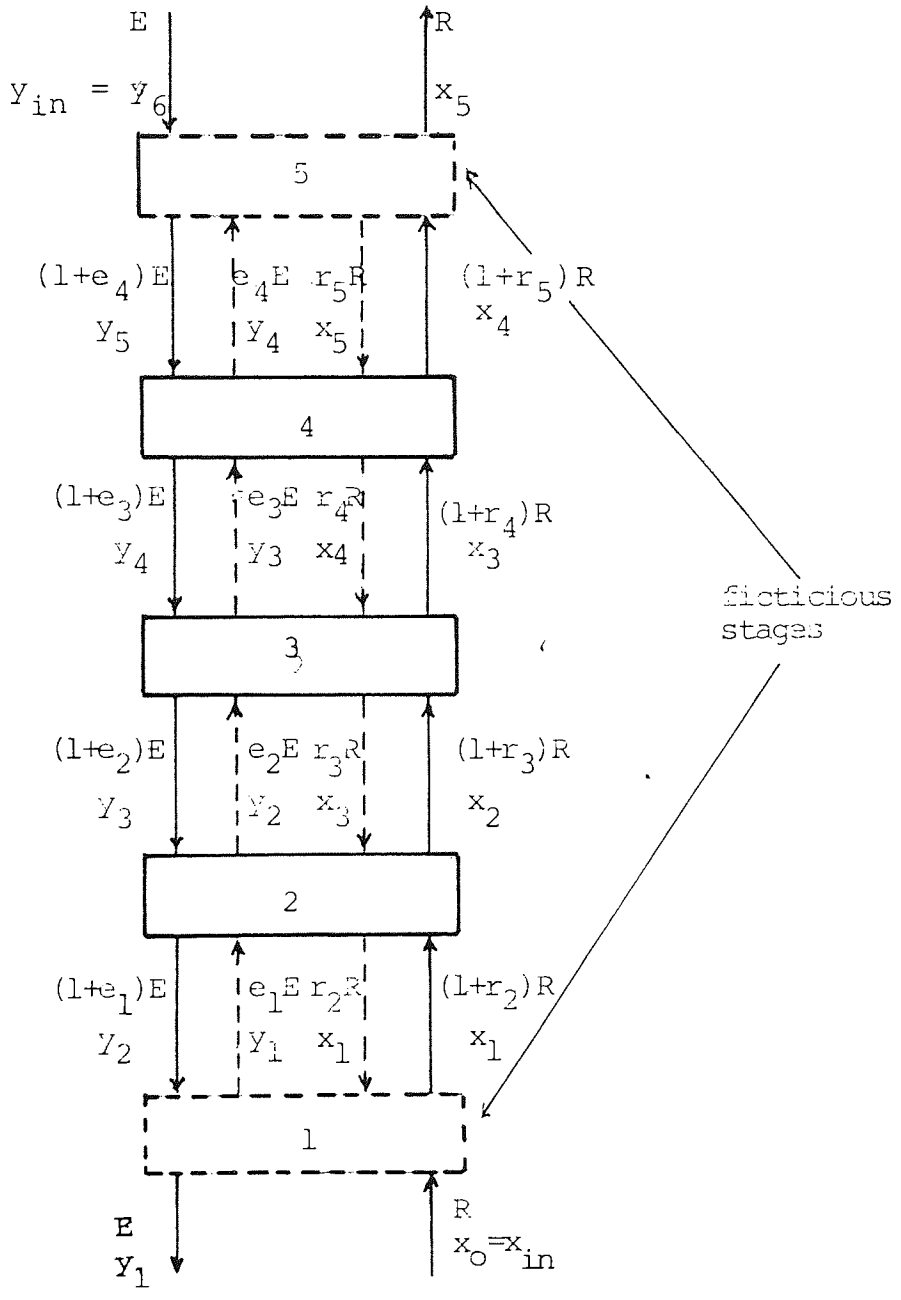

Table 8.9 - Application of Rod Technique to Experimental Profiles

Run	Backflow Coefficient		Dispersed Phase $\frac{K_D(aV_K)}{R}$
	r	e	
P_{M-1}	0.861	2.65	0.564
P_{M-2}	1.00	2.60	1.498
P_{M-3}	0.183	5.95	1.17

Figure 8.13 - Stagewise model fitting. Rod's method

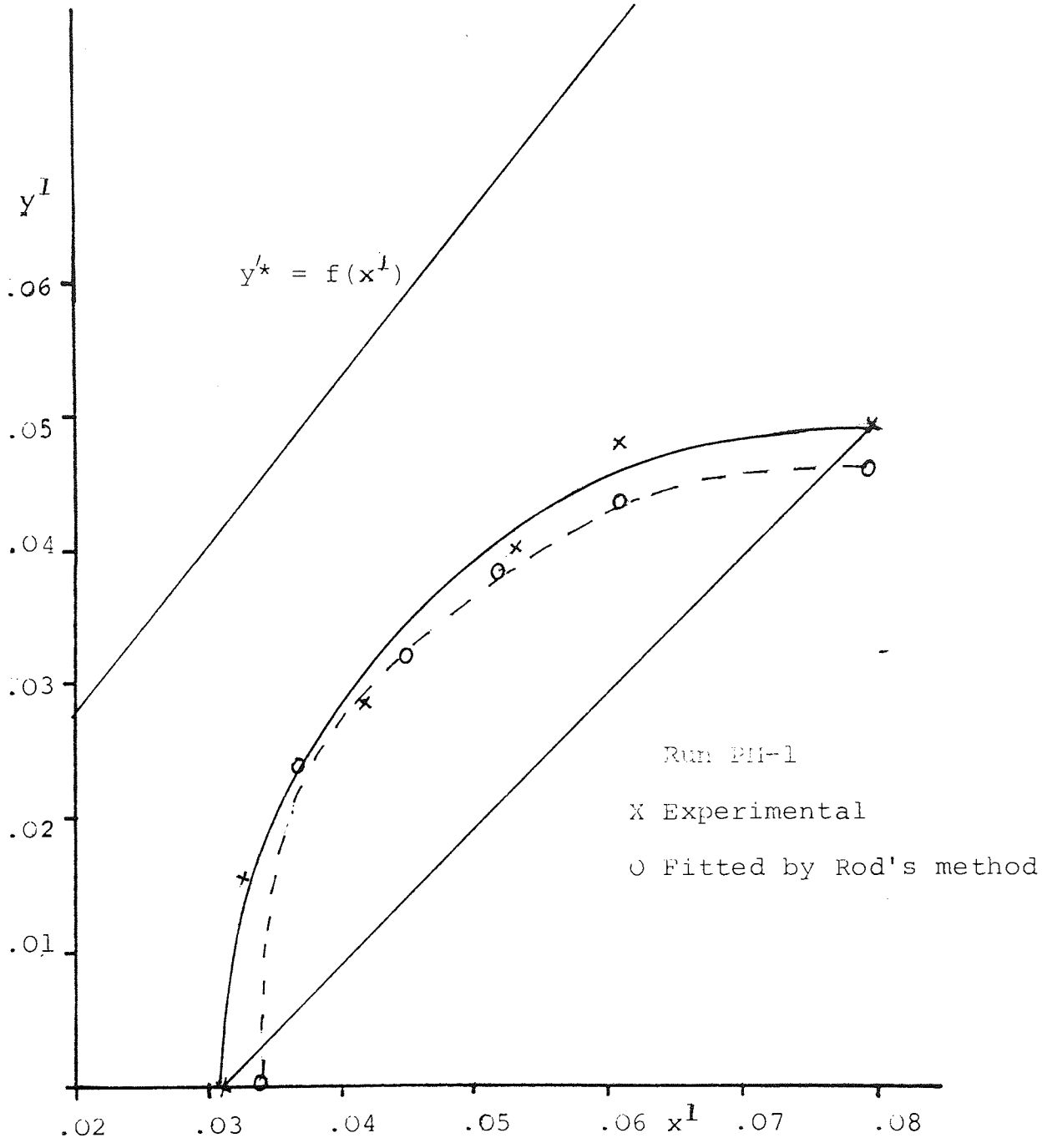

given in Table 8.9 were substituted in the following relationships between stage efficiency and mass transfer coefficient (146).

$$N_{kx} = \frac{K_x \ (a \ V_k)}{R(1+r_k+r_{k+1})} \tag{8.6}$$

$$\eta_k = \frac{(1+\beta_k^1)N_{kx}}{(1+\beta_k^1)+1} \tag{8.7}$$

where

$$\beta_k^1 = \frac{\alpha}{D_k} \ \frac{(1+r_k+r_{k+1})}{(1+\ell_k+\ell_{k-1})} \tag{8.8}$$

The different formulations of the stagewise model were studied. They correspond to Formulation 3 (five parameter model) and Formulation 4 (three parameter model, no axial variations of model parameters) already discussed in Chapter 5. The computer program used in this optimization step is presented in Appendix 2.

Table 8.10 to Table 8.12 present the results of the computations corresponding to Run PM-1 to PM-3. These results show that the stagewise model with back flow describes the behaviour of the column quite well. Even the simplest formulation i.e. no axial variation in the parameters gave a fitting for the profiles with a maximum error (Sum Square of Residuals) SSR = 0.65×10^{-4}.

The formulation based on five parameters model assumes that $\eta_2 = \eta_3 = \eta_4$ and all end effects are included in η_1 and η_5. Then for this model the parameter which

Table 8.10 - Run PM-1. Least Square Fitting. Stagewise Model

Concentration Profiles						
	Experimental		Fitted Formulation 3		Fitted Formulation 4	
k	x_k	y_k	$\hat{x}_k$	$\hat{y}_k$	$\hat{x}_k$	$\hat{y}_k$
0	x_{in} = 0.0802		-		-	
1	0.0614	0.0526	0.06260	0.04957	0.06196	0.05119
2	0.0534	0.04843	0.05107	0.04887	0.05115	0.04574
3	0.04150	0.04004	0.04155	0.03964	0.04188	0.03722
4	0.03263	0.02870	0.03398	0.02849	0.03397	0.02791
5	0.03092	0.01574	0.03065	0.01581	0.02903	0.01836
6		y_{in}=0.00		-		-
			- solution vector		- solution vector	
			η_1=0.038 η_3=0.378 η_5=0.268 r=1.42 e=0.607 -S.S.R.=0.1x10^{-4}		η=0.32 r=0.64 e=1.07 -S.S.R.=0.37x10^{-4}	

Table 8.11 - Run PM-2. Least Square Fitting. Stagewise Model

Concentration Profiles						
	Experimental		Fitted Formulation 3		Fitted Formulation 4	
k	x_k	y_k	$\hat{x}_k$	$\hat{y}_k$	$\hat{x}_k$	$\hat{y}_k$
0	x_{in}=0.08932		-		-	
1	0.06258	0.06666	0.06412	0.06689	0.06482	0.06801
2	0.05591	0.06315	0.05337	0.06423	0.05264	0.05975
3	0.0444	0.05291	0.04323	0.05154	0.04232	0.04851
4	0.03145	0.03809	0.03400	0.03852	0.03306	0.03691
5	0.02774	0.02239	0.02752	0.02233	0.02649	0.02512
6		y_{1n}=0.00		-		-
			- solution vector		- solution vector	
			η_1=0.180 η_3=0.72 η_5=0.65 r=2.11 e =0.032 -S.S.R.=0.2x10^{-4}		η=0.551 r=0.69 e=1.11 -S.S.R.=0.65x10^{-4}	

Table 8.12 - Run PM-3. Least Square Fitting. Stagewise Model

Concentration Profiles						
	Experimental		Fitted Formulation 3		Fitted Formulation 4	
k	x_k	y_k	$\hat{x}_k$	$\hat{y}_k$	$\hat{x}_k$	$\hat{y}_k$
0	x_{in}=0.0846		-		-	
1	0.06383	0.05820	0.06418	0.05810	0.06342	0.05967
2	0.05263	0.05708	0.05139	0.05841	0.05135	0.05507
3	0.04286	0.05152	0.04269	0.05131	0.04288	0.04839
4	0.03412	0.04438	0.03571	0.04230	0.03588	0.04107
5	0.03177	0.03092	0.03185	0.03181	0.03043	0.03359
6		y_{in}=0.00		-		-
			- solution vector		- solution vector	
			η_1=-0.027 η_3=0.522 η_5=0.432 r=1.65 e=1.95 -S.S.R.=0.23x10^{-4}		η=0.517 r=0.181 e=3.544 -S.S.R.=0.40x10^{-4}	

characterize the column performance is η_3, which is associated with the inner part of the column.

Comparing the solution vectors for the two model formulations for the three experimental profiles it can be concluded that both formulations produce similar values of η in the central part of the column. The variation of η with N presents a maximum value at 500 RPM. No improvement in column performance can be obtained by increasing the level of agitation above 500 RPM in spite of the increased mass transfer interfacial area. This behaviour is explained by the fact that the continuous phase back mixing increases sharply for N above 500 RPM, decreasing the mass transfer driving force and also the drops being smaller produce lower mass transfer coefficients.

Further inspection of the solution vector reveals that both formulations produce quite different estimated values of the back flow parameters. This situation can be explained based on the conclusions drawn from the theoretical studies of the different model formulations presented in Chapter 5. It was theoretically shown that the accuracy of the back flow parameters e and r are more influenced by the number of parameters in the model and the experimental errors in the concentrations than the stage efficiency η. Also an increase in the number of parameters in the model produces a significant bias in the values of e and r, which increases with experimental and/or modelling errors. Since the 5-cells with back flow model is still a simple approximation to the real behaviour

of the column (Figure 8.1) which implies large modelling errors, it is believed that the estimated values of the back flow coefficients $\underline{e}$ and $\underline{r}$ based on Formulation 3 are unreliable. On the other hand, the values of the back flow parameters obtained with Formulation 4 give a reasonable and explainable relationship among themselves as well as with the speed of agitation. As was expected, the ratio (e/r) increases with N, since $\underline{r}$ decreases due to a more uniform drop size distribution and $\underline{e}$ increases due to the increase of the true back flow which existence has been experimentally established.

The estimated values of the overall mass transfer coefficients presented in Table 8.13 were obtained by substituting the results from Formulation 4 into equation (8.6) to (8.8). Theoretical mass transfer coefficients were also calculated using the correlations proposed by Newmann (105) for stagnant drops, Garner and Tayeban (102) for circulating drops and Rose and Kintner (103) lately revised by Al-Hassan (112) for oscillating drops.

It is necessary to mention that the K_D's values obtained from the best fitted value of the model parameter n, do not represent a real local value but rather an equivalent value for the simplified column of the model For this reason it is expected that K_D may be correlated with the back flow parameters.

Table 8.13 - Overall Mass Transfer Coefficient
Preliminary Runs

Run	K_D (experimental)	K_D (theoretical)		
		Stagnant	Circulating	Oscillating
P_{M-1}	0.91×10^{-4}	0.16×10^{-4}	0.38×10^{-4}	0.66×10^{-4}
P_{M-2}	1.33×10^{-4}	-	-	0.61×10^{-4}
P_{M-3}	0.72×10^{-4}	0.15×10^{-4}	0.35×10^{-4}	0.66×10^{-4}

The comparison between the theoretical and the estimated mass transfer coefficients reveal that the latter are higher than the expected theoretical value even for oscillating drops. Same behaviour was found in the final experimental program and the discussion of the situation is given in Section 9.3.4.5.

CHAPTER IX

EXPERIMENTAL PROGRAM, RESULTS AND DISCUSSION

EXPERIMENTAL PROGRAM, RESULTS AND DISCUSSION

9.1 Planning of the Investigation

The final experimental programme was planned to interpret the experimental profiles under the cells with backflow model and at the same time identify the variables that have the greatest effect on the process, in order to obtain design information.

The following points were considered:

1. Selection of the operational and design variables
2. Number of levels and range of the variables
3. Most convenient response to study
4. Experimental design

Each of these will be discussed.

9.1.1 Process Variables

The speed of agitation N is a factor that has to be considered since the preliminary investigation was revealed that there was a strong affect of this variable on process operation and performance.

The packing pad height is an important design variable since not only does it control the amount of backflow of the phases but it also influences the column capacity.

The height of the mixing chamber was shown to be within a reasonable range, not important as far as mass transfer is concerned and it will be kept constant throughout the experimentation.

The effect of the mass transfer direction on the column performance had not been analysed in the exploratory investigation. Nevertheless, the results of run PM-4 and PM-5 indicated that there was a strong influence of this variable upon the drop size and dispersed phase hold-up; which justifies its inclusion.

The dispersed and continuous phase superficial velocities V_D and V_C were included in the plan in order to complete the analysis of the operating variables.

Many other variables such as packing element size and voidage, geometric variables (D_I,D_C,W), physical properties of the system and feed solute concentration, may affect the operation as well as the rate of mass transfer in the column. However, only those cited above which are independent and capable of control, were considered initially to be sufficient to start a systematic investigation.

9.1.2 Levels and Range of the Variables

The number of levels of the variables chosen was based on the selected experimental design and a 2^n factorial design, as discussed in Section 9.1.4, was initiated since it was considered to be the most economical and reasonable

initial design in which all variables would be studied at two levels.

9.1.2.1 Impeller Speed

The levels of the variable N chosen were based on the results of the exploratory runs. Speeds below 400r.p.m., did not impart sufficient energy for the dispersion to be fully uniform in each compartment, especially when mass transfer took place from the dispersed to the continuous phase. At speeds of 700r.p.m. and above drop sizes in the case of mass transfer continuous to dispersed were very small and serious difficulties were encountered in obtaining pictures from which drop size could be measured. Therefore, impeller speeds 400 and 600r.p.m. were chosen as representative of the range of normal operating speeds for the column under study.

9.1.2.2 Packing Pad Height and Number of Scheibal Stages

It has been shown in Chapter 8 that, due to the "junction effect" there is total coalescence of the organic dispersed phase inside the packing. Therefore, the function of the packing pads in the column is to act as a coalescer and at the same time, isolate the mixing chambers.

In view of this, the following packing pad heights reported in the literature 5(10), 23(17), and 33(17) cm for 2.5 and 30.5 cm diameter columns, seem unnecessarily large. Since small column heights are convenient practically

and 1.5 cm pad heights had been tested, it was decided to study pads of heights 3.0 and 6.0 cm.

The number of Scheibel stages selected were based on the following points:

1. A small number of stages permit a rapid approach to steady state condition. This is an important limiting factor in view of the relative small feed capacity of the pilot plant (70 litres).

2. The number of stages while small, has to be sufficient to give a representative performance and to be able to apply the model fitting exercise with a sufficiently large number of data points. This last requirement is crucial in the parameter estimation of the cell model as shown in Chapters 5 and 8. Based on the above four Scheibel stages were considered appropriate.

9.1.2.3 Phases Volumetric Flow and Feed Solute Concentration

Initially it may be considered that the levels of V_C and V_D can be chosen considering only the total feed capacity of the unit, the flooding characteristic of the column and the operating time necessary to reach steady state condition, plus some extra time for sampling and picture taking.

The pilot plant utilized in this study is shown in Figure 6.2 and it has a feed capacity of each phase of 70 litres. The time estimated to attain steady state, based on results from the preliminary experiments and Treybal's (7) approximated method, was about 45 minutes. Hence it can be assumed that a total operating time of 60 to 75 minutes is possible per run. Column flooding conditions were measured with the 6.0 cm pads height inserted into the column under no-mass transfer operation and the results obtained are presented and discussed in the following sections. These results together with the selected impeller speeds led to the tentative conclusion that a volumetric feed rate and solvent rate of 1000 ml/min could be accepted as a practical maximum value. Then the choice for levels of V_C and V_D were 500 and 1000 ml/min.

The concentration of the feed was fixed by considering the following:

1. Maximum solute content allowed in each phase while maintaining phase immiscibility,

2. The concentration range in the column should be within the linear portion of the system equilibrium relationship. Based on the systems physico-chemical data presented in Chapter 6 it was decided that the feed concentration be about 8% w/w together with the pure solvent would be used in this study.

An important variable in extraction studies that had not yet been considered is the extraction factor F, defined as

$$F = \frac{mR}{E} \tag{9.1}$$

where m is the distribution coefficient of the equilibrium relationship

$$x^* = f(y) \tag{9.2}$$

An analysis of this variable was made for the case of the aqueous continuous phase i.e. the raffinate phase, since similar conclusions can be drawn from a similar analysis of the opposite mass transfer direction case. The solid lines in Figure 9.1 shows the ideal operating lines for the values of F, 2.55 (a and a') and 0.64 (b) calculated using the levels of V_C and V_D tentatively assumed above. The dotted lines simulate the real operating lines.

For F > 1, case a, Figure 9.1 shows that the existence of a "pinch point" condition is possible at the bottom of the column, depending on the extent of deviation from plug flow exhibited and the number of real stages in the column. This situation must be avoided, since the experimental error affecting the values of the phase concentrations can be a large portion of the total driving force in the "pinch point" region, due to the extremely low values of the x- or y- driving forces. This large error in the experim ental value of the driving force certainly will affect the accuracy of the model parameter estimates.

Figure 9.1 - Analysis of Extraction Factor F

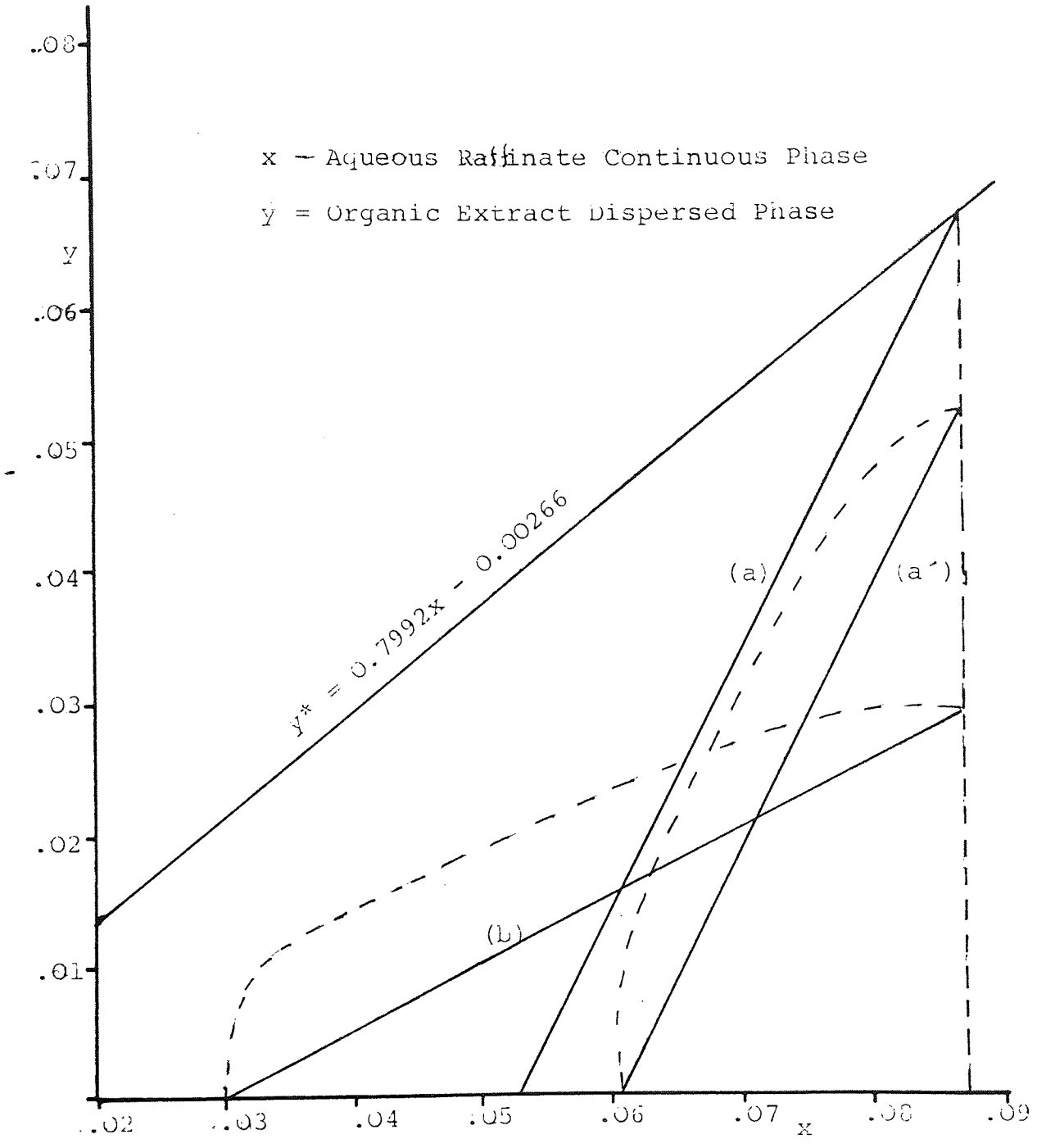

Case b, F < 1, represents the situation of a low extraction factor and also needs careful analysis since problems can arise in the event of large flow non-idealites. From Figure 9.1 it is noticed that, for large axial mixing or backmixing of the extract phase, the concentration profile can become almost horizontal. Under this condition, unavoidable experimental errors and column random variation can mask the extract phase concentration change in the middle part of the column with the consequence of a poor and unacceptable solution of the model fitting stage.

The above discussion indicated that the selected levels of V_C and V_D (500 and 1000 ml/min) are not convenient and that values of F in the range of 0.8 to 1.2 are suitable under operating conditions of organic phase raffinate and dispersed.

Setting two levels of a phase flowrate and F, results in four values of the other dependent flowrate. This may require an experimental design of the type $2^k 4^n$ with k = 4 n = 1 which was considered to be unnecessarily large and it was decided not to study V_C, keeping its value at 500 ml/min, which then gives a reasonable 2^4 = 16 runs complete experimental design.

In summary, the factors to be investigated were chosen to be:

	Factor	(-)	(+)
Impeller Speed, r.p.s.	(A)	6.66	10
Pad Height m	(B)	0.03	0.06
Mass Transfer direction	(C)	D→C	C→D
Volumetric Dispersed Phase Flowrate ml/min	(D)	625	950
Volumetric Continuous Phase Flowrate	- 500 ml/min		

9.1.3 Treatment Response

The mean drop diameter and drop size distribution, the dispersed phase hold-up and the concentration profile of each phase are to be measured in each experiment and later subject to analysis.

Still photographs of several agitated chambers were taken in order to produce a characteristic Sauter mean drop diameter. Although it was shown in the preliminary experimentation that no relationship exists between the mean drop diameter and the column height, the above procedure was considered convenient when mass transfer is taking place. Hold-up determination was made by withdrawing a large two-phase sample from a mixing compartment. More details of these techniques, as well as the sampling technique for concentration measurement are presented in Chapter 7.

9.1.4 Experimental Design

Since large interactions between the factors listed in Section 9.1.1 are expected to exist, the Latin Squares and/or Randomised Blocks experimental designs can not be used.

Each of the statistical treatments presented in Section 9.1.3 may require different experimental designs. The significance of the effects and interactions will be different according to the response of the analysis, and in some case a simple design will supply the information while for others a more complete one is required. Since it is desirable to run a single design, at least as a starting point, a complete 2^4 factorial was considered to be the most economical and reasonable.

The four variables or factors generate sixteen treatment combinations as presented in Table 9.1. The factors are denoted by capital letters and the two levels of each factor by (1) and the corresponding small letter. By convention (1) refers to the lower level, the normal condition or the absence of a condition while the small letter refers to the higher level, the change from normal the presence of a condition, etc. The next table 9.2 shows a more familiar representation of the 2^4 design.

It was decided that each treatment would be tested once giving a total number of sixteen experimental runs. The runs would be made at random. As will be shown in the Data Analysis section, this design requires some interaction mean squares to be used as estimates of the experimental

Table 9.1 - Symbols for Treatment Combinations

Treatment Combination	Level of Factors			
	A	B	C	D
(1)	-	-	-	-
a	+	-	-	-
b	-	+	-	-
ab	+	+	-	-
c	-	-	+	-
ac	+	-	+	-
bc	-	+	+	-
abc	+	+	+	-
d	-	-	-	+
ad	+	-	-	+
bd	-	+	-	+
abd	+	+	-	+
cd	-	-	+	+
acd	+	-	+	+
bcd	-	+	+	+
abcd	+	+	+	+

Table 9.2 - 2^4 Experimental Design

Impeller speed, N r.p.s. (A)	Pad Height H_p, m (B)	Dispersed Phase Superficial Velocity, V_D (D) m/s			
		1.28×10^{-3}		1.94×10^{-3}	
		Mass Transfer Direction (C)		Mass Transfer Direction (C)	
		D→C	C→D	D→C	C→D
6.66	0.03	(1)	c	d	cd
	0.06	b	bc	bd	bcd
10.00	0.03	a	ac	ad	acd
	0.06	ab	abc	abd	abcd

error since a single replication of the experiment will be carried out.

9.2 Experimental Results

9.2.1 Columns Capacity

The flooding characteristics of the columns shown in Chapter 6, Figures 6.3 and 6.4, were investigated under "no mass transfer conditions" in order to assess the maximum flow rates permitted in the columns. Although it was realised that in the mass transfer experiments the flooding characteristics can be quite different, the data shown in Tables 9.3 to 9.7 would serve as a guideline in the selection of the levels of the phases flowrate.

The influence of the agitators location on the flooding behaviour was tested by running the columns alternatively with the impellers positioned at the middle of the mixing chambers and at $D_I/5$ cm from the upper surface of the pads.

The determination of the onset of flooding and the experimental procedures adopted have been described in Chapter 6. In all the runs the system was mutually saturated toluene (dispersed) and water (continuous). The data listed in Tables 9.3 to 9.7 and plotted in the Figures 9.2 to 9.5 are the average values of at least two runs. The position of the onset of flooding reported in the tables was specified relative to the bottom packing pad.

Table 9.3 - Flooding Data - Column 1, 6cm pad height (5)

Volumetric Flowrate ml/min		Impeller speed r.p.m.	Onset Flooding
Q_C	Q_D		
1230	1870	400	Below lst pad from column bottom
1650	1740		"
2070	1350		"
850	2000	500	Below lst pad
1230	1850		"
1230	1650		"
1650	1400		"
2070	600		"
850	1120	700	Below lst pad
1230	720		"
1650	530		"

Impeller Position: Middle of Mixing Chambers

Table 9.4 - Flooding Data - Column 1, 6 cm pad height (5)

Volumetric flowrate ml/min		Impeller Speed r.p.m.	Onset Flooding
Q_C	Q_D		
850	1160	400	Below 1st Pad
1230	1160		"
1650	1000		"
1230	1780	500	Below 1st Pad
1650	1550		"
2070	1350		"
1230	2300	700	Below 1st Pad
1650	1740		"
2070	1300		"

Impeller Position: $D_I/5$ cm from upper surface of the pad

Table 9.5 - Flooding Data - Column 2, 3cm pad height (5)

Volumetric Flowrate ml/min		Impller speed r.p.m.	Onset Flooding
Q_C	Q_D		
850	-	400	Below 5th pad
1225	3100		"
1650	2850		"
1225	1750	700	Below 1st pad
1650	1250		"

Impeller Position: Middle of Mixing Chambers

Table 9.6 - Flooding Data - Column 2, 3cm pad height (5)

Volumetric Flowrate ml/min		Impeller speed r.p.m.	Onset Flooding
Q_C	Q_D		
850	1700	400	Below 1st pad
1250	1400		Below 4th pad
1650	1250		Below 5th pad
2100	1075		Below 5th pad
850	2400	500	Below 5th pad
1225	1950		"
1650	1950		"
850	3500	700	Below 5th pad
1225	2700		
1650	2250		"

Impeller Position: $D_I/5$ cm from upper surface of pads

Table 9.7 - Replicated Flooding Data [1] Column 2, 3cm pad height (5)

Volumetric Flowrate ml/min		Impeller speed r.p.m.	Onset Flooding
Q_C	Q_D		
850	1450	400	Below 4th pad
1230	1350		Below 1st pad
1650	850		Below 1st pad
2070	750		Below 1st pad
850	1650	500	Below 4th pad
1230	1350		Below 4th pad
1650	1260		Below 4th pad
850	1290	700	Below 1st pad
1230	1260		
1650	1075		

Impeller Position: $D_I/5$ cm from upper surface of pads

Figure 9.2 - Flooding Data

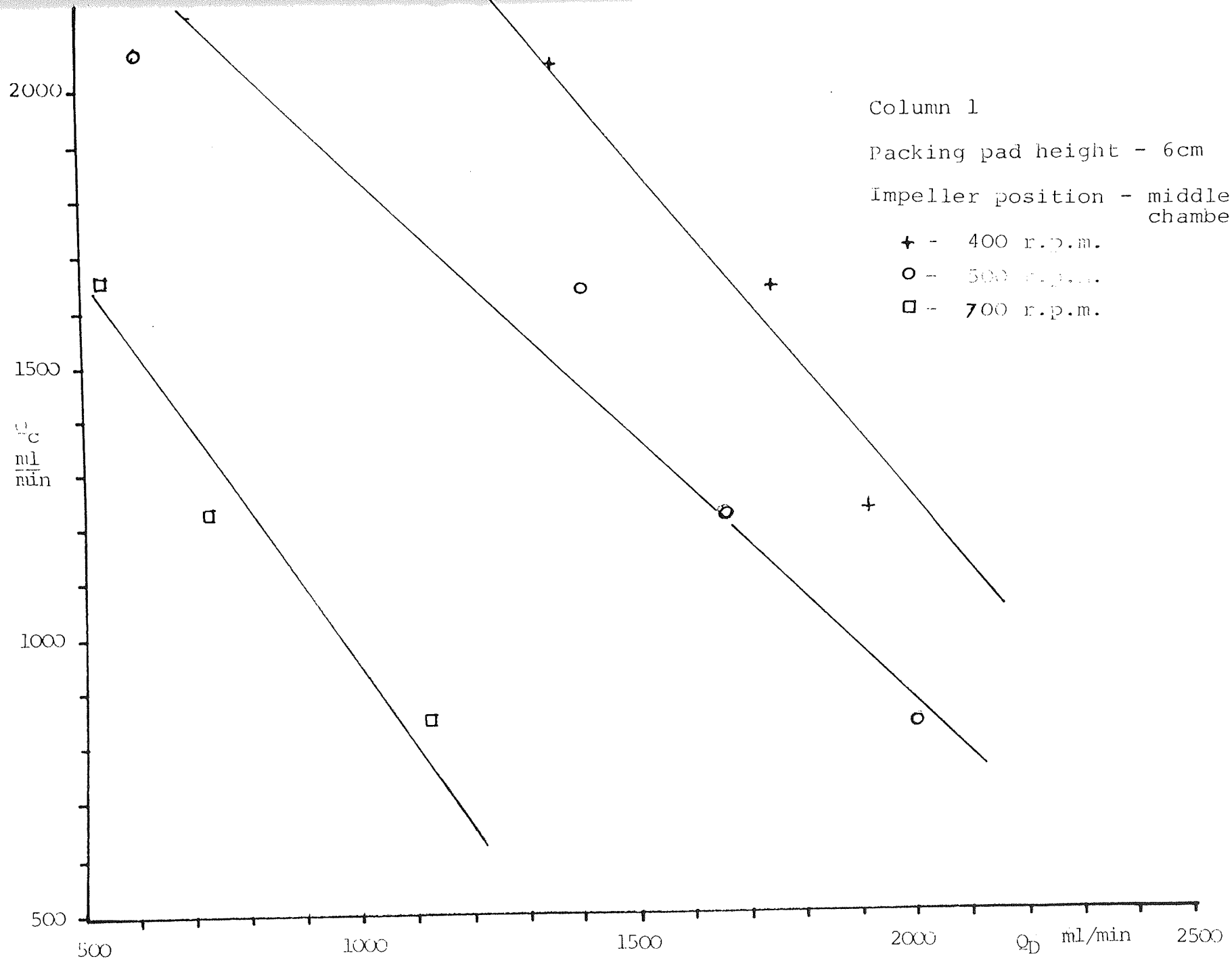

Figure 9.3 - Flooding Data

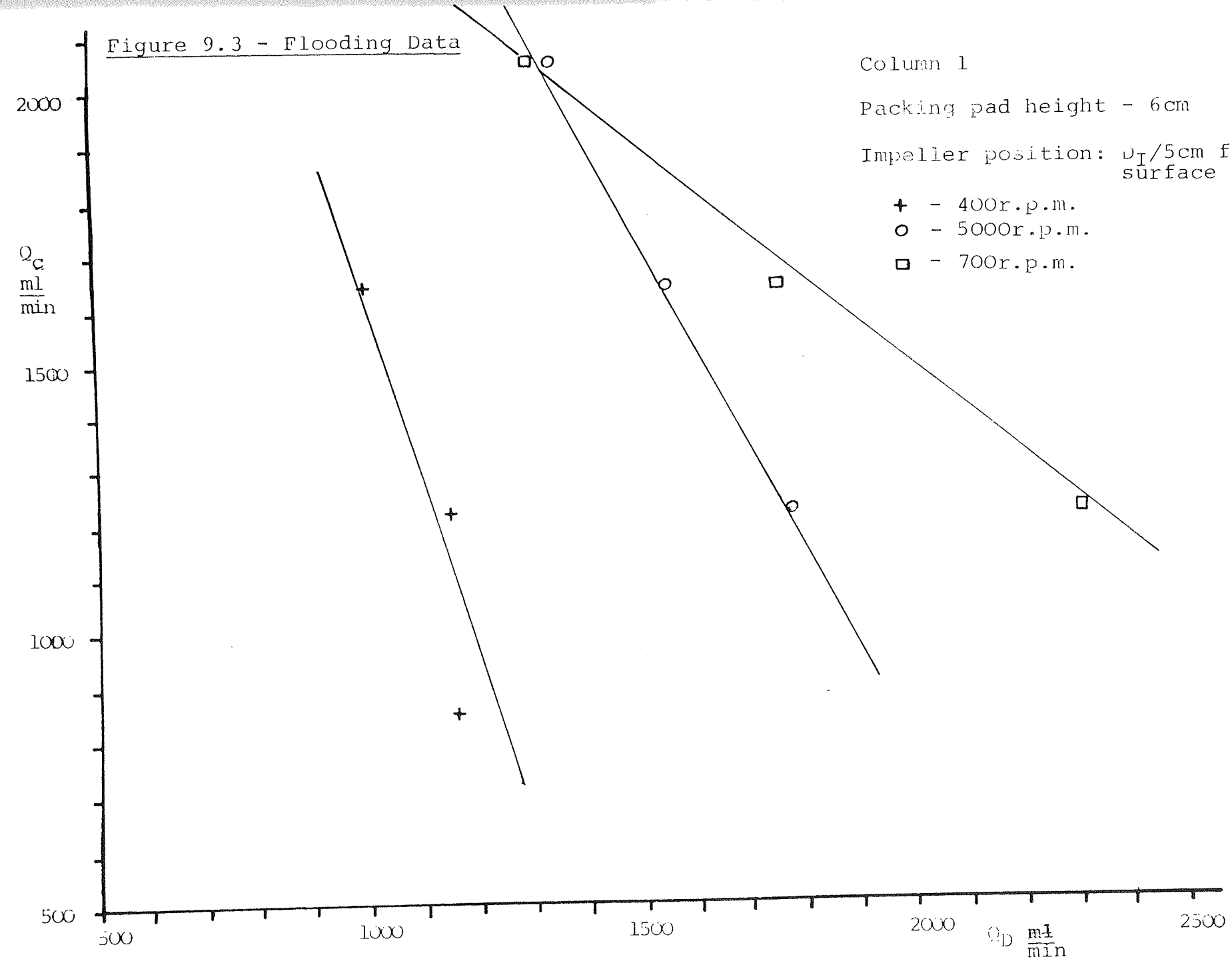

Figure 9.4 - Flooding Data

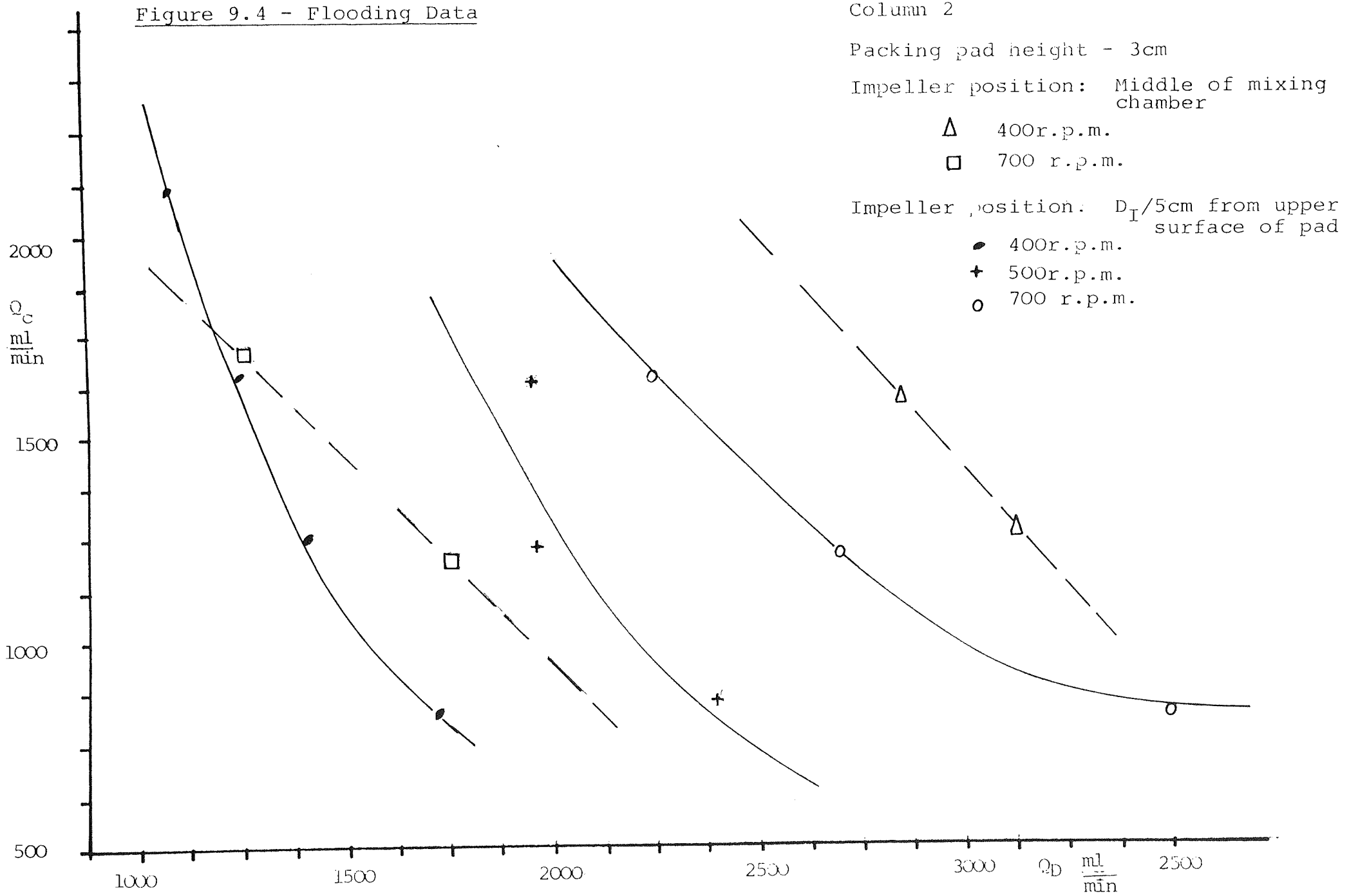

Figure 9.5 - Flooding Data

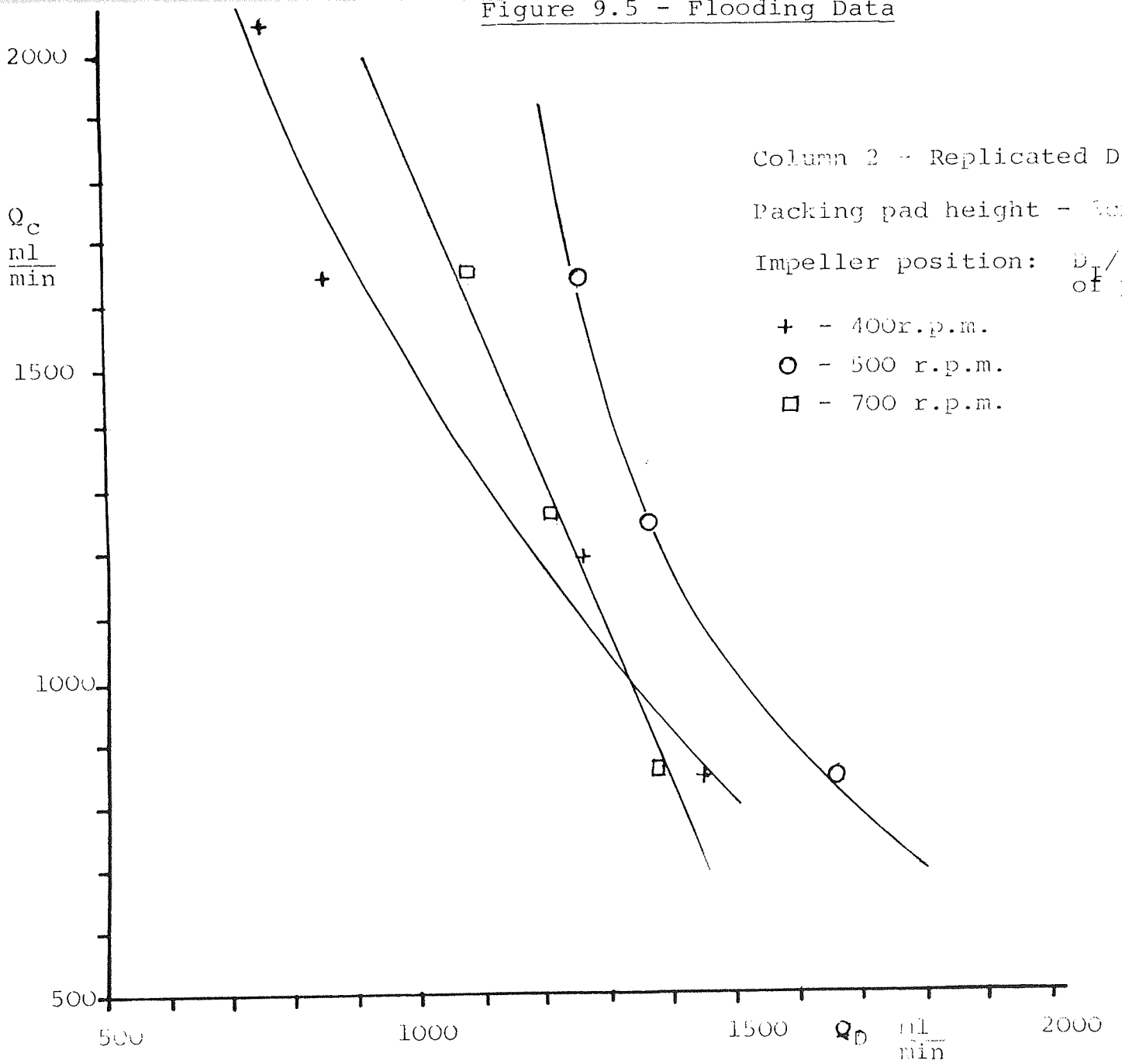

Column 2 - Replicated Data

Packing pad height - [illegible]

Impeller position: D_I/5cm from upper surface of pad

+ - 400r.p.m.

O - 500 r.p.m.

□ - 700 r.p.m.

9.2.1.1 Continuous Phase Entrainment

Tests for entrainment in the continuous phase similar to the ones described in Section 8.3.2.1, were performed in both columns with the impellers positioned at $D_I/5$ cm from the upper surface of the pads. No evidence of backflow or entrainment of the continuous phase was found in either column.

9.2.2 2^4 Factorial Design

This section presents the results of the 2^4 factorial design given in Table 9.2. In all the runs the impellers were positioned at approximately $D_I/5$ cm from the upper surface of the pads. The position of the interface at the top of the column was maintained at about 20 cm from the top distributor plate and carefully monitored in all the runs, in order to avoid random variations which enlarge the experimental error.

The two columns identified as Column 1 for the 6 cm pad height and Column 2 for the 3 cm pad height, were constructed from standard QVF pipe sections of 10 cm diameter. The columns were of such length as to give, as close as possible, comparable end effects. Undetected large differences in the end effects would give bias results which lead to wrong conclusions in the statistical analysis.

Tables 9.8 to 9.12 present the concentration profiles, hold-up and Sauter mean drop diameter obtained for each of the experiments of Table 9.2. A total of 22 samples per run were analysed for Run 1 to 8 inclusive, fourteen samples from inside the columns and two samples from each of the inlet and outlet streams. The samples labelled Dist. T and Dist. W, corresponding to the organic and aqueous phase respectively were taken at the exit ($\sim$1cm) of the distributor plates. For Run 9 to 16, each produced 8 samples from inside the columns, one sample at the exit of each distributor plate and two samples from each of the inlet and outlet streams, giving a total of 19 samples/runs.

Figure 9.6 shows schematically the sampling position and system behaviour at both distributor plates. At the top of the column the dispersed phase coalesces completely in the upper pad leaving it by several jets. This is in agreement with the fact, common to all of the runs, that the 6T and 5T samples have approximately the same concentration. This confirms the conclusion of the preliminary investigation that almost no-mass transfer takes place inside the packing pads.

The organic phase jets hit the internals of the upper distributor plate breaking-up into large oscillating drops which coalesce at the top interface. This behaviour is quantitatively represented by the relatively large concentration difference found between 6T and the organic samples at the column top. This extra amount of solute transfer is considered to be part of the columns top end

Table 9.8 - Column 1. Mass Transfer Direction Dispersed → Continuous

Sample Position Z	Sample Number	b-Run 1 y^1	b-Run 1 x^1	ab-Run 2 y^1	ab-Run 2 x^1	bd-Run 3 y^1	bd-Run 3 x^1	abd-Run4 y^1	abd-Run4 x^1
0.00	Column bottom	4.76	7.65=feed	5.33	7.25=feed	6.90	7.82=feed	7.40	7.55=feed
0.01	Dist. T	-	7.41	-	7.14	-	7.58	-	7.42
0.107	1W, 1T	4.78	7.31	5.40	6.90	6.86	7.31	7.36	7.49
0.259	2W, 2T	4.18	6.60	4.52	5.45	6.24	6.62	6.77	6.85
0.412	3W, 3T	2.92	5.13	3.75	4.61	5.04	5.72	5.92	6.11
0.582	4W, 4T	1.44	3.20	2.52	2.89	3.97	5.01	4.61	5.04
0.735	5W, 5T	1.34	3.06	1.38	1.96	2.82	4.07	3.02	4.01
0.893	6W, 6T	0.45	3.00	0.20	2.01	0.92	4.20	0.89	4.10
0.99	Dist. W	0.51	-	0.25	-	0.75	-	0.88	-
1.00	Column top	0.00	2.84	0.00	1.79	0.00	3.79	0.00	3.31
		d_{32}=2.53 mm (St. Dev.= 1.30 mm)		d_{32}=2.22 mm (St.D. = 1.05)		d_{32}=2.82 mm (St.D. = 1.50)		d_{32}=2.76 mm (St.D. = 1.43)	
		Θ_D=0.045		Θ_D=0.055		Θ_D=0.068		Θ_D=0.0742	

Table 9.9 - Column 1. Mass Transfer Direction Continuous → Dispersed

Position Z	Sample Number	bc-Run 5 y^1	bc-Run 5 x^1	abc-Run 6 y^1	abc-Run 6 x^1	bcd-Run 7 y^1	bcd-Run 7 x^1	abcd-Run 8 y^1	abcd-Run 8 x^1
1.0	Column bottom	0.10	3.51	0.00	2.82	0.00	2.30	0.00	1.70
0.99	Dist. T	0.28	-	0.21	-	0.21	-	0.25	-
0.893	1T, 1W	0.61	3.57	0.41	2.83	0.39	2.33	0.30	1.77
0.7403	2T, 2W	1.75	4.03	1.38	2.99	1.14	2.75	0.84	1.93
0.5877	3T, 3W	2.67	4.95	2.22	4.13	1.68	3.78	1.70	2.89
0.4177	4T, 4W	3.40	6.13	3.09	5.25	2.29	4.71	2.48	4.08
0.2651	5T, 5W	4.19	7.19	3.86	6.35	2.98	5.88	3.55	5.44
0.1071	6T, 6W	4.28	7.86	4.07	7.07	3.06	7.19	3.62	6.45
0.01	Dist. W	-	8.10	-	7.46	-	7.46	-	7.22
0.00	Column top	4.88	8.68=feed	4.37	7.67=feed	3.66	8.20=feed	4.06	7.90=feed
		d_{32}=1.43 mm (St.D. = 0.54)		d_{32}=0.82 mm (St.D. = 0.26)		d_{32}=2.04 mm (St.D. = 0.89)		d_{32}=1.27 mm (St.D. = 0.87)	
		Θ_D=0.080		Θ_D= 0.14		Θ_D=0.10		Θ_D=0.17	

Table 9.10 - Column 2. Mass Transfer Direction Dispersed → Continuous

Position Z	Sample Number	(1)-Run 9 y^1	(1)-Run 9 x^1	a-Run 10 y^1	a-Run 10 x^1	d- Run 11 y^1	d- Run 11 x^1	ad Run 12 y^1	ad Run 12 x^1
0.0	Column bottom	5.04	8.15=feed	5.87	7.98=feed	7.35	8.75=feed	7.74	8.44=feed
0.01	Dist. T	-	8.05	-	7.96	-	-	-	8.42
0.2454	2W, 2T	4.61	5.93	5.58	5.83	7.00	7.76	7.36	7.29
0.4047	3W, 3T	3.22	4.46	3.79	4.35	5.66	6.39	6.01	6.35
0.5549	4W, 4T	1.87	3.75	2.52	3.09	4.27	5.25	4.61	5.42
0.7161	5W, 5T	1.02	3.37	1.24	2.03	1.65	4.64	1.55	4.11
0.99	Dist. W, 6T	0.15	3.36	0.10	1.86	1.06	4.69	0.69	4.07
1.0	Column top	0.00	2.911	0.00	1.84	0.00	4.23	0.00	3.63
		d_{32}=2.96 mm (St.D.=1.55)		d_{32}=2.29 mm (St.D.=1.10)		d_{32}=3.86 mm (St.D.=2.25)		d_{32}=3.28 mm (St.D.=1.76)	
		Θ_D=0.044		Θ_D=0.057		Θ_D=0.072		Θ_D=0.08	

Table 9.11 - Column 2. Mass Transfer Direction Continuous → Dispersed

Position	Sample Number	c-Run 13 y^1	c-Run 13 x^1	ac-Run 14 y^1	ac-Run 14 x^1	cd-Run 15 y^1	cd-Run 15 x^1	acd-Run 16 y^1	acd-Run 16 x^1
1.0	Column bottom	0.00	3.60	0.00	3.27	0.10	2.45	0.13	1.74
0.99	Dist. T	0.16	-	0.10	-	0.33	-	0.21	-
0.7545	2T, 2W	1.49	3.97	1.44	3.20	0.88	2.85	0.77	1.83
0.5952	3T, 3W	2.37	5.19	2.38	4.74	1.42	3.79	1.43	2.87
0.4450	4T, 4W	3.37	6.40	3.06	5.84	2.05	4.65	2.05	4.07
0.2838	5T, 5W	3.75	7.02	3.90	6.93	2.81	5.62	3.11	5.51
0.01	6T, Dist. W	4.21	8.10	4.44	8.12	2.85	7.32	3.20	7.42
0.00	Column top	4.70	8.61=feed	4.73	8.42=feed	3.25	8.29=feed	3.76	8.54=feed
		d_{32}=1.78 mm (St.D.=0.77)		d_{32}=1.32 mm (St.D.=0.62)		d_{32}=2.24 mm (St.D.=1.18)		d_{32}=1.06 mm (St.D.=0.43)	
		Θ_D=0.06		Θ_D=0.124		Θ_D=0.116		Θ_D=0.158	

Table 9.12 - Replicated Runs

Sample		Run 10-1		Sample		Run 14-1	
Position	Number	y^1	x^1	Position	Number	y^1	x^1
0.00	Column bottom	6.70	8.58=feed	1.00	Column bottom	0.00	3.05
0.01	Dist. T	-	8.50	0.99	Dist. T	0.50	-
0.2454	2W, 2T	6.44	6.10	0.7545	2T, 2W	1.76	3.24
0.4047	3W, 3T	4.57	4.70	0.5952	3T, 3W	2.78	4.56
0.5549	4W, 4T	3.02	3.33	0.4450	4T, 4W	3.79	5.88
0.7161	5W, 5T	1.66	2.29	0.2838	5T, 5W	4.76	6.93
0.99	Dist. W, 6T	0.64	2.29	0.01	6T, Dist.W	4.98	7.83
1.00	Column top	0.00	1.95	0.00	Column top	5.18	8.50=feed
		Θ_D=0.062				Θ_D=0.116	

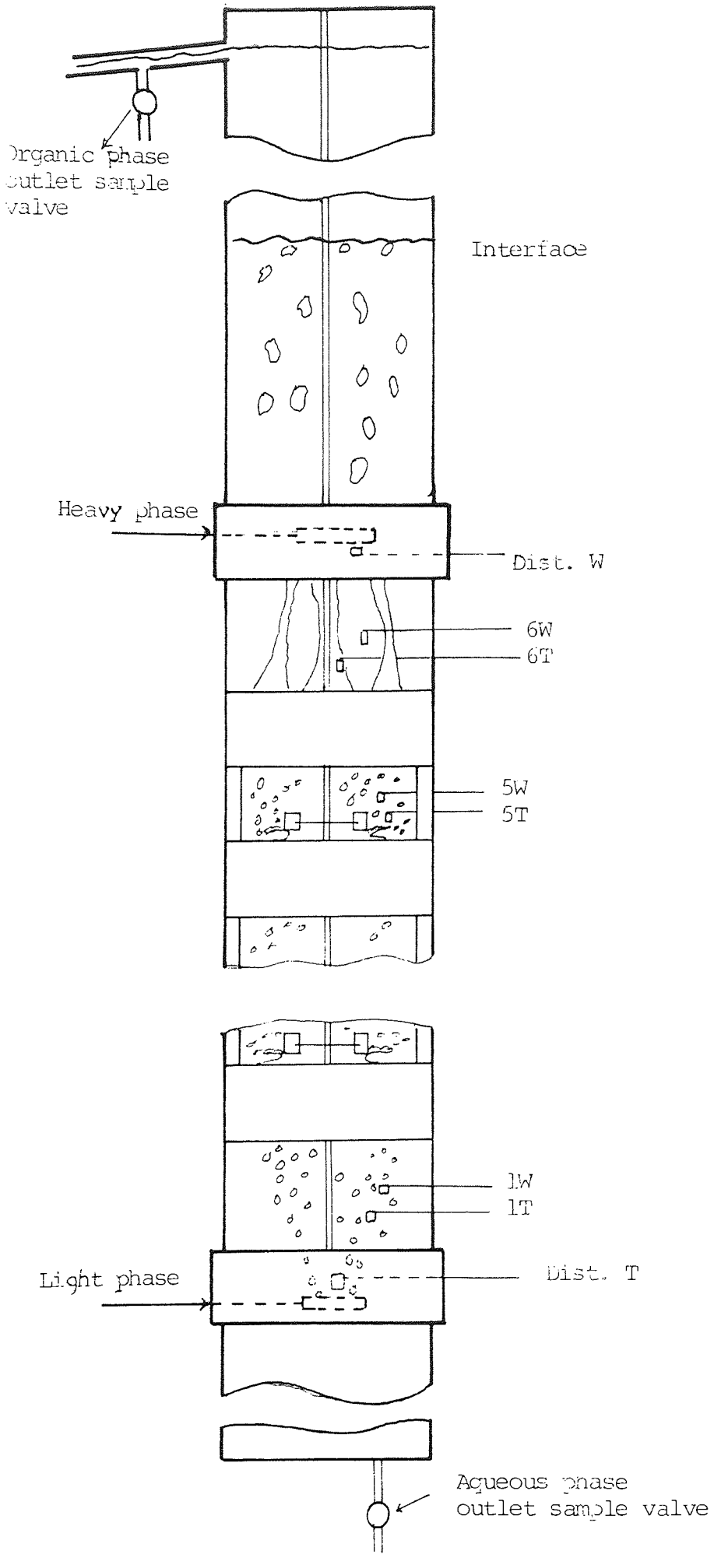

Figure 9.6 - Column 1. Sampling Points

effect and it is partially controlled by keeping the level of the main interface constant. The behaviour of the aqueous phase at the column top also needs careful examination. Sample 6W on Column 1, as well as sample Dist. W in both columns, do not provide a concentration value which accurately characterize the aqueous phase beyond the upper pad. This region behaves approximately as a spray column with large backflow in the aqueous phase which produces concentration gradients below and above the distributor plate. If the concentration changes in both phases at the top of the column are compared, it must be realised that the aqueous phase concentration jump at the distributor is the result of a mixing process and not of a solute transfer mechanism.

The portion of the column between the lower distributor plate and the first packing pad behaves also as a spray column. The organic phase concentration jump measured is the result of mass transfer at drop formation. The magnitude of the jump was, in all the runs, substantially smaller than the organic phase concentration change across any Scheibel stage. This reveals as far as mass transfer is concerned, an important difference between the two mechanism of drop formation. No relationship was found between the operating variables and the organic phase concentration jump, probably because the experimental error was large compared to the magnitude of the jump.

Figures 9.7 to 9.14 show the concentration profiles. The columns are schematically presented with the sampling positions and the hold-up valve clearly indicated. In drawing these profiles it was the author's intention to represent, as close as possible, the real axial concentration variation of the phases inside the columns. Thus, no mass transfer inside the packing pads, total mixing of the phases in the agitated chambers and total solute transfer located only at the impeller zones, were the conditions used in the drawings.

9.3 Analysis of Data

9.3.1 Flooding

The observation reported in Section 8.3.1.1 regarding the unusual behaviour of the preliminary flooding studies, was quantitatively confirmed in the final experimental programme. The tables of flooding data and their corresponding figures presented in Section 9.2.1 clearly show that by positioning the impellers close to the upper surface of the pads, the column capacity increases with the impeller speed.

Flooding data on Column 2 were replicated, under the condition of impellers close to the upper surface of the pads, at the end of the factorial experiment program. The results listed in Table 9.7 still show the unusual behaviour mentioned above but the reproducibility is so poor that it is necessary to conclude that another variable, besides impeller position in mixing chamber, exists which has a

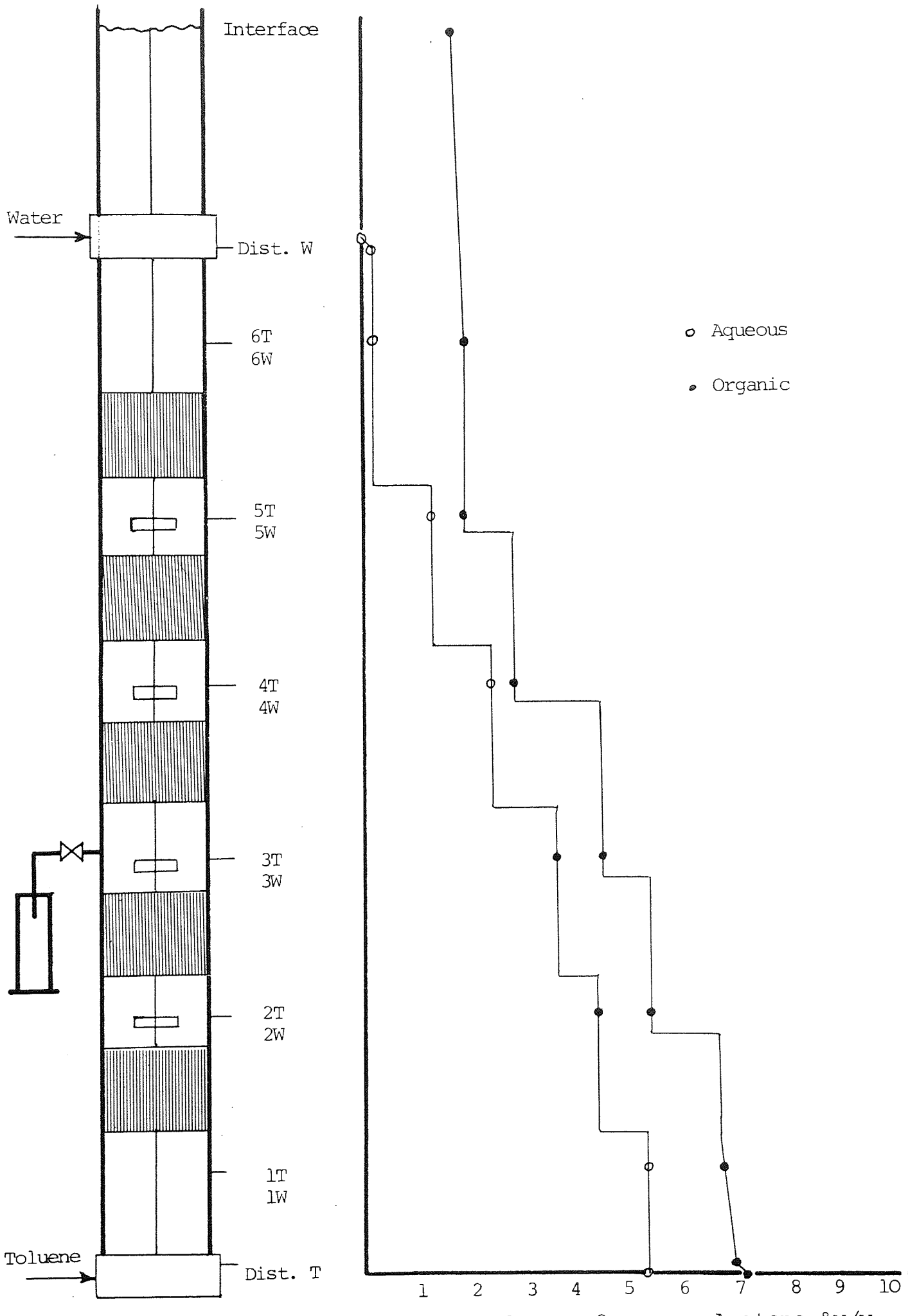

Figure 9.7 - Concentration Profile Run 2

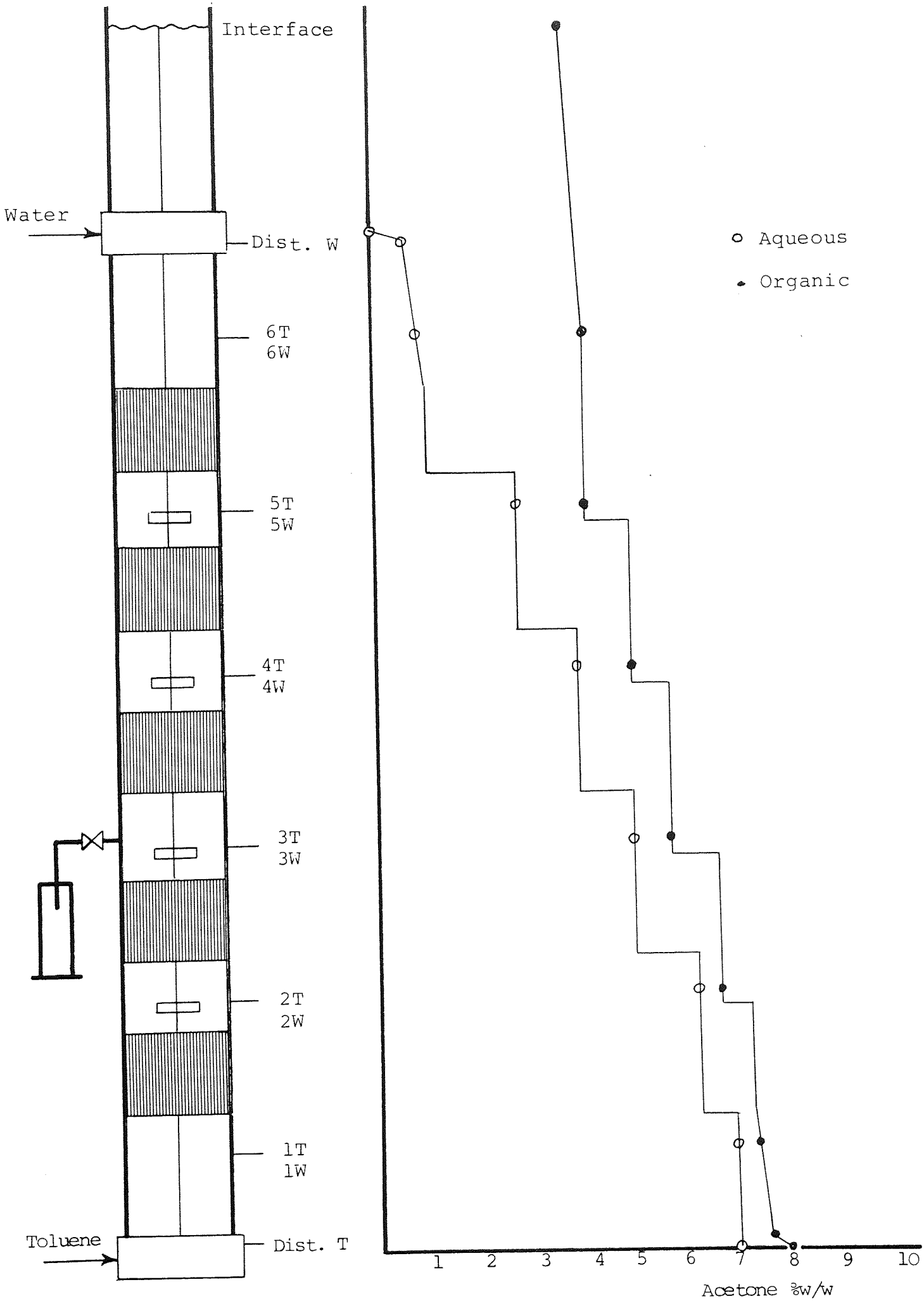

Figure 9.8 - Concentration Profile Run 3

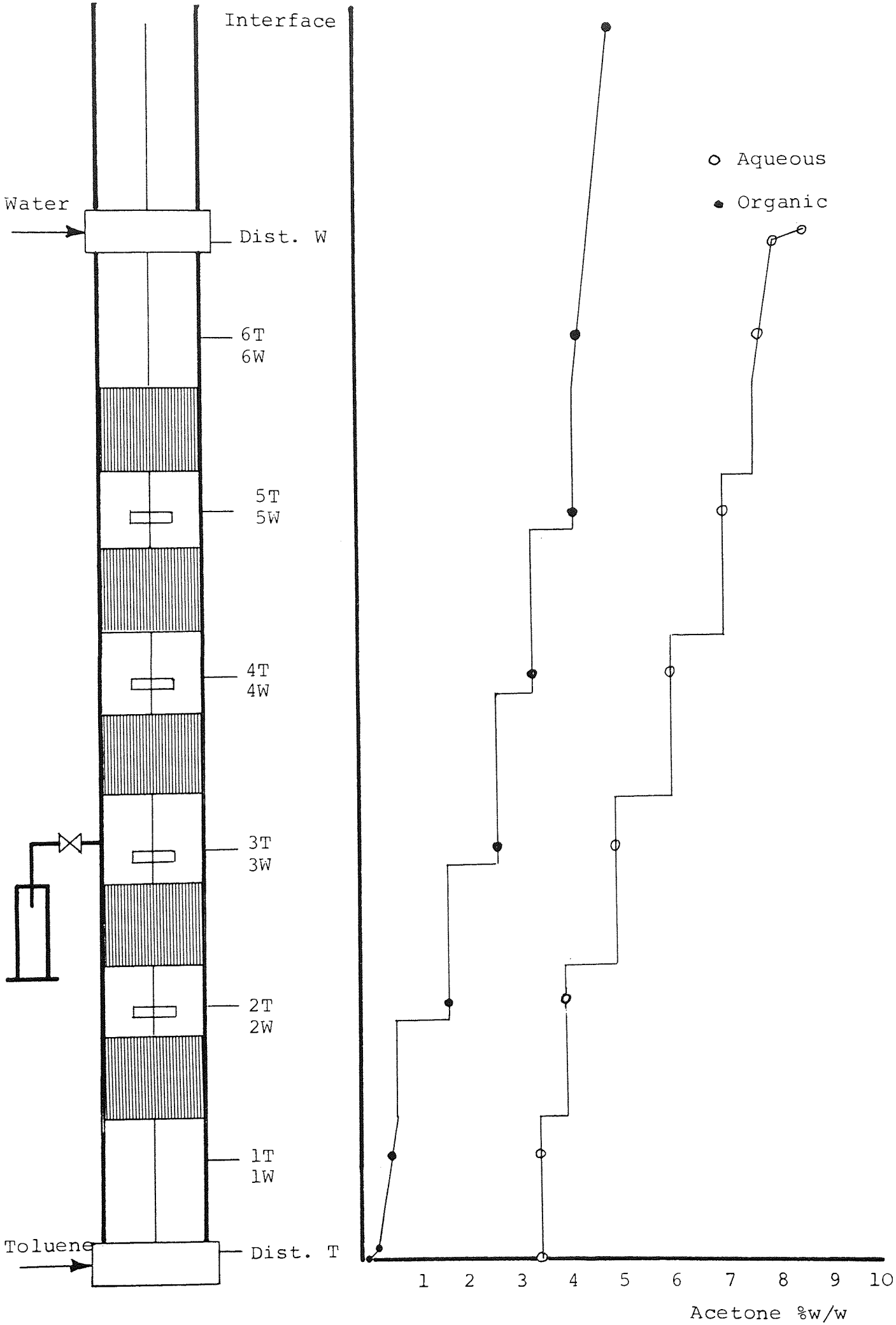

Figure 9.9 - Concentration Profile Run 5

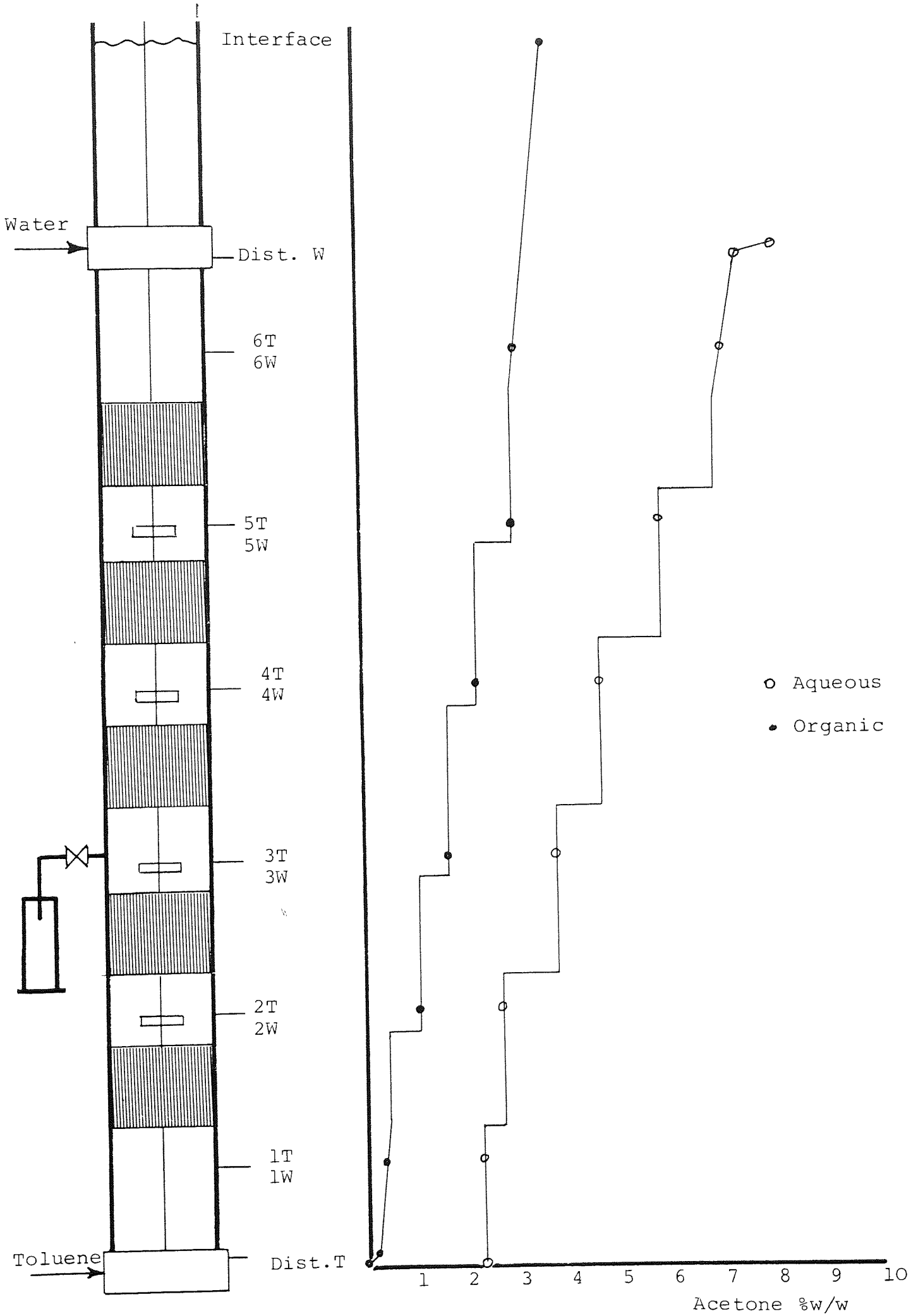

Figure 9.10 - Concentration Profile Run 7

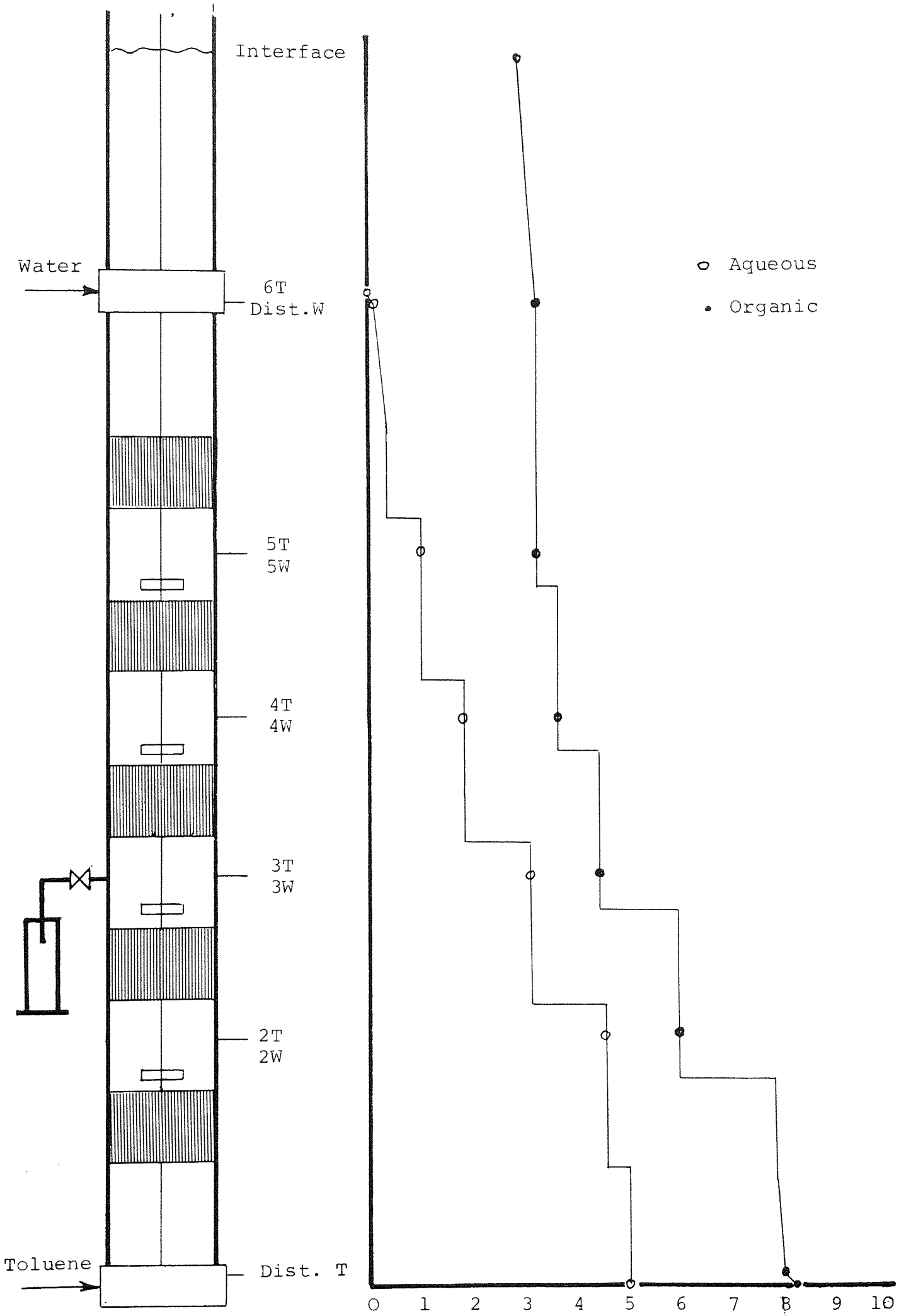

Figure 9.11 - Concentration Profile Run 9

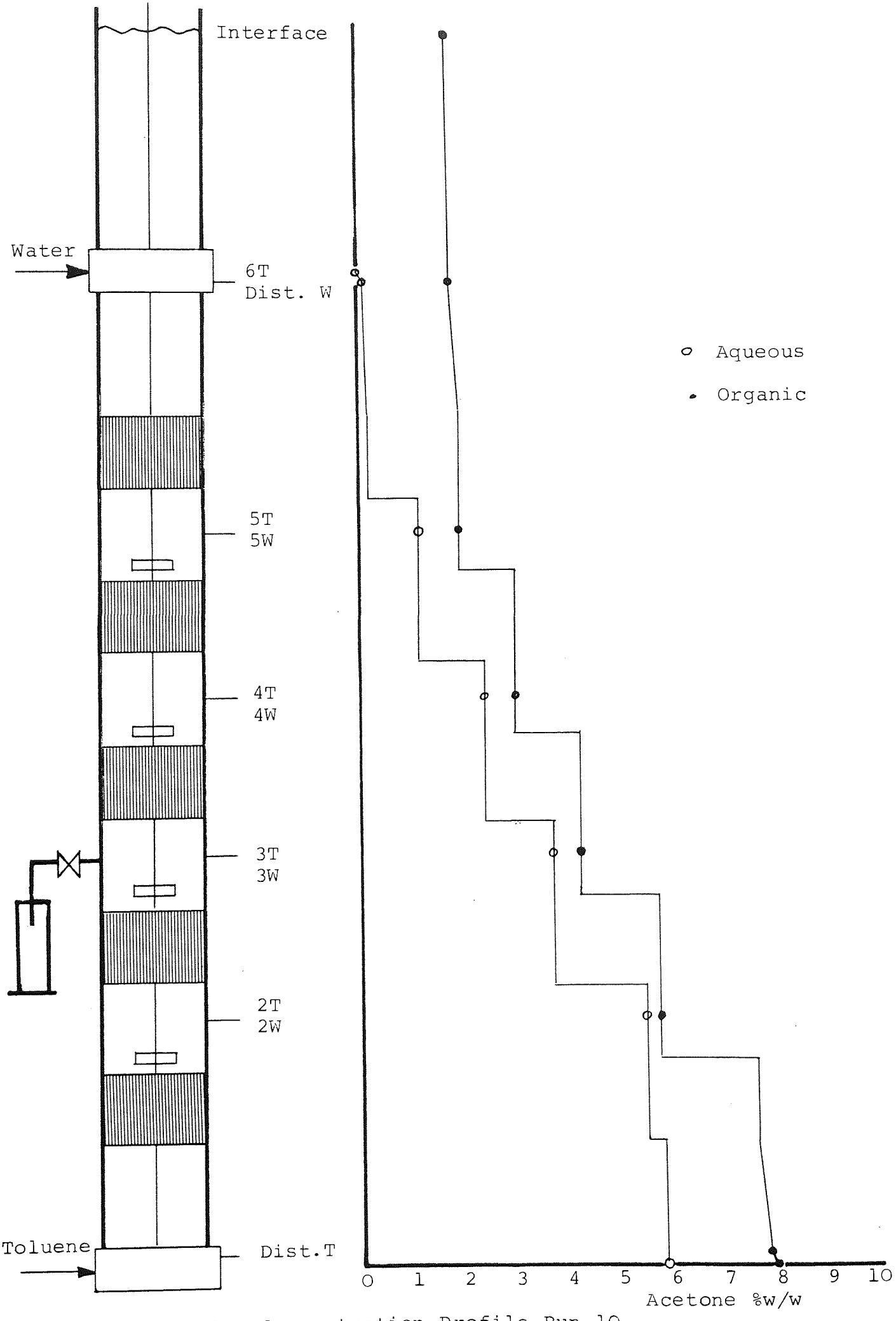

Figure 9.12 - Concentration Profile Run 10

Figure 9.13 - Concentration Profile Run 13

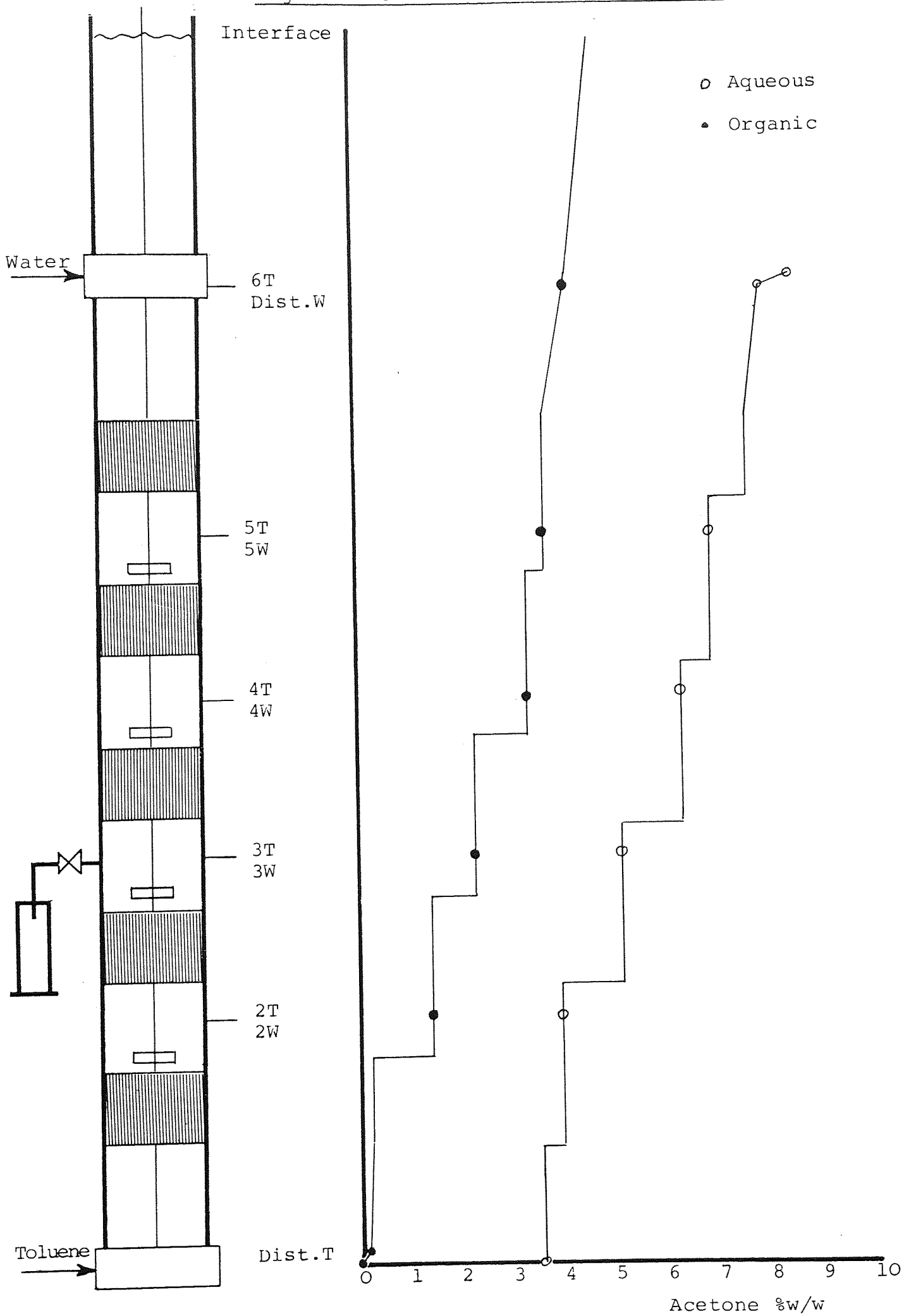

Figure 9.14 - Concentration Profile Run 16

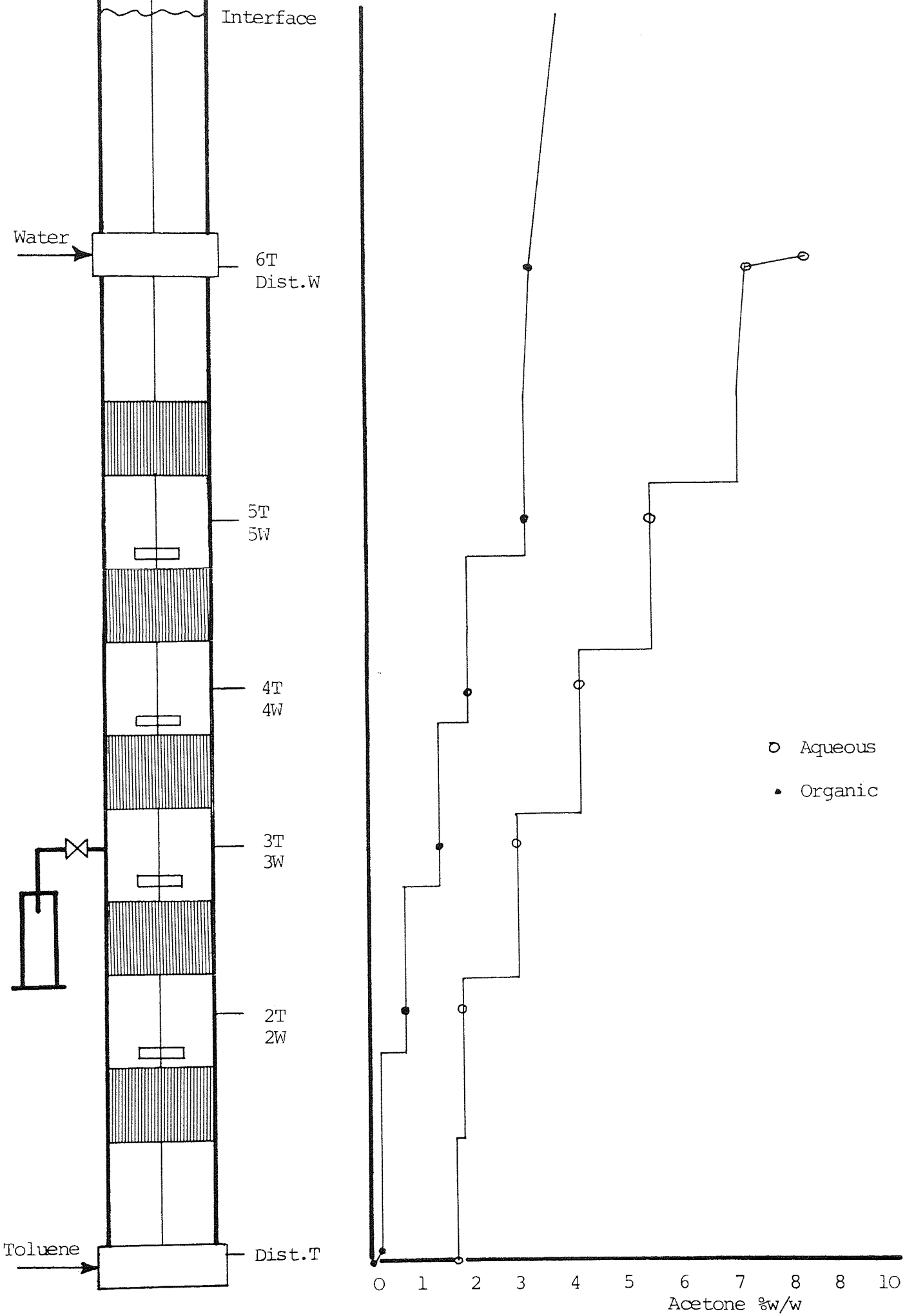

strong influence upon the flooding mechanism. It is suspected that this unknown variable has a random nature and it is closely related to the voidage distribution inside the pad.

The very important practical implications and the consequences that the finding describes above could have over the future commercial applications of the Scheibel column, indicate that the problem requires a more complete and carefully planned investigation in which new variables describing the physical nature of the packing pad must be analysed.

9.3.2 Drop Size

9.3.2.1 Statistical Analysis

The characteristic of this variable or response is that its normally reported value is not a deterministic one but a mean from a distribution curve. This situation has not always been recognised when drop size data were subjected to an analysis of variance. It is better to use all the measured drop diameters instead of the single valued mean drop diameter. That is, if in any particular experiment the drop size is characterized by, say, 100 drops, measured from still photograps, then in the analysis of variance each drop diameter is considered to be a response of a treatment which has been replicated 100 times.

This approach can be criticized on the fact that the tabulated significance levels for the Fisher's test (F-test) used in the analysis of variance is based on the assumption that the observed responses in repeated trials of one treatment are distributed normally with the true response as mean, and variance σ_o^2 (error variance). It is well known that drop sizes distributions in agitated columns in general, departs from normality and more often they are of the log-normal or Mugele-Evans distribution types. Nevertheless, the degree of freedom of the effects is 1, in which case F is equal to t^2 (student t-distribution) and since t is not strongly influenced by departure from normality the above criticism is not important.

The Sauter mean diameters listed in Tables 9.8 to 9.11 are the result of measuring the drop sizes in several photographs taken when possible from all the mixing chambers and these are the values (d_{32}) used in the correlations presented in the next section.

In the following analysis of variance only the individual drop diameters of the pictures taken from the second mixing chamber were considered. Each of the of the runs in the factorial design were characterized by the measurement of the diameters of 100 drops and in those experiments in which more than 100 drops were measured, those in excess of 100 were eliminated randomly using a table of random numbers. This ensures that the design is symmetrical in all the factors and the main effects and interactions can be independently estimated without entanglement (orthogenality).

The calculation of the effects and mean squares was done using the Yates' Method (150). The corresponding ANOVA (analysis of variance) table is presented in Table 9.13. For 1 and infinite degrees of freedom the 5% probability of F is 3.84, so that using the calculated error variance, mean squares greater than 3.84 x 0.623 = 2.39 are significant at the 5% level. It is seen that all effects except AD,BD,CD,ACD and ABCD are highly significant at the 5% level.

The magnitude of the significant effects are;

Main Effects	Agitator Speed (A)	= -0.266
	Pad Height (B)	= -0.179
	Mass Transfer Direction (C)	= -0.742
	Dispersed Phase Superficial Velocity (D)	= 0.179
Two Factor Interaction	A B	= 0.117
	A x C	= -0.104
	B x C	= 0.241
Three Factor Interaction	A x B x C	= -0.198
	A x B x D	= 0.083
	B x C x D	= 0.168

The effects of A,C and D upon drop diameter agrees with observations made during the preliminary runs. The relatively high magnitude of the main effect C; that is drop diameter decrease when the mass transfer direction changes from dispersed → continuous to continuous → dispersed phase, is an indication that this variable is the most

Table 9.13 - Analysis of variance of drop diameter data

Source of variation	Degrees of freedom	Sum Square	Mean Square	F^a
Mean		2871.11		
A	1	28.30	28.30	48.40***
B	1	12.88	12.88	20.60***
C	1	220.55	220.55	354.01***
D	1	12.88	12.28	20.60***
AB	1	5.56	5.56	8.90**
AC	1	4.34	4.34	6.96**
AD	1	0.03	0.03	-
BC	1	23.29	23.29	37.38***
BD	1	0.18	0.18	-
CD	1	1.08	1.08	-
ABC	1	15.71	15.71	25.20***
ABD	1	2.75	2.75	4.42**
ACD	1	0.56	0.56	-
BCD	1	11.42	11.42	18.33***
ABCD	1	0.99	0.99	-
Error	$1584=99x2^4$	987.37	0.623	
Total	$1599=100x2^4-1$	4199.02		

a Fisher test made at 5% significant level, F(1,00)=3.84

*** Highly significant

** Significant

important one in controlling the degree of dispersion and that the selection of the phase (continous or dispersed) can not be done arbitrarily.

The significance of the pad height over the drop diameter was unexpected. The analysis shows that increasing pad height (3 → 6cm) results in a decrease in drop sizes, which is larger when the mass transfer direction is dispersed to continuous phase (two factor interaction B x C > 0). A direct comparison of the data presented in Tables 9.8 to 9.11 reveal that Sauter mean drop diameter and their corresponding standard deviations are lower for the experiments performed in Column 1 (6 cm pad height) than the ones in Column 2 under the same mass transfer direction. Since total coalescence of the dispersed phase inside the pads has been experimentally demonstrated, a possible explanation for the behaviour above could be that for lower pad height their particular voidage distribution allows a portion of the coalesced phase to leave the pads far from the impeller region contributing in this manner with larger drops which increase the mean values as well as the spread of the distribution. Nevertheless, further work must be done to clarify this point.

9.3.2.2 Correlations

The Sauter mean diameter data from the factorial design plus the ones obtained during the preliminary experimentation were correlated using the regression models

$$\frac{d_{32}}{D_I} = K_1 (\Theta_D)^{K_2} (Re_I)^{K_3} (We)^{K_4} \left(\frac{H_P}{H_M}\right)^{K_5} \qquad (9.3)$$

$$d_{32} = K_1 . 10^{(1+K_2 \Theta_D)} . (\bar{\epsilon})^{K_3} (H_P)^{K_4} \qquad (9.4)$$

$$\frac{d_{32}}{D_I} = (K_1 + K_2 \Theta_D)(We)^{K_3} \qquad (9.5)$$

where

$$We = \frac{D_I^{\,3} N^2 \rho_c}{\sigma}$$

$$Re_I = \frac{D_I^{\,2} N \rho_c}{\mu_c}$$

$$\bar{\epsilon} = \frac{4.4 N^3 D_I^{\,5} \rho_c}{\frac{\pi D_c^{\,2}}{4} . H_m . \bar{\rho}}$$

being 4.4 the value of the power number for a fully turbulent flow in a baffled agitated vessel (151). The coefficients and exponents of equation (9.3) and (9.5) were evaluated by linear regressions of the logarithms of the independent variables, that is, a logarithmic fit. For this purpose the ICL Statistical Package X DS-3, available at the University of Aston Computer Centre, was used. Correlations were made with all of the terms included

in the above equations and also with some terms ignored for mass transfer in both directions.

Equation (9.5) could not be linearised, requiring an optimisation method to evaluate the coefficients and exponents. The Gauss-Newton method based on the minimisation of an objective function of the type "sum of squares of residuals" was used. The NAG-E04FDF computer program, available at the Computer Centre of the University of Aston, is an "easy to use" modified version of the Gauss-Newton technique and it was the one used.

Table 9.14 lists the resulting correlations using the basic three regression models mentioned above. The correlations from the linearised models show the exponents with their standard errors. For comparison, the "residual error" or "standard error" defined as

$$r.e. = \sqrt{\frac{\Sigma(\hat{d}_{32}-d_{32})^2}{n_{data}-n_{param}}}$$

n_{data} = number of data points

n_{param} = number of parameters to be estimated

was calculated for each correlation. The lower the value of residual error, the better the correlation.

For mass transfer in each direction, the correlations were improved by discarding H_p (height of packing pad). This is another indication that the influence of this variable on drop size has not been fully established since the above results contradict the conclusion of the

Table 9.14 - Regression Models for d_{32} Correlation

a) Mass transfer direction dispersed→continuous phase

Regression Model	Correlation Coefficient	Residual Error
1) $\frac{d_{32}}{D_I}=(Re)^{0.135\pm0.159}(We)^{-0.506\pm0.179}(\Theta_D)^{0.457\pm0.224}(\frac{H_P}{H_M})^{-0.039\pm0.073}$	0.999	3.859×10^{-4}
2) $\frac{d_{32}}{D_I}=(We)^{-0.351\pm0.050}(\Theta_D)^{0.282\pm0.090}$	0.999	3.733×10^{-4}
3) $\frac{d_{32}}{D_I}=(Re)^{-0.150\pm0.070}(We)^{-0.234\pm0.127}$	0.999	4.363×10^{-4}
4) $\frac{d_{32}}{D_I}=(Re)^{0.112\pm0.142}(We)^{-0.472\pm0.161}(\Theta_D)^{0.433\pm0.212}$	0.999	3.809×10^{-4}
5) $d_{32}=(1.098\times10^{-4}\pm0.436\times10^{-4}).10^{[1+(3.564\pm1.602)\bar{\Theta_D}]}(\bar{\epsilon})^{-0.291\pm0.069}(H_p)^{-0.038\pm0.071}$	1.00	3.715×10^{-4}
6) $d_{32}=(1.240\times10^{-4}\pm0.313\times10^{-4}).10^{[1+(3.407\pm1.516)\bar{\Theta_D}]}(\bar{\epsilon})^{-0.277\pm0.0617}$	1.00	3.673×10^{-4}
7) $d_{32}=(2.10\times10^{-4}\pm0.166\times10^{-4})(\bar{\epsilon})^{-0.206\pm0.0618}$	1.00	4.363×10^{-4}
8) $d_{32}/D_I=(0.304+4.099\Theta_D)(We)^{-0.4}$	-	3.714×10^{-4}

Table 9.14 (continued)

b) Mass Transfer Direction Continuous → Dispersed Phase

	Regression Model	Correlation Coefficient	Residual Error
9)	$\frac{d_{32}}{D_I}=(Re)^{0.271\pm0.281}(We)^{-0.974\pm0.391}(\Theta_D)^{0.422\pm0.328}(\frac{H_P}{H_M})^{-0.105\pm0.110}$	0.999	2.429×10^{-4}
10)	$\frac{d_{32}}{D_I}=(We)^{-0.597\pm0.047}(\Theta_D)^{0.115\pm0.106}$	0.999	2.460×10^{-4}
11)	$d_{32}=(3.809\times10^{-5}\pm2.640\times10^{-5}).10^{[1+(1.895\pm1.453)\Theta_D]}.(\bar{\epsilon})^{(-0.583\pm0.183)}$ $(H_p)^{(-0.113\pm0.112)}$	1.000	2.434×10^{-4}
12)	$d_{32}=(6.197\times10^{-5}\pm3.017\times10^{-5}).10^{[1+(1.216\pm1.291)\Theta_D]}.(\bar{\epsilon})^{-0.500\pm0.163}$	1.000	2.391×10^{-4}
13)	$d_{32}=(8.880\times10^{-5}\pm1.043\times10^{-5})(\bar{\epsilon})^{-0.368\pm0.085}$	1.000	2.610×10^{-4}
14)	$\frac{d_{32}}{D_I}=(1.763+16.117\Theta_D)(We)^{-0.907}$	-	2.26×10^{-4}

analysis of variance (Table 9.13).

The best correlations found were

$$d_{32} = (1.240 \times 10^{-4}).10^{(1+(3.407)\Theta_D)} (\bar{\epsilon})^{-0.277} \quad (9.6)$$

for mass transfer direction dispersed ⟶ continuous phase and

$$\frac{d_{32}}{D_I} = (1.763 + 16.117\,\Theta_D)We^{-0.907} \quad (9.7)$$

for continuous ⟶ dispersed phase. Since equation (9.6) is not a dimensionless correlation, care must be taken to use them with the correct units.

In these correlations, the influence of V_D over d_{32} is implicit, being included in the hold-up factor. The influence of the agitator speed can be isolated from the correlations to give

$d_{32} \propto N^{-0.8}$ Dispersed ⟶ Continuous

$d_{32} \propto N^{-1.8}$ Continuous ⟶ Dispersed

Kolmogoroff's law is not stictly followed in either case ($d_{32} \propto N^{-1.2}$), nevertheless, the exponents of the correlations for mass transfer direction Continuous ⟶ Dispersed phase were found to be in the range 1.2 to 1.8; close to 1.2 required by the above law. The values of d_{32} are in the range 2.2×10^{-3} to 3.8×10^{-3}m for Dispersed ⟶ Continuous and 0.8×10^{-3} to 2.0×10^{-3}m for Continuous ⟶ Dispersed. The integral scale of Turbulence Le, calculated according

to the approximation given by Cutter (55) (30) for the impeller-discharge stream of an agitated, baffled vessel, Le = 0.08 D_I is 2.7×10^{-3}m and the Kolmogoroff's length scale η is in the range 0.05×10^{-3} to 0.03×10^{-3}m. Therefore, the drops for the condition dispersed $\longrightarrow$ continuous phase transfer, are most likely similar in size to the large and medium size eddies for which isotropic turbulence does not exist and consequently, Kolmogoroff's law can not be applied, as has been shown numerically. Less deviation from Kolmogoroff's law is expected when mass transfer is in the opposite direction since the sizes of the drops are around the upper limit of the domain G of isotropic and homogeneous turbulence.

9.3.3 Hold-up

9.3.3.1 Statistical Analysis

Hold-up data from the factorial experiment were subject to an analysis of variance with the effects and interactions calculated using Yates' technique.

Table 9.15 shows the ANOVA table. An estimate of the experimental error variance is required by which the significance of the effects and interactions may be judged. There was insufficient background information, especially from the preliminary investigation, to provide a reliable external estimate and a true internal estimate from the experiment itself, as was done in the drop size analysis , was not possible since only a single replication of the experiment was carried out. Since the higher

Table 9.15 - Analysis of variance of hold-up data

Source of Variation	Degrees of Freedom	Mean Squares	F
A	1	47.680	95.58***
B	1	0.366	0.733
C	1	129.846	260.30***
D	1	33.698	67.54***
AB	1	0.308	0.617
AC	1	25.452	51.02***
AD	1	0.297	0.59
BC	1	1.311	2.62
BD	1	1.550	3.10
CD	1	1.311	2.62
ABC, ABD, ACD, BCD, ABCD (Error)	1, 1, 1, 1, 1 = 5	0.632, 0.648, 0.011, 0.648, 0.555	$= \frac{2.494}{5} = 0.498$

F(1,5) = 6.61 at 5% level

F(1,5) = 16.30 at 1% level

*** Highly significant

interactions are small, it was thought unlikely that they would be significant and it was decided to combine the three and four-factor interactions to give an estimate of the error variance. In order to have an experimental confirmation of the validity of this step a test based on the Bartlett's criterion (15) was performed.

The Bartlett's criterion is a test for the equality of several variances. When this hypothesis is shown to be true, the compared variances are in fact estimates of the same variance and may therefore be used as an estimate of error. Since this test was used in the rest of the data analysis in this chapter, a detailed presentation is considered appropriate.

Consider the variances $\sigma_1^2, \sigma_2^2, \ldots \sigma_k^2$ based on $\phi_1, \phi_2, \ldots \phi_k$ degrees of freedom. The criterion for measuring the divergence in the variance is based on the value of a random variable M defined by

$$M = \phi \ln \sigma^2 - \sum_{i=1}^{k} \phi_i \ln \sigma_i^2 \qquad (9.8)$$

where ϕ is the total number of degrees of freedom and σ^2 is the average variance defined as

$$\sigma^2 = \frac{\sum_{i=1}^{k} \phi_i \sigma_i^2}{\phi} \qquad (9.9)$$

When the variances differ greatly the value of M is large and is equal to zero when all the variances are equal.

In our case,

$$M = 5 \times \ell n\ 0.498 - \ell n(0.632 \times 0.648 \times 0.011 \times 01648 \times 0.555)$$

$$M = 2.576$$

From the table of significance points of M when each variance has a single degree of freedom, given by Nair (150), it is seen that a value of 12.0 is required for significance at the 5% level. Since the value obtained here is lower there is no evidence of heterogenity and the procedure to estimate the error variance is adequate.

The results of the application of the Yates' method produces the following magnitude and sign of the significant effects

Main Effect	Agitator Speed (A)	=	3.45
	Mass Transfer Direction (C)	=	5.69
	Dispersed Phase Superficial Velocity (D)	=	2.90
Two Factor Interaction	AC	=	2.52

Table 9.15 shows that all factors, except pad height are significant with positive effects on the response; that is hold-up increases when the level of the factor increases. The relatively large interaction Agitator Speedx Mass Transfer Direction indicates that the positive effect of Agitator Speed on hold-up is greater at the mass transfer direction continuous $\longrightarrow$ dispersed phase. This strongly suggests that when hold-up data

are correlated, a factor must be included to represent the effect of the direction of transfer or correlations for each direction be obtained.

9.3.4 Stagewise Model Parameter Estimates

9.3.4.1 Compartments with Backflow Model - Fitting Results

The interpretation of the sixteen concentration profiles was carried out in terms of the 5-stage with backflow model schematically presented in Figure 9.15 The three parameter model (Formulation 4) was fitted to the profiles, using the Marquardt's algorithm (Appendix 4) to minimise the sum squares of the residual objective function.

Table 9.16 to 9.24 present the results of the computations. The solute concentrations are expressed in weight fractions on a solute free base (y and x) and the values between the brackets are the resulting concentration fitted.

In Runs 8 and 14 the computations very slowly approached toward the minimum and in both cases, convergence was not achieved. This was due to the fact that one of the parameters (e) of the solution vector lies outside the boundaries of the constraints given by

$$-0.01 \leq \begin{bmatrix} \eta \\ r \\ e \end{bmatrix} \leq 10$$

Figure 9.15 - 5 stages model with backflow

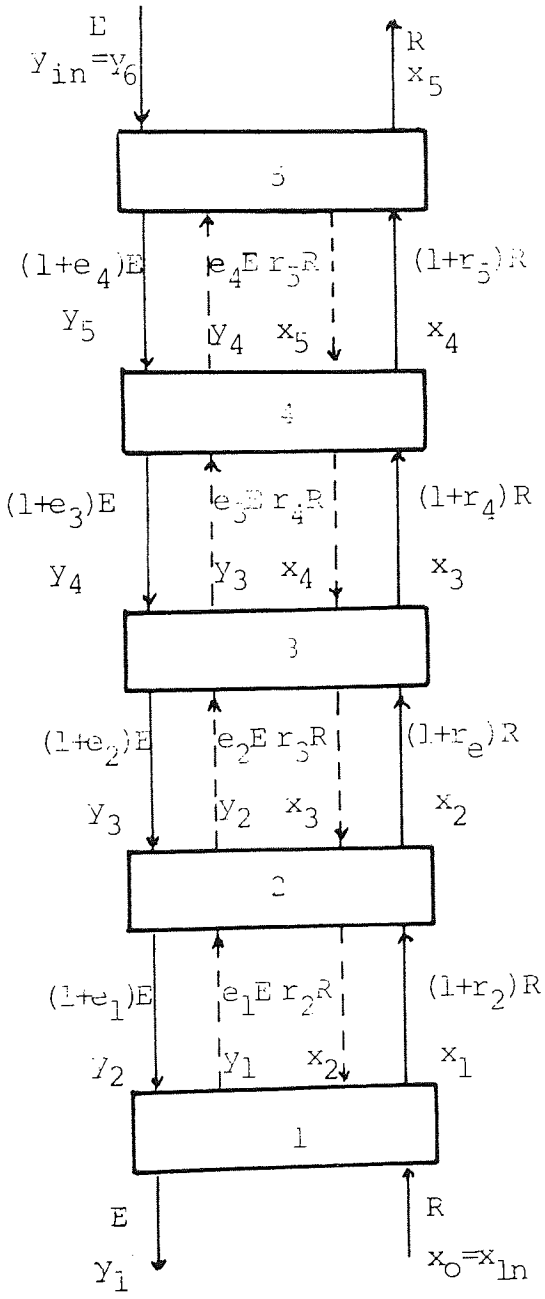

Table 9.16 - Runs 1 and 2

	Run 1		Run 2	
K	x_k	y_k	x_k	y_k
0	x_{in}=0.828		x_{in}=0.0782	
1	0.0700	0.0499	0.0577	0.0562
	(0.650)	(0.0528)	(0.0572)	(0.0577)
2	0.0540	0.0436	0.0483	0.0473
	(0.531)	(0.0423)	(0.0441)	(0.0478)
3	0.0331	0.0301	0.0298	0.0389
	(0.0423)	(0.0308)	(0.0333)	(0.0362)
4	0.0310	0.0146	0.0201	0.0258
	(0.0328)	(0.0202)	(0.0238)	(0.0252)
5	0.0292	0.0136	0.0182	0.0140
	(0.0261)	(0.0100)	(0.0167)	(0.0151)
		y_{in}=0.0		y_{in}=0.00
- Solution vector:		η=0.393 r=0.485 e=0.075	- Solution vector:	η=0.606 r=0.289 e=0.68
Number of iterations = 10			Number of iterations = 14	
$(S.S.R.)_{opt}$ = 0.17x10^{-3}			$(S.S.R.)_{opt}$ = 0.574x10^{-4}	

Table 9.17 - Runs 3 and 4

	Run 3		Run 4	
K	x_k	y_k	x_k	y_k
0	x_{in} = 0.0848		x_{in}=0.0820	
1	0.0708	0.0741	0.0735	0.0794
	(0.0697)	(0.0738)	(0.0719)	(0.0810)
2	0.0606	0.0666	0.0650	0.0726
	(0.0614)	(0.0666)	(0.0629)	(0.0726)
3	0.0527	0.0530	0.0531	0.0629
	(0.0531)	(0.0555)	(0.0537)	(0.0608)
4	0.0424	0.0414	0.0417	0.0482
	(0.0451)	(0.0425)	(0.0436)	(0.0472)
5	0.0394	0.0291	0.0342	0.0311
	(0.0396)	(0.0271)	(0.0333)	(0.0319)
		y_{in}=0.00		y_{in}=0.00
- Solution vector:		η=0.412 r=0.969 e=0.605	- Solution vector:	η=0.626 r=0.017 e=0.946
Number of iterations = 10			Number of iterations = 13	
$(S.S.R.)_{opt}$=0.208x10^{-4}			$(S.S.R.)_{opt}$=0.203x10^{-4}	

Table 9.18 - Runs 5 and 6

	Run 5		Run 6	
K	x_K	y_k	x_k	y_k
0	x_{in} = 0.0951		x_{in} = 0.0830	
1	0.0775 (0.0758)	0.0513 (0.0518)	0.0678 (0.0659)	0.0455 (0.0471)
2	0.0653 (0.0652)	0.0437 (0.0448)	0.0554 (0.0561)	0.0402 (0.0397)
3	0.0521 (0.0546)	0.0352 (0.0363)	0.0431 (0.0461)	0.0318 (0.0317)
4	0.0420 (0.0441)	0.0276 (0.0272)	0.0308 (0.0360)	0.0227 (0.0233)
5	0.0364 (0.0358)	0.0178 (0.0171)	0.0291 (0.0271)	0.0140 (0.0142)
		y_{in}=0.001		y_{in}=0.000
- Solution vector:		η=0.655 r=0.823 e=0.290	- Solution vector:	η=0.801 r=0.775 e=0.091
Number of iterations = 8			Number of interations = 42	
- $(S.S.R.)_{opt}$		=0.175x10^{-4}	- $(S.S.R.)_{opt}$	=0.482x10^{-4}

Table 9.19 - Runs 7 and 8

	Run 7		Run 8	
K	x_k	y_k	x_k	y_k
0	x_{in} = 0.0893		x_{in} = 0.0857	
1	0.0624 (0.0625)	0.0381 (0.0381)	0.0575 (0.0566)	0.0423 (0.0441)
2	0.0495 (0.0493)	0.0307 (0.0316)	0.0426 (0.0431)	0.0368 (0.0329)
3	0.0392 (0.0386)	0.0235 (0.0241)	0.0298 (0.0319)	0.0254 (0.0237)
4	0.0283 (0.0295)	0.0171 (0.0171)	0.0196 (0.0225)	0.0173 0.0161)
5	0.0233 (0.0231)	0.0115 (0.0107)	0.0172 (0.0142)	0.0084 (0.0099)
		y_{in}=0.000		y_{in}=0.010
- Solution vector:		η=0.633 r=0.621 e=0.613	- Solution vector:	η=1.085 r=0.798 e=0.010
- Number of iteration = 7			Number of iteration = no convergence	
- $(S.S.R.)_{opt}$=0.367x10^{-5}			- (S.S.R.) = 0.479x10^{-4}	

Table 9.20 - Runs 9 and 10

	Run 9		Run 10	
K	x_k	y_k	x_k	y_k
0	x_{in} = 0.0887		x_{in} = 0.0867	
1	0.0631 (0.0609)	0.0530 (0.0542)	0.0619 (0.0605)	0.0623 (0.0652)
2	0.0467 (0.0505)	0.0482 (0.0443)	0.0455 (0.0460)	0.0591 (0.0525)
3	0.0390 (0.0412)	0.0332 (0.0334)	0.0318 (0.0338)	0.0394 (0.0388)
4	0.0349 (0.0335)	0.0191 (0.0228)	0.0207 (0.0234)	0.0258 (0.0264)
5	0.0299 (0.0286)	0.0103 (0.0117)	0.0187 (0.0157)	0.0125 (0.0151)
		y_{in}=0.000		y_{in}=0.000
- Solution vector:		η=0.379 r=1.569 e=0.050	- Solution vector:	η=0.682 r=0.439 e=0.441
- Number of iterations = 19			- Number of iteration = 32	
- $(S.S.R.)_{opt}$=0.607x10^{-4}			- $(S.S.R.)_{opt}$=0.810x10^{-4}	

Table 9.21 - Runs 11 and 12

K	Run 11 x_k	Run 11 y_k	Run 12 x_k	Run 12 y_k
	x_{in} = 0.0959		x_{in} = 0.0922	
1	0.0841 (0.0800)	0.0793 (0.0828)	0.0786 (0.0786)	0.0839 (0.0878)
2	0.0683 (0.0700)	0.0753 (0.0719)	0.0678 (0.0681)	0.0794 (0.0755)
3	0.0554 (0.0597)	0.0600 (0.0576)	0.0573 (0.0569)	0.0638 (0.0604)
4	0.0486 (0.0485)	0.0447 (0.0418)	0.0428 (0.0452)	0.0483 (0.0437)
5	0.0442 (0.0418)	0.0167 (0.0237)	0.0377 (0.0351)	0.0157 (0.0248)
		y_{in}=0.000		y_{in}=0.000
- Solution vector:		η=0.451 r=0.730 e=0.199	- Solution vector:	η=0.593 r=0.446 e=0.125
- Number of iterations = 28			- Number of iterations = 24	
- $(S.S.R.)_{opt}$=0.131x10^{-3}			- $(S.S.R.)_{opt}$=0.160x10^{-3}	

Table 9.22 - Runs 13 and 14

K	Run 13 x_k	Run 13 y_k	Run 14 x_k	Run 14 y_k
0	x_{in} = 0.0942		x_{in} = 0.0920	
1	0.0755 (0.0760)	0.0493 (0.0496)	0.0744 (0.0729)	0.0497 (0.0508)
2	0.0683 (0.0657)	0.0389 (0.0424)	0.0620 (0.0626)	0.0405 (0.0426)
3	0.0547 (0.0551)	0.0349 (0.0336)	0.0497 (0.0519)	0.0315 (0.0339)
4	0.0414 (0.0449)	0.0243 (0.0244)	0.0330 (0.0414)	0.0244 (0.0248)
5	0.0373 (0.0370)	0.0151 (0.0140)	0.0338 (0.0325)	0.0146 (0.0145)
		y_{in}=0.000		y_{in}=0.000
- Solution vector:		η=0.574 r=0.827 e=0.143	- Solution vector:	η=0.713 r=0.922 e=0.01
- Number of iterations = 16			- Number of iterations = no convergence	
- $(S.S.R.)_{opt}$		$=0.350x10^{-4}$	- $(S.S.R.)_{opt}$	$=0.910x10^{-4}$

Table 9.23 - Runs 15 and 16

	Run 15		Run 16	
K	x_k	Y_k	x_k	Y_k
0	x_{in}=0.0904		x_{in}=0.0934	
1	0.0596 (0.0602)	0.0336 (0.0337)	0.0584 (0.0578)	0.0391 (0.0405)
2	0.0488 (0.0483)	0.0288 (0.0277)	0.0424 (0.0425)	0.0321 (0.0299)
3	0.0394 (0.0384)	0.0210 (0.0210)	0.0295 (0.0308)	0.0210 (0.0209)
4	0.0290 (0.0304)	0.0144 (0.0149)	0.0187 0.0217)	0.0145 (0.0138)
5	0.0257 (0.0254)	0.0088 (0.0091)	0.0177 (0.0149)	0.0077 (0.0082)
		Y_{in}=0.001		Y_{in}=0.001
- Solution vector:		η=0.494 r=1.251 e=0.229	- Solution vector:	η=0.896 r=0.455 e=0.358
- Number of iterations = 9			- Number of iterations = 25	
- $(S.S.R.)_{opt}$=0.446x10^{-5}			- $(S.S.R.)_{opt}$=0.264x10^{-4}	

Table 9.24 - Runs 10 and 14

	Replicated Run 10		Replicated Run 14	
K	x_k	y_k	x_k	y_k
0	x_{in}=0.0938		x_{in}=0.0928	
1	0.0649 (0.0643)	0.0718 (0.0747)	0.0744 (0.0744)	0.0546 (0.0559)
2	0.0493 (0.0495)	0.0688 (0.0605)	0.0624 (0.0640)	0.0499 (0.0476)
3	0.0344 (0.0369)	0.0478 (0.0456)	0.0477 (0.0530)	0.0393 (0.0388)
4	0.0234 (0.0258)	0.0311 (0.0319)	0.0334 (0.0415)	0.0285 (0.0295)
5	0.0198 (0.0170)	0.0168 (0.0194)	0.0314 (0.0300)	0.0179 (0.0192)
		y_{in}=0.000		y_{in}=0.000
- Solution vector:		η=0.785 r=0.465 e=0.557	- Solution vector:	η=0.934 r=0.900 e=0.029
- Number of iterations = 10			- Number of iterations = 14	
- $(S.S.R.)_{opt}$=0.109x10^{-3}			- $(S.S.R.)_{opt}$=0.106x10^{-3}	

specifically $e_{opt.} < -0.01$. The results from replicated run 14 confirms the above explanation. Experimental and model errors, plus the proximity of the solution vector to the origen can lead to a negative value of the backflow parameter. In the following analysis of variance the parameters with negative values were considered to have zero values since negative ones do not have any physical meaning in the model under study.

The sum squares of the residuals at the optimum $(SSR)_{opt.}$, serves as an internal criterion to compare the fitting of the model to the various experimental profiles. The following Figures 9.16 to 9.31 help to visualize the goodness of fit of the model. It is seen that overall the model describes the behaviour of the column quite well.

The results from Run 8 show a stage efficiency slightly greater than one. To conclude that a significant amount of mass transfer took place inside the pads is not justifiable since it is seen from the result of the extract phase backflow parameter ($e < 0$) that an error greater than the average contaminates the profile and it could be responsible for the large value of η. Nevertheless, a statistical analysis of the stage efficiency will clarify the point.

Table 9.25 summarizes the results of the factorial experiment. The column labelled M.B.C. gives the material balance closure percentage error.

Figure 9.16 - Run 1

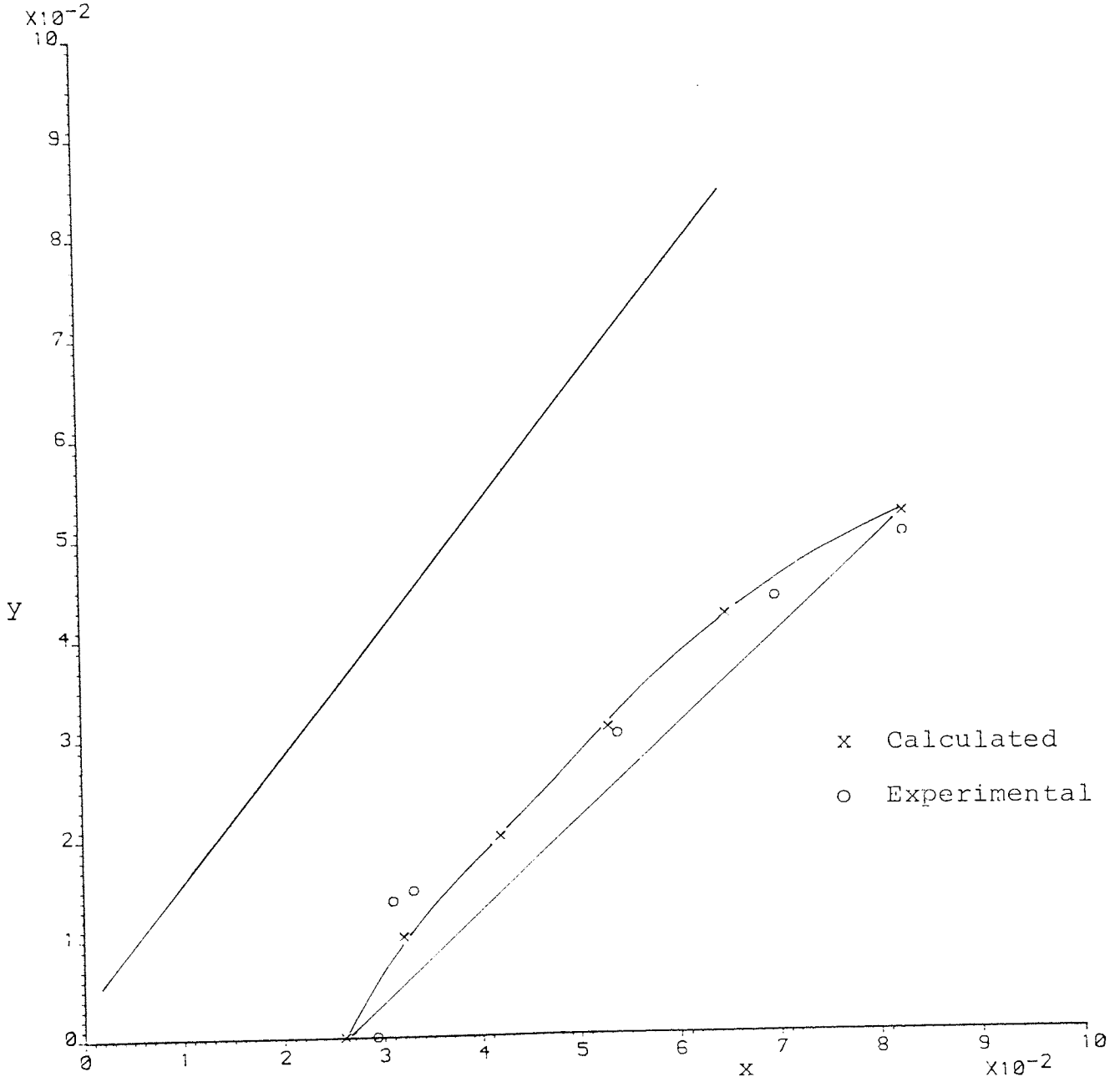

Figure 9.17 - Run 2

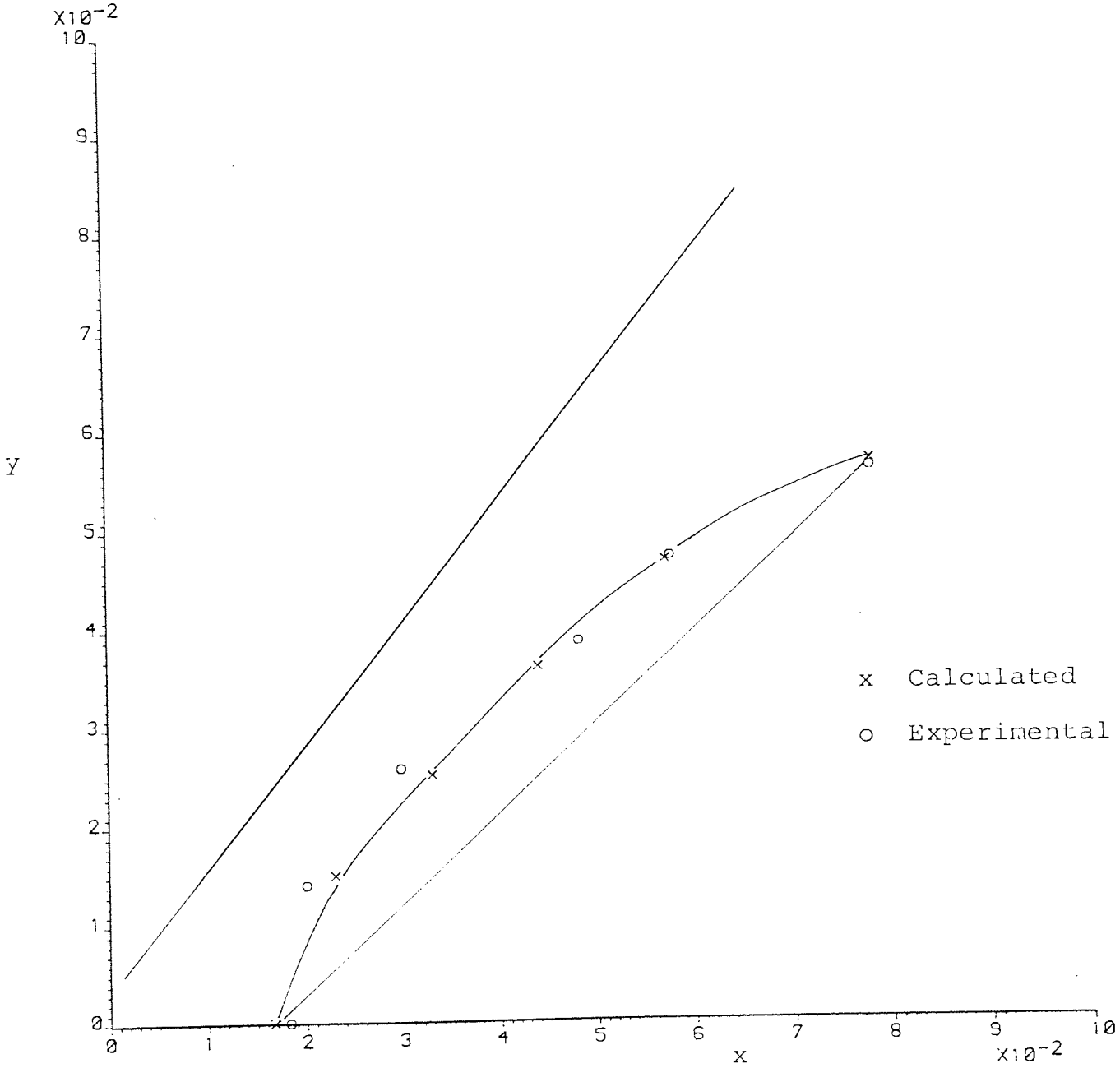

Figure 9.18 - Run 3

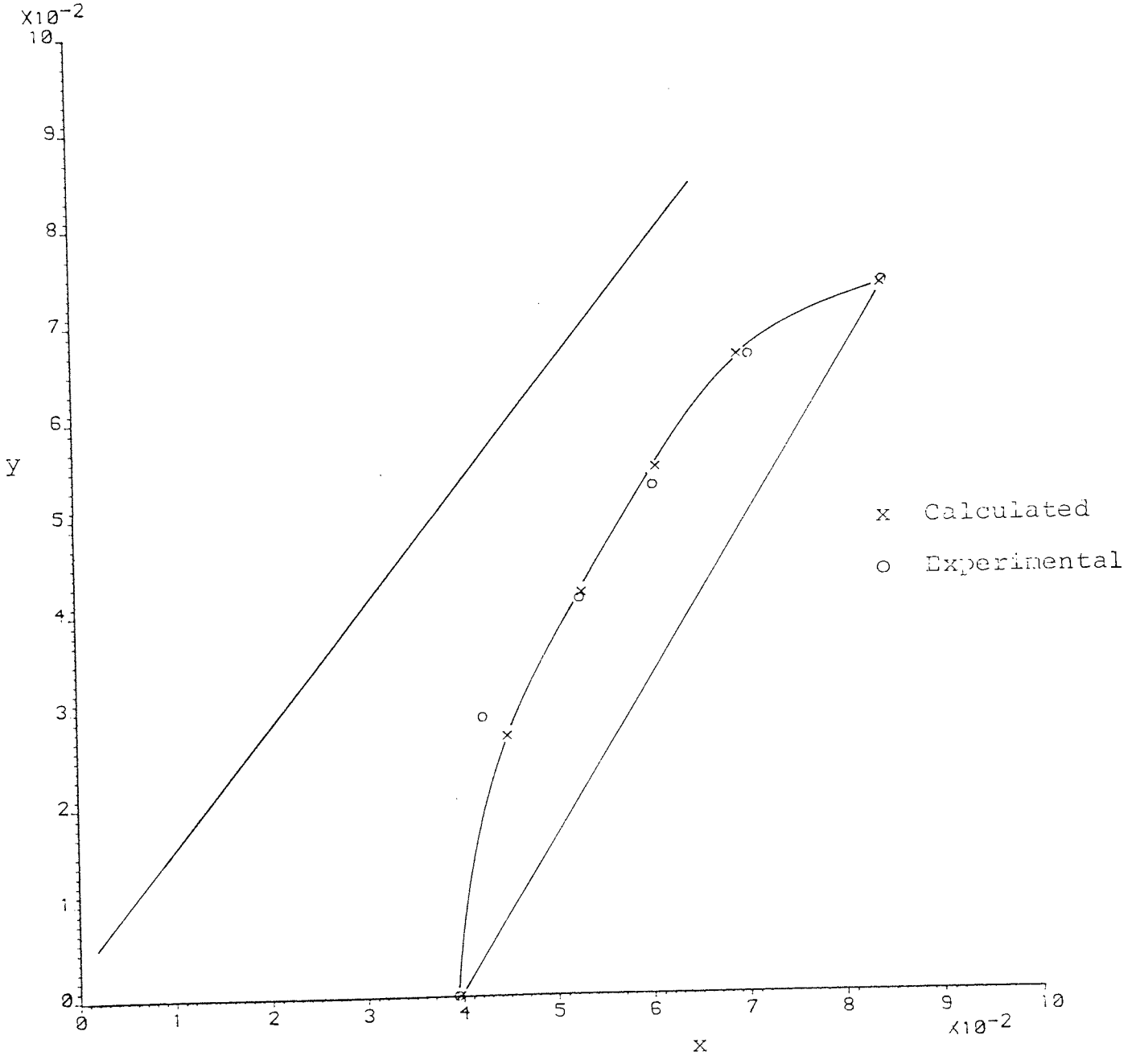

Figure 9.19 - Run 4

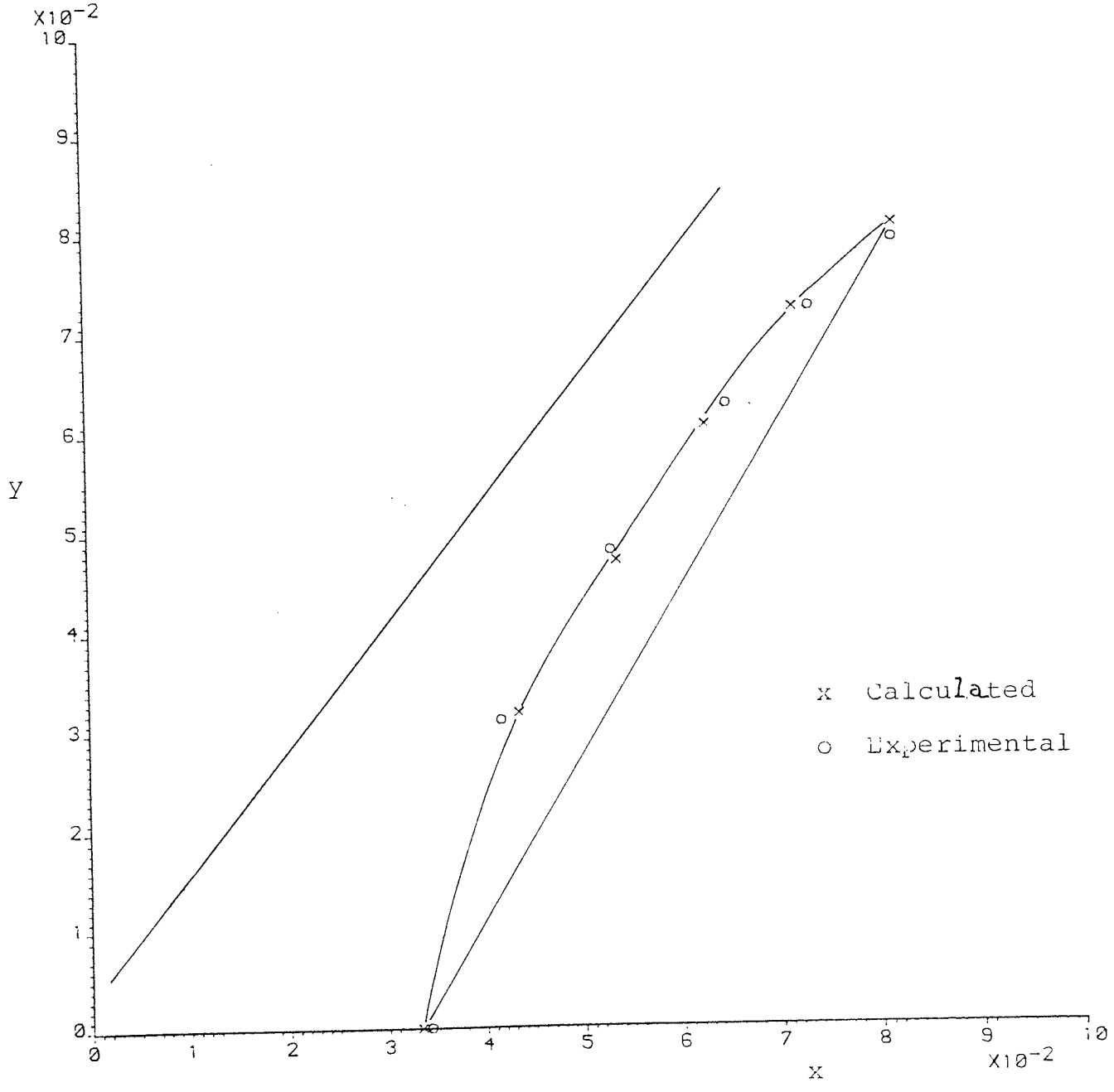

Figure 9.20 - Run 5

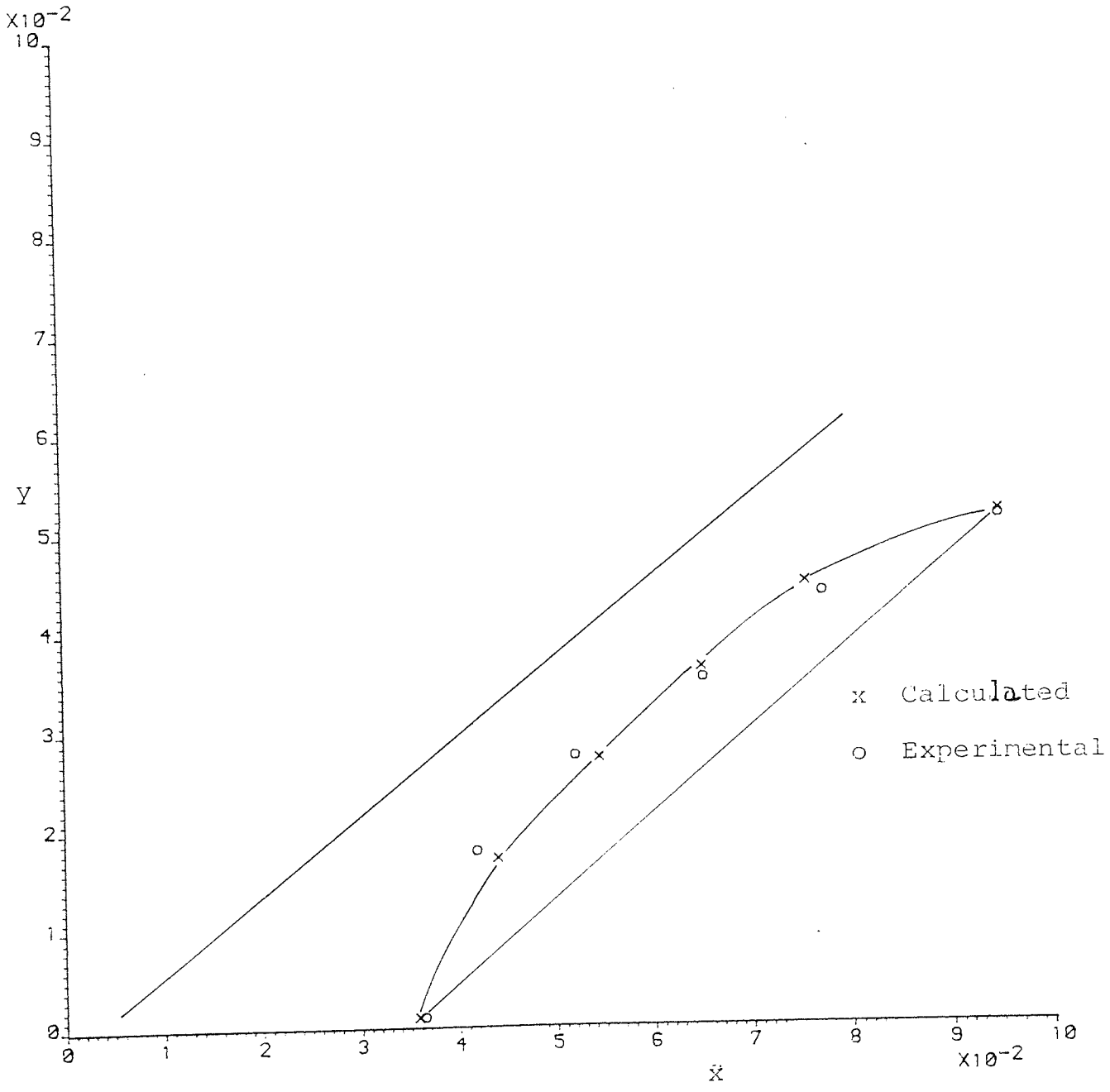

Figure 9.21 - Run 6

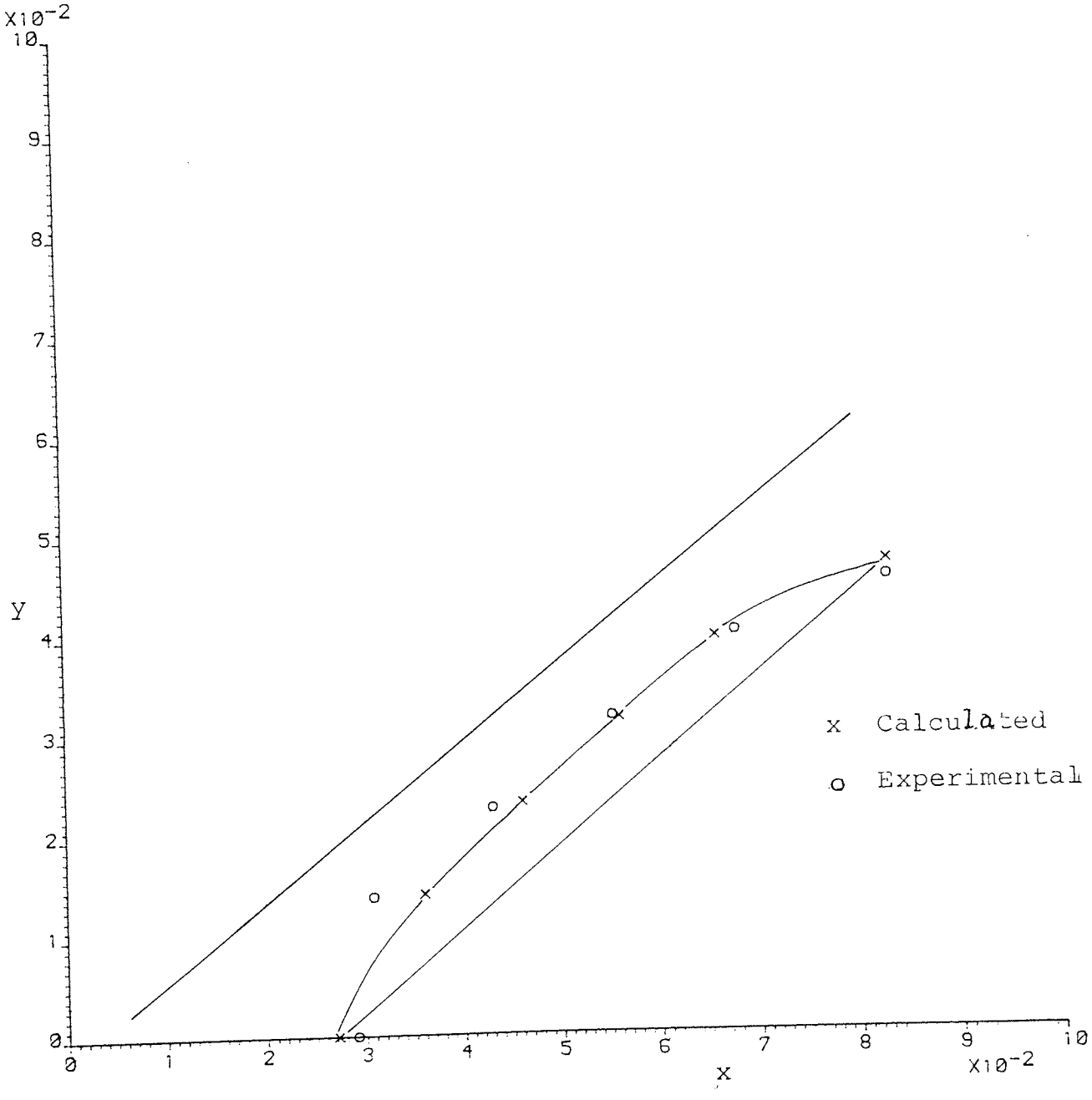

Figure 9.22 - Run 7

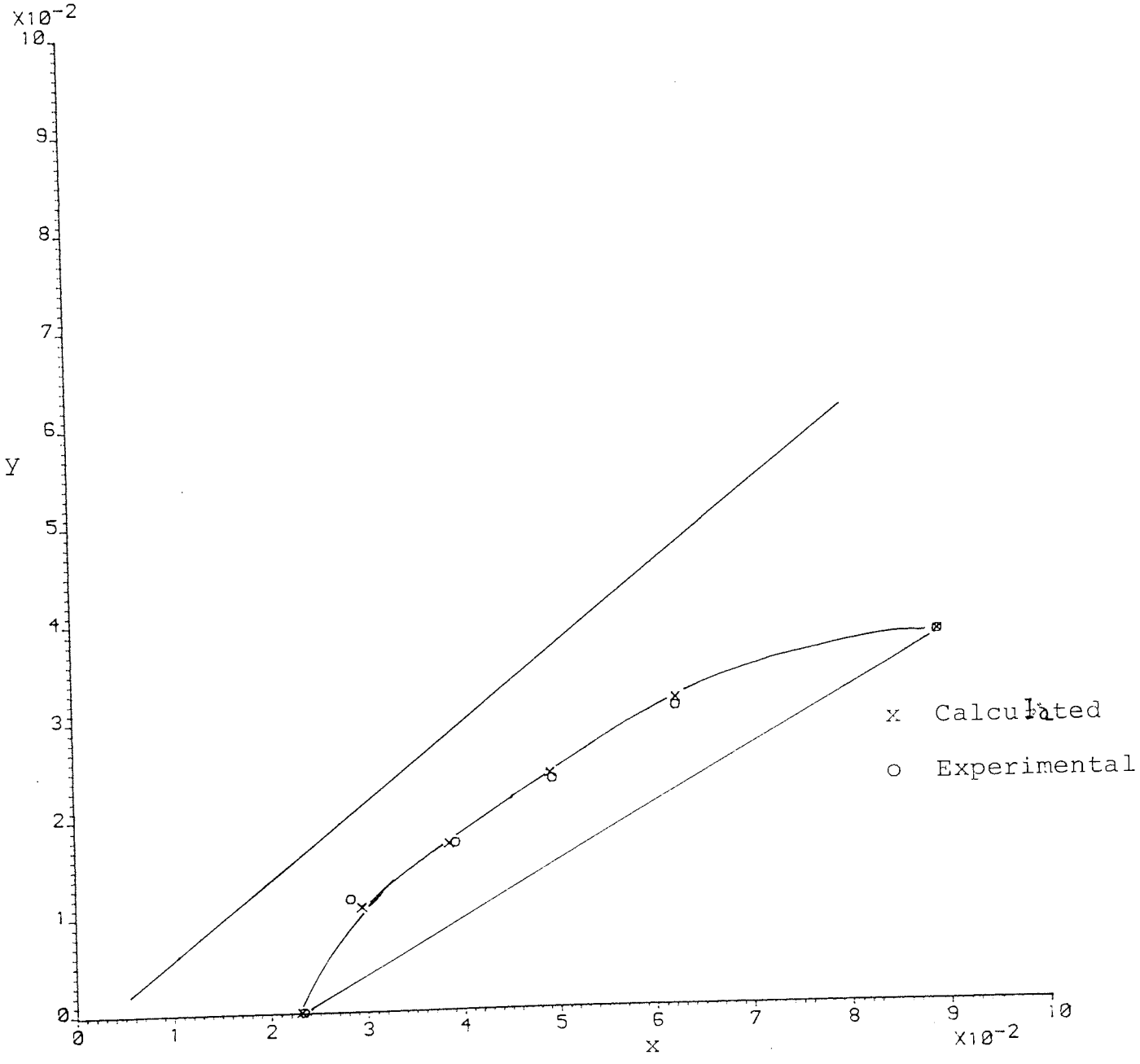

Figure 9.23 - Run 8

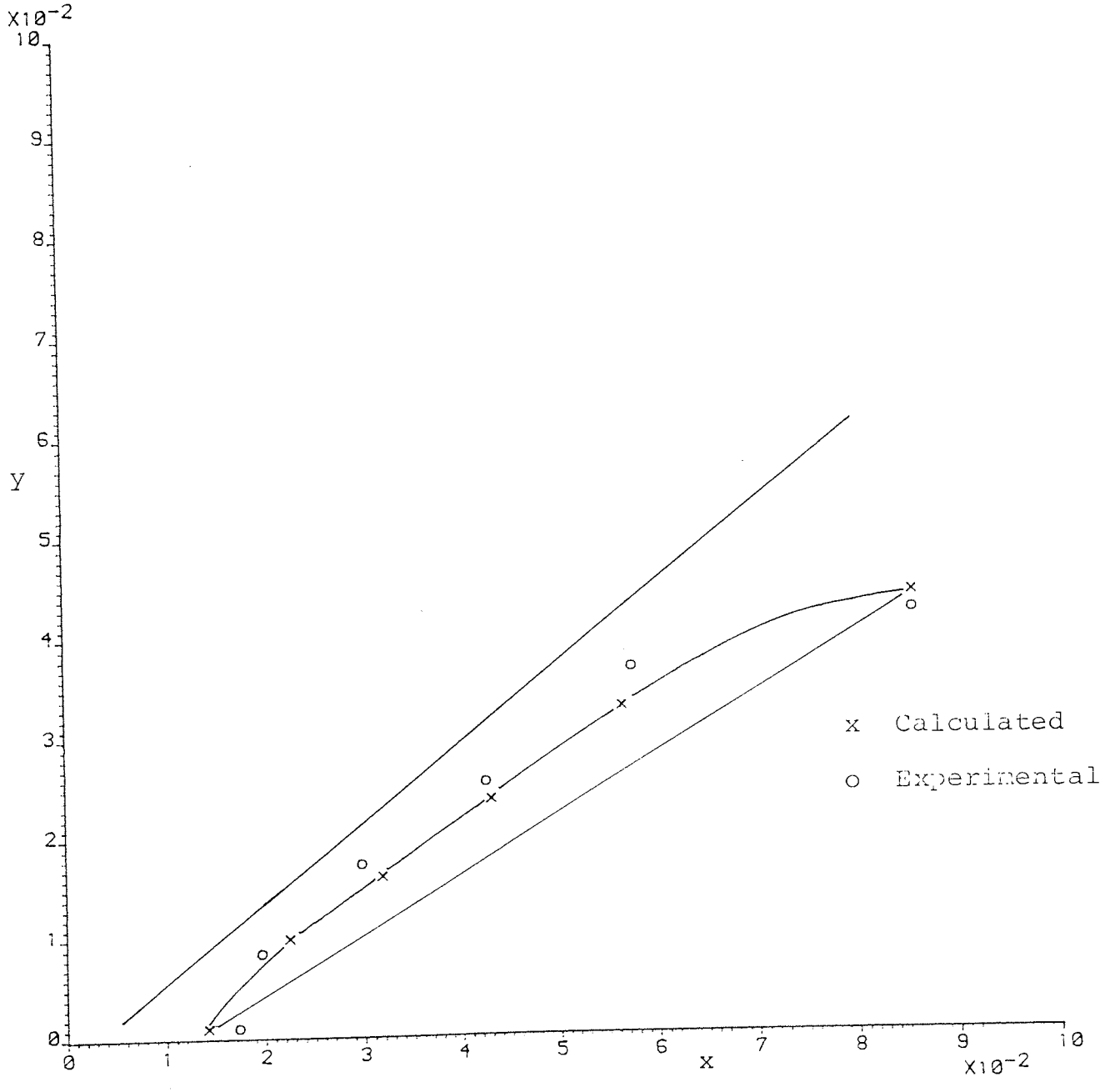

Figure 9.24 - Run 9

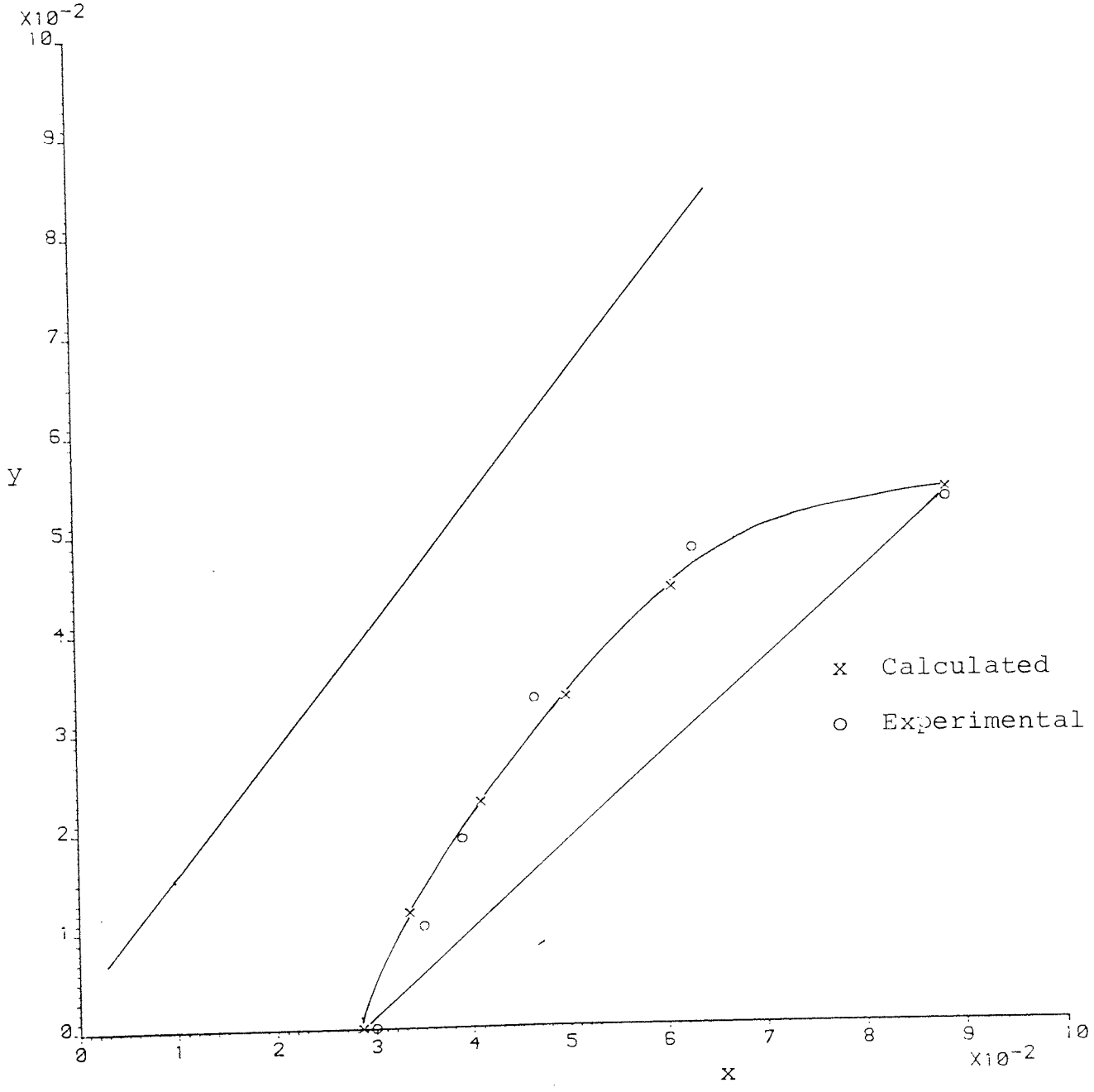

Figure 9.25 - Run 10

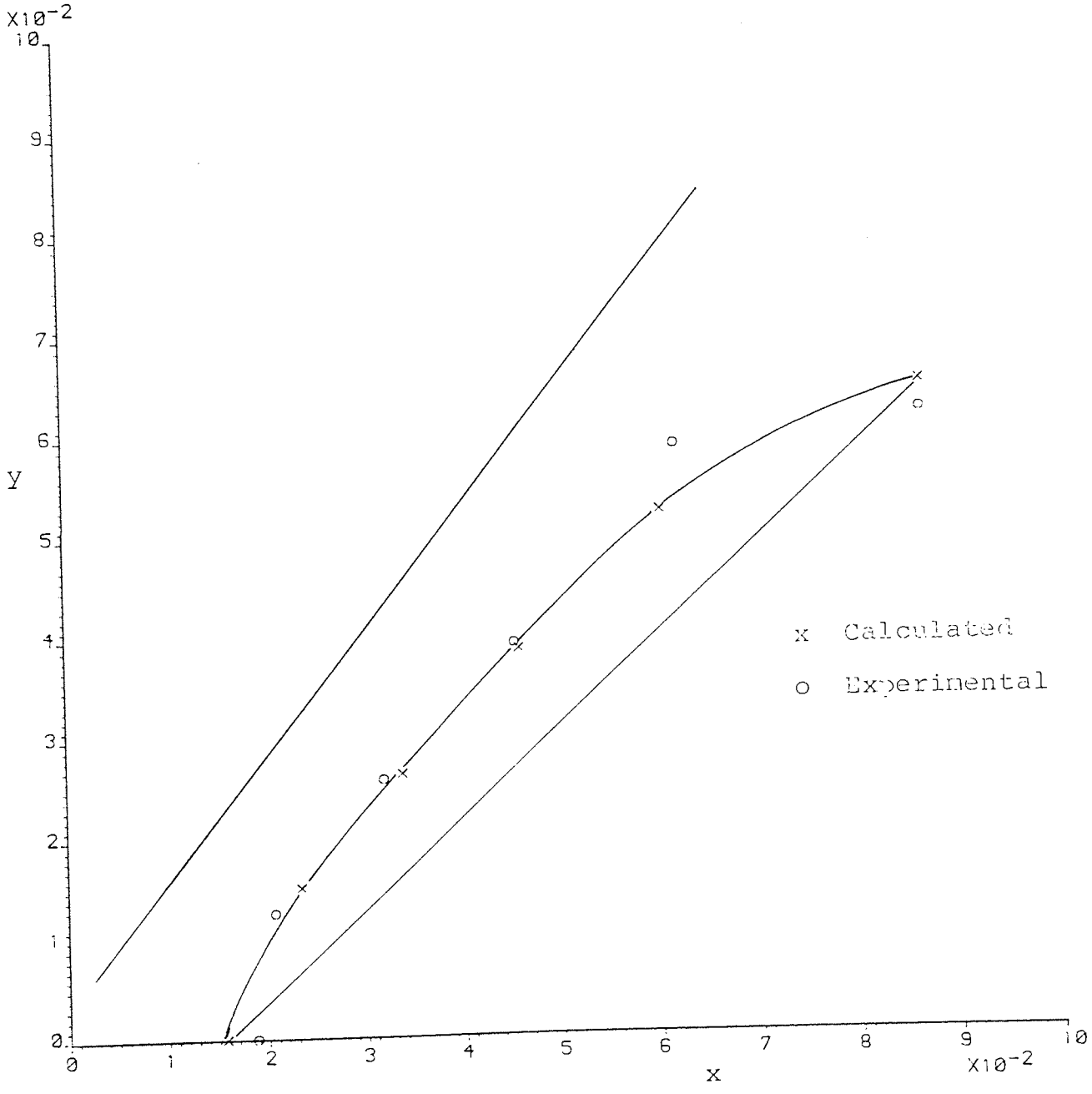

Figure 9.26 - Run 11

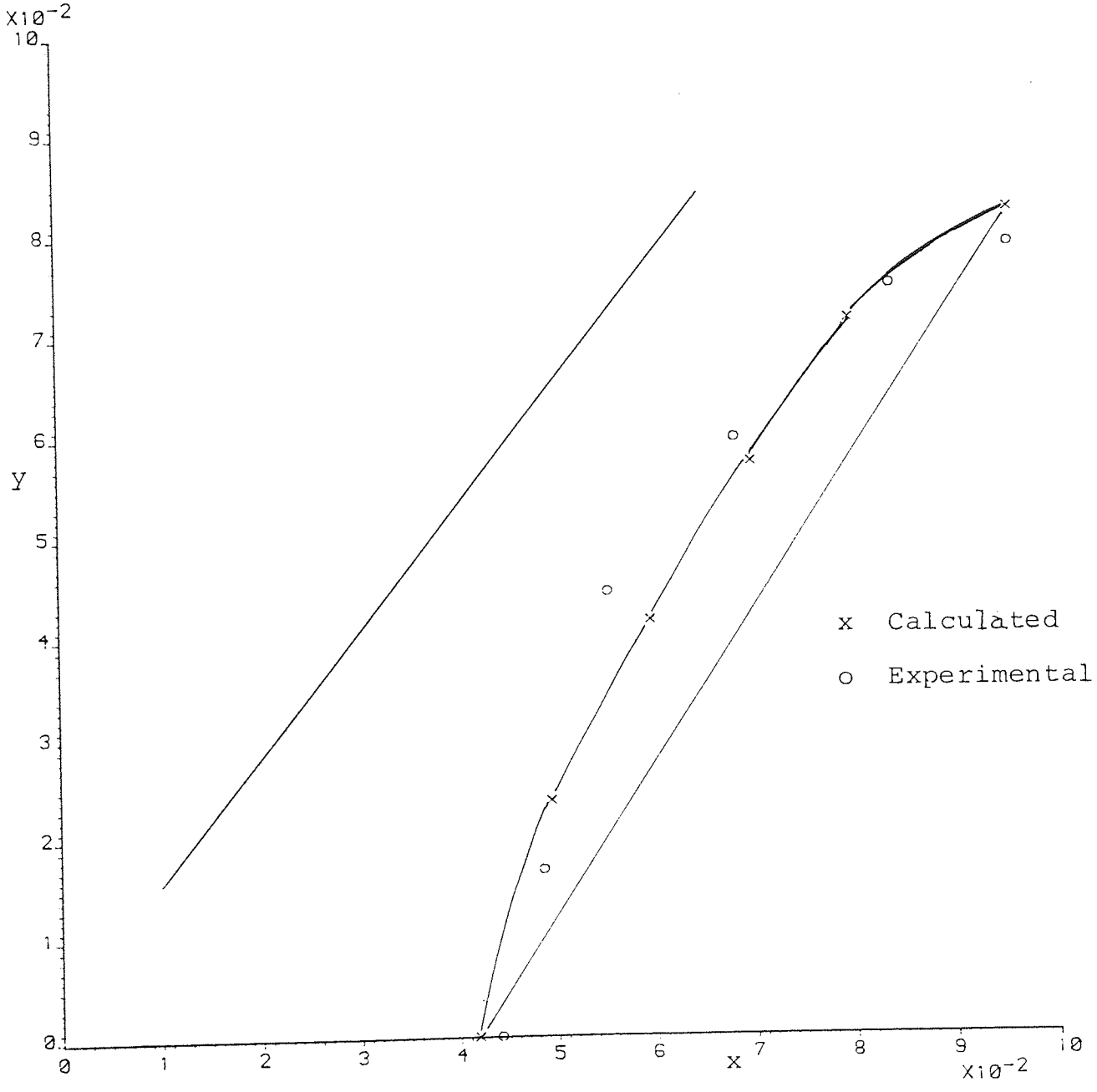

Figure 9.27 - Run 12

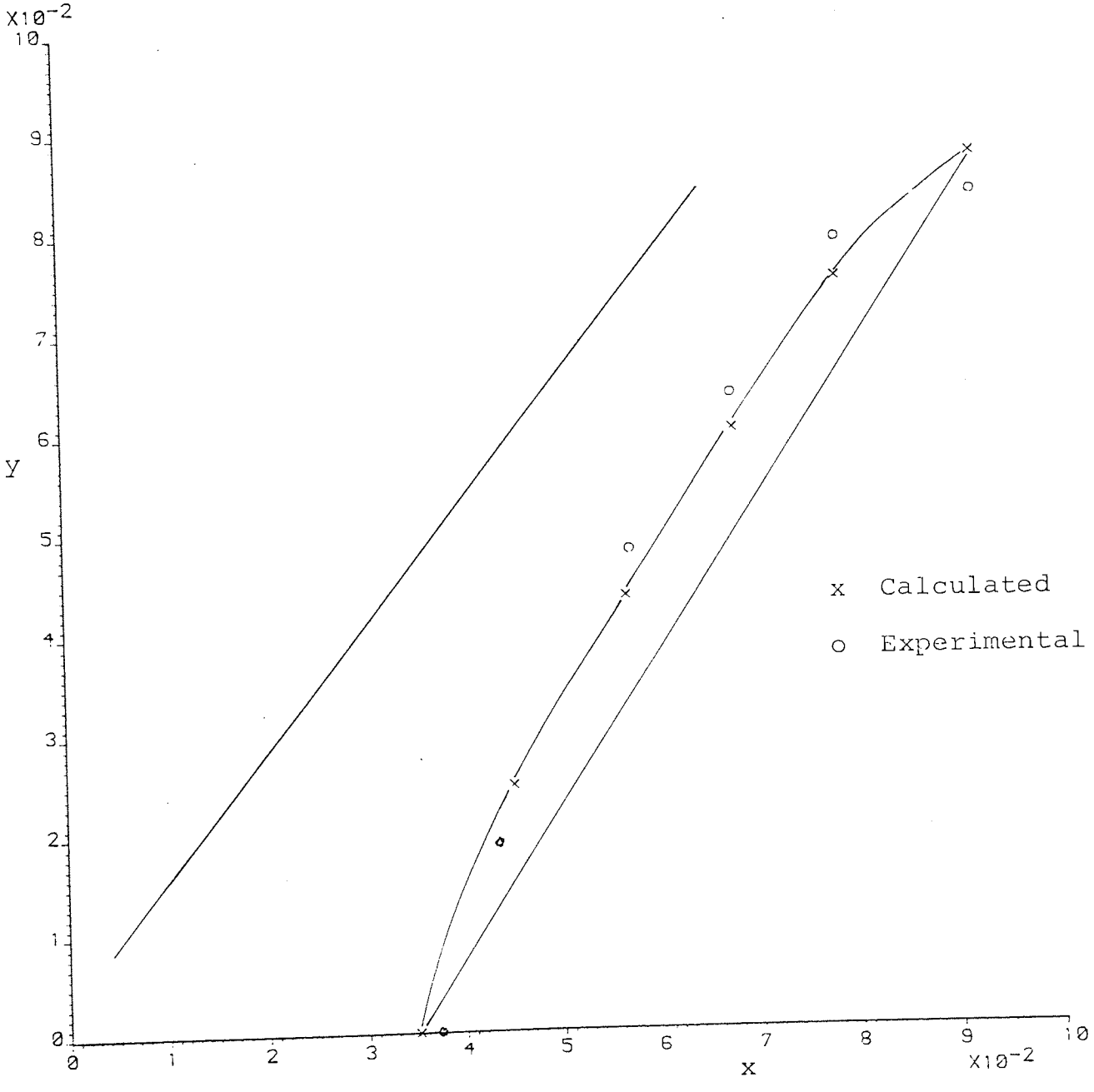

Figure 9.28 - Run 13

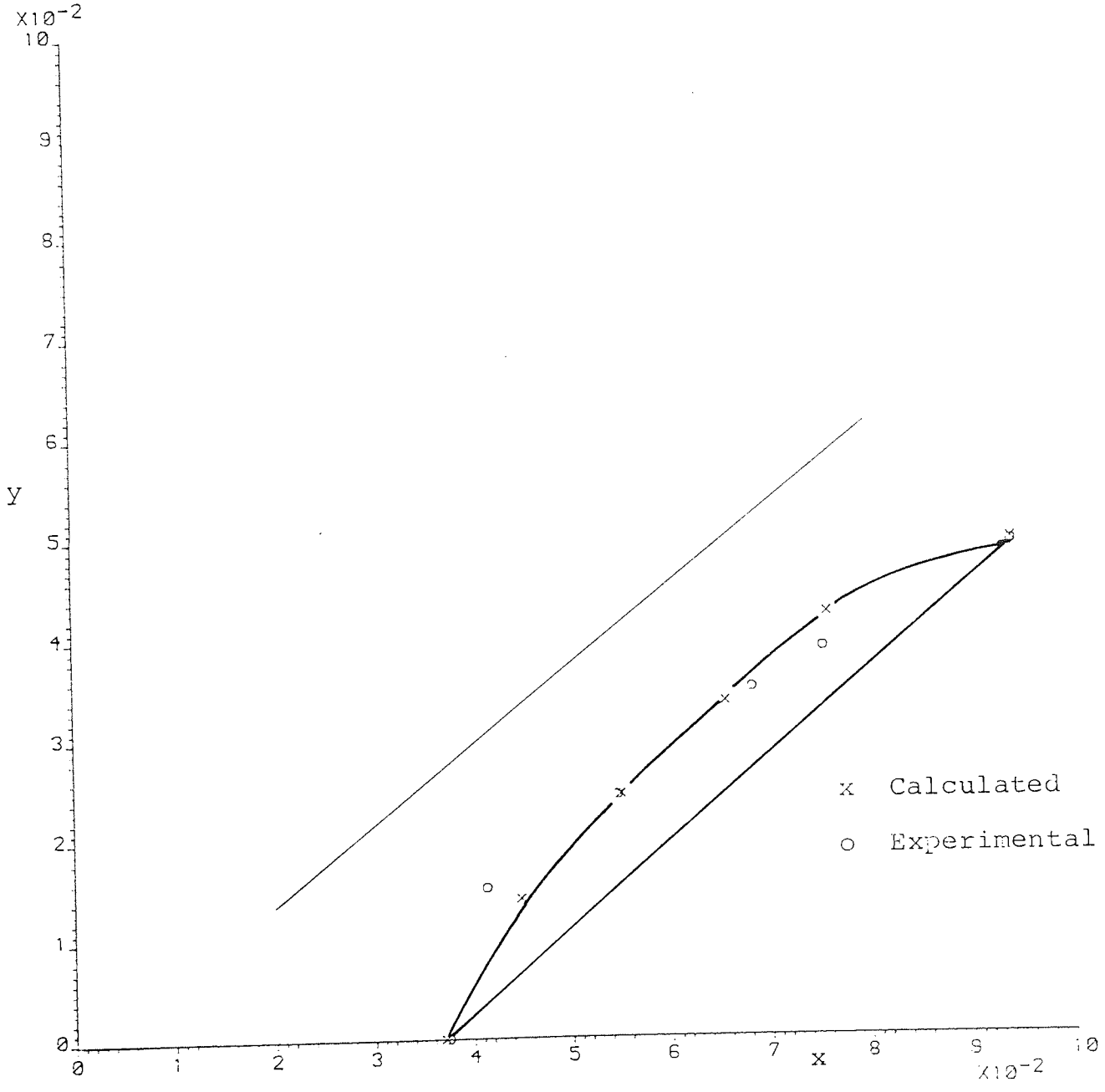

Figure 9.29 - Run 14

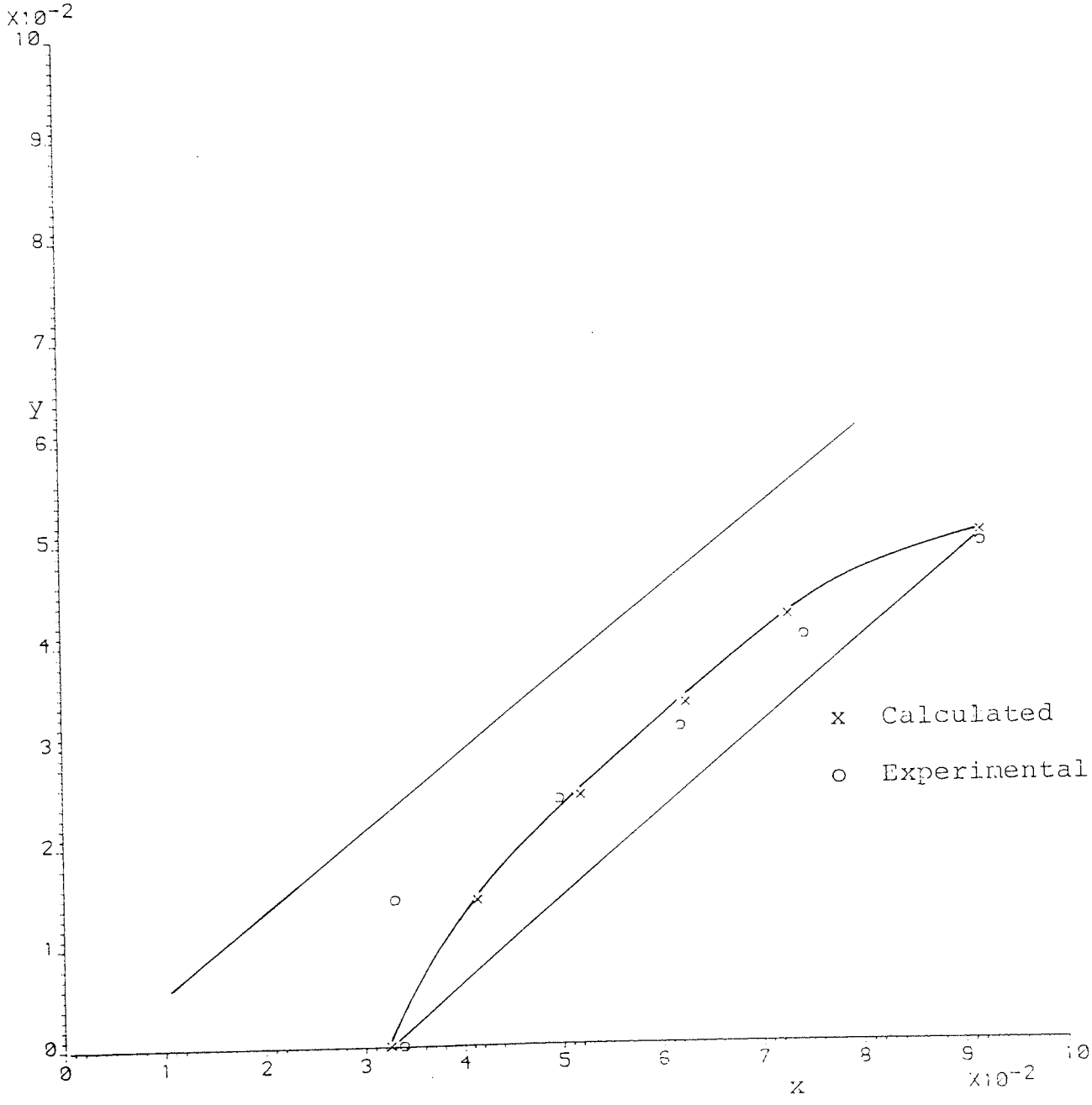

Figure 9.30 - Run 15

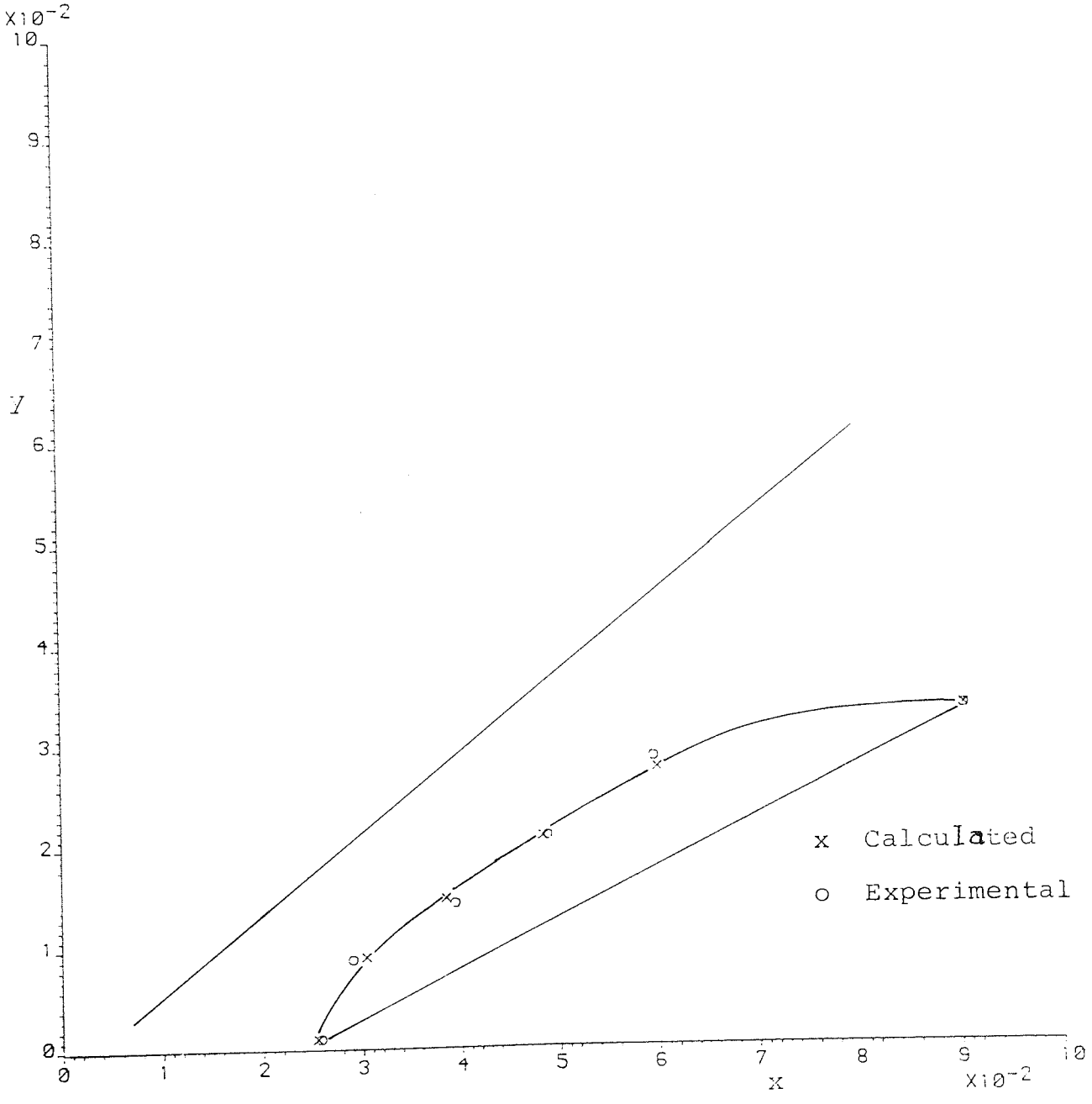

Figure 9.31 - Run 16

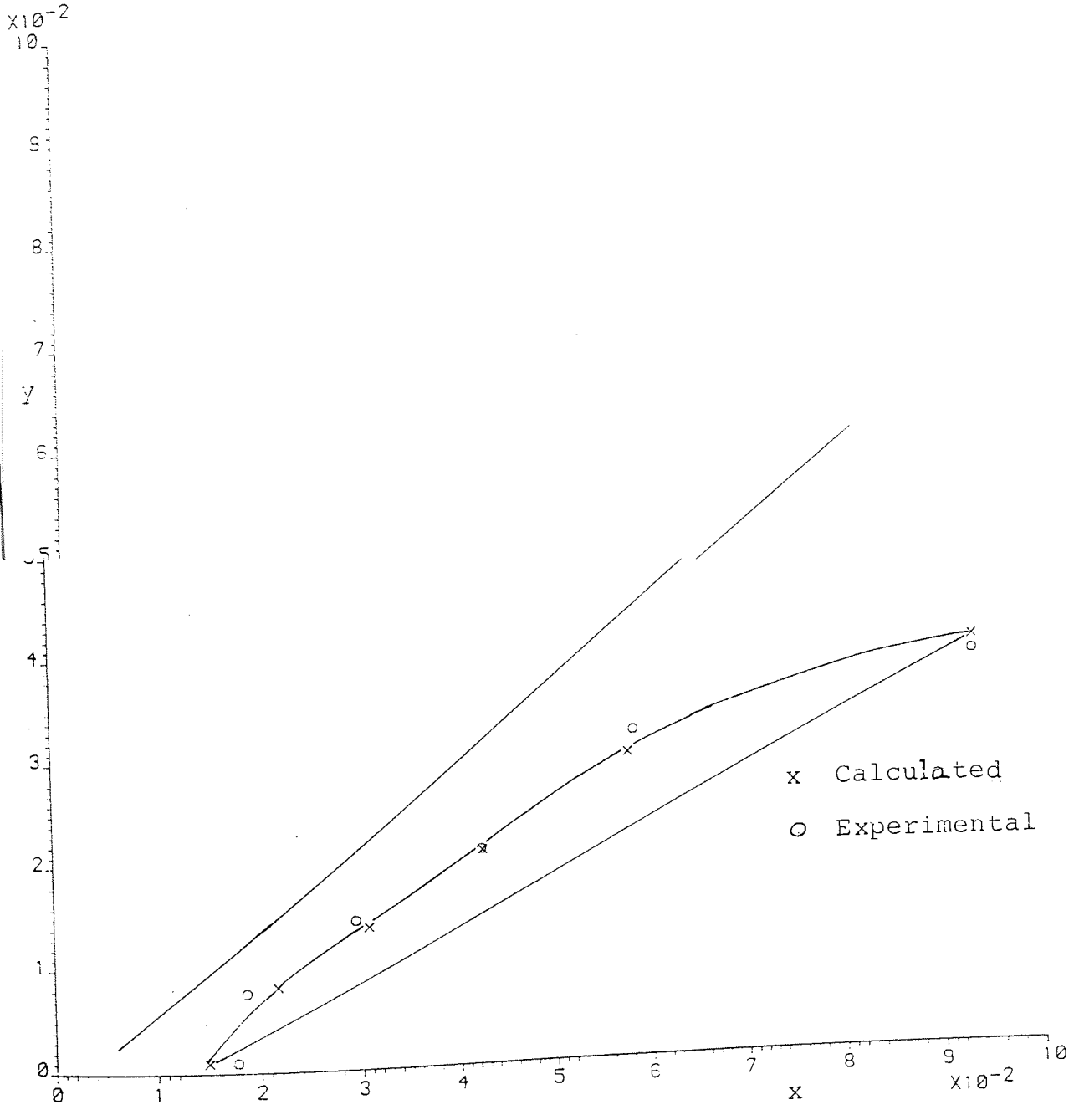

Table 9.25 - Results of Factorial Experiment

Run	MTD	Pad Height	$x10^{-3}$ V_D	N	% MBC	Θ_D	$x10^{-3}$ d_{32} (st. Dev.)	$x10^{-2}$ a	η	r	e	$x10^{-5}$ K_D
1	D → C	0.06	1.28	6.66	2.50	0.045	2.53 (1.30)	1.06	0.393	0.485	0.75	5.58
2			1.28	10.00	2.10	0.055	2.22 (1.05)	1.48	0.606	0.289	0.641	11.40
3			1.94	6.66	2.90	0.068	2.82 (1.5)	1.44	0.412	0.969	0.605	9.06
4			1.94	10.00	4.70	0.074	2.76 (1.43)	1.61	0.626	0.017	0.946	13.73
5	C → D		1.28	6.66	0.76	0.080	1.43 (0.54)	3.34	0.655	0.823	0.290	5.80
6			1.28	10.00	3.10	0.142	0.82 (0.26)	10.32	0.801	0.775	0.091	3.33
7			1.94	6.66	7.00	0.100	2.04 (0.89)	2.93	0.633	0.621	0.613	8.33
8			1.94	10.00	11.00	0.171	1.27 (0.47)	8.03	1.085	0.798	-0.010	-
9	D → C	0.03	1.28	6.66	3.00	0.044	2.96 (1.55)	0.89	0.379	1.569	0.050	11.00

Continued/....

Table 9.25 - Continued

Run	MTD	Pad Height	$x10^{-3}$ V_D	N	% MBC	Θ_D	$x10^{-3}$ d_{32} (st. Dev.)	10^{-2} a	η	r	e	$x10^{-5}$ K_D
10			1.28	10.00	1.71	0.057	2.29 (1.10)	1.49	0.682	0.439	0.441	17.83
11			1.94	6.66	2.40	0.072	3.86 (2.25)	1.12	0.451	0.730	0.199	13.83
12			1.94	10.00	2.51	0.080	3.28 (1.76)	1.46	0.593	0.446	0.125	15.50
13	C → D		1.28	6.66	1.52	0.060	1.78 (0.77)	2.02	0.574	0.827	0.143	8.16
14			1.28	10.00	4.82	0.124	1.32 (0.62)	5.63	0.713	0.922	-0.01	4.73
15			1.94	6.66	4.30	0.116	2.24 (1.18)	3.10	0.494	1.251	0.229	6.70
16			1.94	10.00	2.10	0.158	1.06 (0.43)	8.94	0.896	0.455	0.358	15.41
10-1			1.28	10.00	4.00	0.062	-	-	0.785	0.465	0.557	
14-1			1.28	10.00	1.10	0.116	-	-	0.934	0.906	-0.029	

9.3.4.2 Statistical Analysis - Stage Efficiency

The stage efficiencies resulting from the model fitting steps werestudied in an analysis of variance using the Yates' technique to calculate effects and interactions.

Table 9.26 presents the ANOVA table. The error variance was estimated combining the three- and four-factor interactions. The application of the Bartlett's test led to a value of M of 7.20 which is below the one required for significance and therefore there is no evidence of heterogeneity.

Table 9.26 shows that only agitator speed (effect A) and mass transfer direction (effect C) are significant. An important finding is that packing pad height, within the studied levels, do not influence η and therefore it can be concluded that noappreciable mass transfer took place inside the packing.

The calculated sign and magnitude of the significant effects are,

Agitator Speed (A) = 0.2513

Mass Transfer Direction (C) = 0.2141

Both factors affect the stage efficiency positively, η increases with the level of the factors, and have approximately the same magnitude. The combined effect of increasing interfacial area and decreasing dispersed phase backflow parameter, as presented in the next section with the increasing level of the factors A and C explains

Table 9.26 - Analysis of Variance - Stage Efficiency

Source of variation	Degree of freedom	Mean Square	F
A	1	0.2527	33.73 ***
B	1	0.0115	1.53
C	1	0.1833	24.43 ***
D	1	0.0092	1.22
AB	1	0.0000	0.00
AC	1	0.0044	0.00
AD	1	0.0100	1.33
BC	1	0.0202	2.69
BD	1	0.0028	0.37
CD	1	0.0074	0.98
ABC	1	0.0003	
ABD	1	0.0026	
ACD } Error	1 :5	0.0330	= 0.0374/5 = 0.0075
BCD	1	0.0007	
ABCD	1	0.0008	

F(1,5) = 6.61 at 5% level

F(1,5) = 16.30 at 1% level

*** Highly Significant

the behaviour of the stage efficiency.

9.3.4.3 Statistical Analysis - Dispersed Phase Backflow Parameter

The data corresponding to the raffinate backflow parameter (r) for the experiments with mass transfer direction Dispersed ⟶ Continuous phase and to the extract backflow parameter (e) for the experiments with the opposite mass transfer direction were analysed in terms of an analysis of variance.

Table 9.27 presents the result of the analysis. The application of the Bartlett criterion to the three- and four-factor interaction gave M = 3.97, therefore, the estimated variance of the higher interactions can be combined to estimate the error variance. The analysis indicates that only agitator speed and mass transfer direction have a significant influence over the value of the dispersed phase non-ideal flow parameter. The magnitude and sign of these effects were calculated to be

Agitator Speed (A)	=	-0.4280
Mass Transfer Direction (C)	=	-0.4048

and since interactions are not significant, both main effects are independent. The decrease in the value of the backflow parameter with N is the result of a more uniform drop size distribution, as indicated by the decrease in the standard deviations of the distributions

Table 9.27 - Analysis of Variance - Dispersed Phase Backflow Parameter

Source of variation	Degree of freedom	Mean Square	F
A	1	0.7357	7.12**
B	1	0.0898	0.86
C	1	0.6556	6.34*
D	1	0.0000	0.00
AB	1	0.0147	0.142
AC	1	0.1951	1.88
AD	1	0.0000	0.00
BC	1	0.1881	1.82
BD	1	0.0395	0.382
CD	1	0.0965	0.934
ABC	1	0.0743	
ABD	1	0.3033	
ACD } Error	1 :5	0.0024 } = $\frac{0.5166}{5}$ = 0.1033	
BCD	1	0.0910	
ABCD	1	0.0456	

F(1,5) = 6.61 at 5% level

F(1,5) = 4.06 at 10% level

** Significant

* Probable Significance

("forward mixing" effect). The same results can be achieved by changing the direction of mass transfer from dispersed → continuous to continuous → dispersed phase (e.g. Run 2 and 6, Run 10 and 14 etc). With the exception of Run 16, the combination of high agitator speed and mass transfer direction continuous → dispersed phase leads, practically to an ideal flow behaviour of the dispersed phase (backflow parameter $\triangleq$ 0).

The insignificant effect of the dispersed phase superficial velocity (Factor D) came out to be a surprise. In order to give an explanation the following points need to be considered:

1. The non-ideality of the dispersed phase in this column is affected not only by the measurable spread of the drop size distribution but also by possible by-pass or/and accumulation of the phase on the internals which are not always noticed and much less measured. All these factors, whose presence increases the non-ideality, are at their minimum value at high agitator speeds. The increase of V_D is expected to increase both the spread of drops size distribution and the possibility of existence of a dispersed phase by-pass, at least at low N (400r.p.m.). For some experiments, (Run 1 and 3, Run 5 and 7, Run 13 and 15) the results follow the above; that is at equal N (400r.p.m.) the dispersed phase backflow increased with V_D, while for other experiments the opposite situation or at least no change (N = 600r.p.m.) occurred. This brings us to

the next point of the degree of reliability of the estimate of the solution vector.

2. The study carried out in Chapter 5 concerning the properties of the solution vector of the compartmental model showed that the concentration profile is less sensitive to changes in the backflow parameters as compared with the stage efficiency. This implies that the backflow parameters $\underline{r}$ and $\underline{e}$ can be estimated with a relatively low accuracy. The estimated experimental error variances of η, dispersed phase backflow and continuous phase backflow, presented in the corresponding ANOVA tables, reflect the above property of the solution vector.

Response	Estimated Error Variance
Stage efficiency	0.0075
Continuous phase backflow parameter	0.0488
Dispersed phase backflow parameter	0.1033

Since the dispersed phase backflow presents the largest error, one can conclude that the high probable existence of a significant effect of V_D is masked by the total error (true experimental plus lack of fit).

9.3.4.4 Statistical Analysis - Continuous Phase Backflow Parameter

Table 9.28 presents the results of the analysis of variance of the data corresponding to the continuous phase backflow parameter. The application of the Bartlett's test to the higher interactions resulted in a value of M of 9.39, which is lower than the vaulue of 12.0 required for significance. Therefore, the procedure to estimate the error variance is adequate.

The analysis shows that the Mass Transfer Direction (Factor C) is significant at the 5% level and the interactions Agitator Speed x Mass Transfer Direction (interaction A x C) and Pad Height x Mass Transfer Direction (interaction B x C) are significant at the 10% level. The corresponding sign and magnitude of the significant effects are

Mass Transfer Direction	=	0.422
Agitator Speed x Mass Transfer Direction	=	-0.226
Pad Height x Mass Transfer Direction	=	-0.236

If very little or no reliance is placed on the 10% level of significance, the only significant mean square is the one associated with Mass Transfer Direction. The sign of this main effect indicates that an increase in the backflow parameter results from a change in the mass transfer direction from dispersed $\rightarrow$ continuous to continuous $\rightarrow$ dispersed phase. Since physical backflow has been experimentally shown not to exist (section 9.2.1.1), and assuming other effects being constant or negligible,

Table 2.98 - Analysis of Variance - Continuous Phase Backflow Parameter

Source of variation	Degree of freedom	Mean Square	F
A	1	0.0251	0.51
B	1	0.0617	1.26
C	1	0.7131	14.60 **
D	1	0.0116	0.23
AB	1	0.1253	2.56
AC	1	0.2040	4.17 *
AD	1	0.1159	2.37
BC	1	0.2227	4.56 *
BD	1	0.0460	0.94
CD	1	0.0490	1.00
ABC	1	0.0035	
ABD	1	0.1140	
ACD } Error	1 :5	0.0001	$= \frac{0.2442}{5} = 0.0488$
BCD	1	0.0789	
ABCD	1	0.0477	

$F(1,5) = 16.3$ at 1% level

$F(1,5) = 6.61$ at 5% level

$F(1,5) = 4.06$ at 10% level

** Significant

* Probable Significance

i.e. end effects, the channelling effect in the continuous phase, created by the high continuous phase linear velocity in the packed section which persists in the vicinity of the wall at the mixing section, is considered to be wholly responsible for any change in the continuous phase non-ideal flow parameter. This phenomenon which is associated with a poor radial diffusivity depends entirely on the intensity of turbulence in the continuous phase and its distribution on the vicinity of the chamber wall. A high level of turbulence increases the radial diffusivity and eliminates the channelling at the wall. It has been suggested in the literature that the degree of turbulence decreases as drop concentration or hold-up increases. The data obtained in the factorial experiment indicate that for equal agitator speed, the hold-up increases in the range of 150% to 200% when solute transfer direction changes from dispersed→ continuous to continuous→ dispersed phase, therefore a change in the continuous phase backflow parameter is expected.

Using the above assumed relationship between intensity of turbulence and hold-up it is reasonable to expect a significant influence of impeller speed on the backflow parameter. Such a situation did not occur and the variation of the backflow parameter with N is seen to be completely random leading to a non-significant effect. A tentative explanation could be that increasing impeller speed increases intensity of turbulence and hold-up and since both have opposite effects on the continuous phase

backflow coefficient, they may cancel out. The same results were observed in the preliminary experimentation for N in the range 400-500r.p.m. The above discussion points out to the need of further experimentation at higher levels of the impeller speed.

9.3.4.5 Overall Mass Transfer Coefficient

The overall dispersed phase mass transfer coefficient, K_D, for each experiment was calculated using Equations (8.6) to (8.8). These equations (145) were based on the assumption of perfect mixing of the phases within a stage. This assumption is reasonable in view of the results obtained in the preliminary experimentation.

To solve the above equations the total interfacial area for mass transfer in a stage ($a.V_K$) must be known. The complexities of the drop formation process shown in Figure 8.6 makes it extremely difficult to measure or to predict, with a reasonable degree of accuracy, the total interfacial area for mass transfer in the impeller region. The results of the experiment presented in Figure 8.8 and the characteristics of the dispersed phase fluid dynamics at drop formation shown in Figure 8.6 suggests that all the mass transfer takes place in the region where drops are detached from the jets created by the vortex behind the impeller blades. Even in very carefully controlled experiment of drop formation under jetting condition (152,153) the interfacial area at drop detachment is so difficult to measure accurately that it is normally assumed to be

equal to the surface area of all free drops. This assumption has been adopted by the author and the total interfacial area for mass ($a.V_k$) was calculated as

$$a.V_k = \frac{6\Theta_D}{d_{32}} \cdot (H_m + H_p) \cdot \frac{\pi D_c^2}{4} \qquad (9.10)$$

The calculated overall mass transfer coefficient given in Table 9.29 are based on completely mixed stages and the values reported therefore, include allowance for the non-ideality in the stages.

For the purpose of comparison, theoretical overall mass transfer coefficients were calculated using well known correlations derived from single drop mass transfer studies. Individual dispersed phase mass transfer coefficients were calculated using the correlation proposed by Neumann and later simplified by Vermeulen (106) for stagnant drops, Kronig and Brink (107) later simplified by Calderbank (110) for circulating drops and Rose and Kinter (103) for oscillating drops. The continuous phase coefficients were calculated using the correlations given by Garner and Tayeban (102) for the case of stagnant and circulating drops. Diffusion coefficients were calculated using the correlations derived by Wilkie and Chang (154). Both individual coefficients were substituted in the usual equation (4.86) to give the overall coefficient of mass transfer. Not all the experiments were used to calculate the theoretical K_D's only those which most represent the whole range of operating conditions were chosen.

Table 9.29 lists the experimental and theoretical overall dispersed phase mass transfer coefficient. The theoretical cofficients for the oscillating single drop case were calculated for two different modes of oscillation n = 2 and n = 3.

If drop size is the criteria used to select the appropriate single drop mechanism, the results of Table 9.29 show that all the experimental coefficients are larger than the corresponding theoretical. Drops in Run 6 were expected to behave as rigid drops, in Run 4 as circulating-oscillating drops, in Run 7 as circulating drops, and so on. In fact, all of the coefficients came out to be one order higher in a scale of "intensity of drop motion". The result is that the predictions tend to underestimate the experimental values and is readily understood in terms of the violent nature of the drop formation mechanism. Thus, even the most likely, stagnant drops of Run 6, probably began their free rise existence with some degree of oscillation induced by the break-up process, so that mass transfer coefficient estimates based on completely stagnant drops would be on the low side. The circulating-oscillating drops of Run 4 probably experienced enhanced oscillation due to the violence of the swirling jet break-up, compared with a free oscillating drop created at a nozzle.

The overall result is that predicted mass transfer coefficients are on the conservative side, which is a desirable feature for design purposes.

Table 9.29 - Experimental and Theoretical Overall Dispersed Phase Mass Transfer Coefficient

Run	d_{32}-3 x10-3	$K_D \times 10^{-5}$ (Experimental)	$K_D \times 10^{-5}$ (theoretical)			
			Stagnant Drop	Circulating Drop	Oscillating Drop	
					n = 2	n = 3
1	2.53	5.58	1.61	3.75	6.61	6.98
4	2.76	13.73	1.51	3.52	6.18	6.46
5	1.43	5.80	1.51	3.51	7.14	7.45
6	0.82	3.33	-	3.64	7.63	7.86
7	2.04	8.33	1.45	3.37	6.39	6.70

CHAPTER X

CONCLUSIONS AND RECOMMENDATIONS FOR FUTURE WORK

CONCLUSIONS AND RECOMMENDATIONS FOR FUTURE WORK

A study of the hydrodynamics and mass transfer performance of a four-stage Scheibel column under total coalescence in the packing sections has been undertaken. The experimental results obtained, using the system toluene-acetone-water, were used in a model fitting exercise in order to calculate the mass transfer performance parameter (stage efficiency) and the non-ideal flow parameters (rafinate and extract phase backflow).

10.1 Conclusions

The main conclusions arising from this study are:

1. In order to select the appropriate packing material for a Scheibel Column, it is necessary to know the desired voidage, and the average sizes of interstices inside the pads for each of the materials, since they control the fluid flow resistances and the column capacity. Since measurements of interstices sizes can be extremely difficult and laborious to perform when knitted mesh packings are studied, it was found that the number of stitches per unit length in the vertical and horizontal direction in the mesh gave a good relative measurement of the size of the interstices and it can be used as a guideline in the selection of the packing.

2. Column capacity increased considerably when the packing pads are wetted by the dispersed phase and the impellers positioned in the vicinity of D_I/5cm from thepads upper surface.

3. Sauter mean drop sizes under no mass transfer conditions can be estimated by equation (8.1), developed in this study. When mass transfer occurs Equation 9.6 or Equation 9.7 may be used depending on the direction of mass transfer. Deviations from Kolmogoroff's law are large in the cases of no mass transfer and when the mass transfer direction is dispersed to continuous phase.

4. The phases inside the 5.0cm height agitated compartments behave as totally mixed.

5. No significant amount of mass transfer takes place inside a dispersed phase wetted knitted mesh pad. The major part of the solute transfer within a Scheibel stage occurs in the region of the impeller.

6. The "cells in series with backflow" model best represents the behaviour of the Scheibel column. The non-ideal behaviour of the dispersed phase measured in terms of a backflow parameter is a function of the variance of the drop size distribution. The backflow parameter in the continuous phase is a function of the degree of turbulence in the mixing chamber which in turn is related to the speed of the agitator and the dispersed phase hold-up. The column performance

measured in terms of the stage efficiency, η, depends on the impeller speed and the direction of mass transfer; increasing when the mass transfer was continuous to dispersed.

7. Experimental overall dispersed phase mass transfer coefficient based on completely mixed stages are larger than the corresponding theoretical coefficient calculated in base of single drop mechanism.

10.2 Recommendations for Future Work

1. Study of the column capacity for different sizes of knitted meshes, impeller position and voidage distribution within the pads.

2. Determine quantitatively the amount of physical backflow of the phases as function of impeller speed and position, pad thickness and type of knitted mesh.

3. Study the total flow non-identity of each phase under different operating conditions using the technique of "pulse injection of a tracer". Compare the obtained results with the ones reported in this thesis using the model fitting method.

NOMENCLATURE

a	Specific interfacial area, m^2/m^3
a'	Activity
A^*	Solubility of solute A in the phase where it is transferred, $grmole/m^3$
A	Proportionality constant in equation (4.52)
a_s	Packing surface/packing volume, m^2/m^3
a_p	Amplitude
B^o	Concentration of B in bulk of B-phase, $gmol/m^3$
C_D	Drag coefficient Equation (4.76)
C^*	Equilibrium concentration, Kg/m^3
C_x	Raffinate phase solute concentration, Kg/m^3
C_y	Extract phase solute concentration, Kg/m^3
d	Drop diameter, m
d_{32}	Sauter mean drop diameter, m
d_c	Collision diameter, m
$(dp)_{crit.}$	Critical packing size, m
D_I	Impeller diameter, m
D_c	Column diameter, m
d_o	Diameter of uncombined drops, m
$D_{turb.}$	Coefficient of turbulent diffusion of particles m^2/s
dp	Characteristic packing size, m
E	Solute free extract phase mass flowrate, Kg/s
E_{MD}	Murphree dispersed phase stage efficiency

E_C	Axial eddy diffusivity of continuous phase m^2/s
E_D	Axial eddy diffusivity of dispersed phase m^2/s
e_c	Axial dispersion coefficient continuous phase, $E_x \times \Theta_D$, m^2/s
e_D	Axial dispersion coefficient dispersed phase, $E_D \times (1 - \Theta_D)$, m^2/s
E_a	Energy of adhesion between two-drops, N.m
E_O	Eotuos number = $\frac{g\Delta\rho d^2}{\sigma}$
e_k	Fractional backflow coefficient in k^{th} stage, extract phase (also ℓ_k)
F	Extraction factor
F(h)	Force of adhesion between drops, N
g	Acceleration due to gravity m/s^2
H	Lenght of mixing vessel or stage, m
$(HTU)_{OD}$	Height of overall dispersed phase transfer unit, m
h_o	Minimum distance between two drops, m
H_P	Packing pad thickness, m
H_M	Height of mixing compartment in a Scheibel stage, m
I_o/I	Extinction ratio
K_D	Dispersed phase overall mass transfer coefficient, m/s
k_D	Dispersed phase mass transfer coefficient, m/s
k_c	Continuous phase mass transfer coefficient, m/s
K'	Overall mass transfer coefficient based on activity, $Kg/s\ m^2$

k_2	Second order reaction rate constant, m^2/g mole.s
k_L^o	Liquid side mass transfer coefficient, m/s
L	Height of active extraction part of a column, m
l	Numerical constant in Equation (4.5)
Le	Integral scale of turbulence, m
m	Distribution coefficient
N	Impeller speed, r.p.s.
$(NTU)_{OD}$	Number of overall dispersed phase transfer unit, also $(No)_x$ or $(No)_y$
n_o	Number of drops per unit volume of dispersion
N_P	Power number, defined by Equation (4.54
N_A	Mass flux of solute A Kg/s.m^2
n	Mode of oscillation
Pe	Peclet number
P	Power, J/s
p	Turbulent fluctuation of static pressure $\frac{N}{m^2}$
Q_c	Volumetric flowrate of continuous phase ml/min
Q_D	Volumetric flowrate of dispersed phase ml/min
R	Solute free raffinate phase mass flow rage Kg/s
r_k	Fractional backflow coefficient in k^{th} stage, rafinate phase
R_x	Total rate of solute transfer per unit volume of dispersion Kgmole/s.m^3
R_x	Jump ratio, raffinate phase
R_y	Jump ratio, extract phase
r	Magnitude of interval vector
r_{SD}	Radius of stable drop, m
$(Re)_I$	Tank or impeller Reynold number = $D_I^2.N.\rho_c/\mu_c$
Re	Drop Reynolds number = $V_t.d.\rho_c/\mu_c$

SS	Stator ring opening, m
Sw	Surface area/weight, m^2/kg
$\bar{S}_c$	Mean distance between collision, m
Sh	Sherwood number = $k.d/\mathcal{D}$
Sc	Schmidt number = $\nu/\mathcal{D}$
s	Fractional surface renewal rate, s^{-1}
S	Area of time dependent surface, m^2
S_o	Charactarestic reference area for constant surface, m^2
$\bar{t}$	Average time between collision, s
t_c	Penetration or contact time, s
t_{ci}	Circulation time, s
t_k	Kolmogoroff's time scale, s
U_i	Instantaneous velocity, m/s
$\bar{U}_i$	Time average velocity, m/s
u_i	Instantaneous fluctuation velocity m/s
u_i'	Root mean square fluctuation velocity, m/s
U_x	Same as $\bar{v}_r$
U_o	Same as $\bar{v}_o$
$U_{o,\Theta}$	Velocity defined by Equation (4.71)
V_D	Dispersed phase superficial velocity based on extractor cross-section, m/s
V_c	Continuous phase superficial velocity based on extractor cross-section, m/s
$\bar{v}_o$	Characteristic velocity, m/s
$\bar{V}$	Linear velocity, i.e. $\bar{V}_D = V_D/\Theta_D$, m/s
V	Volume, m^3
v_λ	Fluctuation velocity at scale of motion λ, m/s

V_s	Stokes terminal velocity, m/s
$\bar{v}_r$	Relative or slip velocity, m/s
V_t	True drop terminal velocity, m/s
V_k	Volume of the k^{th} Scheibal stage, m^3
W_e	Vessel Weber number = $D_I{}^3.N^2\rho_c/\sigma$
w_i	Relative fluctuation velocity in the i-direction, m/s
w_c	Collision frequency per unit volume $(s.m^3)^{-1}$
W	Impeller blade width, m
w	Frequency of oscillation, s^{-1}
x'	Raffinate phase solute concentration, w/w%
x	Raffinate phase solute concentration, weight fraction solute free base
X	Dimensionless concentration, rafinate pahse
X'	Hypothetical concentration defined by Equation (5.5), Kg/m^3
y'	Extract phase solute concentration w/w%
y	Extract phase solute concentration, weight fraction solute free base
Y_o	Film thickness, m
Y	Dimensionless concentration, extract phase
Y'	Hypothetical concentration defined by Equation (5.6) Kg/m^3
Z_s	Stoichiometric number
z	Coalescence coefficient
Z	Dimensionless axial column length
Θ_D	Dispersed phase volumetric fractional hold-up
σ	Interfacial tension, N/m
ρ	Density, Kg/m^3
μ	Dynamic viscosity, $N.s/m^2$

$\Delta\rho$	Density difference, Kg/m^3
ε	Fractional voidage of packing $\frac{(m^3 \text{ void space}}{(m^3 \text{ packed volume})}$
$\mathcal{D}$	Molecular diffusion coefficient m^2/s
β	Numerical constant in Equation (4.5)
β_{dd}	Universal function
$\epsilon, \bar{\epsilon}$	Local and average enery input per unit mass and time or energy dissipation per unit mass, respectively, m^2/s^3
ν	Kinematic viscosity, m^2/s
η	Kolmogoroff's lenght scale, m
η	Stage efficiency
v	Kolmogoroff's velocity scale, m/s
λ	Eddy characteristic length or scale of motion, m
ϵ'	Dimensionless amplitude factor
θ_c	Time between coalescence and redispersion

APPENDIX 1

Drop Size Analysis - Computer Program

```
5  REM                    DROP  SIZE  ANALYSIS  PROGRAM
7  REM                     ============================
8  REM
10 REM                    MIXING CHAMBERS- SCHEIBAL COLUMN
12 REM
15 REM
16 REM
20 DIM A(48),I(48),D(48),M(6),S(6),V(4),U(4),X(4)
22 DIM K(4,48),Y(4,48)
24 REM
26 REM          INPUT RUN IDENTIFICATION
28 INPUT R
30 REM
32 REM          READ ZEISS ANALIZER MID POINT RANGES
34 FOR I=1,48: READ A(I): NEXT I
36 REM
38 FOR R=1,4
40  J1=0:J2=0:J3=0:J4=0:I=0
42 FOR I=1,48:I(I),D(I)=0: NEXT I
44 REM
47 PRINT "RUN =";R,"MIXING CHAMBER NUMBER ";R
50 REM
52 REM          ENTER ZEISS MEASURING RANGE
55 REM          PRINT 0 -STANDARD RANGE , 1 -REDUCED RANGE
60 PRINT "ZEISS ANALIZER MEASURING RANGE =";: INPUT X
65 PRINT "PICTURE MAGNIFICATION FACTOR   =";: INPUT M
70 IF X=1 THEN M=M/3
75 REM
76 REM          INPUT NUMBER OF DROPS IN RANGE
77 V(R)=48
80 FOR I=1,48
85 INPUT I(I)
90 IF I(I)<0 THEN 133
95 D=I(I)+D
100  D(I)=M*A(I)
105 J1=J1+I(I)*D(I)
110 J2=J2+I(I)*(D(I))↑2
115 J3=J3+I(I)*(D(I))↑3
120 J4=J4+I(I)*(D(I))↑4
125 NEXT I
130 GOTO 135
133 V(R)=I-1
135 M(1)=J1/I: REM       ARITHMETIC MEAN
140 M(2)=SQR(J2/I): REM        MEAN SQUARE DIAMETER
145 M(3)=(J3/I)↑.333: REM      MEAN CUBIC DIAMETER
150 M(4)=J2/J1: REM       LINEAL MEAN DIAMETER
155 M(5)=J3/J2: REM       SAUTER MEAN DIAMETER
160 M(6)=J4/J3: REM       VOLUMETRIC MEAN DIAMETER
170 FOR A=1,6
175 S(A)=0
180 FOR J=1,V(R)
185 S(A)=S(A)+I(J)*(D(J)-M(A))↑2
190 NEXT J
195 S(A)=SQR(S(A)/(D-1))
200 NEXT A
205 REM
210 REM                    OUTPUT  SECTION
300 REM                    PRINT "RUN =";R;"MIXING COMP.=";R;"MAGN.FACTOR=";M
305 PRINT "RUN =";R;"MIXING COMP.=";R;"MAGN.FACTOR=";M
307 PRINT
307 PRINT : PRINT
310 FOR I=1,V(R)
315 PRINT D(I),I(I)
320 NEXT I
322 PRINT : PRINT                    =";I
325 PRINT "TOTAL NUMBER OF DROPS         =";M(1);"STD.DEV.=";S(1)
330 PRINT "ARITHMETIC MEAN DROP DIAMETER=";M(2);"STD.DEV.=";S(2)
335 PRINT "SQUARE MEAN DROP DIAMETER     =";M(3);"STD.DEV.=";S(3)
340 PRINT "CUBIC MEAN DROP  DIAMETER     =";M(4);"STD.DEV.=";S(4)
345 PRINT "LINEAL MEAN DROP DIAMETER     =";M(5);"STD.DEV.=";S(5)
350 PRINT "SAUTER MEAN DROP DIAMETER     =";M(6);"STD.DEV.=";S(6)
355 PRINT "VOLUMETRIC MEAN DROP DIAMETER=";M(6);"STD.DEV.=";S(6)
360 PRINT : PRINT : PRINT
365 REM
370 REM
375 FOR J=1,V(R)
380 K(R,J)=D(J): REM       DIAMETER OF RANGE
385 Y(R,J)=I(J): REM       NUMBER OF DROPS IN RANGE
390 NEXT J
395 U(R)=M(5):X(R)=D
400 NEXT R
405 REM
407 REM
410 REM        OUTPUT DIAMETERS AND NUMBER OF DROPS IN RANGE THRU THE
415 REM        HIGH SPEED PUNCHER.
420 REM
430 REM        SET SENSE SWITCH  4
432 REM
435 FOR I=1,4
```

```
200  NEXT A
205  REM
210  REM
300  REM                    OUTPUT  SECTION
305  PRINT "RUN ="IR1"MIXING COMP.="IE1"MAGN.FACTOR="IM
307  PRINT
307  PRINT : PRINT
310  FOR I=1,V(R)
315  PRINT D(I),I(I)
320  NEXT I
322  PRINT : PRINT
325  PRINT "TOTAL NUMBER OF DROPS          ="IT
330  PRINT "ARITHMETIC MEAN DROP DIAMETER="IM(1)"STD.DEV.="IS(1)
335  PRINT "SQUARE MEAN DROP DIAMETER      ="IM(2)"STD.DEV.="IS(2)
340  PRINT "CUBIC MEAN DROP  DIAMETER      ="IM(3)"STD.DEV.="IS(3)
345  PRINT "LINEAL MEAN DROP DIAMETER      ="IM(4)"STD.DEV.="IS(4)
350  PRINT "SAUTER MEAN DROP DIAMETER      ="IM(5)"STD.DEV.="IS(5)
355  PRINT "VOLUMETRIC MEAN DROP DIAMETER="IM(6)"STD.DEV.="IS(6)
360  PRINT : PRINT : PRINT
365  REM
370  REM
375  FOR J=1,V(R)
380  X(R,J)=D(J): REM       DIAMETER OF RANGE
385  Y(R,J)=I(J): REM       NUMBER OF DROPS IN RANGE
390  NEXT J
395  D(R)=M(5):X(R)=T
400  NEXT R
405  REM
407  REM
410  REM       OUTPUT DIAMETERS AND NUMBER OF DROPS IN RANGE THRU THE
415  REM       HIGH SPEED PUNCHER.
420  REM
430  REM       SET SENSE SWITCH  4
432  REM
435  FOR I=1,4
437  PRINT D(I),X(I)
440  FOR J=1,V(I)
445  PRINT X(I,J),Y(I,J)
450  NEXT J
460  NEXT I
465  REM
470  REM         RELEASE SENSE SWITCH 4 WHEN PUNCHER STOP
475  REM
480  REM
485  DATA 1.49,2.04,2.59,3.14,3.7,4.25,4.8,5.35,5.9
495  DATA 6.46,7.01,7.56,8.11,8.66,9.22,9.77,10.32,10.87,11.42
500  DATA 11.98,12.53,13.08,13.63,14.18,14.74,15.29,15.84,16.39
505  DATA 16.94,17.5,18.05,18.6,19.15,19.7,20.26,20.81
510  DATA 21.37,21.91,22.46,23.02,23.57,24.12,24.67,25.22,25.78
512  DATA 26.33,26.88,27.43
515  STOP
520  END

?
```

APPENDIX 2

Computer Program to Calculate Concentration Profiles - Compartments with Backflow Model

```
 *****    ****   ****    *****   *****   *****    *
**   *  *    *  *   *  *     *  *    *  *    *   *
**   *  *    *  *   *  *     *  *    *  *    *   *
 ****   *    *  ****    *****   *****   *    *   *
**   *  *    *  *       *     *  *  *    *    *  *
**   *  *    *  *       *     *  *   *   *    *  *
 *****   ****   *       *****   *    *  *****    *

                                                                    :ECP2204.STAPROF

#LISTING OF :ECP2204.STAPROF(1/8180)    PRODUCED ON 23NOV21 AT 11.47.57

#G8.64AB AT ASTON    IN :ECP2204.STAPROF ON 23NOV21 AT 11.48.43 USING  U15

DOCUMENT    :ECP2204.STAPROF(1/8180)

   STARTED :ECP2204,STAPROF,23NOV21 11.35.46 TYPE: BACK  ID ; STREAM   ; PRIORITY 2 ; ENTERED WILL 23NOV21 11.32.18
11.35.46* JOB :ECP2204,STAPROF
   11.35.46 JOB IS NOW FULLY STARTED
11.35.46* STAPROF
   11.35.46* UAFORTRAN LIB NAGF,LINES 2000
ENTERING :MACROS.UAFORTRAN(227/)
   11.35.47*        TA A5,CM,JL

 FORTRAN COMPILATION BY FXFIV MK 39    DATE  23/11/21  TIME  11/36/ 9


      0000                LIST (LP)
      0001                PROGRAM (FXXX)
      0002                INPUT  1 = CR0
      0003                INPUT  5 = TR0
      0004                INPUT  5 = CR1
      0005                OUTPUT 2 = LP0/132
      0006                OUTPUT 6 = LP1/132
      0007                COMPRESS INTAGER AND LOGICAL
      0008                COMPACT PROGRAM
      0009                EXTENDED DATA
      0010                TRACE 2
      0011                END


      0012                TRACE 1
      0000                TRACE 2
      0001                MAST P JOB
      0002          C
      0003          C     PROGRAM CALCULAT. CONC. PROFIL   STAG  MULTI-STAGE  EFFICI NCY
      0004          C
      0005          C     WHEN FV(*) IS SET TO 1. THE MODEL P RAMETERS ARE CONSID RED
      0006          C     CONSTANT. OTHERS VALUES CORRESPON TO THE NUMB R OF UNKNOWNS
      0007          C     THE PROGRAM WAS WRITTEN FOR 5, 7, 9 STAGES COLUMN
      0008          C
      0009                DIMENSION FV(10)
      0010                DIMENSION XC(10),XPC(10),XS (10)
      0011                DOUBLE PRECISION XCSID  XI , XJ , XD , XMLE
      0012                DOUBLE PRECISION XC,XXC
      0013                COMMON XCI,XIS , ,D, LE
      0014          1     F A2(1, 2)**,KK,FV(1)
      0015                F,    1(   , F1   )
      0016                IF(FV(1) .EQ. 0.)GO T
      0017                   DO ,KK
      0018          1     ,   ,XC(J)
      0019                F   *(   ,*)
```

```
0020                 READ(1,05)XIN,YIN,D,G
0021              05 FORMAT(4F10.5)
0022                 READ(1,01)ALF
0023              01 FORMAT(D1.4)
0024                 READ(1,20)FV(2)
0025              20 FORMAT(F10.5)
0026                 WRITE(2,23)XIN,YIN,D,G,ALF,NN,KK,FV(2),FV(1)
0027              23 FORMAT(//1X,5D1.5,2I1 ,2F1.  )
0028                 CALL PROFIL(NN,KK,XC,XXC,FV)
0029                 DO 17 J=1,KK
0030              17 WRITE(2,16)XC(J)
0031              16 FORMAT(5 X,D1F.5)
0032                  DO 10 J=1,NN
0033              10 WRITE(2,11)XXC(J)
0034              11 FORMAT(2X,D15.5)
0035                 GO TO 101
0036                 STOP
0037                 END
```

END OF SEGMENT, LENGTH 17A, NAME JOB

```
0038                 SUBROUTINE PROFIL(M,N,XC,XXC,FV)
0039                 DIMENSION FV(10)
0040                 DIMENSION XC(11),XXC(11 ),A(10, ),B(11 ),C(11 ,11)
0041                 DIMENSION BFF(5),BMP(5),BMF(5), T(5)
0042                 DIMENSION X(12),XX (12)
0043                 DOUBLE PRECISION XC,XXC,A,B1,C, FF, MP, F, I, ,XXC,XIN,YI
0044                 DOUBLE PRECISION D,G, LF
0045                 COMMON XIN,YIN,D,G, LF
0046           C
0047           C      K=NUMBER OF STAGES
0048           C
0049                 K=M/2
0050                 DO 1  I=1,2*K
0051                 B1(I)=0.00
0052                 DO 1  J=1,2*K+2
0053                 A(I,J)=0.00
0054              1  C(I,J)=0.00
0055                 DO 11 I=1,K
0056                 B T(I)=0.01
0057                 BFF(I)=0.00
0058                 BMP(I)=0.00
0059              11 BMF(I)=0.00
0060                 IF(FV(2) .EQ. 1.)GO TO 2
0061                 BFF(1)=XC(1)
0062                 B X( )=XC(2)
0063                 BMF(1)=XC(2)
0064                 FF( )=FF(1)
0065                 FF( )= FF(1)
0066                 FF( )=FF(1)
0067                 FF(5)=FF(1)
0068                 X( )= X(2)
0069                 X( )= X(2)
0070                 X( )= X(3)
0071                 X( )= X(3)
0072                 X( )= X(1)
0073                 X( )= X(1)
0074                 GO TO 3
0075              2  IF(FV(2) .EQ. 1.)GO TO 20
0076                 FF( )= X(1)
0077                 FF( )= X(2)
0078                 FF( )= X(2)
0079                 FF( )=X(3)
0080                 FF( )= X(3)
```

```
      BMR(2)=XC(6)
      BMR(3)=XC(7)
      BMR(4)=XC(8)
      BMR(5)=XC(9)
      BME(1)=XC(10)
      BME(2)=XC(11)
      BME(3)=XC(12)
      BME(4)=XC(13)
      GO TO 300
   22 IF(FV(2) .NE. 1.)GO TO 230
      EFF(1)=XC(1)
      EFF(2)=XC(2)
      EFF(3)=XC(3)
      EFF(4)=XC(4)
      EFF(5)=XC(5)
      EFF(6)=XC(6)
      EFF(7)=XC(7)
      BMR(1)=XC(8)
      BMR(2)=XC(9)
      BMR(3)=XC(10)
      BMR(4)=XC(11)
      BMR(5)=XC(12)
      BMR(6)=XC(13)
      BME(1)=XC(14)
      BME(2)=XC(15)
      BME(3)=XC(16)
      BME(4)=XC(17)
      BME(5)=XC(18)
      BME(6)=XC(19)
      GO TO 300
  230 IF(FV(2) .NE. 2.)GO TO 240
      DO 5  J=1,K
    5 EFF(J)=XC(J)
      II=1
      DO 6  J=K+1,17
      II=II+1
    6 BMR(II)=XC(J)
      JJ=0
      DO 7  J=2*K,25
      JJ=JJ+1
    7 BME(JJ)=XC(J)
      DO 8  J=1,K
    8 WRITE(2,82)EFF(J),BMR(J),BME(J)
   82 FORMAT(1X,3D15.8)
      GO TO 300
  240 STOP
  300 CONTINUE
      WRITE(2,26)XIN,FIN,D,G,ALF,A,E(1),E(2)
   26 FORMAT(///1X,5D15.5,I10,2F10.2)
      DO 12 I=1,K-1
   12 B(I)=ALF*(1.+BMR(I)+BMR(I+1))/(D*(1.+BME(I-1)+BME(I)))
      DO 13 K1=2,K-1
      A(2*K1,2*K1-2)=ALF*(1.+BME(K1))
      A(2*K1-1,2*K1-2)=(1.-EFF(K1))*(1.+
      B(2*K1,2*K1-1)=BMR(K1-1)
      A(2*K1-1,2*K1-1)=
      A(2*K1,2*K1)=-ALF*(1.+BME(K1)+
      A(2*K1-1,2*K1)=-(1.+
      A(2*K1-1,2*K1)=(2*K1-1,2*K1)+
      A(2*K1,2*K1+1)=-(1.+
      A(2*K1-1,2*K1+1)=EFF(K1)*(1.+
      A(2*K1,2*K1-1)=
      A(2*K1-1,2*K1-1)=(1.-
      A(2*K1,2*K1+1)=
   13 CONTINUE
```

```
0147                BET(1)=ALF*(1.+BMR(2))/(D*(1.+BME(1)))
0148                A(2,1)=ALF
0149                A(2,2)=-ALF*(1.+BMR(2))
0150                A(2,3)=-(1.+BME(1))
0151                A(2,4)=ALF*BMR(2)
0152                A(2,5)=(1.+BME(1))
0153                A(1,1)=1.-EFF(1)
0154                A(1,2)=-(1.+BMR(2))*(1.+(1.-EFF(1))*BET(1))/(1.+BET(1))
0155                A(1,3)=EFF(1)*(1.+BMR(2))/(D*(1.+BET(1)))
0156                A(1,4)=(1.-EFF(1))*BMR(2)
0157          C     ELEMENTS A-MATRIX FOR LAST STAGE
0158                BET(K)=ALF*(1.+BMR(K))/(D*(1.+BME(K-1)))
0159                A(2*K,2*K-2)=ALF*(1.+BMR(K))
0160                A(2*K,2*K-1)=BME(K-1)
0161                A(2*K,2*K)=-ALF*(1.+BMR(K))
0162                A(2*K,2*K+1)=-(1.+BME(K-1))
0163                A(2*K,2*K+2)=1.
0164                A(2*K-1,2*K-2)=(1.-EFF(K))*(1.+BMR(K))
0165                A(2*K-1,2*K-1)=0.
0166                A(2*K-1,2*K)=-(1.+BMR(K))*(1.+(1.-EFF(K))*BET(K))/(1.+BET(K))
0167                A(2*K-1,2*K+1)=EFF(K)*(1.+BMR(K))/(D*(1.+BET(K)))
0168          C     ELEMENTS OF COLUMN VECTOR B
0169                J=-1
0170                DO 22 I=1,K
0171                J=J+2
0172             22 B1(J)=A(J,J+2)*S
0173          C     IF FV(1) WAS SET EQUAL 1 THE CALCULATION PROCEED ACCORDING
0174          C     WITH OBJ. FUNCTION  SUM(XIEXP -IAV(I)* )**A . (I.E.
0175          C     REQUIRE MODIFICATIONS TO A-MATRIX TO CONFORM A SQUARE MATRIX AND
0176          C     MODIFICATIONS TO B-VECTOR
0177                B1(1)=B1(1)-A(1,1)*XIN
0178                B1(2)=-ALF*XIN
0179                B1(2*K)=-YIN
0180                DO 100 I=1,2*K
0181                DO 100 J=1,2*K
0182            100 C(I,J)=A(I,J+1)
0183                CALL SOLLEQ(K,C,B1,XXC)
0184                RETURN
0185                END

      END OF SEGMENT, LENGTH  2716, NAME  PROFIL

0186                SUBROUTINE SOLLEQ(K,Z,B1,XXC)
0187          C
0188          C     SOLUTION OF A SET OF LINEAR EQUATIONS -CROUT FACTORIZATION
0189          C
0190                DOUBLE PRECISION Z,B1,XXC
0191                DIMENSION Z(1,1),B1(1),XXC(1)
0192                DIMENSION A(10,10),B(10),C(10),AA(10,10),IKS1(20),IKS2(20)
0193                N=2*K
0194                IA=2*K
0195                IAA=2*K
0196                IFAIL=0
0197                DO 1 I=1,N
0198                B(I)=B1(I)
0199                DO 1 J=1,N
0200             1  A(I,J)=Z(I,J)
0201                CALL F O F DF(A,I,,,C,B,IA,IAA,IKS1,IKS2,IFAIL)
0202                IF(IFAIL .EQ. 0)GO TO 2
0203                WRITE(6,IFAIL
0204             5  FORMAT(2H= E=0  IFAIL = ,I)
0205                STOP
0206             2  DO 3 I=1,N
0207             3  XXC(I)=C(I)
```

```
END OF SEGMENT, LENGTH   1[illegible], [illegible]   [illegible]

0210              FINISH

END OF COMPILATION -  NO [illegible]

    S/C SUBFILE   :      50 BUCKETS USED
  FIRST WORKFILE  :      48 BUCKETS USED
 SECOND WORKFILE  :      48 BUCKETS USED
CONSOLIDATED BY XPCK 12H    DATE    23/11/81   TIME 11/44/03

        *SHORTLIST

        *IN ED (FORTSEMICOMP)

        *LIB ED (SUBGROUPNAGF.SUBROUTINES)

        *LIB ED (SUBGROUPSRF4.SUBROUTINES)

        *WORK ED (FORTWORKFILE)

        ****

PROGRAM FXXX
EXTENDED DATA (22AM)
COMPACT PROGRAM (DBM)
CORE              12928

DISPLAY : TRACE 2 USED
 ALLOT        *CRO     N
 0.27: MONITOR
 ALLOT        *LPO     N
 0.28: MONITOR
 11.47.54 FREE *CRO ,50 TRANSFERS
 11.47.54 FREE *LPO ,134 TRANSFERS
 0.39 DELETED : 00
 11.47.55 0.39 DELETED,CLOCKED 0.27
 DISPLAY: UAFORTRAN: NORMAL EXIT
 11.47.56 0.39 FINISHED : 2 LISTFILES
 11.47.56 JOBTIME USED 40 ; MAXIMUM CORE USED 32576
 11.47.56 JOB UNITS 88

*BBBBBBBBBBBBBBBBBBBBBBBBBBBBBBBBBBBBBBBBBBBBBBBBBBBBBBBBBBBBBBBBBBBB*
*BBEEBBE                         [illegible]*
*BBBBBBB      NUMBER OF PAGES    5     [illegible]*
*EBBBB35
*BBBBBBBBBBBBBBBBBBBBBBBBBBBBBBBBBBBBBBBBBBBBBBBBBBBBBBBBBBBBBBBBBBBB*
```

APPENDIX 3

Computer Program to Calculate Concentration Profiles - Diffusion Model

```
#LISTING OF :ECP2204.CONTPROF(/B16C)   PRODUCED ON 20OCT80 AT 13.14.06
#68.63EC AT ASTON     IN :ECP2204.CONTPROF* ON 20OCT80 AT 13.17.02 USING  U15

DOCUMENT     :ECP2204.CONTPROF(/B16C)

 STARTED :ECP2204,CONTPROF,20OCT80 13.06.20 TYPE: BACK  10 ; STREAM A ; PRIORITY 2 ; ENTERED WELL 20OCT80 12.47.00
13.06.21* JOB :ECP2204,CONTPROF
 13.06.23 JOB IS NOW FULLY STARTED
13.06.23* CONTPROF
 13.06.23* UAFORTRAN
ENTERING :MACROS.UAFORTRAN(223/)
 13.06.24*        TA A6,CM,JL

 FORTRAN COMPILATION BY #XFIV MK 3B     DATE  20/10/80  TIME  13/07/40


 0000                    LIST (LP)
 0001                    PROGRAM (FXXX)
 0002                    INPUT  1 = CR0
 0003                    INPUT  3 = TR0
 0004                    INPUT  5 = CP1
 0005                    OUTPUT 2 = LP0/132
 0006                    OUTPUT 6 = LP1/132
 0007
 0008                    COMPRESS INTEGER AND LOGICAL
 0009                    COMPACT PROGRAM
 0010                    EXTENDED DATA
 0011                    TRACE 2
 0012                    END


 0013                     TRACE 1
 0000                      MASTER EX1
 0001                     DIMENSION TLAND(4),B(4),AA(4),DA1(4)
 0002                     DIMENSION X(11),Y(11),Z(11),A(7,5),B(2,5)
 0003                   10 READ(1,3)F,PER,PEE,TNTU
 0004                    3  FORMAT(4F10.5)
 0005                      IF(F .EQ.0.0)GO TO 15
 0006                      CALL COEF(PER,PEE,TNTU,F,TLAND,B,AA,2,B,DA1)
 0007                      DO 20 K=1,11
 0008                      N=K
 0009                      Z(K)=(K-1.)/10.
 0010                      X(K)=0.
 0011                      Y(K)=0.
 0012                      DO 20 N=1,4
 0013                      X(K)=X(K)+A(N)*EXP(TLAND(N)*Z(K))
 0014                   20 Y(K)=Y(K)+A(N)*AA(N)*EXP(TLAND(N)*Z(K))
 0015                      WRITE(2,4)F,PER,PEE,TNTU
 0016                    4  FORMAT(//4X,4F10.4//)
 0017                      WRITE(2,62)
 0018                   62 FORMAT(//20X,21HCONCENTRATION PROFILE//)
 0019                      DO 30 I=1,11
 0020                   30 WRITE(2,60)Z(I),X(I),Y(I)
 0021                   60 FORMAT(1H ,20X,3F10.4)
 0022                      GO TO 10
 0023                   15  STOP
 0024                      END


END OF SEGMENT, LENGTH   1A2, NAME  EX1

 0025                    SUBROUTINE COEF(P1,P2,P3,P4,P5,P6,P7,P8,P9)
```

```
      SUBROUTINE COEF(P1,P2,T,F,TL,A,AA,B,D,DA1)
      DIMENSION TL(4),A(4),AA(4),B(3,5),D(3,5),DA1(4)
      ALF=P1-P2
      BET=T*P1+P1*P2+T*P2*F
      GAM=(1.-F)*T*P1*P2
      P=(ALF/3.)**2+BET/3.
      Q=(ALF/3.)**3+ALF*BET/6.+GAM/2.
      TL(1)=0.0
      S=ALF/3.
      SS=2.*SQRT(P)
      U=ACOS(Q/(P**1.5))
      TL(2)=S+SS*COS(U/3.)
      TL(3)=S+SS*COS(U/3.+3.1416*2./3.)
      TL(4)=S+SS*COS(U/3.+3.1416*4./3.)
      DO 6 I=1,4
    6 AA(I)=1.+TL(I)/T-TL(I)**2/(T*P1)
      DO 80 I=1,3
      DO 80 J=1,3
       NP=J
      GO TO (1,2,5),NP
    1 B(J,I)=1.-TL(I+1)/P1
      D(J+2,I)=(1.+TL(I+1)/P2)*AA(I+1)*EXP(TL(I+1))
      GO TO 80
    2 B(J,I)=TL(I+1)*AA(I+1)
      D(J-1,I)=B(J,I)
      GO TO 80
    5 B(J,I)=TL(I+1)*EXP(TL(I+1)-TL(3))
      D(J-1,I)=B(J,I)
   80 CONTINUE
C  ADD COLUMNS 4 AND 5 TO B AND D
      DO 30 I=1,2
      M=3+I
      DO 30 J=1,3
      B(J,M)=B(J,I)
   30 D(J,M)=D(J,I)
C  EVALUATE THE DETERMINANTS
      X1=0.
      X2=0.
      X3=0.
      X4=0.
      DO 40 I=1,3
      S2=1.
      S3=1.
      S4=1.
      S1=1.
      K=I
      K=2+I
      DO 35 J=1,3
      S1=S1*B(J,M)
      S2=S2*B(J,K)
      S3=S3*D(J,M)
      S4=S4*D(J,K)
      K=K+1
   35 K=K-1
      X1=X1+S1
      X2=X2+S2
      X3=X3+S3
      X4=X4+S4
   40 CONTINUE
      A(1)=X3-X4
      A=DA1(1)-(X1-X2)
```

```
0080                    X2=X2+S2
0081                    X3=X3+S3
0082                    X4=X4+S4
0083                 40 CONTINUE
0084                    DA1(1)=X3-X4
0085                    DA=DA1(1)-(X1-X2)
0086                    DA1(2)=-(B(2,2)*B(3,3)-B(2,3)*B(3,2))
0087                    DA1(3)=B(2,1)*B(3,3)-B(2,3)*B(3,1)
0088                    DA1(4)=-(B(2,1)*B(3,2)-B(2,2)*B(3,1))
0089                    DO 50 I=1,4
0090                 50 A(I)=DA1(I)/DA
0091                    RETURN
0092                    END

END OF SEGMENT, LENGTH   512, NAME  COEF

0093                    FINISH

END OF COMPILATION -  NO ERRORS

      S/C SUBFILE  :     15 BUCKETS USED

CONSOLIDATED BY XPCK 10H    DATE    20/10/80   TIME 13/11/20

          *SHORTLIST

          *IN ED (F.RTSE*ICOMP)

          *LIB ED (SUBGR.UPSRF4_SUBROUTINES)

          *WORK ED (FORT.ORKFILE)

          ****

  PROGRAM FXXX
EXTENDED DATA (224K)
  COMPACT PROGRAM (24K)
CORE                6080

  ALLOT       *CPO     N
0.15: MONITOR
  ALLOT       *LPO     N
0.15: MONITOR
  13.13.57 FREE *CR  ,7 TRANSFERS
13.13.57 FREE *LPO ,121 TRANSFERS
  0.17 :DELETED : 00
13.13.57 0.17 DELETED,CLOCKED 0.06
  DISPLAY: UAFORTRS.: NO MAL EXIT
13.14.01 0.16 FINISHED : 2 LISTFILES
  13.14.01 JOBTIME USED 00 ; MAXIMUM CORE USED 1757
13.14.01 JOB UNITS 34
```

APPENDIX 4

Parameter Estimation Computer Program

Compartments with Backflow Model

ECP2200 :ECP2200.MOPJMGF

#LISTING OF :ECP2200.JULIO(17) PRODUCED ON 27MAY 1 AT 11.40.20

#G8.63EG AT ASTON IN :ECP2200.MOPJMGF' ON 27MAY81 AT 10.05.01 USING U15

DOCUMENT JULIO

```
JOB :ECP2204,STAG1410,JD(JT1200)
UAFORTRAN LIB NAGF,LINES 3000
      MASTER JCF
C     SCHEIBAL COLUMN-CONC.PROFILE ANALYSIS
C     PERFECT MIXING CELLS WITH BACKFLOW MODEL
C     STAGE EFFICIENCY TYPE
C     AXIAL VARIATION OF BACKFLOW COEFF. AND STAGE
C     EFFICIENCIES ARE ESTIMATED BY THIS MODEL
C     OPTIMAZATION METHOD-MARQUARDT ALGORITHM
C     OBJECTIVE FUNCTION  SUM(A*X-B)**2
      DIMENSION F(130),A(10,10),AC(10,10),XXE(10),B(10),Z(10)
      DIMENSION Y(10),HV(10), MIN(10),MAX(10)
      DIMENSION FV(10),DV(10)
      DOUBLE PRECISION F,A,AC,XXE,B,Z,Y,EV,MIN,MAX,FV,DV,XIN,YIN
      DOUBLE PRECISION D,G,ALF,FNC,FLT,TAL,HS,MIN,PH,EPS
      EXTERNAL FUNC
      COMMON XXE,XIN,YIN,D,G,ALF
C
      NI=1
      NO=2
C
C     READ IN NUMBER OF EQUATIONS & UNKNOWNS
      READ(NI,011)NN,KK
  011 FORMAT(2I10)
C
C     READ IN LIMITS ON VARIABLES
C
      READ(NI,012)(MIN(J),J=1,KK)
      READ(NI,012)(MAX(J),J=1,KK)
C
  101 CONTINUE
C     READ IN INITIAL GUESSES OF PARAMETERS TO BE ESTIMATED
C
      READ(NI,012)(B(J),J=1,KK)
  012 FORMAT(3D.4)
      IF(B(1) .EQ. 0.0)GO TO 1 00
C
C     READ IN INDEPENDENT VARIABLES
      READ(NI,013)(XXE(J),J=1,NN)
  013 FORMAT(2D10.4/5D10.0)
C
      READ(NI,014)XIN,YIN,D,...
  014 FORMAT(4...)
C
C     ...
C     DO ...
      ...
    ...
      ...
C
      END...
```

```
      FNU=0.D0
      FLA=0.D0
      TAU=0.D0
      EPS=0.D0
      PHMIN=0.D0
      I=0
      KD=KK
      DO 100 J=1,KK
      BV(J)=1.D0
  100 CONTINUE
      ICON=KK
      ITER=0
      IP=0
      WRITE(NO,015)
  015 FORMAT(1H1,10X,27HSOLVE REGRESSION ALGORITHM)
      SET FV(1)=1 IF OBJ. FUNCTION SUM(XEXP. - XCALC)**2 IS REQUIRED
C     FOR THIS CASE DEPENDENT VARIABLE Y(J) IS EQUAL TO XXE(J)(EXP.. CONC.PROF.
C     CALCULATED PROFILE US OBTAINED BY SOLVING  INV(A)*B
      READ(NI,017)FV(1)
  017 FORMAT(F10.0)
      IF(FV(1) .NE. 1.)GO TO 200
      DO 2 L=1,NN
    2 Y(L)=XXE(L)
C
  200 CALL BSOLVE(KK,B,NN,Z,Y,PH,FNU,FLA,TAU,EPS,PHMIN,I,ICON,FV,DV,V,
     1BMIN,BMAX,P,FUNC,DERIV,KD,A,AC,GAMM)
C
      ITER=ITER+1
      IF(ITER .GT. 100) GO TO 400
      IF((ITER-IP) .NE.  2) GO TO 116
      WRITE(NO,001)ICON,PH,ITER
  001 FORMAT(/,2X,6HICON = ,I3,4X,5HPH = ,D25.1 ,4X,16HITERATION NO. =
     *,I3)
      WRITE(NO,112)FLA,GAMM
  112 FORMAT(1X,6H FLA= ,D12.5,7X,7H GAMM= ,D10.5)
      WRITE(NO,114)(B(J),J=1,KK)
  114 FORMAT(/,2X,10H BASE POINT ,/D16.6)
      WRITE(NO,115)(Z(J),J=1,NN)
  115 FORMAT(1X,10D10.5)
      IP=ITER
  116 IF(ICON)10,300,200
   10 IF(ICON+1)20,60,200
   20 IF(ICON+2)30,70,200
   30 IF(ICON+3)40,70,200
   40 IF(ICON+4)50,90,200
   50 GO TO 75
   60 WRITE(NO,004)
  004 FORMAT(//,2X,32HNO FUNCTION IMPROVEMENT POSSIBLE)
      GO TO 300
   70 WRITE(NO,005)
  005 FORMAT(//,2X,2 MORE UNKNOWN THAN FUNCTIONS )
      GO TO 300
   90 WRITE(NO,006)
  006 FORMAT(//,2X,24HTOTAL VARIABLES  ARE ZERO)
      GO TO 300
   95 WRITE(NO,007)
  007 FORMAT(//,2X,/,2HEXPLANATION  WITH  ,
     1LA=1 FACT =(FLA) TITLE LA= )
      GO TO
      FORMAT(//,
      FORMAT(//,
      FORMAT(//,
      FORMAT(//,
      GO TO
```

```
      WRITE(NO,003)J,B(J)
  003 FORMAT(/,2X,2HB(,I2,4H) = ,D16.8)
  400 CONTINUE
      GO TO 101
 1000 STOP
      END
      SUBROUTINE FUNC(KK,B,NN,Z,FV)
      DIMENSION FV(10)
      DIMENSION XXE(12),Z(25),B(25),XXC(25)
      DOUBLE PRECISION XXE,Z,B,XXC,FV,XIN,YIN,D,G,ALF
      COMMON XXE,XIN,YIN,D,G,ALF
      CALL PROFIL(NN,KK,B,XXC,FV)
      DO 100 JJ=1,NN
      Z(JJ)=XXC(JJ)
  100 CONTINUE
      RETURN
      END
C
      SUBROUTINE PROFIL(M,N,XC,XXC,FV)
      DIMENSION FV(10)
      DIMENSION XC(10),XXC(10),A(10,12),E1(10),C(10,12)
      DIMENSION EFF(5),BMR(5),BME(5),BET(5)
      DIMENSION X(12),XXE(12)
      DOUBLE PRECISION XC,XXC,A,E1,C,EFF,BMR,BME,BET,X,XXE,XIN,YIN
      DOUBLE PRECISION D,G,ALF
      COMMON XXE,XIN,YIN,D,G,ALF
C
C     INPUT NUMBER OF STAGES K
      K=5
      DO 10 I=1,2*K
      E1(I)=0.D0
      DO 10 J=1,2*K+2
      A(I,J)=0.D0
   10 C(I,J)=0.D0
      DO 11 I=1,K
      BET(I)=0.D0
      EFF(I)=0.D0
      BMR(I)=0.D0
   11 BME(I)=0.D0
      EFF(1)=XC(1)
      BMR(2)=XC(2)
      BME(1)=XC(3)
      EFF(2)=EFF(1)
      EFF(3)=EFF(1)
      EFF(4)=EFF(1)
      EFF(5)=EFF(1)
      BMR(3)=BMR(2)
      BMR(4)=BMR(2)
      BMR(5)=BMR(2)
      BME(2)=BME(1)
      BME(3)=BME(1)
      BME(4)=BME(1)
      DO 12 I=2,K-1
   12 BET(I)=ALF*(1.+BMR(I)+[illegible](I+1))/([illegible]*(1.+[illegible](I-1)+BME(I)))
      DO 20 K1=[illegible],K-1
      A(2*K1,2*K1-[illegible])=ALF*(1.+[illegible]-1))
      A(2*K1-1,[illegible]1-[illegible])=(1.-[illegible]F[illegible])*(1.-[illegible](K1))
      A(2*K1,[illegible]K1-1)=[illegible]1-1
      A([illegible]K1-1,2*K1-1)=[illegible]
[illegible]
```

```
      20 CONTINUE
C       ELEMENTS A-MATRIX FOR FIRST STA
        BET(1)=ALF*(1.+BMR(2))/(D*(1.+B
        A(2,1)=ALF
        A(2,2)=-ALF*(1.+BMR(2))
        A(2,3)=-(1.+BME(1))
        A(2,4)=ALF*BMR(2)
        A(2,5)=(1.+BME(1))
        A(1,1)=1.-EFF(1)
        A(1,2)=-(1.+BMR(2))*(1.+(1.-EFF(1))*BET(1))/(1.+BET(1))
        A(1,3)=EFF(1)*(1.+BMR(2))/(D*(1.+BET(1)))
        A(1,4)=(1.-EFF(1))*BMR(2)
C       ELEMENTS A-MATRIX FOR LAST STAGE
        BET(K)=ALF*(1.+BMR(K))/(D*(1.+BME(K-1)))
        A(2*K,2*K-2)=ALF*(1.+BMR(K))
        A(2*K,2*K-1)=BME(K-1)
        A(2*K,2*K)=-ALF*(1.+BMR(K))
        A(2*K,2*K+1)=-(1.+BME(K-1))
        A(2*K,2*K+2)=1.
        A(2*K-1,2*K-2)=(1.-EFF(K))*(1.+BMR(K))
        A(2*K-1,2*K-1)=0.
        A(2*K-1,2*K)=-(1.+BMR(K))*(1.+(1.-EFF(K))*BET(K))/(1.+BET(K))
        A(2*K-1,2*K+1)=EFF(K)*(1.+BMR(K))/(D*(1.+BET(K)))
C       ELEMENTS OF COLUMN VECTOR
        J=-1
        DO 22 I=1,K
        J=J+2
     22 B1(J)=A(J,J+2)*G
C       IF FV(1) WAS SET EQUAL 1 THE CALCULATION PROCEED ACCORDING
C       WITH OBJ. FUNCTION  SUM(EXP -INV(A)*B)**2. THIS
C       REQUIRE MODIFICATIONS TO A-MATRIX TO CONFORM A SQUARE MATRIX AND
C       MODIFICATIONS TO B-VECTOR
        IF(FV(1) .NE. 1.) GO TO 23
        B1(1)=B1(1)-A(1,1)*XIN
        B1(2)=-ALF*XIN
        B1(2*K)=-XIN
        DO 100 I=1,2*K
        DO 100 J=1,2*K
    100 C(I,J)=A(I,J+1)
        CALL SOLLEQ(K,C,B1,XC)
        GO TO 145
     23 DO 140 I=1,2*K+2
        IF(I .EQ. 1)GO TO 121
        IF(I .EQ. 2*K+2)GO TO 122
        X(I)=XXB(I-1)
        GO TO 140
    121 X(I)=XIN
        GO TO 140
    122 X(I)=0.
    140 CONTINUE
C       CALCULATE RESIDUAL VECTOR  A*X-
        DO 130 I=1,2*K
        XXC(I)=0.
        DO 130 J=1,2*K+2
    130 XXC(I)=XXC(I)+A(I,J)*X(J)
        DO 135 I=1,2*K
    135 XXC(I)=XXC(I)-B1(I)
        IF(FV(1)
        CALL
    115 FV=
        F(1)=
    145
C
C
```

```
      BY CROUT FACTORIZATION METHOD (SLS FACTF)
      DOUBLE PRECISION Z,B1,XXC
      DIMENSION Z(10,10),B1(10),XXC(10)
      DIMENSION A(10,10),B(10),C(10),AA(10,10),KK1(20),KK2(20)
      N=10
      IA=10
      IAA=10
      IFAIL=0
      DO 1 I=1,N
      B(I)=B1(I)
      DO 1 J=1,N
    1 A(I,J)=Z(I,J)
      CALL F04ATF(A,IA,B,N,C,AA,IAA,KK1,KK2,IFAIL)
      IF(IFAIL .EQ. 0)GO TO 20
      WRITE(2,5)IFAIL
    5 FORMAT(25H ERROR IN SOLLEQ IFAIL = ,I2)
      STOP
   20 DO 2 I=1,N
    2 XXC(I)=C(I)
      RETURN
      END
      SUBROUTINE HSOLVE(KK,B,NN,Z,Y,PM,ENU,FLA,TAU,EPS,
     1PHMIN,I,ICON,FV,DV,EV,EMIN,HMAX,P,FUNC,VERIO,KO,A,AC,GAMM)
      DIMENSION B(10),Z(10),Y(10),DV(1 ),EMIN(10),HMAX(10)
      DIMENSION P(120),A(10,1 ),AC(10,12),F(10),FV(10),DV(10)
      DOUBLE PRECISION B,Z,Y,PM,ENU,FLA,TAU,EPS,PHMIN,DV,EV,EMIN
      DOUBLE PRECISION HMAX,P,A,AC,GAMM,C,C1,C2,FL,DN,DD
      DOUBLE PRECISION  COSG,ARCOS,PHI

      K=KK
      N=NN
      KP1=K+1
      KP2=KP1+1
      KB11=K*(
      KB12=K*11+K
      KZI=KB1(+K
      IF(ENU .LE. 0.)ENU=10.000
      IF(FLA .LE. (.)FLA=0.01
      IF(TAU .LE. 0.)TAU=.00100
      IF(EPS .LE. 0.)EPS=EXP(A*F( 0)
      IF(PHMIN .LE. 0.)PHMIN= .01
  120 KS=0
  130 DO 160 I1=1,K
  160 IF(DV(I1) .NE. 0.)KS=KS+1
      IF(KS .GT. 0) GO TO 170
  162 ICON=-3
  163 GO TO 2120
  170 IF( .NE. K) GO TO 500
  180 ICON=-2
  190 GO TO 2120
  500 I1=1
  550 IF(I .GT. 0) GO TO 1550
  555 DO 560 J1=1,K
      J2=KB11+J1
      P(J2)= (J1)
      J3=KB12+J1
  560 (J3)=(J1)+1.
      GO TO 1
   57 IF(I .GT. . . . . .
      DO 2, J1=1,
      J1=(J1-1)*
      IF( (J1,J
    1 CONTINUE
      IF(J .GT. 1 . . -1)
      (J1)=1.
      DO 2 J=1,
```

```
      J3=KBI1+J2
  606 P(J3)=B(J2)
      J3=KBI1+J1
      J4=KBI2+J1
      DEN=0.001*AMAX1(P(J4),A S(P(J3)))
      IF (P(J3) + DEN .LE. BMAX(J1)) GO TO 55
      P(J3)=P(J3) - DEN
      DEN=-DEN
      GO TO 56
   55 P(J3)=P(J3) + DEN
   56 CALL FUNC(K,P(KBI1+1),N,P(N1+1),FV)
      DO 610 J2=1,N
      JB=J2+N1
  610 P(JB)=(P(JB) - Z(J2))/DEN
  620 CONTINUE
C
C     SET UP CORRECTION EQUATIONS
C
  625 DO 725 J1=1,K
      N1=(J1-1)*N
      A(J1,KP1)=0.
      IF(PV(J1))630,692,630
  630 DO 640 J2=1,N
      N2= N1+J2
  640 A(J1,KP1)=A(J1,KP1)+P(N2)*(Y(J2)-Z(J2))
  650 DO 680 J2=1,K
  660 A(J1,J2)=0.
  665 N2 = (J2-1)*N
  670 DO 680 J3=1,N
  672 N3=N1+J3
  674 N4=N2+J3
  680 A(J1,J2)=A(J1,J2)+P(N3)*P(N4)
      IF(A(J1,J1) .GT. 1.E-20) GO TO 725
  692 DO 694 J2=1,KP1
  694 A(J1,J2)=0.
  695 A(J1,J1)=1.0
  725 CONTINUE
      GN=0.
      DO 729 J1=1,K
  729 GN=GN + A(J1,KP1)**2
C
C     SCALE CORRECTION EQUATIONS
C
      DO 726 J1=1,K
  726 A(J1,KP2) = SQRT(A(J1,J1))
      DO 727 J1=1,K
      A(J1,KP1) = A(J1,KP1)/A(J1,KP2)
      DO 727 J2=1,K
  727 A(J1,J2) = A(J1,J2)/(A(J1,KP2)*A(J2,KP2))
  730 FL=FLA/FNU
      GO TO 810
  800 FL=FNU*FL
  810 DO 840 J1=1,K
  820 DO 830 J2=1,KP1
  830 AC(J1,J2)= A(J1,J2)
  840 AC(J1,J1)=AC(J1,J1) + FL
C
C     SOLVE CORRECTION EQUATIONS
C
      D[illegible] L1=1,[illegible]
      L[illegible]=L1+1
      [illegible]
   [illegible] AC(L1,[illegible]
      D[illegible]
      IF(L1-[illegible]
      D[illegible]
```

```
      925 AC(L3,L4)=AC(L3,L4)-AC(L1,L4)*AC(L3,L1)
      930 CONTINUE
C
      DN=0.
      DG=0.
      DO 1028 J1=1,K
      AC(J1,KP2) = AC(J1,KP1)/A(J1,KP2)
      J2= KBI1 + J1
      P(J2) = AMAX1(GMIN(J1),AMIN1(GMAX(J1),B(J1)+AC(J1,KP2)))
       DG = DG + AC(J1,KP2)*A(J1,KP1)*A(J1,KP2)
      DN = DN + AC(J1,KP2)*AC(J1,KP2)
 1028 AC(J1,KP2)=P(J2)-B(J1)
      COSG = DG/SQRT(DN*GN)
      JGAM = 0
      IF(COSG) 1100,1110,1110
 1100 JGAM = 2
      COSG = -COSG
 1110 CONTINUE
      COSG = AMIN1(COSG,1.0)
      GAMM=ARCOS(COSG)*180./(3.1415926)
      IF(JGAM .GT. 0) GAMM=180. -GAMM
 1030 CALL FUNC(K,P(K+I1+1),N,P(KZI+1),FV)
 1500 PHI = 0.
      DO 1520 J1=1,N
      J2=KZI + J1
 1520 PHI=PHI+(P(J2)-Y(J1))**2
      IF(PHI .LT. 1.E-15)GO TO 3000
      IF(I .GT. 0) GO TO 1540
 1521 ICON = K
      GO TO 2110
 1540 IF(PHI .GE. FH) GO TO 1550
C
C     EPSILON TEST
C
 1200 ICON=0
      DO 1220 J1=1,K
      J2=KBI1+J1
 1220 IF(ABS(AC(J1,KP2))/(TAU + ABS(P(J2))) .GT. EPS) ICON=ICON+1
      IF(ICON .EQ. 0) GO TO 1400
C
C     GAMMA LAMBDA TEST
C
      IF(FL .GT. 1.0 .AND. GAMM .LT. 90.0) ICON =-1
      GO TO 2105
C
C     GAMMA EPSILON TEST
C
 1400 IF(FL .GT. 1.0 .AND. GAMM .LT. 90.0) ICON=-1
      GO TO 2105
C
 1550 IF(I1-2)1551,1551,2310
 1551    I1=I1+1
         GO TO (1552,1553,1554),I1
 2310 IF(FL .LT. 1.0E+7) GO TO 1520
 1320 ICON=-1
C
 2105 FLAMFL
      DO 2110 J=1,
      J1=K+I1+J
      P(J1) = P(J)
 2110 P(J)=P(J1)
      I=I+1
```

```
      2120 RETURN
      3000 ICON=0
           GO TO 2105
C
           END
           FUNCTION ARCOS(Z)
C
           DOUBLE PRECISION X,Z,ARCOS
            X=Z
            KEY=0
           IF(X .LT. (-1.)) X=-1
           IF(X .GT. 1.) X=1.
           IF(X .GE. (-1.) .AND. X .LT. 0.) KEY=1
           IF(X .LT. 0.) X=ABS(X)
           IF(X .EQ. 0.) GO TO 10
           ARCOS=ATAN(SQRT(1.-X*X)/X)
           IF(KEY .EQ. 1) ARCOS=3.1415926535 -ARCOS
           GO TO 999
        10 ARCOS=1.5707963
       999 RETURN
           END
           FINISH
             1                    3
    -10.00   -10.00   -10.00
     10.00    10.00    10.00
   0.71000   0.4200  0.00100
   0.0744900 0.0546000 0.0064700 0.0009100 0.0004900
   0.0394500 0.0305500 0.0126500 0.0031600 0.0011400
   0.0029400       0.000 0.0009200 -0.0002700
     1.
   0.62000   0.4400  0.44000
   0.0650400 0.0714400 0.0494000 0.0300000 -0.0044000
   0.0479700 0.0235500 0.0111900 0.0 -0.0015400
   0.0029400       0.000  1.25110  0.
     1.
```

APPENDIX 5

Parameter Estimation Computer Program

Diffusion Model

```
DOCUMENT     :ECP2204.TRIAL(1/@180)

STARTED :ECP2204,TRIAL,23OCT81 12.59.29 TYPE: BACK  IO ; STREAM A ; PRIORITY 2 ; ENTERED WELL 23OCT81 12.59.07
12.59.29* JOB :ECP2204,TRIAL
12.59.29 JOB IS NOW FULLY STARTED
12.59.29* TRIAL
12.59.29* UAFORTRAN LIB NAGF,LINES 3000
ENTERING :MACROS.UAFORTRAN(227/)
12.59.30*          TA AB,CM,JL

FORTRAN COMPILATION BY #XFIV MK 3B     DATE  23/10/81   TIME  12/59/41

0000                    LIST (LP)
0001                    PROGRAM (FXXX)
0002                    INPUT  1 = CR0
0003                    INPUT  3 = TR0
0004                    INPUT  5 = CR1
0005                    OUTPUT 2 = LP0/132
0006                    OUTPUT 6 = LP1/132
0007                    COMPRESS INTEGER AND LOGICAL
0008                    COMPACT PROGRAM
0009                    EXTENDED DATA
0010                    TRACE 2
0011                    END

0012                    TRACE 1
0000                    MASTER JCB
0001          C         SCHEIBAL COLUMN -CONC. PROFILE ANALYSIS
0002          C         CONTINUOUS DIFFERENTIAL AXIAL-MIXING MODEL
0003          C         MODEL PARAMETERS ARE : NTU,RAFIN,TL AND EXTRACT PECLET NUMBERS
0004          C         OPTIMIZATION METHOD - MARQUARDT ALGORITHM
0005          C         VALUE OF FLAG FV(1) IDENTIFY THE OBJECTIVE FUNCTION
0006          C
0007          C         FV(1)=1    OBJ.FUNC. = SUM((Y-X) EXP. -(Y-X)CALC.)**2
0008          C                    OPTIMIZE DIFFERENCE OF THE CONC.-PROFILES
0009          C
0010          C         FV(1)=2    OBJ.FUNC. = SUM(YEXP. - YCALC.)**2
0011          C                    OPTIMIZE THE Y-PROFILE
0012          C
0013          C         FV(1)=3    OBJ.FUNC. = SUM(XEXP. - XCALC.)**2
0014          C                    OPTIMIZE THE X-PROFILE
0015          C
0016          C         IN ALL THIS CASES THE EXP.DATA ARE LABELLED AS Y(J)
0017                    DIMENSION F(130),A(1?,?0),AC(?,?),X(1?)
```

```
      DOUBLE PRECISION BMAX,BMIN,FV,PH,ENU,FLA,TAU,EPS,PHMIN,B,DV,BV,
     COMMON XX,XIN,XOUT,YIN,YOUT,D1,G
     EXTERNAL FUNC
     NI=1
     NO=2
C
C    READ IN NUMBER OF DATA POINTS AND UNKNOWN PARAMETERS
C    READ(NI,011)NN,KK
 011 FORMAT(2I10)
C    READ IN LIMITS ON PARAMETERS
C
     READ(NI,012)(BMIN(J),J=1,KK)
     READ(NI,012)(BMAX(J),J=1,KK)
C
 017 CONTINUE
C
C    READ IN VALUE OF FV(2)=F
     READ(NI,113)FV(2)
C    READ IN VALUE OF FLAG FV(1)
C
     READ(NI,110)FV(1)
 110 FORMAT(F10.5)
C
     IF(FV(1) .EQ. 0.) GO TO 1000
C
C    READ IN INITIAL GUESSES OF PARAMETERS TO BE ESTIMATED
C
     READ(NI,012)(B(J),J=1,KK)
 012 FORMAT(3D10.5)
C
C    READ IN EXP.VALUES ACCORDING WITH SELECTED OBJ. FUNCTION -Y(J)
C    AND THE CORRESPONDING COLUMN HEIGHT-XX
     READ(NI,013)(Y(J),J=1,NN)
     READ(NI,013)(XX(J),J=1,NN)
 013 FORMAT(7D10.5)
C
C
     READ(NI,014)XIN,YIN,XOUT,YOUT,D1,G
 014 FORMAT(6D10.5)
     ENU=0.0D0
     FLA=0.0D0
     TAU=0.0D0
     EPS=0.0D0
     PHMIN=0.0D0
     I=0
     KD=KK
     DO 100 J=1,KK
     DV(J)=1.D0
 100 CONTINUE
     ICON=KK
     ITER=0
     IP=0
     WRITE(NO,015)
 015 FORMAT(1H1,10X,27HDSOLVE REGRESSION ALGORITHM//)
C
 200 CALL DSOLVE(KK,B,NN,Y,PH,ENU,FLA,TAU,EPS,PHMIN,I,ICON,FV,DV,BV,
    1BMIN,BMAX,F,FUNC,DERIV,KD,A,NC,IMM)
C
     ITER=ITER+1
     IF((ITER-IP) .NE. 10) GO TO 111
     WRITE(NO,201)ICON,PH,ITER
 201 FORMAT(//,20X,6HICON =,I2,4X,5HPHI =,D12.7,4X,
    *,I5)
     WRITE(NO,112)FLA,GAMA
 112 FORMAT(1X,24H FLA= ,D12.7,7X,7H GAMA= ,D10.5)
     WRITE(NO,114)(B(J),J=1,KK)
```

```
0086                WRITE(NO,114)(B(J),J=1,KK)
0087            114 FORMAT(/,2X,12H BASE POINT ,/,(2D12.6))
0088                WRITE(NO,115)(Z(J),J=1,NN)
0089            115 FORMAT(1X,7D15.5)
0090                IP=ITER
0091            116 IF(ICON)10,300,200
0092             10 IF(ICON+1)20,60,200
0093             20 IF(ICON+2)30,70,200
0094             30 IF(ICON+3)40,80,200
0095             40 IF(ICON+4)50,90,200
0096             50 GO TO 95
0097             60 WRITE(NO,004)
0098            004 FORMAT(//,2X,32HNO FUNCTION IMPROVEMENT POSSIBLE)
0099                GO TO 300
0100             70 WRITE(NO,005)
0101            005 FORMAT(//,2X,28HMORE UNKNOWS THAN FUNCTIONS )
0102                GO TO 300
0103             80 WRITE(NO,006)
0104            006 FORMAT(//,2X,24HTOTAL VARIABLES ARE ZERO)
0105                GO TO 300
0106             90 WRITE(NO,007)
0107            007 FORMAT(//,2X,79HCORRECTIONS SATISFY CONVERGENCE REQUIREMENTS BUT
                   1LAMDA FACTOR(FLA) STILL LARGE)
0108                GO TO 300
0109             95 WRITE(NO,008)
0110            008 FORMAT(//,2X,20HTHIS IS NOT POSSIBLE)
0111                GO TO 300
0112            300 WRITE(NO,002)
0113            002 FORMAT(//,2X,26HSOLUTIONS OF THE EQUATIONS)
0114                DO 400 J=1,KK
0115                WRITE(NO,003)J,B(J)
0116            003 FORMAT(/,2X,2HB(,I2,4H) = ,D16.8)
0117            400 CONTINUE
0118                GO TO 017
0119           1000 STOP
0120                END
0121

END OF SEGMENT, LENGTH   335, NAME  JCB

                    SUBROUTINE FUNC(KK,B,NN,Z,FV)
0122                DIMENSION XX(10),B(10),XXC(10),Z(10),FV(10)
0123                DIMENSION TLAND(4),A(4),AA(4),DA1(4)
0124                DOUBLE PRECISION XX,XIN,XOUT,YIN,YOUT,D1,G,B
0125                DOUBLE PRECISION  XXC,Z,TLAND,A,AA,DA1
0126                COMMON XX,XIN,XOUT,YIN,YOUT,D1,G
0127                CALL PROFIL(NN,KK,B,XXC,TLAND,A,AA,DA1,FV)
0128                DO 100 JJ=1,NN
0129                Z(JJ)=XXC(JJ)
0130            100 CONTINUE
0131                RETURN
0132                END
0133

END OF SEGMENT, LENGTH    67, NAME  FUNC

                    SUBROUTINE PROFIL(M,X,XC,YYY,TLAND,A,AA,DA1,FV)
0134
0135            C
0136            C       THIS SUBROUTINE OUTPUT THE CALC. PROFIL ACCORDING WITH TH
0137            C       SELECTED OBJECTIVE FUNCTION
0138            C
0139                    DIMENSION DA1(4),TLAND(4),A(4),AA(4),X(2,5),XC(2)
0140                    DIMENSION XX(10),XC(10),YYY(10)
0141                    DIMENSION FV(10)
```

```
0142                  DIMENSION XX(50),XIN,XOUT,YIN,YOUT,D1,G,XC,FV,DA1,TLAND,A,AA
0143                  DOUBLE PRECISION XX,XIN,XOUT,YIN,YOUT,D1,G,XC,FV,DA1,TLAND,A,AA
0144                  DOUBLE PRECISION ET,F,PER,PEE,TNTU
0145                  DOUBLE PRECISION X,Y
0146                  COMMON XX,XIN,XOUT,YIN,YOUT,D1,G
0147            C
0148            C     CALCULATE EXTRACTION FACTOR = F
0149            C     THE CALCULATION OF EXT. FACTOR F MAY REQUIRE MODIFICATIONS
0150            C     ACCORDING WITH THE USER DEFINITION OF THE Y- AND- PHASES
0151                  F=FV(2)
0152                  GO TO 01
0153                  F=(XOUT-XIN)/(YIN-YOUT)
0154                  F=F/D1
0155             01   CONTINUE
0156                  PER=XC(1)
0157                  PEE=XC(2)
0158                  TNTU=XC(3)
0159                  CALL COEF(PER,PEE,TNTU,F,TLAND,A,AA,B1,D,DA1)
0160                  NP=FV(1)
0161                  DO 15 K=1,M
0162                  Y(K)=0.000
0163                  X(K)=0.000
0164                  DO 18 N1=1,4
0165                  X(K)=X(K)+A(N1)*EXP(TLAND(N1)*XX(K))
0166             18   Y(K)=Y(K)+A(N1)*AA(N1)*EXP(TLAND(N1)*XX(K))
0167                  GO TO (10,20,30),NP
0168             10   YYY(K)=ABS(X(K)-Y(K))
0169                  GO TO 15
0170             20   YYY(K)=Y(K)
0171                  GO TO 15
0172             30   YYY(K)=X(K)
0173             15   CONTINUE
0174                  RETURN
0175                  END

      END OF SEGMENT, LENGTH   323, NAME  PROFIL

                      SUBROUTINE COEF(P1,P2,T,F,TL,A,AA,B1,D,DA1)
0176
0177            C
0178                  DIMENSION TL(4),A(4),AA(4),B1(3,5),D(3,5),DA1(4)
0179                  DOUBLE PRECISION XX,XIN,XOUT,YIN,YOUT,D1,G,TL,A,AA,B1,D,DA1,P1,P2
0180                  DOUBLE PRECISION T
0181                  DOUBLE PRECISION F,ALF,BET,GAM,P,Q,S,SS,U,X1,X2,X3,X4,S1,S2,S3,S4
0182                  COMMON XX,XIN,XOUT,YIN,YOUT,D1,G
0183            C
0184                  ALF=P1-P2
0185                  BET=F*P1*P1*P2+T*P2*P
0186                  GAM=(1.-F)*T*P1*P2
0187                  P=(ALF/3.)**2+BET/3.
0188                  Q=(ALF/3.)**3+ALF*BET/6.+GAM/2.
0189                  TL(1)=0.000
0190                  S=ALF/3.
0191                  SS=2.*SQRT(P)
0192                  U=ACOS(Q/(P**1.5))
0193                  TL(2)=S+SS*COS(U/3.)
0194                  TL(3)=S+SS*COS(U/3.+2.094395102)
0195                  TL(4)=S+SS*COS(U/3.+4.188790205)
0196                  DO 6 I=1,4
0197             6    A(I)=1.*TL(I)/T-TL(I)**2/(2.*T)
0198                  DO 1 I=1,3
0199                  DO 1 J=1,3
0200                  NP=J
0201                  GO TO (1,2,5),NP
0202             1    B1(J,I)=1.-TL(I+1)/B1
```

```
0203                    D(J+2,I)=(1.+TL(I+1)/P2)**A(I+1)*EXP(TL(I+1))
0204                    GO TO 80
0205                  2 B1(J,I)=TL(I+1)**A(I+1)
0206                    D(J-1,I)=B1(J,I)
0207                    GO TO 80
0208                  5 B1(J,I)=TL(I+1)**EXP(TL(I+1)-TL(2))
0209                    D(J-1,I)=B1(J,I)
0210                 80 CONTINUE
0211               C  ADD COLUMNS 4 AND 5 TO B AND D
0212                    DO 30 I=1,2
0213                    K=3+I
0214                    DO 30 J=1,3
0215                    B1(J,K)=B1(J,I)
0216                 30 D(J,K)=D(J,I)
0217               C  EVALUATE THE DETERMINANTS
0218                    X1=0.0D0
0219                    X2=0.0D0
0220                    X3=0.0D0
0221                    X4=0.0D0
0222                    DO 40 I=1,3
0223                    S2=1.D0
0224                    S3=1.D0
0225                    S4=1.D0
0226                    S1=1.D0
0227                    N=I
0228                    K=2+I
0229                    DO 35 J=1,3
0230                    S1=S1*B1(J,N)
0231                    S2=S2*B1(J,K)
0232                    S3=S3*D(J,N)
0233                    S4=S4*D(J,K)
0234                    N=N+1
0235                 35 K=K-1
0236                    X1=X1+S1
0237                    X2=X2+S2
0238                    X3=X3+S3
0239                    X4=X4+S4
0240                 40 CONTINUE
0241                    DA1(1)=X3-X4
0242                    DA=DA1(1)-(X1-X2)
0243                    DA1(2)=-(B1(2,2)*B1(3,3)-B1(2,3)*B1(3,2))
0244                    DA1(3)=B1(2,1)*B1(3,3)-B1(2,3)*B1(3,1)
0245                    DA1(4)=-(B1(2,1)*B1(3,2)-B1(2,2)*B1(3,1))
0246                    DO 50 I=1,4
0247                 50 A(I)=DA1(I)/DA
0248                    RETURN
0249                    END
```

END OF SEGMENT, LENGTH 862, NAME COEF

```
                        SUBROUTINE BSOLVE(KK,B,NN,Z,Y,BB,ENU,FLA,TAU,EPS,
0250                   1PHMIN,I,ICON,FV,DV,BMAX,PMIN,SMAX,P,FUNC,DERIV,KU,A,AC,GAMM)
0251                    DIMENSION B(10),Z(10),Y(10),BV(10),ENU(10),BB(10)
0252                    DIMENSION B(130),A(10,10),AC(10,12),X(10),FV(10),DV(10)
0253                    DOUBLE PRECISION B,Z,Y,BB,ENU,FLA,TAU,EPS,PHMIN,DV,FV,BV
0254                    DOUBLE PRECISION BMAX,P,A,AC,SMAX,X,DUM,GR,FLA,FUNC,DG
0255                    DOUBLE PRECISION COEF,XCOEF,PHI
0256
0257               C
0258                    K=KK
0259                    N=NN
0260                    KP1=K+1
0261                    KP2=KP1+1
0262                    KB11=K*K
0263                    KB12=KB11+K
0264                    KZ1=KB12+K
```

```
0264                KB1=KB12+K
0265                IF(FNU .LE. 0.)FNU=10. D0
0266                IF(FLA .LE. 0.)FLA=0.0100
0267                IF(TAU .LE. 0.)TAU=0.001D0
0268                IF(EPS .LE. 0.)EPS=X02AAF(RR)
0269                IF(PHMIN .LE. 0.)PHMIN=0.D0
0270          120 KE=0
0271          130 DO 160 I1=1,K
0272          160 IF(BV(I1) .NE. 0.)KE=KE+1
0273                IF(KE .GT. 0) GO TO 170
0274          152 ICON=-3
0275          153 GO TO 2120
0276          170 IF(N .GE. KE) GO TO 500
0277          180 ICON=-2
0278          190 GO TO 2120
0279          500 I1=1
0280          530 IF(I .GT. 0) GO TO 1530
0281          550 DO 560 J1=1,K
0282              J2=KB11+J1
0283              P(J2)=B(J1)
0284              J3=KB12+J1
0285          560 P(J3)=ABS(B(J1))+1.0E-32
0286              GO TO 1030
0287          590 IF(PHMIN .GT. PH .AND. I .GT. 1) GO TO 625
0288              DO 620 J1=1,K
0289              N1=(J1-1)*N
0290              IF(BV(J1))601,620,605
0291          601 CALL DERIV (K,B,N,Z,P(N1+1),FV,DV,J1,JTEST)
0292              IF(JTEST .NE. (-1)) GO TO 620
0293              BV(J1)=1.0
0294          605 DO 606 J2=1,K
0295              J3=KB11+J2
0296          606 P(J3)=B(J2)
0297              J3=KB11+J1
0298              J4=KB12+J1
0299              DEN=0.001*AMAX1(P(J4),ABS(P(J3)))
0300              IF (P(J3) + DEN .LE. BMAX(J1)) GO TO 55
0301              P(J3)=P(J3) - DEN
0302              DEN=-DEN
0303              GO TO 56
0304           55 P(J3)=P(J3) + DEN
0305           56 CALL FUNC(K,P(KB11+1),N,P(N1+1),FV)
0306              DO 610 J2=1,N
0307              JB=J2+N1
0308          610 P(JB)=(P(JB) - Z(J2))/DEN
0309          620 CONTINUE
0310        C
0311        C     SET UP CORRECTION EQUATIONS
0312        C
0313          625 DO 735 J1=1,K
0314              N1=(J1-1)*N
0315              A(J1,KP1)=0.
0316              IF(BV(J1))630,692,630
0317          630 DO 640 J2=1,N
0318              N2=N1+J2
0319          640 A(J1,KP1)=A(J1,KP1)+P(N2)*(Y(J2)-Z(J2))
0320          650 DO 660 J2=1,K
0321          660 A(J1,J2)=0.
0322          665 N2=(J2-1)*N
0323          670 DO 680 J3=1,N
0324          672 N3=N1+J3
0325          674 N4=N2+J3
0326          680 A(J1,J2)=A(J1,J2)+P(N3)*P(N4)
0327              IF(A(J1,J1) .GT. 1.E-20) GO TO 735
0328          692 DO 694 J2=1,KP1
0329          694 A(J1,J2)=0.
0330              A(J1,J1)=1.0
```

```
0330          725 A(J1,J1)=1.0
0331              CONTINUE
0332              GN=0.
0333              DO 729 J1=1,K
0334          729 GN=GN + A(J1,KP1)**2
0335          C
0336          C     SCALE CORRECTION EQUATIONS
0337          C
0338              DO 726 J1=1,K
0339          726 A(J1,KP2) = SQRT(A(J1,J1))
0340              DO 727 J1=1,K
0341              A(J1,KP1) = A(J1,KP1)/A(J1,KP2)
0342              DO 727 J2=1,K
0343          727 A(J1,J2) = A(J1,J2)/(A(J1,KP2)*A(J2,KP2))
0344          730 FL=FLA/FNU
0345              GO TO 810
0346          800 FL=FNU*FL
0347          810 DO 840 J1=1,K
0348          820 DO 830 J2=1,KP1
0349          830 AC(J1,J2)= A(J1,J2)
0350          840 AC(J1,J1)=AC(J1,J1) + FL
0351          C
0352          C     SOLVE CORRECTION EQUATIONS
0353          C
0354              DO 930 L1=1,K
0355              L2=L1+1
0356              DO 910 L3=L2,KP1
0357          910 AC(L1,L3)=AC(L1,L3)/AC(L1,L1)
0358              DO 930 L3=1,K
0359              IF(L1-L3) 920,930,920
0360          920 DO 925 L4=L2,KP1
0361          925 AC(L3,L4)=AC(L3,L4)-AC(L1,L4)*AC(L3,L1)
0362          930 CONTINUE
0363          C
0364              DN=0.
0365              DG=0.
0366              DO 1028 J1=1,K
0367              AC(J1,KP2) = AC(J1,KP1)/A(J1,KP2)
0368              J2= KBI1 + J1
0369              P(J2) = AMAX1(BMIN(J1),AMIN1(BMAX(J1),B(J1)+AC(J1,KP2)))
0370               DG = DG + AC(J1,KP2)*(J1,KP1)*A(J1,KP2)
0371              DN = DN + AC(J1,KP2)*AC(J1,KP2)
0372          1028 AC(J1,KP2)=P(J2)-B(J1)
0373              COSG = DG/SQRT(DN*GN)
0374              JGAM = 0
0375              IF(COSG) 1100,1110,1110
0376          1100 JGAM = 2
0377              COSG = -COSG
0378          1110 CONTINUE
0379              COSG = AMIN1(COSG,1.0)
0380              GAMM=ARCOS(COSG)*180./(3.14159265)
0381              IF(JGAM .GT. 0) GAMM=180. -GAMM
0382          1030 CALL FUNC(K,P(KBI1+1),N,P(KZI+1),FV)
0383          1500 PHI = 0.
0384              DO 1520 J1=1,N
0385              J2=KZI + J1
0386          1520 PHI=PHI+(P(J2)-Y(J1))**2
0387              IF(PHI .LT. 1.E-15)GO TO 1535
0388              IF(I .GT.  ) GO TO 154
0389          1521 ICON = K
0390              GO TO 211.
0391          1540 IF(PHI .GE. PH) GO TO 1510
0392          C
0393          C       EPSILON TEST
0394          C
0395          1210 ICON=0
0396               DO 1 J1=1,K
```

```
0396                  DO 1220 J1=1,K
0397                  J2=KBI1+J1
0398            1220  IF(ABS(AC(J1,KP2))/(TAU + ABS(P(J2))) .GT. EPS) ICON=ICON+1
0399                  IF(ICON .EQ. 0) GO TO 1400
0400            C
0401            C     GAMMA LAMBDA TEST
0402            C
0403                  IF(FL .GT. 1.0 .AND. GAMM .GT. 90.0) ICON =-1
0404                  GO TO 2105
0405            C
0406            C     GAMMA EPSILON TEST
0407            C
0408            1400  IF(FL .GT. 1.0 .AND. GAMM .LE. 45.0) ICON=-4
0409                  GO TO 2105
0410            C
0411            1530  IF(I1-2)1531,1531,2310
0412            1531     I1=I1+1
0413                  GO TO (530,590,800),I1
0414            2310  IF(FL .LT. 1.0E+8) GO TO 800
0415            1320  ICON=-1
0416            C
0417            2105  FLA=FL
0418                  DO 2091 J2=1,K
0419                  J3=KBI1+J2
0420            2091  Q(J2)=P(J3)
0421            2110  DO 2050 J2=1,N
0422                  J3=KZI+J2
0423            2050  Z(J2) = P(J3)
0424                  PH=PHI
0425                  I=I+1
0426            2120  RETURN
0427            3000  ICON=0
0428                  GO TO 2105
0429            C
0430                  END

END OF SEGMENT, LENGTH  1481, NAME  BSOLV1


0431                  FUNCTION ARCOS(Z)
0432            C
0433                  DOUBLE PRECISION X,Z,ARCOS
0434                   X=Z
0435                   KEY=0
0436                  IF(X .LT. (-1.)) X=-1
0437                  IF(X .GT. 1.) X=1.
0438                  IF(X .GE. (-1.) .AND. X .LT. 0.) KEY=1
0439                  IF(X .LT. 0.) X=ABS(X)
0440                  IF(X .EQ. 0.) GO TO 10
0441                  ARCOS=ATAN(SQRT(1.-X**2)/X)
0442                  IF(KEY .EQ. 1) ARCOS=3.1415926 -ARCOS
0443                  GO TO 999
0444             10   ARCOS=1.5707963
0445             999  RETURN
0446                  END

END OF SEGMENT, LENGTH   171, NAME  ARCOS

0447                  FINISH

END OF COMPILATION -  NO ERRORS
```

```
S/C SUBFILE :      56 BUCKETS USED
CONSOLIDATED BY XPCK 12H    DATE    23/10/81   TIME 13/01/23

          *SHORTLIST

          *IN ED (FORTSEMICOMP)

          *LIB ED (SUBGROUPNAGF.SUBROUTINES)

          *LIB ED (SUBGROUPSRF4.SUBROUTINES)

          *WORK ED (FORTWORKFILE)

          ****

PROGRAM FXXX
EXTENDED DATA (22AM)
COMPACT PROGRAM (DBM)
CORE               12992

ALLOT       *CRO    N
0.34: MONITOR
ALLOT       *LFO    N
0.34: MONITOR
13.02.23 FREE *CRO ,11 TRANSFERS
13.02.23 FREE *LFO ,23 TRANSFERS
0.46 :DELETED : CO
13.02.23 0.46 DELETED,CLOCKED 0.32
DISPLAY: UAFORTRAN: NORMAL EXIT
13.02.25 0.46 FINISHED : 2 LISTFILES
13.02.25 JOBTIME USED 47 ; MAXIMUM CORE USED 32575
13.02.25 JOB UNITS 103

*XXXXXXXXXXXXXXXXXXXXXXXXXXXXXXXXXXXXXXXXXXXXXXXXXXXXXXXXXXXXXXXXXXXXXXXXXXXXXXXXXXXXXXXXXXXXXXXXXX*
*XXXXX X                                   XXXXXXXXXXXXXXXXXXXXXXXXXXXXXXXXXXXXXXXXXXXXXXXXXXXXXXXXX*
*XXXXXXX         NUMBER OF PAGES     0     XXXXXXXXXXXXXXXXXXXXXXXXXXXXXXXXXXXXXXXXXXXXXXXXXXXXXXXXX*
*XXXXXXX                                   XXXXXXXXXXXXXXXXXXXXXXXXXXXXXXXXXXXXXXXXXXXXXXXXXXXXXXXXX*
*XXXXXXXXXXXXXXXXXXXXXXXXXXXXXXXXXXXXXXXXXXXXXXXXXXXXXXXXXXXXXXXXXXXXXXXXXXXXXXXXXXXXXXXXXXXXXXXXXXX*
```

References

1. Karr, A. and Scheibel, E.G., Chem. Eng. Prog. Symp. Series, (1954), Vol.50. Part No.10, 73.
2. Honekamp, J.R. and Burkhart, L.E., Ind. and Eng. Chem. Process Design and Development. 1, 3, 177, (1962).
3. Piper, H.B., Ph.D. Thesis, University of Manchester, (1969).
4. Gelperin, N.L. et al., Teor. Osn. Khim, Tekhnol. 1(5) 666-74, (1967).
5. Hanson, C., Chem. Engr. January 19, 86, (1976).
6. Reissinger, K.H. and J. Schroeter., Chem. Engr. Nov (1978), 109.
7. Treybal, R., Liquid-Liquid Extraction. McGraw-Hill (1963).
8. Jeffreys, G.V. and Hawksley, J.L., Droplet Phenomena Symposium A.I.Ch.E.J. Pittsburgh (1964).
9. Miyauchi, T. and Vermeulen, T., Ind. and Eng. Chem. Fundamentals 2, 113 (1963).
10. Sleicher, C.A., A.I.Ch.E.J. 5, No.2, 145 (1959).
11. Strand, C.P., Olney, R.B. and Ackerman, G.H., A.I.Ch.E.J. 8, No.2, 252 (1962).
12. Pratt, H.R.C. Ind. Eng. Chem. Process Design and Development 14, No.1, 74 (1975).
13. Misek, T., 'Rotating Disc Contactor' (1964) (Prague Statni Nakadelokri Technicke Literatury).
14. Misek, T., Coll. Czech. Chem. Comm. 28, 1631 (1963).
15. Scheibel, E.G., (to Hoffman La Roche Co.), U.S. Patent 2.493.265 (Jan. 3 1950).
16. Scheibel, E.G., Chem. Engr. Progr. 44, No.9, 681 (1948).
17. Scheibel, E.G. and Karr, A.E., Ind. Eng. Chem. 42, No.6, 1048 (1950).

18. Scheibel, E.G., A.I.Ch.E.J. 2, No.1, 74 (1956).

19. Lewis, J.B., Jones, I. and Pratt, H.R.C., Trans. Instn. Chem. Engrs. Vol29, 126 (1951).

20. Gayler, R. and Pratt, H.R.C., Trans. Instn. Chem. Engrs, Vol.29, 110 (1951).

21. Honekamp, J.R., Ph.D. Thesis, Iowa State University (1960).

22. Gayler, R., Roberts, N.W. and Pratt, H.R.C., Trans. Instn. Chem. Engrs. Vol.31, 57 (1953).

23. Crawford, J.W. and Wilke, C.R., Chem. Engr. Prog. 47, No.8, 423, (1951).

24. Jeffreys, G.V., Davies, G.A. and Piper, H., Paper 75 I.S.E.C. '71, The Hague (1971).

25. Levenspiel, O. and Smith, W.K., Chem. Engr. Soc. 6, 227 (1957).

26. Guttoff, E.B., A.I.Ch.E. Journal, 11, No.4, 712 (1965).

27. Nanda, A.K. and Sharma, M.M., Chem. Engr. Sci. 21, 707, (1966).

28. Purinak, S.A. and Sharma, M.M., Chem. Engr. Sci, 25, 257 (1970).

29. Fernandez, J.B., Ph.D. Thesis, University of Bombay (1967).

30. Weinstein, B. and Treybal, R., A.I.Ch.E.J. 19, No.2, 304, (1973).

31. Coulaloglou, C. and Tavlarides, L., A.I.Ch.E.J. 22, No.2, 289, (1976).

32. Hinze, J.O., A.I.Ch.E.J. 1, No.3, 289 (1955).

33. Kolmogoroff, A.M., C.R.Acad. Sci. URSS 30, 301 (1941).

34. Hinze, J.O., "Turbulence" 1st Ed. (1959) p. 239, McGraw Hill.

35. Batchelor, G.K., Proc. Camb. Phil. Soc. 43, 533 (1947).

36. Levich, V.G., "Physicochemical Hydrodynamics" (1962), Prentice-Hall.

37. Kolmogoroff, A.M., Dokl., Akad. Nauk SSSR 66, 825 (1949).

38. Shinner, R.J., Fluid Mech. 31, 365 (1961).

39. Howarth, W., Chem. Eng. Sci. 19, 33 (1964).

40. Misek, T., Coll. Czech Chem. Comm. 22, 2086 (1964).

41. Smoluchowski, J., Z. Phys. Chem. 92, 129 (1917).

42. Harper, W.R., Trans. Farad. Sco. 32, 1139 (1936).

43. Misek, T., Coll. Czech. Chem. Comm 29, 2089 (1964)

44. Levich, U.G., Dokl. Akad. Nauk SSSR 99, 809 (1954).

45. Doulah, M. and Davies, G.A., I.S.E.C. Vol.1, 533 (1974).

46. Shiloh, K. Sideman, S. and Resnick, W., Paper A.I.Ch.E. 68th National Meeting Houston, Texas (1971).

47. Koetsier, W. and Thoener, D., Proceedings of 5th European Symposium in Chem. Reactor Engr. 133-15 Amsterdam, Holland, (May 1972).

48. Dallavalle, J.M., "Micromeritics, the Technology of Fine Particles" 2nd Ed. N.Y. Pitman Publishing Co. (1948).

49. Sprow, F.B., Chem. Engr. Sci. 22, 435 (1967).

50. Van Heuven, J. and Hoevenaar, J.C., Proc. 4th European Symp. Chem. React. Engr. Brussels. Pergammon Press, Oxford (1968).

51. Brown, D.E. and Pitt, K., Chemeca '70 Inst. of Chem. Engrs. Symp. Ser. No.33, Session 5 p.83, Butterworth, Australia.

52. Rushton, J. E. Costich and H. Everett., Chem. Engr. Prog. 46, 395 (1950).

53. Brodkey, R.S., "The phenomenon of fluid motion" Addisson-Wesley Redding, Mass. (1967).

54. Nagata, S., "Mixing Principle and Applications" John Wiley and Sons. (1975).

55. Cutler, L., A.I.Ch.E.J. 12, No.1, 35 (1966).

56. Vermeulen, T., Williams, G.M. and Langleis, G.E., Chem. Engr. Prog. 51, 85F (1955).

57. Calderbank, P.H., Trans. Instn. Chem. Engr. 36, 43 (1958).

58. Chen, H.T. and Middleman, S., A.I.Ch.E.J. 13, No.5, 989, (1967).

59. McManamey, W., Chem. Engr. Sci. 34, 432 (1979).

60. Brown, D.E. and Pitt, K., Chem. Engr. Sci, 29, 345 (1974).

61. Coulaloglou, C., Ph.D. Thesis. Illinois Inst. Technology. Chicago (1975).

62. Logsdail, D. Thornton, J. and Pratt, H., Trans. Instn. Chem. Engrs. 35, 301 (1957).

63. Groothuis, H. and Zuiderweg, F.J., Chem. Engr. Sci. 12, 288 (1960).

64. Jeffreys, G.V. and Lawson, G., Trans. Inst. Chem. Engrs. 43, 294 (1965).

65. Sawistowski, H., "Recent Advances in Liquid-Liquid Extraction" Ed. C. Hanson (1971).

66. Misek, T., Coll. Czech. Chem. Com. 28, 426 (1963).

67. Ferrarin, V.D.J., Forschungsheft Nr. 551.

68. Fisher, A., Ferfahrenstechnik 5, 360 (1971).

69. Mlynek, Y. and Resnick W., A.I.Ch.E.J. 18, No.1, 122 (1972).

70. Arnold, D.R., Ph.D. Thesis, University of Aston, Birmingham (1974).

71. Steinour, H.H., Ind. Eng. Chem. 36, 618 (1944).

72. Gayler, R. and Pratt, H.R.C., Trans. Instn. Chem. Engr. Vol.31, 69 (1953).

73. Thornton, J.D., Chem. Engr. Progr. Nuclear Engineering Series Vol. III.

74. Thornton, J.D. and Prat, H.R.C., Trans. Instn. Chem. Engrs. 31, 289 (1953).

75. Thornton, J.D., Chem. Engr. Sci. 5, 201 (1956).

76. Hayworth, C.B. and Treybal, R.E., Ind. Engr. Chem. 42, 1174 (1950).

76. Steinour H.S., Ind. Engr. Chem. 36, 618 (1944).

77. Perry's Handbook 5-64 5th Edition.

78. Resnick, W., Paper presented to the 3rd CHISA Congress, Marianske Lanze (1969).

79. Hu, S. and Kintner, R.C., A.I.Ch.E.J. 1, 42, (1955).

80. Klee, A.J. and Treybal, R.E., A.I.Ch.E.J. 2, 444, (1956).

81. Al;Hemeri, A., Ph.D. Thesis University of Aston (UK) (1973).

82. Biband, R.E. and Treybal, R.E., A.I.Ch.E.J. 12, 472 (1966).

83. Breckenfeld, R.R. and Wilke, C.R., Chem. Engr. Progr. 46, 187 (1950).

84. Crawford, J.W. and Wilke, C.R., Chem. Engr. Progr. 47, 423 (1951).

85. Dell, F.R. and Pratt, H.R.C., Trans. Instn. Chem. Engr. 29, 89 (1951).

86. Watson, J.S. et al., A.I.Ch.E.J. 6, 1080, (1975).

87. Sarkar, S., Ph.D. Thesis, University of Aston (UK), 1976.

88. Nernst, W., Z. Phys. Chem. 47, 52 (1904).

89. Whitman, W.G., Chem. Met. Engr. 29, 146 (1923).

90. Higbie, R., Trans. Am. Instn. Chem. Eng. J. 31, 365 (1935).

91. Danckwerts, P.V., Ind. Engr. Chem. 43, 1460 (1951).

92. Sherwood, T.K. Pigford, R.L. and Wilke, C.R., "Mass Transfer" McGraw Hill (1975).

93. Skelland, A.H.P., "Diffusional Mass Transfer" J. Wiley International (1974).

94. Scriven, L.E., Chem. Engr. Educ. 2, 150 (Fall 1968), 26 (Winter 1969), 94 (Spring 1969).

95. Lamont, J.C. and Scott, D.S., A.I.Ch.E. Journal 16, 513 (1970).

96. Ranz, W.E. and Marshall, W.R., Chem. Engr. Progr. 48, 173, (1952).

97. Frossling, N., Beitr. Geophys. 52, 170 (1938).

98. Kinard, G.E. Manning, F.S. and Manning, W.P., Brit. Chem. Engr. 8, 326 (1963).

99. Garner, F.H., Foord, A. and Tayeban, M., J. Appl. Chem. 9, 315 (1959).

100. Boussinesf, J., J. Math. Pure Appl. 11, 285 (1905).

101. Ruckenstein, E., Chem. Engr. Sci. 10, 22 (1959).

102. Garner, F.H. and Tayeban, M., An. R. Soc. Esp. Fis. Quim. 56B, 479 (1960).

103. Rose, P.H. and Kintner, R.C., A.I.Ch.E. J. 12, 530 (1966).

104. Angelo, J. Lightfoot, E. and Howard, D., A.I.Ch.E.J. 12, 751 (1966).

105. Newman, A.B., Trans. Am. Inst. Chem. Engrs, 27, 203 (1931).

106. Vermeulen, T., Ind. Eng. Chem. 45, 1664, (1953).

107. Kronig, R. and Brink, J.C., Appl. Scient. Res., A2, 142 (1960).

108. Rybczynski, W., Bull. Acad. Sci. Cracovie, Ser. A. 40, (1911).

109. Hadamard, J.S., C.R. Acad. Sci. Paris, 152, 1735 (1911).

110. Calderbank, P.H. and Korchinski, I.J., Chem. Eng. Sci, 6, 65 (1956).

111. Handlos, A.E. and Baron, T., A.I.Ch.E.J. 3, 127 (1957).

112. Al-Hassan, T., Ph.D. Thesis, University of Aston (UK), (1979).

113. Sternling, C.V. and Scriven, L.E., A.I.Ch.E.J. 5, 515 (1959).

114. Barker, J.J. and Treybal, R.E., A.I.Ch.E.J. 6, 289 (1960).

115. Schindler, H.D. and Treybal, R.E.. A.I.Ch.E.J. 14, 790 (1968).

116. Harricot, P. A.I.Ch.E.J. 8, 93 (1962).

117. Holmes, D.B., Voncken, R.M. and Dekker, J.A., Chem. Eng. Sci. 19, 201, (1964).

118. Mok, Y.I. and Treybal, R.E., A.I.Ch.E.J. 17, 914, (1971).

119. Hughmark, G.A., Ind. Eng. Chem. Fund. 6, 408 (1967).

120. Calderbank, P.H. and MooYoung, M.B., Chem. Eng. Sci., 16, 39 (1961).

121. Keey, R.B. and Glen, J.B., A.I.Ch.E.J. 15, 942, (1969).

122. Lin, C. et al., Ind. Eng. Chem. 45, 636 (1953).

123. Skelland, A.H. and MoonLee, J., A.I.Ch.E.J. 27, 99 (1981).

124. Geankoplis, C.J. and Hixson, A.N., Ind. Eng. Chem. 42, 1141 (1950).

125. Gier, T.E. and Hougen, J.O., Ind. Eng. Chem. 45, 1362 (1953).

126. Cavers, S.D. and Ewanchyna, J.E., Can. J. Chem. Eng., 35, 113 (1957).

127. Smoot, L.D. and Babb, A.L., Ind. Eng. Chem. Fund. 1, 93 (1962).

128. Souhrada, F. Prochazka, J. and Landau, J., Coll. Czech. Chem. Comm. 31, 1695 (1966).

129. Chin, L.L., M.Eng. Thesis, University of Florida (USA), (1963).

130. Treybal, R.E., Ind. Eng. Chem. 47, 2435 (1955).

131. Rod, V., Brit. Chem. Eng. 9, 300 (1964).

132. Pollock, G.G. and Johnson, A.I., Can. J. Chem. Eng. 48, 64 (1970).

133. Bonnet, J.C. and Jeffreys, G.V., Paper 4-8,7th CHISA Congress, Prague (1981).

134. Newman, M.L., Ind. Eng. Chem. 44, 2457 (1952).

135. Wen, C.Y. and Fan, L.T., "Models for Flwo System and Chemical Reactors" Dekker (1975).

136. Danckwerts, P.V., Chem. Eng. Sci. 2, 1, (1953).

137. Eguchi, W. and Nagata, S., Chem. Eng. Tokyo, 22, 2181 (1958).

138. Sleicher, C.A., A.I.Ch.E.J. 6, 529 (1960).

139. Hartland, S. and Mecklenburgh, J.C., Chem. Eng. Sci. 21, 1209 (1966).

140. Mecklenburgh, J.C. and Hartland, S., Ind. Chem. Eng. Symp. Series 26, 121 (1967).

141. Pratt, H.R.C., Ind. Eng. Chem. Proc. Des. and Dev. 14, 74 (1975).

142. Mecklenburgh, J.C. and Hartland, S., "The Theory of Backmixing" J. Wiley and Sons (1975).

143. Sherwood, T.K. and Jenny, F.I., Ind. Eng. Chem. 27, 265, (1935).

144. Colburn, A.P.,Ind. Eng. Chem. 28, 526 (1936).

145. Misek, T. and Rod, V., "Recent Advances in Liquid-Liquid Extraction" Ed. C. Hanson (1971).

146. Prochazka, J. and Landau, J., Coll. Czech Chem. Comm. 31, 1685 (1966).

147. Miyauchi, T. and Vermeulen, T., Ind. Eng. Chem. Fund. 2, 304 (1963).

148. Slavickova et al., Coll. Czech. Chem. Comm. 43, 2682 (1978).

149. Ricker, N.L., Nakasio, F. and King, C.J., A.I.Ch.E.J. 27, 277 (1981).

150. Davies, O., "Design and Analysis of Industrial Experiments" 2nd Ed. Longman for I.C.I. Ltd (1978).

151. Uhl, V.W., "Mixing : Theory and Practice" Academic Press (1966).

152. Shelland, A.P. and Huang, Y.F., A.I.Ch.E.J. 23, 701 (1977).

153. Shelland, A.P. and Huang, Y.F., A.I.Ch.E.J. 25, 80 (1979).

154. Wilke, C.R. and Chang, P., A.I.Ch.E.J, 1, 264 (1955).

155. Bouyatiotis, B.S. and Thornton, J.D., Inst. Chem. Engr. (London), Symp. Ser. 26, 43 (1967).

156. Calderbank, P.H., Trans. Instn. Chem. Engr. 36, 43, (1958).

157. Von Berg, R.L. and Henkel, W.M., Proc. I.S.E.C. Vol.II, 852 (1971).

158. Rod, V., Coll. Czech. Chem. Comm. 30, 3822, (1965).

159. Chilton, T.H. and Colburn, A.P., Ind. Eng. Chem. 27, 255, (1935).

160. Marguardt, D., J. Soc. Ind. Appl. Math. 11, 432, (1963).

161. Henley, H. and Rosen, L., "Material and Energy Balance Computation, J. Wiley and Sons (1969).

162. Staffin, H.K., D.Ch.E. Dissertation, Pol. Inst. of Brooklyn, (1959).

163. Thomas, R.J. and Mumford, C.J., Proceedings of ISEC (1971). The Hague.

164. Kessler, D.D. and York, J.L., A.I.Ch.E.J. 16, 369 (1970).

165. Littlewood, A.B., "Gas Chromatography" Acad. Press. (London), (1962).

166. Davies, G.A. Jeffreys, G.V. and Afzal, M., Brit. Chem. Eng. 17, 709 (1972).

167. U.K. Patent No. 1409045, 1427704.

168. Othmer, D.F., White, R.E. and Trueger, E., Ind. Eng. Chem. 32, 1240 (1941).

169. Mumford, C.J., Ph.D. Thesis, University of Aston (UK) (1970).